



The
University
Of
Sheffield.

Breast Cancer Immunotherapy Using Magnetised Oncolytic Virus

By:

Haider Hussein Naser Al-Janabi

A thesis submitted in partial fulfilment of the requirements for the degree of
Doctor of Philosophy

The University of Sheffield
Faculty of Medicine, Dentistry and Health
School of Medicine
Department of Oncology and Metabolism

June 2019

Acknowledgements

There are many people I would like to give thank for their support during my study. First, I am thankful to the Ministry of Higher Education and Scientific Research in Iraq and its representative in the UK, the Iraqi cultural attaché, which has funded this research project. I would also like to thank my supervisor Dr. Munitta Muthana for providing me with guidance, education and support from day one of my PhD. In addition, for giving me a chance to take part in international conferences. I am also grateful for her patience, understanding and massive knowledge.

Additional thanks must go to Dr Faith Howard for helping to proofread my thesis. Big thanks also go to Dr. Joe Conner for providing the virus that used in my PhD study. I am also thankful to Ms. Zainab Taher for the assistance with the chemical part of this study. I want also to thank Mr. Richard Allen and Mr. Matthew Fisher for offering immense technical expertise. Huge thanks also go to Muthana group; Areej, Taewoo, Priya, Natalie and Amy, for their help when needed. I am also thankful for Mohammed Ridha and Muslim Idan for providing assistance when needed. I would also like to thank all my friends; Noori, Samer, Sarmed and Nasar for all the fun times we have shared.

My special thanks are extended towards my mother, Hanan Al-Janabi, who always prayed for me, and my father, Hussein Al-Janabi, for their support, advice and encouragement. To my sisters; Alyaa and Alaa and my brother; Ali for their continued support.

Many thanks must go to my wife, Sarah ALwattar for her understanding, solidarity and advice that was provided through the long journey. Lastly, thank you to my sons, Jood and Majd, for making my day happy.

Publications

- 1- AL-JANABI, H., CONNER, J., TAHER, Z., STANILAND, S. & MUTHANA, M. 2018. *Breast cancer immunotherapy using magnetised oncolytic viruses. European Journal of Cancer, 92, S4.*
- 2- SONG, W., GREGORY, D. A., AL-JANABI, H., MUTHANA, M., CAI, Z. & ZHAO, X. 2019. *Magnetic-silk/polyethyleneimine core-shell nanoparticles for targeted gene delivery into human breast cancer cells. International Journal of Pharmaceutics, 555, 322-336.*

List of the conferences attended:

1	Yorkshire Immunology Group meeting, University of Leeds. UK 2017.	Oral presentation
2	Understanding tumour immunology Workshop, Beatson institute. Glasgow, UK 2017	Poster
3	5th Edition of the ImmunoTherapy of Cancer Conference, Berlin, Germany 2018.	Oral presentation
4	International Oncolytic Virus Conference 2018, Oxford, UK 2018	Oral presentation
5	Canadian Cancer Immunotherapy Consortium (CCIC) and ImmunoBC 2018, Vancouver, Canada 2018	Oral presentation
6	American Association for Cancer Research Annual Meeting 2019, Atlanta, Georgia, USA 2019	Poster

List of Contents

Abstract.....	xiii
Chapter 1	1
Introduction and literature review	1
1.1 Introduction.....	2
1.2 Breast Cancer	3
1.3 Cancer Immunotherapy	3
1.4 Oncolytic Virotherapy	7
1.5 Clinical trials and development of oncolytic HSV	11
1.6 The mechanism of action of HSV on tumour cells.....	14
1.7 HSV infection and host cell defence mechanisms against infection.....	16
1.7.1 Virion and genome of HSV-1.	16
1.7.2 HSV viral entry into host cells	17
1.7.3 HSV replication.....	18
1.7.4 Activation of the MEK pathway is necessary for HSV replication	18
1.7.5 Proliferating cell nuclear antigen (PCNA) is important for HSV replication	19
1.7.6 Cell death pathways and HSV	20
1.7.6.1 Autophagy.....	20
1.7.6.2 Apoptosis.....	21
1.8 HSV induces immunogenic cell death	22
1.9 Systemic delivery of HSV	25
1.10 Magnetic nanoparticles (MNPs)	28
1.10.1 Iron oxide particles	28
1.10.2 Coated iron oxide MNPs.....	29
1.10.3 Challenges of MNPs	30
1.10.3.1 Toxicity of nanoparticles	32
1.10.3.2 Controlling and guiding MNPs via an external magnetic field.....	32
1.10.4 Magnetotactic bacteria and magnetosomes	33
1.10.4.1 Applications of MTB and Magnetosomes	37
1.11 Hypothesis and Aims	40
Chapter 2	41
Materials and Methods.....	41
2.1 Materials	42
2.1.1 List of reagents	42
2.1.2 List of materials.....	43
2.1.3 List of equipment and Apparatus.....	44
2.1.4 List of Primers.....	45
2.1.5 List of commercial kits	47
2.1.6 List of solutions	47
2.1.7 List of software.....	47
2.1.8 Human Materials	47
2.2 Methods.....	48
2.2.1 Preparation of Magnetosomes (MAG)	48
2.2.1.1 Bacterial culture.....	48
2.2.1.2 AMB-1 culture medium.....	48

2.2.1.3 AMB-1 inoculation.....	51
2.2.1.4 Harvest and lysis of AMB-1 cells.....	51
2.2.1.5 Sterilization of MNPs.....	52
2.2.1.6 Sonication of MNPs.....	52
2.2.2 Culturing of human breast cancer cells.....	52
2.2.3 Cell harvesting and seeding densities.....	53
2.2.4 Primary cells isolation.....	53
2.2.5 Incubation of magnetic nanoparticles (MNPs) with cell lines.....	54
2.2.6 Flow cytometry (FACS) to assess MNP uptake and cell death in MDA-MB-231s.....	54
2.2.7 Prussian blue staining to visualise MNP uptake.....	54
2.2.8 MTT assay to assess cell viability.....	55
2.2.9 HSV1716 oncolytic virus.....	55
2.2.10 Preparation of Magnetic Viral Complexes.....	55
2.2.11 Characterisation of MAG and MAG-OV complex.....	55
2.2.11.1 Transmission Electron Microscopy (TEM).....	55
2.2.11.1.1 TEM sample preparation.....	56
2.2.11.1.2 Preparation of MAG-OV infected cells for TEM.....	56
2.2.11.2 MNP size determination by TEM.....	56
2.2.11.3 qNano.....	56
2.2.11.4 Zeta potential analysis.....	57
2.2.11.5 Magnetic susceptibility measurements (MSM).....	57
2.2.11.6 Inductively coupled plasma Atomic Emission Spectrometer (ICP-AES).....	57
2.2.12 Cell death and uptake of magnetic viral complexes.....	57
2.2.13 Tumour spheroid experiments.....	58
2.2.14 Measuring mRNA gene expression after OV infection.....	58
2.2.14.1 RNA extraction.....	58
2.2.14.2 Complementary DNA (cDNA) Synthesis.....	59
2.2.15 Cytokine Protein Level Expression Analysis with Cytokine Bead Array (CBA).....	61
2.2.16 Virus neutralization.....	62
2.2.17 HMGB1 ELISA.....	62
2.2.18 ATP assay.....	62
2.2.19 Immunocytochemistry.....	63
2.2.20 <i>IN VIVO</i>	63
2.2.20.1 Murine model of breast cancer.....	63
2.2.20.2 HSV1716 <i>in vivo</i> neutralisation experiment.....	64
2.2.20.3 Tissue preparation of samples for post-mortem analysis.....	65
2.2.20.4 Dissociation of EO771 cells tumours.....	65
2.2.20.5 Preparation of tumour cells for flow cytometry.....	65
2.2.20.6 Immunofluorescent staining of tumours.....	68
2.2.20.7 Haematoxylin and Eosin staining.....	69
2.2.20.8 NanoString gene expression analyses.....	69
2.2.21 Statistical analysis.....	70
Chapter 3.....	71
Characterisation of MAG-OV.....	71
3.1 Introduction.....	72
3.2 Results.....	74
3.2.1 Characterization of bacterial derived MNPs.....	74

3.2.2 Breast cancer cell internalisation of MNPs.....	75
3.2.3 Breast cancer cell viability following incubation with MAG	77
3.2.4 Characterization of MAG-OV	78
3.2.5 Transmission electron microscopy of MAG-OV cell internalisation.	81
3.2.6 MAG-OV induce MDA-MB-231 cell oncolysis.....	81
3.2.7 MAG-OV induce MCF7 cell oncolysis	83
3.2.8 MAG-OV induced tumour spheroid cell death	85
3.3 Discussion.....	87
3.3.1 Characterisation of MAG.....	87
3.3.2 MAG internalisation and viability by breast cancer cells	89
3.3.3 Characterisation of magnetic viral complexes	90
3.3.4 Oncolytic potential of magnetic viral complexes on breast cancer cells	91
Chapter 4	94
Oncolytic potential of MAG-OV	94
4.1 Introduction.....	95
4.1.1 HSV1716 entry into tumour cells	95
4.1.2 HSV1716 mechanisms of cell death and influence on the TME	96
4.1.3 Pre-existing immunity to HSV1716	97
4.2 Results	99
4.2.1 MAG-OV induces tumour cell oncolysis.....	99
4.2.2 Viral replication genes	100
4.2.3 Cell Death Mechanisms	101
4.2.4 Immunogenic cell death.....	102
4.2.5 MAG-OV induces changes in Pro-Inflammatory cytokines and Anti- Inflammatory cytokines	105
4.2.6 Primary cells infection	108
4.2.7 Viral neutralisation	109
4.3 Discussion.....	110
Chapter 5	117
Targeting delivery and immunotherapy of MAG-OV in tumour-bearing mice using an external magnetic field	117
5.1 Introduction.....	118
5.2 The antitumour efficacy of MAG-OV in the E0771 mammary carcinoma model.....	121
5.2.1 <i>In vivo</i> study Design	121
5.2.2 Magnetic guidance of MAG-OV shrinks primary mammary tumours and promotes survival.....	122
5.2.3 Increased MAG-OV in primary breast tumours following magnetic guidance.....	124
5.2.4 Increased MAG-OV viral replication following magnetic guidance	125
5.2.5 MAG-OV induces anti-tumour properties following magnetic guidance.....	126
5.2.6 MAG-OV treated tumours induce anti-tumour immunity: NanoString analysis.....	129
5.2.7 Magnetic targeting of MAG-OV increased immune cell infiltrates – Flow cytometry..	134
5.2.8 Magnetic targeting of MAG-OV increased immune cell infiltrates: Immuno-fluorescence	135
5.2.9 Magnetic targeting of MAG-OV increases T cell activation	137
5.3 Magnetising HSV1716 protect the virus from neutralisation	138
5.3.1 <i>In vivo</i> study design.....	138

5.3.2 MAG-OV protects HSV1716 from neutralising antibodies	139
5.4 Discussion.....	140
5.4.1 Magnetic guidance of MAG-OV shrinks primary mammary tumours and promotes survival.....	141
5.4.2 Increased MAG-OV targeting in primary breast tumours following magnetic guidance	144
5.4.3 Increased MAG-OV viral replication following magnetic guidance	145
5.4.4 MAG-OV induces anti-tumour immunity following magnetic guidance.....	146
5.4.5 MAG-OV treated tumours induce expression of immune-related genes.....	147
5.4.6 MAG-OV recruits immune cells into the tumour microenvironment	149
5.4.7 MAG-OV protection from neutralising antibodies.....	150
Chapter 6	151
Summary of main outcomes and general conclusion	151
6.1 Summary of main outcomes and general conclusion.....	152
6.2 Limitations of studies.....	155
6.3 Future work.....	157
References.....	159
Appendix.....	181

List of Figures

Figure 1.1: The recent advancement and growth of cancer immunotherapy acceptance.....	7
Figure 1.3: A. Genome of wild type HSV 1. B. shows the deletion in HSV1716.....	17
Figure 1.5: OV's induce ICD of cancer cells that leads to antitumor immunity.	23
Figure 1.6: Virus neutralisation during systemic delivery.	26
Figure 1.7: Transmission electron microscopy (TEM) images.	34
Figure 1.8: Transmission electron microscopy (TEM) images of different crystal shapes of magnetite magnetosome crystals that organise into chain(s) within magnetotactic bacteria.	36
Figure 2.1: shows an example melt curve from a good primer pairs have a single peak.	61
Figure 3.1: High-resolution Transmission electron microscopy of magnetotactic bacteria and purified MAG.	75
Figure 3.2: MAGs were internalised by MDA-MB-231 cells.	77
Figure 3.3: MDA-MB-231 remain viable after incubation with MAG.	78
Figure 3.4: Diagram of the self-assembly of MAG and OV.	79
Figure 3.5: The size distribution of the OV and MAG-OV.....	80
Figure 3.6: TEM images showing stability of MAG-OV over time.....	80
Figure 3.7: TEM images of MAG-OV inside MDA-MB-231 cells.....	81
Figure 3.8: MAG-OV induce MDA-MB-231 cell oncolysis.....	82
Figure 3.9: MAG-OV induce MDA-MB-231 cell oncolysis.....	83
Figure 3.10: MAG-OV induce MCF7 cell oncolysis.	84
Figure 3.11: MAG-OV induce MCF7 cell oncolysis.	85
Figure 3.12: MAG-OV infects and kills MDA-MB-231 spheroids.	86
Figure 3.13: MAG-OV infects and kills MCF7 spheroids.....	87
Figure 3.14: Viral and cellular membrane components that contribute to HSV1716 entry.....	92
Figure 4.1: A simplified illustration of HSV1716 replication.	96
Figure 4.3: OV and MAG-OV induce oncolysis in a panel of human and murine breast cancer cell lines.....	100
Figure 4.4: MAG-OV undergoes viral replication in breast cancer cells.	101
Figure 4.5: Increased expression of cell death markers following MAG-OV infection.....	102
Figure 4.6: Extracellular levels of immunogenic cell death markers ATP and HMGB1 in human breast cancer cells.	103
Figure 4.7: Increased expression of calreticulin (CRT) on the cell surface of human breast cancer cells following MAG-OV infection.....	104
Figure 4.8: MAG-OV induces pro-Inflammatory cytokine mRNA expression in human breast cancer cells.....	106
Figure 4.9: MAG-OV induces pro-Inflammatory cytokines protein expression in human breast cancer cells.....	107
Figure 4.10: MAG-OV infected primary cells.....	108
Figure 4.11: MAG-OV is protected from anti-HSV neutralising antibodies and induces MDA-MB-231 oncolysis.	110
Figure 5.1: Treatment scheme in C57BL/6 female mice with a mammary carcinoma.	122
Figure 5.2: Magnetic targeting of MAG-OV shrinks primary mammary tumours.	123
Figure 5.3: Increased systemic targeting of MAG-OV to mammary tumours in the presence of an external magnetic field.	125
Figure 5.4: Increased viral replication of MAG-OV in mammary tumours in the presence of an external magnetic field.....	126
Figure 5.5: MAG-OV increases tumour necrosis and immunogenic cell death.	128
Figure 5.6: Volcano plots show MAG-OV increases expression of genes related to an immune response.....	130

Figure 5.7: MAG-OV upregulates tumour infiltrating immune cells.	132
Figure 5.8: Magnetic targeting of MAG-OV upregulated the expression of a range of immune- pathway genes.....	133
Figure 5.9: Magnetic targeting of MAG-OV upregulated infiltration of immune cells into tumours.	134
Figure 5.10: Magnetic targeting of MAG-OV increases antitumour immunity.	136
Figure 5.11: MAG-OV activated T cells to express interferon and PD1.	138
Figure 5.12: MAG-OV is protected from neutralising antibodies.....	140

List of Tables

Table 1.1: Active connections between cancer and the immune system...	5
Table 1.2: The advantages and disadvantages of current OVs that are being used as cancer treatments in clinical studies.	9
Table 1.3: Features of HSV that has made this virus clinically relevant.	11
Table 1.4: The oncolytic HSV's in clinical trials.	14
Table 1.5: Compares magnetosomes derived from <i>M. gryphiswaldense</i> with chemically synthesised MNPs (Fischer et al., 2011, Liu et al., 2010, Sun et al., 2008a).	35
Table 1.6: This table shows applications of whole MTB.	37
Table 1.7: This table shows applications of magnetosomes.	39
Table 2.1: AMB-1 growth medium.	49
Table 2.2: Welfer's vitamins solution.	50
Table 2.3: Volume of vitamins and minerals and ferric-quinate that was added to 400ml medium.	50
Table 2.4: Ferric quinate 0.01M.	50
Table 2.5: Welfer's mineral solution.	51
Table 2.6: Components of 2X RT Mastermix.	59
Table 2.7: Thermocycler parameters for generation of cDNA	60
Table 2.8: Components of 2X qPCR Mastermix.	60
Table 2.9: q-PCR Conditions	61
Table 2.10: Antibodies of analysing immune cells infiltration into the tumours	66
Table 2.11: Details of antibodies and controls used in flow cytometry experiments.	67
Table 2.12: Antibodies used in immunofluorescent staining experiment.	69
Table 3.1: The physicochemical properties of MAG purified from magnetospirillum magneticum AMB-1.	75
Table 3.2: The physicochemical properties of the OV and MAG-OV.	79
Table 5.1: Top 20 genes differentially regulated in MAG-OV treated tumours.	131
Table 5.2: Different mouse stains respond differently to HSV1716.	144

List of Abbreviations

- 3D** Three-dimensional
- Ad** Adenovirus
- AMF** Alternating magnetic field
- ATP** Adenosine triphosphate
- BCG** Bacillus Calmette–Guérin
- CBA** Cytokine Bead Array
- cDNA** Complementary DNA
- CRT** Calreticulin
- CI** Cancer immunotherapies
- CS** Chitosan
- CTLA-4** Cytotoxic T-Lymphocyte-associated antigen-4
- DCs** Dendritic Cells
- DMEM** Dulbecco’s Modified Eagle's Medium
- DMSO** Dimethyl Sulfoxide
- DNA** Deoxyribonucleic acid
- DPBS** Dulbecco's Phosphate Buffered Saline
- dsDNA** double stranded DNA
- E** Early
- EDTA** Ethylenediaminetetraacetic acid
- eIF2** Eukaryotic Initiation Factor 2
- FACS** Fluorescence-activated cell sorting
- FBS** Foetal Bovine Serum
- FDA** Food and Drug Administration
- FSC** Forward scatter
- GFP** Green fluorescent protein
- GM-CSF** Granulocyte macrophage-colony stimulating factor
- HDAP** Herpes Simplex Virus Dependent Apoptosis
- HER2** Human epidermal growth factor
- HIV** Human Immunodeficiency Virus
- HMGB1** High Mobility Group Box 1
- HRTEM** High-resolution transmission electron microscopy
- HSV** Herpes simplex virus

ICD Immunogenic cell death
ICP-AES Inductively coupled plasma Atomic Emission Spectrometer
iDC Immature dendritic cells
IE Immediate early
MAG Magnetosomes
MAG-OV Magnetosomes- Oncolytic virus
MAPK Mitogen-activated protein kinases
MNPs Magnetic nanoparticles
MOI Multiplicity of Infection
MRI Magnetic resonance imaging
MSM Magnetic susceptibility measurements
MTB Magnetotactic bacteria
MV Millivolts
NaOH Sodium hydroxide
OCT Optimal cutting temperature
OV Oncolytic viruses
PBS Phosphate Buffered Saline
PCNA Proliferating cell nuclear antigen
PD-1 Programmed cell death protein 1
PEG Polyethylene glycol
PEI Polyethylenimine
PFU Particle Forming Units
PI Propidium iodide
PKR Protein kinase R
PMMA Polymethyl methacrylate
PP1 α Protein phosphatase 1 alpha
PyMT Polyoma middle T antigen
q-PCR Quantitative PCR
RECIST Response Evaluation Criteria in Solid Tumors
RES Reticuloendothelial system
RNA Ribonucleic acid
RPMI Roswell Park Memorial Institute
RT Room temperature
SABR Stereotactic ablative radiotherapy

SAR Specific absorption rate
SCCE Squamous cell carcinoma of the esophagus
SCCHN Squamous cell carcinoma of the head and neck
SEM Standard error of the mean
SF Silk fibrion
SI System International
siRNA Small interfering ribonucleic acid
SPIO Super Paramagnetic Iron Oxide
SSC Side scatter
TEM Transmission electron microscopy
VISTA V-domain Ig suppressor of T cell activation
VSV Vesicular stomatitis virus

Abstract

Background: Oncolytic viruses (OV) are encouraging new immunotherapies for cancer. OVs, replicate in cancer cells inducing immunogenic cell death (ICD) and activating antitumour immunity. To date, clinical use has focused on intratumoural delivery due to concerns over inadequate tumour targeting following systemic administration. We **hypothesise** that magnetising OVs and magnetic guidance strategies will improve their systemic delivery by protecting the viruses from inactivating immune mechanisms but at the same time promote anti-tumour immunity.

Methods: To investigate this, we synthesised and characterised complexes of magnetised oncolytic herpes simplex virus (HSV1716) co-assembled with biocompatible magnetic nanoparticles (MAG) derived from magnetotactic bacteria (AMB-1) to give MAG-OV complexes. Characterization of the physical, chemical and oncolytic potential of MAG-OV was performed. The safety and efficacy of this nanomedicine in combination with magnetic guidance strategies was assessed *in vivo*.

Results: Stable MAG-OV complexes of ~160nm diameter successfully infected human and murine breast cancer cells in a dose-dependent manner, and induced tumour oncolysis. Following MAG-OV infection a significant increase in viral replication (ICP0, gB, ICP8), ICD (HMGB1, CALR, ATP) and apoptotic (CASP 3, CASP8, FASL) signals were detected. Intravenous delivery of MAG-OV resulted in reduced tumour burden in the presence of magnetic guidance (MAG-OV 448.3mm³ vs. HSV1716 670.6mm³; $p \leq 0.05$, n=6-9 mice/group) and an increase in tumour-infiltrating T-cells, NK cells and neutrophils. Furthermore, MAG-OV were protective in the presence of neutralising Abs both *in vitro* and *in vivo*.

Conclusion: This study indicates that MAG are more small and uniform in size and form complexes with OV in such a way that the virus does not change its properties. MAG-OV is able to enter and replicate inside breast cancer cells, at the same time inducing tumour cell death as good as OV alone but with the addition of protecting the virus from neutralising Ab and in combination with magnetic guidance reduces tumour burden and induces anti-tumour immunity.

Chapter 1
Introduction and literature review

1.1 Introduction

Oncolytic viruses (OVs) are emerging as new cancer immunotherapies in clinical and preclinical studies. These OVs comprise of a set of therapeutically useful and non-pathogenic viruses capable of selectively infecting and destroying tumour cells without causing damage to healthy cells. Such can arise via direct tumour cell oncolysis or through improving tumour cell death in combination with other treatments for example radio- and chemotherapy (Goldufsky et al., 2013, Russell et al., 2012, Almstätter et al., 2015a). In addition, OVs can be modified to increase tumour cell death via the induction of potent host anti-tumour immune responses (Achard et al., 2018). Tissue infectivity of OVs is a fundamental feature that is determined by tropism for a particular cell type and natural specificity for tumour cells has already been demonstrated by many OVs (Howells et al., 2017). Tumour cells are attractive to OVs as these cells avoid immune detection and destruction in addition to resisting apoptosis and translational suppression, all these properties are active in normal cells and work to prevent viral infection and spread (Russell, Peng and Bell, 2012). Numerous OVs for example, Herpes simplex virus (HSV), vesicular stomatitis virus (VSV) and adenovirus (Ad) are under examination as cancer therapies and to date the first FDA approved OV for clinical use is Amgen's T-VEC (an oncolytic HSV) in melanoma (Almstätter et al., 2015a). In addition, H101 adenovirus has been approved for head and neck cancer in China (Garber, 2006, Yuan et al., 2003)

In spite of these hopeful developments, use of OVs in the clinic comes with many challenges, such as innate host antiviral immune responses (e.g. neutralising antibodies and complement), OV pathogenicity, together this results in poor targeting to tumour sites particularly following administration into circulation. Success of oncolytic virotherapy has therefore relied on direct injection of the OV into the tumour. This approach is useful for superficial or accessible tumours but systemic delivery is necessary for the therapy of metastatic disease or hard to reach tumours (e.g. in the brain). To overcome this several approaches have been taken to improve systemic OV delivery to tumours and these will be discussed later. The overall objective is to exceed the 'viremic threshold' above which the virus infects a critical number. To achieve this, it is necessary to develop strategies that avoid OV deactivation by serum factors (antibodies and complement), reduce OV imprisonment in the liver and spleen, direct the OVs to the tumour vascular endothelial cells and selectively enhance virus permeability.

One such approach to achieve this is magnetic targeting of the OVs. Magnetic nanoparticles (MNPs) mixed with adenovirus (Ad) or vesicular stomatitis virus (VSV) has been shown to increase viral entry into a cell in the presence of an applied external magnetic field, a technique

known as magnetofection (Almstätter et al., 2015a, Tresilwised et al., 2012b). The MNPs serve as a metal shield to protect the OV (Sapet et al., 2012) and this has the potential to prevent the virus from unwanted attack in the blood stream. Moreover, an external magnetic field could be used to guide the therapy to the tumour improving its tumour targeting potential and at the same time avoiding delivery to healthy tissues and organs. This approach is the focus of this PhD thesis and in this chapter an introduction to immunotherapy using oncolytic viruses and the challenges of oncolytic virotherapy will be discussed.

1.2 Breast Cancer

Breast cancer is described to be the leading cause of death among women below 40 and the second leading killer among women aged over 40 (Silverstein et al., 2016). Although early stage Breast Cancer (BC) has been treated with a high success rate, the challenge is in managing late stage breast cancer. This suggests there are limitations of existing therapeutic options to control advanced breast cancer (Silverstein et al., 2016, Goldhirsch et al., 2009). It is reported that advanced stage BC tends to develop resistance to conventional chemotherapies, which only leaves patients with palliative care options (Brocato et al., 2014). Current available therapeutic options for breast cancer treatment can be divided into three main categories: cytotoxic, hormonal and immunotherapeutic options (Confortini and Krong, 2015). All of these therapeutic categories proved to be less efficacious in the context of controlling advanced breast cancer, and often yield toxic effects such as neurological and cardiac disorders which drastically affect the quality of life as well as development of new primary cancers (Chen et al., 2013, Roukos et al., 2009). Though combination therapies involving two or more categories of the above-described therapeutic options proved to be useful in terms of high response rate and survival rate, resistance to these therapies is still an issue (Davies and Hiscox, 2011). A new avenue for treating breast cancer, is the application of oncolytic viruses which represent an engineered version or are derived from naturally occurring viruses (Holl et al., 2016).

1.3 Cancer Immunotherapy

Cancer immunotherapy is now considered the fifth pillar of cancer therapy and is rapidly advancing to join the level of surgery, radiation, cytotoxic chemotherapy and targeted therapy. The role of the immune system in cancer was first highlighted by Virchow et al over 150 years ago. Virchow found that cancers developed inflammation and this was accompanied with the infiltration of white blood cells. Afterward, many reports showed that tumours regressed in response to acute associated infections including hepatitis, tuberculosis, smallpox, influenza

and gonorrhoea (Balkwill and Mantovani, 2001, Nauts and McLaren, 1990). The potential relationship between cancer and the immune system was embraced by William Coley. Coley's experiments included direct injection of Gram-positive (*Streptococcus pyogenes*) and Gram negative (*Serratia marcescens*) bacteria into tumours or metastatic lesions. Despite some negative indicators such as treatment related deaths and reporting contradiction, Coley's toxins resulted in spontaneous reduction in numerous tumours including lymphoma and sarcoma (Nauts and McLaren, 1990) and this led to development of the Bacillus Calmette–Guérin (BCG) vaccine for bladder cancer (Fuge et al., 2015).

A major challenge for immunotherapy is to make non-responder patients into responders. This will likely require the use of powerful combination immunotherapies that successfully control the cancer immunity cycle, which achieves the balance between the recognition of non-self and the prevention of autoimmunity (Chen and Mellman, 2013). Cancer treatments lead to tumour cell death as well as release of tumour antigens. Dendritic cells then present these antigens in the tumour-draining lymph nodes to control and stimulate tumour immunity. Tumour-specific T cells then infiltrate into the circulation to penetrate the tumour mass. Additional tumour antigens that prolong the cycle are released by T cell-mediated cancer cell lysis. Tumour immunity could be enhanced at each step of this cycle by numerous opportunities for therapeutic intervention (summarised in **Table 1.1**). Understanding the deficiencies of the tumour microenvironment in antigen processing and presentation and the type, quality, number and infiltration of immune cells and the pathways that control them as well as developing novel immunotherapeutic agents and defining synergistic drug combinations are critical for continuing clinical achievement. This will also provide an opportunity to treat patients who do not respond to immunotherapies.

Table 1.1: Active connections between cancer and the immune system.

Process	Opportunities for combination therapy	Immune components involved
Cancer cell death	Chemotherapy Radiation therapy Targeted therapies	Release of tumour antigens
Tumour antigen presentation	Cancer vaccines Interferon- α GM-CSF Anti-CD40 agonist TLR agonist STING agonist	Dendritic cells, APCs
Priming and activation	Anti-CTLA-4 Anti-CD137 agonist Anti-OX40 agonist Anti-CD27 agonist Interleukin-2 Interleukin-12	APCs and T lymphocytes
Trafficking of T cells to tumours	Chemokine modulators	CTLs
Infiltration of T cells into tumours	Bevacizumab Ramucirumab Endothelin B receptor Antagonist	CTLs, endothelial cells
Recognition of cancer cells by T cells	CAR T cells TCR-modified T cells TIL therapy	CTLs, tumour cells
Recognition of cancer cells by NK cells	Anti-PD-1 Anti-PD-L1	NK cells, tumour cells
Tumour cell lysis resulting in antigen release	Anti-PD-1 Anti-PD-L1 IDO inhibitor A2AR antagonists	T cells, NK cells, tumour cells

Abbreviations: APCs, antigen-presenting cells; GM-CSF, granulocyte-macrophage colony stimulating factor; TLR, toll-like receptor; STING, stimulator of interferon genes; CTLs, cytotoxic T lymphocytes; CTLA-4, cytotoxic T lymphocytes antigen-4; NK, natural killer; CAR, chimeric antigen receptor; TCR, T cell receptor; TIL, tumour-infiltrating lymphocyte; NK, natural killer; PD-1, programmed death-1; PD-L1, programmed death ligand-1; IDO, indoleamine dioxygenase; A2AR, adenosine A2A receptor (Emens et al., 2017).

Cancer immunotherapies (CI), such as preventive and therapeutic cancer vaccines (Garland et al., 2007, Kantoff et al., 2010), immune checkpoint inhibitors (Hodi et al., 2010, Robert et al., 2014, Topalian et al., 2014), bi-specific T-cell engagers (Topp et al., 2011), Car T cells and OV's are now accepted as cancer treatments (Andtbacka et al., 2015). These are highlighted in **Figure 1.1**. One of the most advancing fields of CI is antibodies to inhibit immune checkpoint molecules. To date, they have shown spectacular results but only in a subset of malignancies,

including melanoma (Emens et al., 2017). Recently, meta-analysis of a monoclonal antibody (mAb) which targets the immune checkpoint receptor cytotoxic T-lymphocyte-associated antigen-4 (CTLA-4), showed that 20% of metastatic melanoma patients survived 10 years later with no evidence of disease after receiving a single round of treatment (Schadendorf et al., 2015). The survival rate of 10-year was below 10% before this treatment (Luke et al., 2017). Adding a checkpoint inhibitor as a combination therapy such as nivolumab, a monoclonal antibody that targets the PD-1 receptor on T-cells, demonstrates even more potential when used with ipilimumab. This resulted in a 50% response rate in metastatic melanoma (142 patients) (Postow et al., 2015).

Combination therapy with other treatment modalities (“immuno-oncology”) has also revealed success in other types of malignancies and are demonstrating outstanding benefits (Langer et al., 2016, Patel et al., 2017). A previous study demonstrated that combination therapy using stereotactic ablative radiotherapy (SABR) and anti-PD1 antibody induced significant reduction of non-irradiated tumours in preclinical animal models of melanoma and renal cell carcinoma (Park et al., 2015). Recently, prostate cancer patients have been treated with anti-CTLA-4 (Ipilimumab) resulting in an increase in the level of T-cells in tumours and increase expression of PD-1 and VISTA inhibitory checkpoints. Suggesting that mixtures of checkpoint inhibitors targeting CTLA-4, PD-1, and VISTA would appear promising (Gao et al., 2017).

There are also several challenges with cancer immunotherapies particularly checkpoint inhibitors for example immune-associated toxicity, treatment resistance, and clinical advantage restricted to only a portion of patients. A group of toxicities identified as immune-related adverse events, which is a form of autoimmune-like reactions resulting from an increased efficiency of the immune system, are often associated with immunotherapies like immune checkpoint inhibitors. These toxicities can generate symptoms, such as fatigue or fever, or can lead to damage to specific organ that leads to rash, pneumonitis, colitis and adrenal or thyroid insufficiency, among many others (Naidoo et al., 2015, Michot et al., 2018, Picchi et al., 2018). Therefore, these adverse events need to be understood comprehensively so clinicians can avoid, diagnose and suitably treat each specific reaction when using immune checkpoint therapy. Interruption of treatment and a short course of steroids resolve most adverse events. Colitis refractory of steroids and serious pneumonitis may need treatment with biological agents such as infliximab (Champiat et al., 2016, Dine et al., 2017, Linardou and Gogas, 2016, Gupta et al., 2015).

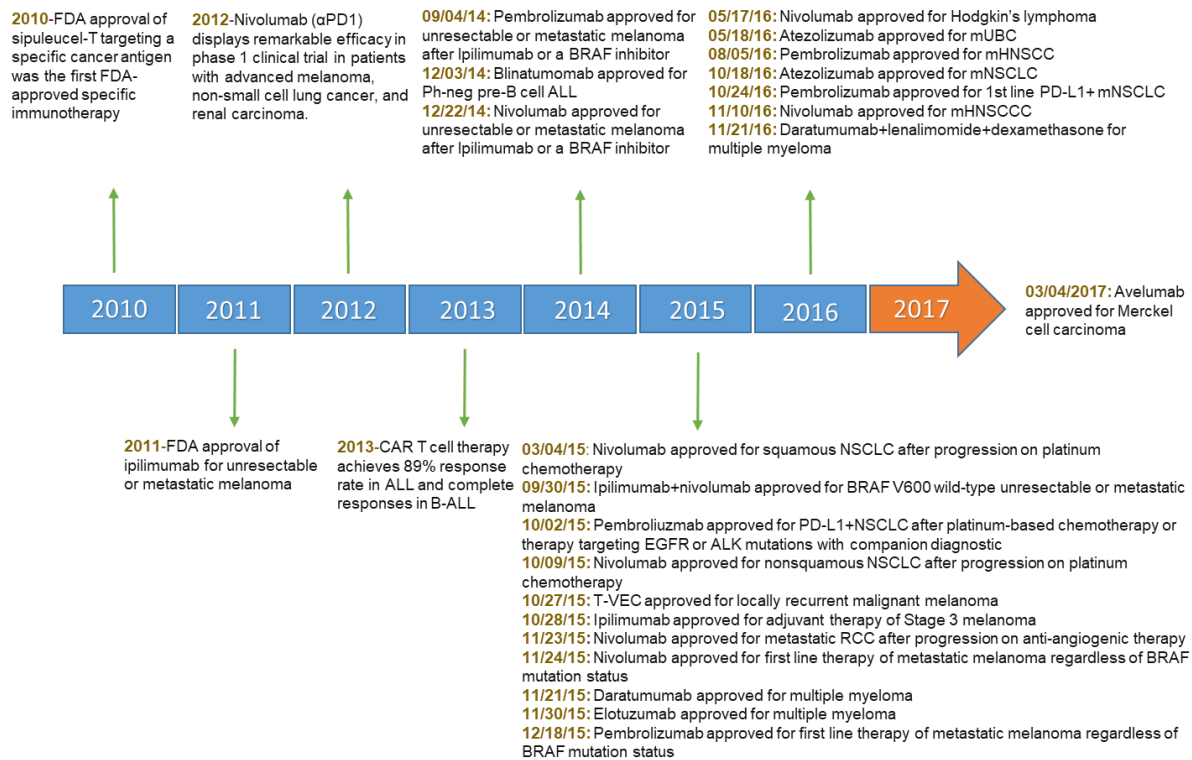


Figure 1.1: The recent advancement and growth of cancer immunotherapy acceptance. A timeline shows regulatory approvals in the United States from 2010.

OVs are becoming increasingly recognised as immune stimulators via an overabundance of tumour antigens emitted by viral-induced destruction of cancer cells (Choi et al., 2016). Clinical trials of other OVs are underway for the treatment of different types of cancer, and some of these trials are combined with other kinds of cancer therapies. The following section will discuss OVs in more detail.

1.4 Oncolytic Virotherapy

Oncolytic virotherapy is an emerging cancer treatment modality that has attracted attention through the last ten years because of its achievements in clinical trials, high cancer specificity, tumour regression and low toxicity. OV are non-pathogenic viruses, which have the aptitude to selectively target and replicate inside tumorous tissues in the absence of producing any damage to healthy tissues (Russell and Peng, 2007). The most important feature of OV is cellular tropism, this decides which tissues are favourably infected, then later, what disease is initiated. For example, hepatitis B virus damages hepatocytes, rabies virus damages neurons, influenza leads to damage of airway epithelium and HIV damages T helper cells. Most naturally arising OVs contain a special tropism for tumour cells and these can be genetically engineered to increase immunity as well as express proteins, that assist in tumour cell death

(Russell et al., 2012). OV's can kill tumour cells using different mechanisms. Death of cells via apoptosis, autophagy or necrosis is not considered to be the sole mechanism for inducing tumour cell death following viral infection. This is because the OV is able to take control of the molecular cell death machinery of the infected tumour cells, enabling cells to die after exploiting available cellular resources for the structure and assembly of new viruses (Russell et al., 2012). Besides destruction of infected cells, OV's are able to kill uninfected tumour cells via indirect techniques for example disrupting the tumour vasculature, inducing antitumor immune responses or via the overexpression of transgene-encoded proteins produced from engineered OV's (Russell et al., 2012).

A whole library of novel OV's have been developed for cancer therapy including parvoviruses, reovirus, Newcastle Disease Virus, Moloney leukaemia virus, mumps virus, these viruses contain a tropism for tumour cells, whilst other viruses for example Vesicular Stomatitis Virus, measles, adenovirus, Herpes Simplex Virus and vaccinia have been engineered or adapted to make them tumour-specific (Patel and Kratzke, 2013). The main advantages and disadvantages of the most common OV's in both preclinical and in clinical trials are described in **Table 1.2**.

Table 1.2: The advantages and disadvantages of current OV's that are being used as cancer treatments in clinical studies.

OV's	Main advantages	Main disadvantages
HSV-1	Multimodal mechanism of action High yields and low viral antigen load Possibility of adding DNA transgenes Broad biodistribution of receptors Does not integrate into the host genome Antiviral agents -acyclovir/ganciclovir	Potential for virus to return to a latent state in the peripheral nervous system (PNS) and therefore not enter lytic replication cycle
Adenovirus	Possible to be produced at high titre Possibility of adding DNA transgenes	Dependent on receptor chimeric antigen receptor (CAR) expression Dependent of loss of tumour protein 53 (TP53) Potential for significant local tissue inflammation /immune Rx
Coxsackie	Naturally preference for tumour cells	Infection depends on the presence of specific receptor molecules
Maraba	High potency Strong anti tumour	Not well studied
Measles virus	Oncolytic	Pathogenic Narrow tropism
Myxoma	Nonpathogenic to humans	Replicates only in cells with activated STAT1
Newcastle disease virus	Nonpathogenic in humans Moderate efficiency No permanent infection in host Oncolytic High potency	Unclear mechanism Not well studied Non-recombinant viruses used Transgene reduces viral replication
Parvovirus	Strongly oncolytic	Small – unable to insert transgenes
Polio virus	Oncolytic	Narrow tropism, Pathogenic, Difficult manipulation
Respiratory enteric orphan virus (Reovirus)	Mild pathogen Unable to infect normal cells Specific oncolytic activity	Previous antigens exist Infects only cells with activated Ras
Vesicular Stomatitis Virus	Relatively non-pathogenic Oncolytic	Difficult to manipulate Requires interferon-resistant cells
Vaccinia virus	High transduction efficiency Systemic dissemination - resistant to clearance Possibility of adding DNA transgenes Long history of human use Antiviral agents – vaccinia Ig or cidofovir	Activated Ras dependent Different forms of the virus may affect Production Immune response /adverse reactions to vaccination (1:50000)

Clinical trials combining OV's with chemotherapy or radiation have been shown to lead to high frequency tumour responses. For example, the combination of oncolytic reovirus alongside paclitaxel were demonstrated in a phase I/II clinical trial in 31 patients with advanced head and neck cancer (Karapanagiotou et al., 2012). The combination of reovirus plus paclitaxel was well tolerated where one patient had a complete response, 6 patients had partial responses, 2 patients had major clinical responses, 9 patients had stable disease, and 8 patient's disease progressed. This has now led to a randomized phase III study. H101 is a genetically modified type 5 adenovirus approved by Chinese regulators in 2005. This virus expresses the viral early gene (E1B) that encodes a protein that is 55-kDa in size (E1B-55KD), this allows E1B to

interact with cellular P53 resulting in cell inactivation but enabling the virus to replicate. Head and neck cancer patients treated with chemotherapy plus intratumoural H101 showed significant improvement compared to chemotherapy alone (Russell et al., 2012). JX594 (Pexa-Vec), is also engineered to express GM-CSF, this is an oncolytic vaccinia virus. In a study by Park and colleagues, patients with non-resectable hepatocellular carcinoma were given intratumoural injections of this virus in a phase I clinical trial. The virus was shown to have limited toxicity and in relation to the Response Evaluation Criteria in Solid Tumours (RECIST), 3 patients had limited response, 6 had constant disease, and 1 had developed disease (Park et al., 2008). This has since developed into a phase II trial where high- or low- dose JX-594 was infused into liver tumours of 30 patients on days one, fifteen and twenty-nine of treatment. Injection caused demonstrable viral replication and GM-CSF expression. However, patient survival was remarkably dependent on dosage, with high doses of virus significantly prolonging patient survival compared to low doses (Heo et al., 2013a). Furthermore, in a phase 3 clinical trial, patients squamous cell carcinoma of the head and neck (SCCHN) and squamous cell carcinoma of the oesophagus (SCCE), were treated using Cisplatin plus 5-fluorouracil (PF) or PF with adenovirus H101. An overall 39.6% response rate was observed, however when PF was given with adenovirus H101 a remarkably greater response of 78.8% was observed (Goldufsky et al., 2013).

Many OV's are currently being used in Phase I/II clinical trials worldwide. However, for OV's to be more accepted as off the shelf anticancer agents, issues such as efficacy and safety should be open to pharmacological study in humans. Of all current OV's that are being studied, the first one that has become an approved and licensed as a cancer therapeutic in the Europe and US is the oncolytic herpes simplex viruses (HSV). The FDA approved Herpes simplex-1 virus (HSV- 1) or Talimogene Laherparepvec (T-VEC) in 2015. This has been modified to express GM-CSF an activator of immune cell proliferation and is injected directly into parts of a melanoma that a surgeon cannot eliminate (Hughes et al., 2014). **Table 1.3** describes the features of HSV that have led to clinical success. HSV1716 will be the OV used in this PhD project and therefore will be discussed further.

Table 1.3: Features of HSV that has made this virus clinically relevant.

FEATURE	ADVANTAGE	REFERENCES
Replicates only within tumour cells to generate multiple doses	Infection results in cytolysis of tumour cells and propagation beyond the cancer cells infected initially. Self-limiting –the virus only replicates within cancer cells leaving normal cells unaffected .	(Sanchala et al., 2017)
Emerging evidence of safety and synergy with other anti-cancer treatments	OV may work synergistically with other forms of anti-cancer treatments.	(Sanchala et al., 2017)
Unique lytic mechanism of action	Decreases risk of resistance developing to oHSV therapy and of cross resistance to other cancer therapies.	(Sanchala et al., 2017)
Immunogenic cell death and tumour specific infection promotes antitumour immune response	Lysis is an immunogenic form of cell death (ICD). This ICD stimulates an immune response to both virus and tumour. OVs are therefore important cancer immunotherapeutics.	(Bardett et al., 2013)
Can be armed to enhance tumour specific immunological reactions	OVs can be engineered to carry therapeutic or immuno-stimulatory genes. For example, by arming viruses with immunomodulatory genes such as IL12, IL2, soluble B7.1- Ig or Granulocyte Macrophage Colony-Stimulating Factor (GM-CSF) to help promote the antitumor immune response the modified viruses are more efficacious.	(Toda et al., 1998, Varghese et al., 2006, Parker et al., 2005) (Carew et al., 2001) (Todo et al., 2001) (Hu et al., 2006, Malhotra et al., 2007, Kaufman and Bines, 2010, Kaufman et al., 2010)
Replication/lysis of cancer stem cells	OVs have been shown to replicate within and destroy cancer stem cells	(Li et al., 2012)
Can be engineered to express additional transgenes that enhance tumour cell killing	Virus directed enzyme prodrug therapy (VDEPT) systems have also been utilised with oncolytic HSV. For example, HSV 1γCD – a modified HSV coding for the yeast cytosine deaminase (CD) enzyme, which converts the non toxic 5-fluorocytosine (5-FC) into 5-FU, a highly toxic chemotherapeutic agent. rRp450 ,carrying rat cytochrome P450 (CYP2B1) which converts cyclophosphamide (CPA) into the alkylating toxin phosphoramidate mustard(PM) Nitroreductase (NTR) which converts the prodrug CB1954 to an active alkylating agent. oHSV have also been armed to increase a cells sensitivity to radiation therapy.	(Nakamura et al., 2001) (Chase et al., 1998) (Braidwood et al., 2009). (Sorensen et al., 2012)

1.5 Clinical trials and development of oncolytic HSV

The clinical activities of oncolytic HSV has significantly accelerated. For example, the engineered HSV (T-VEC) expressing granulocyte-macrophage colony-stimulating factor (GM-CSF) has been administered intratumorally to 50 patients with metastatic malignant melanoma (Eissa et al., 2018). This is thought to lead to direct tumour oncolysis and GM-CSF expression should stimulate closure of the tumour vasculature and induce anti-tumoural immunity as mentioned above. The study showed that the OV was tolerated well with

promising efficacy and improved patient survival compared to GMCSF alone. Despite these promising results, response rates were not evident in patients with visceral metastatic disease (Senzer et al., 2009). In another study, 93% of patients with SCCHN had complete remission when administered directly into the tumour with T-VEC strain when combined with radiotherapy and cisplatin (Russell et al., 2012). The main HSV currently in clinical progress are listed in **Table 1.4**.

Table 1.4: The oncolytic HSV's in clinical trials. References are given where possible but in numerous cases there is no published data so the clinical trial identifier (from clinicaltrials.gov) is given.

HSV strain	Genetic Modification	Indication	Phase	Status	Result	References/ Clinicaltrial.gov
OncoVex GM-CSF (T-Vec) IMMLYGIC	Deletion in both copies of ICP34.5 + ICP47 Disruption US11 expressed as an immediate early gene Encodes GMCSF	Solid Tumours SCCHN Melanoma Melanoma	I I/II II III	Approved and licenced for the treatment of melanoma. Current trials ongoing in melanoma in combination with Keytruda	Evidence of virus replication in injected and adjacent uninjected tumours (head and neck). Regression of injected and uninjected tumors in late stage melanoma	NCT02658812 NCT02819843 (Liu et al., 2003), (Hu et al., 2006) (Harrington et al., 2010) (Sheridan, 2013, Andtbacka et al., 2015)
R7020 (NV1020)	Deletion of 1 copy of ICP34.5 + tk under ICP4 promoter control + deletion in UL24, 55 and 56.	Colorectal cancer liver metastases	I II	Completed	In phase II disease, stabilisation in 40-45% cases	(Kemeny et al., 2006) (Kelly et al., 2008) (Geevarghese et al., 2010) (Sze et al., 2012)
G207	Deletion in both copies of ICP34.5 + disruption of UL39	Recurrent brain cancer glioma, astrocytoma glioblastomas Recurrent brain tumours	I/II	Completed Ongoing	Well tolerated. Evidence of viral replication, radiographic and neuropathological signs of anti tumour activity	(Yazaki et al., 1995) (Mineta et al., 1995) (Hunter et al., 1999) (Todo et al., 2000), (Markert et al., 2000) (Markert et al., 2009) (Aghi and Chiocca, 2009) NCT02457845

G47Δ	Third generation HSV, ICP47 null	Glioma	I/II	ongoing		(Todo, 2012)
M032	Deletion in both copies of ICP34.5, expresses IL-12	Glioma	I	Ongoing	Safe in preclinical models	NCT02062827 (Roth et al., 2014)
HSV1716	Deletion in both copies of ICP34.5	Glioma Melanoma HNSCC Non-CNS solid tumours Malignant pleural mesothelioma	I I/II a	Ongoing Ongoing	No toxicity. In phase I/II (recurrent glioblastomas) 3 of 12 patients showed disease stabilization. No toxicity in melanoma or HNSCC	NCT01721018 NCT00931931 (Harrow et al., 2004, Papanastasiou et al., 2002, Rampling et al., 2000, McKie et al., 1996), (Mace et al., 2007)
HF10	Spontaneous generation of HSV-1 variant	Pancreatic cancer Recurrent breast cancer Bladder cancer HNSCC	I	Ongoing in solid tumours. Active in melanoma Complete HNSCC	No adverse events and possible therapeutic potential	NCT02428036 NCT02272855 NCT01017185 (Nakao et al., 2011)
rQNestin-34.5	Expresses ICP34.5 under a synthetic Nestin promoter	Malignant Glioma	I	Ongoing		(Ning and Wakimoto., 2014)

Abbreviations: HNSCC, Head and neck squamous cell carcinoma; SCCHN, Squamous cell carcinoma of the head and neck; GM-CSF, Granulocyte-macrophage colony-stimulating factor.

1.6 The mechanism of action of HSV on tumour cells

HSV-1 has been genetically engineered for virotherapy and considered the most common herpes virus. There are a number of HSVs currently used in the cancer setting including T-Vec, G207, G47Δ, HSV1716, is a selectively duplicating oncolytic HSV type I virus, it replicates in actively dividing cells however not in terminally differentiated cells. It has double stranded DNA and causes the common cold sore and genital warts. It has about 80 known genes that have been sequenced and encoded within their whole genome. It can be genetically engineered to have beneficial transgenes which can induce immune mediated killing of tumour cells (Kaur

et al., 2012a). *In vivo* and *in vitro* experiments have presented data where this virus replicates in actively dividing cells in diverse tumour cell types such as mesothelioma, melanoma, glioma, non-small cell lung carcinoma, medulloblastoma, and human embryonal carcinoma, reviewed in (Mace et al., 2008).

Both copies of the RL1 gene that translate the neurovirulent ICP-34.5 protein have been deleted from HSV1716. ICP-34.5 allows the virus to kill normal cells. So, deleting such a gene ensures that the virus is no longer able to replicate in normal tissues (Benencia et al., 2008).

HSV1716 is tumour specific due to the fact that tumour cells have reduced expression of protein kinase R (PKR) compared to healthy cells. When a healthy cell becomes infected with this virus, PKR dimerizes and undergoes phosphorylation leading to phosphorylation of the α -subunit of the Eukaryotic Initiation Factor 2 (transcription factor eIF2). This prevents more protein production from arising inside the cells, stopping the virus from replicating as shown in **Figure 1.2**. However, due to the oncogenic stimulation of the mitogen-activated protein kinase (MAPK) signalling pathway, PKR is down regulated in cancer tissues, enabling uninhibited virus replication (Kaur et al., 2012b).

The efficiency and safety of HSV1716 has nowadays been assessed and defined in many progressive tumours for example squamous cell carcinoma of the skin (see **Table 1-4**). A novel phase I/IIa study of HSV1716 therapy for Malignant Pleural Mesothelioma (MPM) opened in Sheffield in November 2012 (NCT01721018). This trial established an acceptable safety profile of intra-pleural HSV1716 with evidence of viral replication and anti-tumour immunogenicity in 12 patients (Danson et al., 2017). This supports further studies in mesothelioma, possibly involving combination with immune checkpoint inhibitors. The following sections will discuss the mechanisms of HSV infection, cell mediated killing mechanisms and the antitumour response.

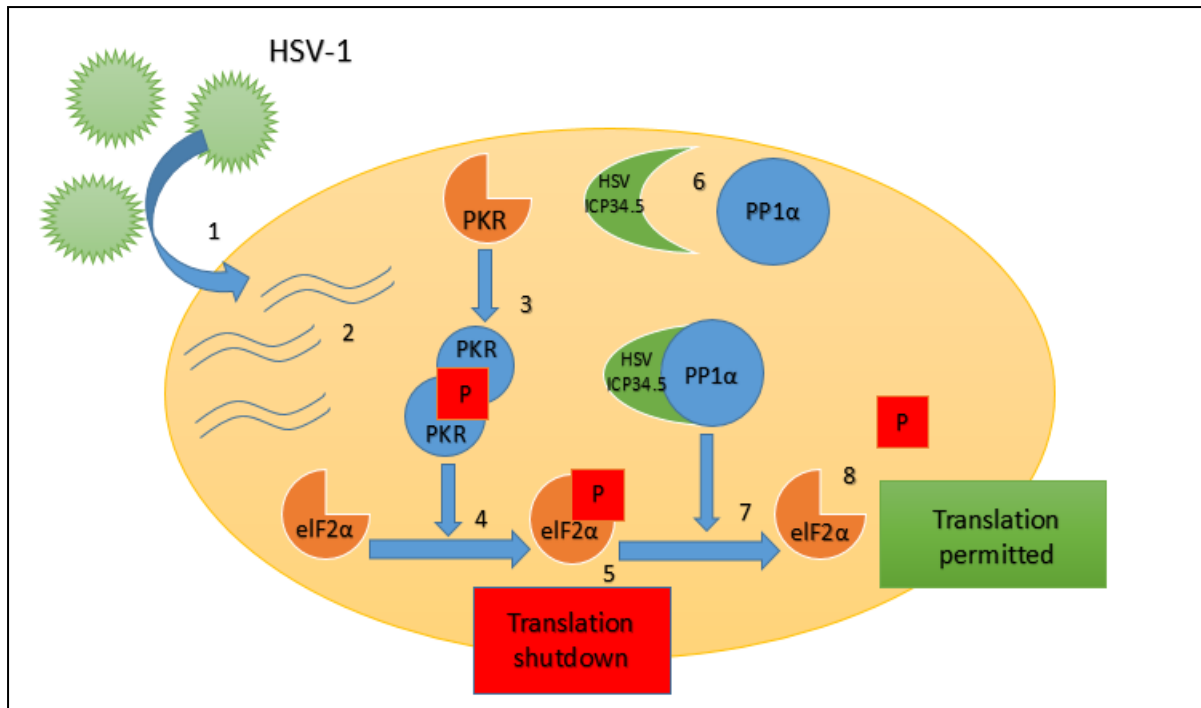


Figure 1.2: HSV-1 mechanism of action in healthy cells.

1. HSV1716 gets in the host cell and starts replication. 2. dsRNA produced by annealing of Complementary RNA. 3. PKR linked to dsRNA, dimerizes resulting in activation and auto phosphorylation. 4. eIF2 α phosphorylated by Phosphorylated PKR. 5. The stopping translation of host cell caused by Phosphorylated eIF2 α and thus prevents viral replication. 6. HSV presented ICP34.5 that creates a protein complex with PP1 α . 7. eIF2 α dephosphorylated by ICP34.5 PP1 α complex resulting in viral replication 8. Replication can continue unimpeded.

Abbreviations: HSV, herpes simplex virus; PKR, protein kinase R; P, phosphorylation; PP1 α , protein phosphatase 1 alpha; eIF2 α , eukaryotic initiation factor 2; ICP, infected cell polypeptide.

1.7 HSV infection and host cell defence mechanisms against infection

1.7.1 Virion and genome of HSV-1.

It is known that HSV1716 is a deletion mutant of HSV-1 which is a human neurotropic virus. The morphological structure of this HSV-1 virion, is distinguished by a core dsDNA genome surrounded by a central icosahedral capsid, which is further surrounded by the tegument. In turn, this tegument is enclosed by the envelope, which is a protein-containing lipid bilayer. The tegument is a substance formed of different viral proteins (Kelly et al., 2009) whereas the envelop mainly contains lipids obtained from the membrane of the host cell, into which are inserted HSV glycoproteins. Most of viral functions such as HSV-1 entry into the cell, cell fusion, cell-to-cell spread and immune evasion is arranged by membrane glycoproteins (Carmichael et al., 2018).

The HSV-1 genome is 152 kb long as illustrated in **Figure 1.3A**. It is a linear two-fold stranded DNA containing two unique regions, long and short (called UL and US). Internal repeats (IRL

& IRS) are linked to these regions in either orientation. Further, terminal repeats (TRL and TRS) are located at the non-linker end of the unique regions. Within L or S regions are a large portion of the known genes named according to their location. The immediate – early (IE), early (E) genes or late (L) genes as described in **Figure 1.3** are considered the main class of HSV-1 genes.

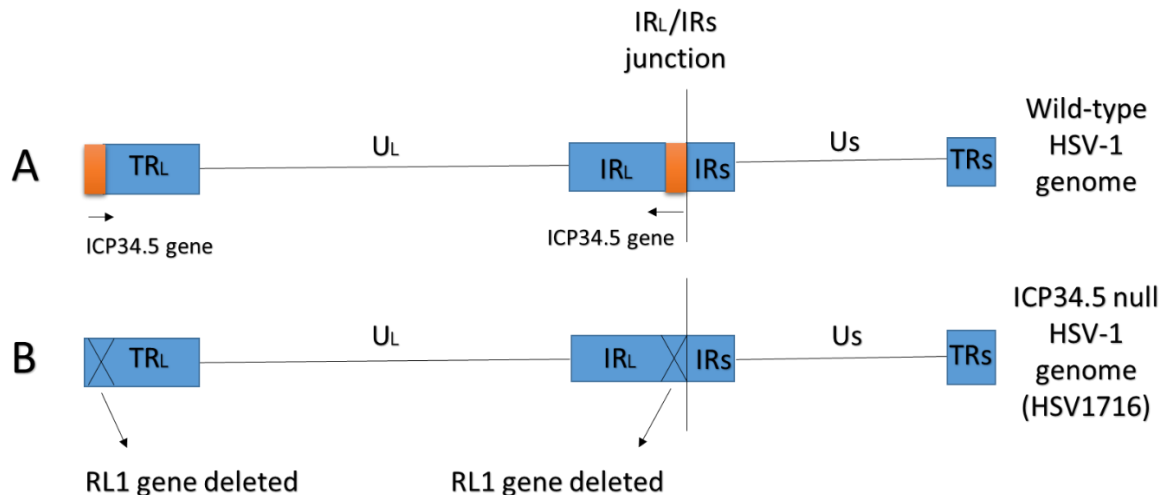


Figure 1.3: A. Genome of wild type HSV 1. B. shows the deletion in HSV1716. Both copies of the RL1 gene that translate the neurovirulent ICP-34.5 protein have been deleted from HSV1716. ICP-34.5 allows the virus to kills normal cells. Therefore, deleting such a gene ensures that the virus is no longer able replicate in normal tissues.

1.7.2 HSV viral entry into host cells

HSV1716 utilizes indistinguishable cell receptors from wild type HSV-1 to infect cells. Associations of a few viral glycoproteins, specifically gB, gD and the heterodimer including gH and gL is included with entry of HSV-1 into the host cell (Campadelli-Fiume et al., 2007). Receptors on the surface of the host cell connect with these glycoproteins that are located on the surface of the enveloped virus.

Interaction between viral gB and cellular heparan sulphate is considered the earliest contact (Shukla and Spear, 2001). Then, the cellular receptors for HSV-1 entry, which incorporate HSV entry mediator (HVEM), nectin-1 and 3-O-sulphated heparin sulphates, interact specifically with gD. The coordinated effectiveness of gB and gH/gL are required for membrane fusion, thus the nucleocapsid obtains access to the cell and infection begins. The primary access for infection of central and peripheral nerve cells is Nectin-1, while HVEM expression is more confined to cells of lymphoid origin (Simpson et al., 2005). HSV-1 entry mediators have an extensive bioavailability and a wide range of human tumour cell types are

permissive to HSV1716 infection (Karasneh and Shukla, 2011). Fusion of the virus envelope with the plasma membrane lets the virus penetrate the cell resulting in viral nucleocapsid being inserted into the cytoplasm of the cell. Then, the genome discharges into the nucleus by binding of the capsid to the nuclear pore to initiate the transcription, replication of viral DNA and progeny nuclear capsid assembly.

1.7.3 HSV replication

HSV-1 gene expression takes place through a very controlled cascade starting with the generation of the immediate early (IE) proteins. The α regulatory proteins, ICP 0, 4, 22, and 27 manage the expression of all classes of viral genes. The proteins that are primarily associated with synthesis of viral DNA, are the β or early (E) gene products for example the viral thymidine kinase (TK)(Roizman, 1996). The γ or late (L) proteins for example the VP16, gD and gC are considered the last batch of viral proteins produced and are the proteins mainly involved in virion structure and assembly (Batterson and Roizman, 1983, Fenwick and Walker, 1978, Read et al., 1993).

The γ or late (L) gene class is additionally divided into the $\gamma 1$ and $\gamma 2$ sets, where $\gamma 2$ expression is totally reliant on viral DNA synthesis. The completed cycle of HSV-1 replication results in eventual damage of the cells.

1.7.4 Activation of the MEK pathway is necessary for HSV replication

MEK is a main controlling kinase triggered via mitogen-activated protein kinase (MAPK) kinases (A-RAF, B-RAF, and C-RAF) that functions to promote cell survival (Ballif and Blenis, 2001, von Gise et al., 2001, Xia et al., 1995). Therefore, MEK and its only identified substrate, MAPKs (ERK1 and ERK 2), are triggered in many tumours as a result of tyrosine kinase receptor activation (Hoshino et al., 1999), dysregulated growth factor secretion (Pouyssegur et al., 2002), activating mutations in RAS isoforms, and somatic activating missense mutations of B-RAF (Davies et al., 2002). Activated MEK plays a main role in suppression of PKR resulting in replication of ICP34.5 mutant virus and destruction of tumour cells (Smith et al., 2006).

As mentioned above, cells from different tumour tissue types can be infected equally well by HSV1716, as confirmed via the equal expression of early viral proteins expressed following viral entry (Smith et al., 2006). This suggests that function of variances in overall viral protein synthesis, rather than differential infectivity could be one of the reasons why there is variability in viral production in different tumour cell types. The occurrence of mechanisms in tumour

cells that circumvent the PKR-mediated antiviral response could be important for replication of HSV1716. Many early studies have shown that the difference in capability of numerous human tumour cell lines to HSV1716 infection was reliant on the stimulation status of the endogenous MAPK kinase (MEK) which can prevent the activation of PKR, (Figure 1.4) (Smith et al., 2006).

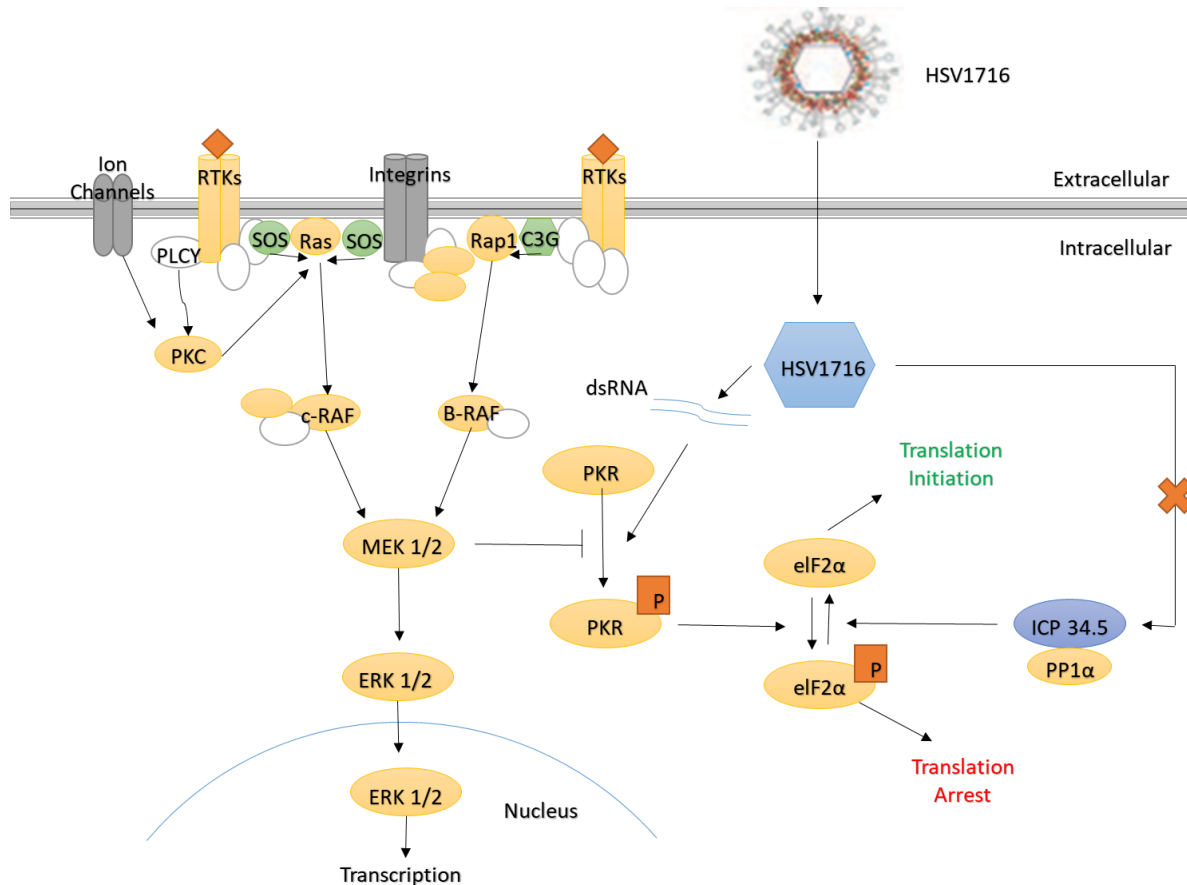


Figure 1.4: The shutdown of host protein synthesis in the presence of HSV1716 infection is blocked by MEK pathway activation in cancer cells. In ICP34.5 (-) mutants, the MEK activated pathway in tumour cell will block PKR activation, and in the absence of ICP34.5 protein, will result in translation initiation and viral replication.

1.7.5 Proliferating cell nuclear antigen (PCNA) is important for HSV replication

Previously, PCNA has been recognised as additional molecular mechanism that participates to the selectivity of HSV for tumour cells. PCNA has been used as a diagnostic and prediction cell-cycle marker because it plays a role in proliferation of cancer cells and cancer transformation (Bologna-Molina et al., 2012). PCNA levels are very high in cycling cells for instance active tumour cells, however levels can normally be much lower than in non-cycling cells. So PCNA could be used as a proliferation cell marker (Bologna-Molina et al., 2012).

Previous studies have shown that HSV neurovirulence factor ICP34.5 forms a complex with

PCNA *in vitro* and *in vivo* via its 63-amino-acid carboxyl domain which is preserved in hamster GADD34, and mouse MyD116 (Brown et al., 1997, Harland et al., 2003). This suggest that both viral and cellular proteins complex *in vitro* and *in vivo* with PCNA and offers solid evidence for the importance and biological relevance of these interactions. Indeed, PCNA is required for HSV replication and recent studies have highlighted that the HSV DNA that enters the cellular nucleus does not have histones (these are responsible for the cellular packaging of DNA into structural units called nucleosomes), but once inside the nucleus histones cover the viral DNA. Using SiRNA knockdown of PCNA and a cytosine arabinoside chemical inhibitor, they demonstrated that PCNA is necessary for histone deposition and in the absence of this process PCNA viral replication was significantly reduced (Sanders et al., 2015).

One of the components of oncolytic specificity that could define its efficiency is tumour expression of PCNA. The in-situ PCNA profiles have been studied in histological sections of tumour biopsies that were gained from patients experiencing craniotomy (Detta et al., 2003). They found that PCNA expression was positive in 10 metastatic tumour biopsies (3 melanoma, 4 carcinoma and 3 adenocarcinoma) via IHC and reinforced the replication of HSV1716. HSV1716 replicated effectively in tumour cells, where PCNA was previously involved in DNA replication, even in the absence of ICP34.5. In spite of this, the association between the PCNA levels and reactivity to HSV1716 in a large group needs to be confirmed.

1.7.6 Cell death pathways and HSV

1.7.6.1 Autophagy

Autophagy acts as a primary cellular conservation mechanism that includes the lysosomal degradation of unnecessary or dysfunctional proteins and organelles. The process of autophagy provides essential cellular energy that ensures cellular survival during starvation. Autophagy proteins, which targets viral components for degradation of lysosomal, plays an antiviral role, and has a role in activating immune responses against viral infection (Alexander et al., 2007). ICP34.5 interferes with autophagy via binding Beclin-1 during wild-type HSV-1 infection. Beclin-1 acts as an important component of numerous extremely regulated complexes controlling the development and maturation of autophagosomes (Alexander and Leib, 2008). Cancer cells often exhibited disorder in autophagy resulting in increased tumorigenesis. HSV1716 cannot bind Beclin-1 to block autophagy because of the ICP34.5 deletion (**Figure 1.4**). However, HSV-1 has US11, a late gene product of HSV-1, that is identified to obstruct autophagy via its interaction with PKR rather than binding to Beclin-1 itself (Lussignol et al.,

2013).

Indeed, two anti-autophagic proteins are encoded by HSV-1, suggesting autophagy develops a strong anti-viral influence. Nevertheless, HSV-1 can replicate *in vitro* in autophagy deficient cells (Murine embryonic fibroblasts (MEFs)) as good as in wild type cells (Alexander et al., 2007). A further study demonstrated that a HSV-1 mutant that had a mutation in ICP34.5 was neuro-reduced in mice suggesting that the neurovirulence of wild type HSV because of the ICP34.5 protein binding with Beclin-1 is contributing to the inhibition of autophagy by HSV-1 (Orvedahl et al., 2007).

A study carried out by a Masters student (Anna Claudia Lima) at the University of Strathclyde in collaboration with Virttu Biologics looked at autophagy with HSV infection in a number of human tumour cell lines, such as Hep3B, HuH7 (liver cancer) and A2780 (ovarian cancer). The autophagy response to HSV infection in the *in vitro* human cancer cell lines studied was variable and independent of ICP34.5 status (this data was presented as a poster at 8th International Oncolytic Viruses meeting, 2014, Oxford, UK).

1.7.6.2 Apoptosis

Host cell apoptotic pathways are activated by HSV-1 infection as a defence mechanism to suppress the spread and replication of the pathogen. HSV-1 infection induces host cell apoptosis via the first class of viral genes (IE genes) expression (Sanfilippo and Blaho, 2006).

Cytopathic effect (CPE) is referred to the major biochemical changes that is induced by productive HSV-1 replication in infected cells. Apoptosis is also activated by the virus in transformed or tumour cells, but not primary cells. Production of virus ICP27 during an apoptotic-prevention window leads to delay of the apoptotic process from damaging the virally infected cells, which eventually enables the beginning of productive viral replication (Aubert et al., 1999). Viral proteins including the immediate early proteins ICP4, ICP24 and ICP27, which act to control apoptosis during viral infection, have been recognised. Loss of any of these proteins results in viruses that activate apoptosis (Thomson, 2001). Previous studies have demonstrated that deletion of either ICP4 or ICP27 resulted in reduced expression of early and late viral gene products. This suggest that immediate early protein ICP4 or ICP27 have regulatory functions (Samaniego et al., 1997).

Apoptosis can be prevented by other early HSV gene products such as US3 (Leopardi et al., 1997), Glycoprotein D (Zhou and Roizman, 2001), R1 (Langelier et al., 2002) and latency

associated transcripts (LAT) (Nguyen and Blaho, 2009). Single loss of any of these late viral genes do not result in apoptosis to the same extent as the ICP4 or ICP27 deleted viruses. This suggest that the late viral genes have unnecessary roles or are able to inhibit apoptosis during HSV infection.

Herpes Simplex Virus Dependent Apoptosis (HDAP) is a process of death used by cells that infected with recombinant viruses with modifications in the anti-apoptotic viral gene. HDAP was firstly studied with transformed cell lines *in vitro*, then when studies were developed to comprise non transformed lines essential variations were detected (Aubert and Blaho, 2001). Transformed, tumourigenic cells are sensitive to HDAP while primary, non-transformed cells are resistant to HDAP. So far, two HDAP sensitivity regulator proteins have been identified, P53 and telomerase, two known key oncogenes (Nguyen et al., 2007). Therefore, HSV infection increases killing in cancer cells, but not normal cells via HDAP. HDAP is reliant on caspases. A study used specific caspases inhibitors in HEp-2 cells and found that caspase 9 inhibitors were able to suppress HDAP, whereas inhibitors of caspase 8 did not. This suggests that HDAP is dependent on the intrinsic pathway of apoptosis (Aubert et al., 2007).

Possibly, As HSV virus is able to induce apoptosis in cancer cells but not in normal cells, this difference could be exploited in tumour therapy. HSV1716, like wild type HSV-1 is able to keep viral proteins that prevent host cell apoptosis. HSV1716 produces progeny virions, preventing cell apoptosis so that viral replication occurs before the host cell is damaged. On the other hand, HSV1716 infection might still leading to tumour cell death, through HDAP, if the production of the viral proteins that prevent apoptosis was blocked. Thus, combination of HSV1716 with antitumour drugs that prevent viral replication could result in tumour cell death through HDAP.

As HDAP occurs through the intrinsic pathway and relies on caspases, looking for increased levels of specific caspases could help measure this enhanced HDAP. Increased apoptosis could be detected by measuring the levels of caspase 3/7, and the differentiation between intrinsic and extrinsic pathways could be identified by measuring caspase 8 or 9.

1.8 HSV induces immunogenic cell death

OV infected tumour cells promote anti-tumour immunity (Bartlett et al., 2013) and this likely a result of immunogenic cell death (ICD). Understandably, ICD is one of the cell death types that involves the adaptive arm of the immune system. Further, ICD stimulates innate and tumour-specific immune cells and generates an anti-tumour immune response, which is able to

eradicate the uninfected cancer cells in primary and metastatic sites (**Figure 1.5**) (Bartlett et al., 2013). HSV-1 RH2 have been shown to induce DAMPs from squamous cell carcinoma SCC cells to induce cell death. In this study they showed that high mobility group box 1(HMGB1) and ATP were released into the extracellular space, while calreticulin (CRT) translocated to the cell membrane after being infected with (RH2) (Takasu et al., 2016). Coxsackievirus B3 virus have also been shown to induce ICD in human non-small cell lung cancer cells (NSCLC; A549, H1299, and H460), including cell surface CRT and release of ATP as well as HMGB1 (Miyamoto et al., 2012).

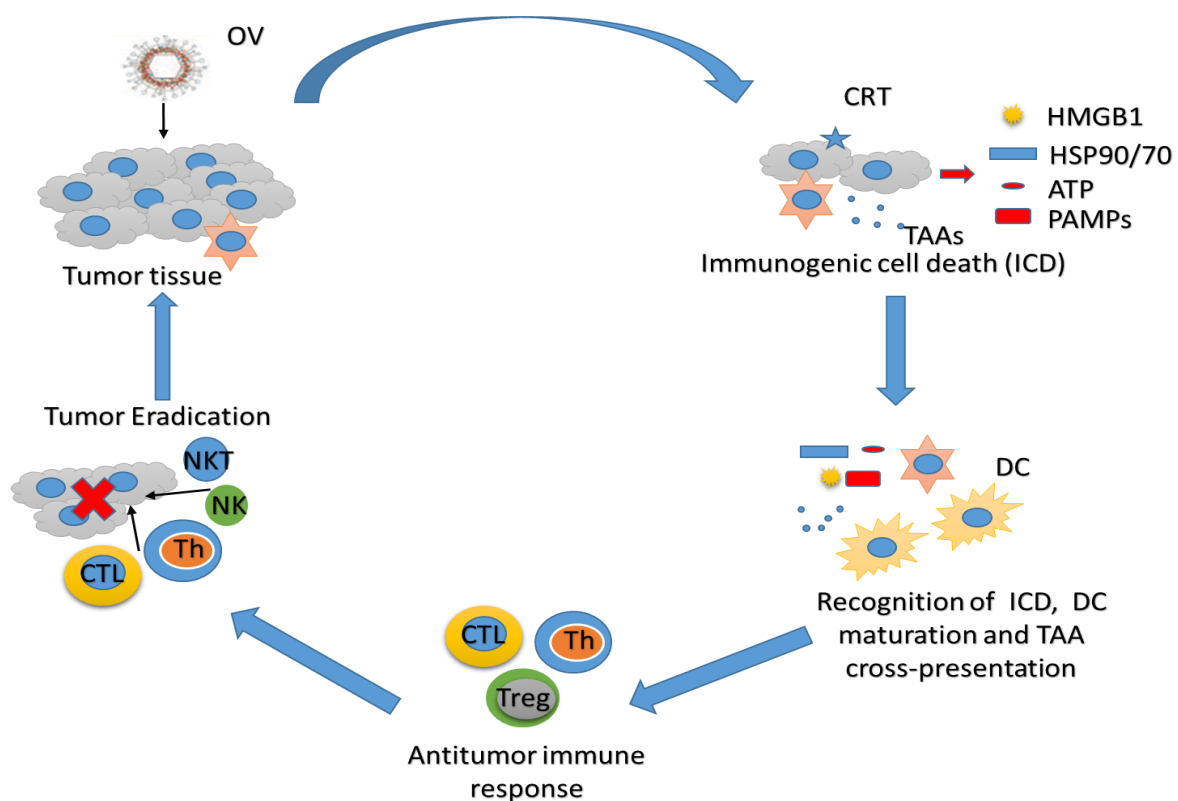


Figure 1.5: OVs induce ICD of cancer cells that leads to antitumor immunity. After delivering the OV into the tumour either intra-tumourally or systemically, replicating OV in tumour and/or stromal cells present eat me signals, DAMPs and PAMPs, on the cell surface and then release danger signals. APC engulfs apoptotic bodies, and TAAs are offered together with MHC complex and co-stimulatory molecules. DCs are activated and matured by released DAMPs (and PAMPs) and TAAs are cross-offered to naïve T-cells. Complete eradication of the tumour mass may be enhanced by causing cytotoxic immune response against the tumour, including CD4 and CD8 T cells. Antitumor immune responses can be helped by other immunotherapies targeting T cells, DCs and the immunosuppressive TME.

The interaction between HSV1716-mediated tumour damage and immune response has been demonstrated in a syngeneic murine intracranial melanoma model (Miller and Fraser, 2000). They found HSV1716 significantly prolonged survival compared with mock-treated mice.

Moreover, they reported complete tumour regression in 60% of the animals treated with HSV1716. There was no change detected between mock and HSV1716 treated groups in the mean survival rates when SCID mice (no adaptive immune system) were used compared to immunocompetent animals. Also, no significant change was found in the mean survival rates of the mock vs. HSV1716 treated mice when leukocytes were depleted using cyclophosphamide in the syngeneic model before and during HSV1716 administration (Miller and Fraser, 2000). Together this suggest that adaptive immune cells are essential for promoting this effect of HSV1716. After viral therapy, infiltration of immune cells into the tumour was also studied. The main early infiltrating cells were macrophages and CD4+ T cells, while polymorphonuclear leukocytes such as NK cells, CD8+ T cells, microglia cells and B cells also infiltrated into the tumour (Miller and Fraser, 2000). NK cells significantly infiltrated on day 7 post therapy, with significant CD4+ T cells infiltration seen on day 12. Staining of HSV-1 antigen was positive in the tumour mass. Treated mice showed downregulation of MHC class I expression 3 days post viral therapy when compared with mock-treated mice. These data are in agreement with prior studies that demonstrate downregulation of MHC class I expression with HSV-1 through ICP47 (Jugovic et al., 1998).

Indeed, various rodent cancer cell lines are unaffected by HSV -1, because the natural hosts for HSV-1 are humans. Transfected mice cell lines and HSV1716 replication-competent cell lines, were used to produce tumours in 4 strains of knockout mice (CD4^{-/-}, CD8^{-/-}, NK^{-/-}, and RAG2^{-/-}) as well as syngeneic C57/BL6 mice. An increase in survival was only shown in immunocompetent C57/BL6 mice when treated with HSV1716. This suggests that the prolongation in survival, which is seen after HSV1716 therapy, was a result of the cells of the immune system (Miller and Fraser, 2003).

A study by Thomas et al., demonstrated that direct tumour injections of HSV1716 was able to inhibit primary tumours growth and improve survival in a 4T1 mouse mammary tumour model. This improvement in survival resulted in reduction in lung metastasis. The establishment of a second challenge of 4T1 tumours also decreased tumour size following HSV1716 therapy. Inflammatory cells, for example neutrophils, were noticed in HSV1716-treated tumours on day 12 post injection of tumour cells. In addition, HSV1716-treated tumours showed an increase in CD4+ and CD8+ T cells compared to the mock-treated tumours. Growth of 4T1 tumours was not reduced after HSV1716 therapy in SCID mice, proposing a function for the T cell infiltrates (Thomas and Fraser, 2003).

In addition, Benencia et al., established the vaccination effect of intra-tumoural injection of HSV1716 in a mouse model of ovarian cancer. They found that tumour growth was reduced significantly by HSV1716, as well as increased mouse survival. Further, mouse ovarian tumour cells displayed a significant increase in expression of gB and gD and were easily phagocytosed by dendritic cells (DCs) after HSV1716 infection. Heparin and anti-HSV gB and gD reduced the improved phagocytosis of tumour-infected cells via DCs. This proposed that collaborations between DCs and tumour apoptotic bodies are improved by viral infection (Benencia et al., 2008).

The type of cell death induced following HSV infection dictates the type of immune response that follows. The induction of antitumour immunity requires ICD that involves the adaptive arm of the immune system. We encourage systemic delivery of HSV into the tumour to induce ICD.

1.9 Systemic delivery of HSV

OV have been modified to increase potency by expressing genes that induce cytotoxicity (Doronin et al., 2000), increase virus replication (Le Boeuf et al., 2013), stimulate killing of bystander cells (Freytag et al., 1998), and improve antitumour immunity (Melcher et al., 2011a). However, these enhancements will not induce effective antitumour responses without successful delivery of virus to the tumour. Traditionally, OV is delivered directly to the tumour by intratumoural injection. However, some of the tumour may contain numerous small nodules spread out over a large area. In addition, direct injection is not always possible for tumours that are not accessible. Systemic delivery is needed for such inaccessible tumours. Furthermore, systemic delivery of some OVs can stimulate antitumour immune responses greater than direct intratumoural injection. For example, Bridle et al showed that a single intravenous dose of Vesicular stomatitis virus expressing human dopachrome tautomerase (VSV-hDCT) into mice bearing intracranial B16 tumours resulted in the induction of antitumour immunity (Bridle et al., 2010).

Although, there are numerous advantages for efficient systemic delivery of HSV, there are several barriers that need to be overcome (**Figure 1.6**). In circulation, the virus can encounter numerous factors that prevent its delivery to the tumour and the host immune system is unable to distinguish between a therapeutic HSV and a pathogenic virus. Therefore, intravenous HSV can encounter circulating factors such as antibodies. These antibodies neutralise virus directly by specific binding, or mark them for destruction via complement and several immune cells

(Ferguson et al., 2012). This is particularly pertinent to viruses that the body has already encountered. Serum proteins as well as circulating cells in the bloodstream also neutralise HSV by nonspecific binding (Ferguson et al., 2012). Virus is also cleared from the bloodstream by organ sequestration, such as the liver, spleen and lung. As these tissues comprise macrophages that filtrate the blood from circulating pathogens (Fisher, 2006). Adaptive immunity produces an extra obstacle to intravenous delivery of HSV. As it capable of growing a significantly more potent and specific immune response to the virus compared with its innate counterpart. Definitely, many of the OV's including vaccinia virus (Heo et al., 2013b), reovirus (White et al., 2008), measles virus (Galanis et al., 2010) and HSV (White et al., 2012) have infected most of the human population resulting in developing immunologic memory to these viruses. Previous preclinical (Power et al., 2007, Ilett et al., 2009, Iankov et al., 2007) and clinical (White et al., 2008, Adair et al., 2012) studies have shown that the amount of infectious virus that can be delivered to the tumour is significantly reduced by neutralising antibodies. Delivery of OV into the tumour bed can also be affected by physical barriers for example tumour extracellular matrix and high interstitial fluid pressure within the tumour resulting in restricted extravasation of OV's into the tumour (Wojton and Kaur, 2010). Although, there are many barriers to systemic delivery of OV's, previous clinical trials have suggested that OV can be delivered into the tumour intravenously by using high doses of virus that perhaps saturate the neutralising mechanisms that exist within the human body (Breitbach et al., 2011a, Adair et al., 2012). In spite of this revolutionary success in the field, there is still space for progress particularly with respect to systemic delivery.

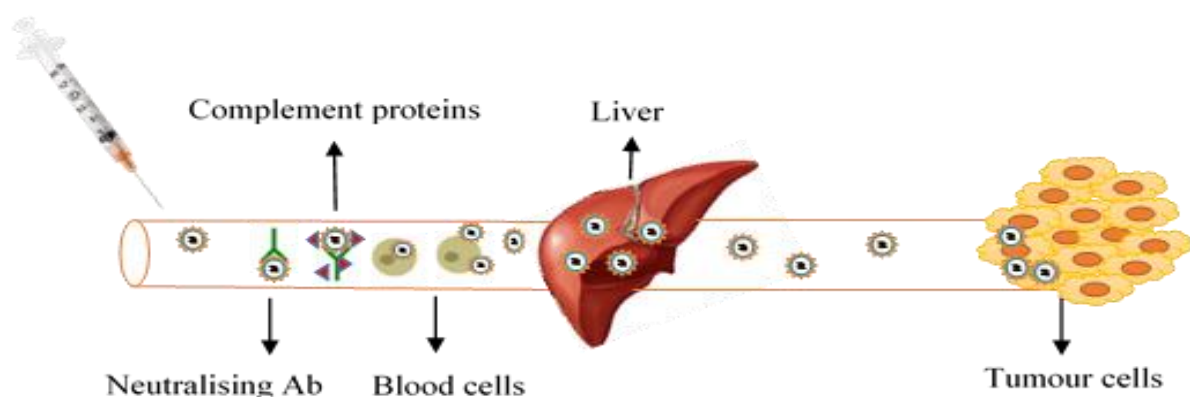


Figure 1.6: Virus neutralisation during systemic delivery. Firstly, virus are neutralised by binding with circulating antibodies in the blood stream and complement proteins resulting in marking them for destruction by immune effector cells. Interaction of the OV with circulating blood cells could result in virus sequestration. Furthermore, the reticulo-endothelial system such as the liver are able to filter viruses from the blood. The tumour extracellular matrix and high interstitial fluid pressure are also able to limit the extravasation of virus into the tumour.

However, as mentioned earlier the most common threat to OV treatments such as HSV1716 is neutralising antibodies from prior encounters with such a common virus. As a result, strategies have been planned to beat this, such as the usage of cell-carriers. There has been considerable interest into the advantages of using live cells to carry OV to tumours at the same time as avoiding antiviral immunity recently (Power and Bell, 2008). The ability of cells to migrate into tissues naturally has led them to be appropriate cell delivery targets for OVs. This has been demonstrated for immune cells for example macrophages and dendritic cells. Jennings et al., demonstrated that overcoming antibody neutralisation can be achieved by inserting reovirus onto either immature dendritic cells (iDC) or Lymphokine-activated killer and dendritic cell LAKDC and reovirus-loaded LAKDC, these were ideal vectors for delivering reovirus to ovarian cancer *in vitro* and stimulated innate and adaptive immunity (Jennings et al., 2014). Macrophages in particular have the advantage in that they home to highly inaccessible hypoxic areas of tumours (Muthana et al., 2011a). Researchers in Sheffield have exploited this for the delivery of adenovirus protected by macrophages in preclinical mouse models of prostate cancer (Muthana et al., 2011a). The same group also demonstrated that viral delivery by macrophages significantly increased the trafficking of macrophages to prostate tumours in mice following chemotherapy and radiotherapy (Muthana et al., 2013). Cell delivery is an attractive approach but clinical studies have demonstrated natural cell trafficking has not been simple. Numerous cell types have been used, such as T cells (Morgan et al., 2006), macrophages (Griffiths et al., 2000) and stem cells (Studený et al., 2004). Most of these types of cells have been located in tumours (albeit in small numbers) following administration but they were also found to enter other organs and tissues and this not only weakens the treatment but also increases the risk of toxicity in other parts of the body if they transfer therapeutic cargo such as viruses.

In a recent paper by Muthana et al., tiny MNPs (Super Paramagnetic Iron Oxide:SPIO) were inserted into cells (monocytes/macrophages) and injected intravenously into tumour bearing mice and subsequently directed into the prostate tumours implanted under the flanks of mice using an external magnetic field. Using this approach, they showed a 3-fold increase in cell delivery (Muthana et al., 2008b). This approach has also been used for delivering anti-cancer drugs, antibodies and for inducing magnetic hyperthermia (Tran and Webster, 2010). Furthermore, Muthana et al., demonstrated that prostate tumour-bearing mice that received HSV1716-carrying macrophages (also loaded with MNPs), which were directed into primary and metastatic tumour sites using magnetic resonance targeting with an MRI scanner, showed marked reduction of the primary tumour than those that received naked HSV1716 (Muthana

et al., 2015b). We propose to use a similar magnetic guidance strategy for delivery and targeting of HSV1716 to tumours but without the need for cells. In order to do this, we must consider how to magnetise our OV and which magnetic nanoparticles (MNPs) are the most suitable. Below is a review of the types of MNPs used in biomedical research and their application.

1.10 Magnetic nanoparticles (MNPs)

Magnetic nanoparticles (MNPs) have been exploited in biomedical applications including hyperthermia, targeted drug delivery and gene delivery. The most vital properties of MNPs in all biomedical applications are biocompatibility, tunable nanomagnetism, low toxicity and exact localization at the biological target. Fe_3O_4 MNPs have been most commonly used in bio-applications because of their unique features, such as strong magnetic susceptibility and superior biocompatibility, one of these bio-applications is gene delivery (Zhou et al., 2014). Moreover, It is well known that Fe_3O_4 MNPs have a big surface area-to-volume ratio, so this kind of MNP tend to conglomerate resulting in low colloidal constancy in physiological circumstances (Dias et al., 2011). There are some major challenges with respect to the use of MNPs in cancer therapy that still need to be addressed. For example, how to increase the uptake of Fe_3O_4 MNPs in tumour cells whilst decreasing accidental side effects to normal cells. Moreover, how to keep the MNPs from clearance by the reticuloendothelial system (RES) so as to increase blood circulation time and ensure they reach their target tissue still needs to be addressed (Sun et al., 2010a, Xie et al., 2007).

Since the 1970s, interest in MNPs for drug delivery systems has been recognised. The use of magnetic fields to guide the MNP-drug conjugates to a specific site because of their ferromagnetism is very attractive. In the last few years, MNPs loaded with anticancer drugs (e.g. carboplatin, doxorubicin, paclitaxel, 5-fluorouracil, epirubicin, etc.) were guided by an external magnetic field to tumour sites. Chao et al. established that growing tumours could be shrunk significantly in mice with hepatocellular carcinomas using doxorubicin-coupled MNPs and external magnetic devices to achieve local enhancement (Chao et al., 2012a).

1.10.1 Iron oxide particles

The most widely used application of iron oxide in the clinic is as MRI contrast agents and because of the extensive scattering of Fe^{3+} in the human body and low toxicity these particles can be exploited for clinical use (McBain et al., 2008, Buyukhatipoglu and Clyne, 2011).

Understanding the structure and property relationship of iron oxide MNPs have led scientists to harness their properties, tailoring and tuning the desired structure, shape and size of the

MNPs (Dadfar et al., 2019). US Food and Drug administration (FDA) have accepted iron oxide MNPs in biomedicine because of their numerous advantages. Certainly, an advantage of iron oxide MNPs is that they are simple to manufacture, non-toxic, biocompatible and can be super paramagnetic. α -Fe₂O₃ (maghemite) and Fe₃O₄ (magnetite) are considered the two major structures of iron oxide particles in medicine to date (Hervault and Thanh, 2014).

1.10.2 Coated iron oxide MNPs

In biomedical applications MNPs are often covered with natural polymers (proteins and carbohydrates), artificial organic polymers (polyethylene glycol), polyvinyl alcohol, poly-L-lactic acid), silica and gold (Kami et al., 2011). Using these compounds can improve chemical and physical stability of the MNPs and their toxicity is reduced (Selvan et al., 2005, Sotiriou et al., 2011). TransMAGPEI iron oxide MNPs stabilised with polyethylenimine (PEI) were the first MNPs used for gene delivery (Mykhaylyk et al., 2012). PEI is a popular choice of coating as this improves cationic gene transport with high effectiveness of transfection in the lungs of mice (Thomas et al., 2005). However, it is highly toxic to cells. The authors found that modifying the PEI to remove the N-acyl groups decreased cytotoxicity and improved its plasmid DNA transfer effectiveness 21 times *in vitro*, in addition to 10,000 times in mice. They also showed that siRNA delivered with PEI coated MNPs missing N-acyl groups inhibited 94% influenza virus infection in the lungs of mice (Thomas et al., 2005). In a study by Sanchez and colleagues, a new nanomagnetic approach for gene delivery and cell separation. They used gene vectors associated with MNPs (PEI-modified silica-iron oxide) to transfect target cells such as hematopoietic stem cells (human and mouse) and human mesenchymal cells when being passaged and isolated using a magnetic field cell separation column. Superior target cell purity and retrieval was yielded using this method (Sanchez-Antequera et al., 2011).

The adjustment of the MNP surface has also been demonstrated with chitosan (CS) because of excellent features such as low immunogenicity, amphiphilicity and biodegradability (Park et al., 2010, Amidi et al., 2010, Rinaudo, 2006). For instance, the core shell nanocomposites decorated by simple coacervation methodology with CS improves the intravenous transfer of the anticancer agent gemcitabine to cancer tissue in a murine tumour model (Arias et al., 2012).

MNPs are very quickly cleared via the reticuloendothelial system (RES) once injected into circulation and this limits their circulation time. Coating the MNPs with polyethylene glycol PEG has been revealed to remarkably increase blood circulation enabling the MNPs to reach their target. PEGylation provides stability, biocompatibility and hydrophobicity (Liu et al.,

2012, Shah et al., 2012). Lui et al, synthesised PEGylated MNPs and found they showed great impedance to phagocytosis by macrophages *in vitro* in addition to minimum uptake via the liver and spleen in mice with tumours. This improved tumour imaging by MRI and required only low doses of MNPs. These properties are basically a result of the considerable protecting effect of the PEG coating and their stability in physiological circumstances (Liu et al., 2011a). The most strong points of MNPs are biocompatibility, tunable nanomagnetism, low toxicity and exact localization at the biological target. Therefore, Many MNPs have been used in preclinical models of cancer using the coatings described above as well as other coatings, these are summarised in **Table 1.5**

Table 1.5: Types of MNPs in preclinical mouse studies of cancer therapy.

MNPs	Drug	Tumour	Reference
Iron oxide nanoparticles with starch coating	Mitoxantrone	Squamous cell carcinoma VX-2 (rabbit) subcutaneous (hind limb)	(Alexiou et al., 2000)
Iron oxide nanoparticles with either citrate or PEG coating	Hyperthermia (alternating magnetic field)	Breast cancer cell line MDA-MB-231 (human)	(Alphandéry et al., 2011)
Iron oxide nanoparticles (Fe ₃ O ₄)	Hyperthermia (alternating magnetic field)	Melanoma cell line B16-F10 (mouse) subcutaneous (rear limb above stifle)	Balivada et al., 2010a)
Iron oxide nanoparticles (Fe ₂ O ₃ , Fe ₃ O ₄)	Hyperthermia (alternating magnetic field)	Squamous cell carcinoma VX-2 (rabbit) kidney	(Bruners et al., 2010)
Iron oxide nanoparticles (Fe ₃ O ₄ /gold)	Doxorubicin	Hepatoma cell line H22 (mouse) subcutaneous (right flank)	Chao et al., 2012)
Iron oxide nanoparticles with dextran coating and ¹¹¹ In-marked L6 monoclonal antibody	Hyperthermia (alternating magnetic field)	Breast cancer cell line HBT3477 (human) subcutaneous (abdomen)	(DeNardo et al., 2007)
Iron oxide nanoparticles with dextran coating	Hyperthermia (alternating magnetic field)	Breast cancer cell line MDA-MB-231 (human) subcutaneous (between the shoulder blades)	(Silvio et al., 2011)
Iron oxide nanoparticles with PEG coating	Arginine-glycine-aspartic acid or chlorotoxin	Glioblastoma cell line U87 (human) subcutaneous	(Dürr et al., 2013)
Iron oxide nanoparticles (Fe ₃ O ₄)	Hyperthermia (alternating magnetic field)	Breast cancer cell line (human) subcutaneous (abdomen)	(Dürr et al., 2013)
Iron oxide nanoparticles with dextran coating and binding for tumor-specific antigen uMUC-1	siRNA against BIRC5	Breast cancer cell line BT-20 (human) subcutaneous	(Kumar et al., 2010)
Iron oxide nanoparticles (Fe ₃ O ₄) coated with poly lactic acid	Arsenic trioxide	Osteosarcoma cell line MG-63 (human) subcutaneous (flank)	(Dürr et al., 2013)
Iron oxide nanoparticles with polylysine coating	NM23-H1 gene (an anti-metastatic gene)	Melanoma cell line B16F10 (mouse)	(Li et al., 2008)

Iron oxide nanoparticles with polyethylenimine coating	Plasmid DNA comprising a cytokine gene	Fibrosarcoma	(Plank et al., 2011)
Iron oxide nanoparticles with dextran coating	Herpes simplex virus vector	Gliosarcoma cell line 9L (rat) brain	(Dürr et al., 2013)
Iron oxide nanoparticles	L6 IgG monoclonal antibody	Lung carcinoma cell line LX-1 (human) brain	(Remsen et al., 1996)
Iron oxide nanoparticles with dextran coating	Human adenovirus type 5 early region 1A (E1A)	Cervix carcinoma cell line HeLa (human) subcutaneous (lower limbs)	(Shen et al., 2010)
Iron oxide nanoparticles (Fe ₃ O ₄) within liposomes	Hyperthermia (alternating magnetic field) combined with dendritic cells	Melanoma cell line B16 (mouse) subcutaneous (right flank)	(Tanaka et al., 2005)
Mn x Zn 1 - x Fe 2 O 4 coated with human albumin and folate	Radionuclide ¹⁸⁸ Rhenium cisplatin (hyperthermia possible)	Ovarian cancer cell line SKOV3 (human) subcutaneous (right side)	(Dürr et al., 2013)
Iron oxide nanoparticles covered with starch, dextran or mannan for uptake in tumor-associated immunosuppressive phagocytes	Hyperthermia (alternating magnetic field)	Ovarian cancer cell line ID8-Defb29/Vegf-a (mouse) intraperitoneal	(Toraya-Brown et al., 2013)
Iron oxide nanoparticles (Fe ₃ O ₄)	Adenoviruses	Pancreatic carcinoma cell line 181RDB-fLuc (human) subcutaneous (right flank)	(Tresilwised et al., 2010c)
Iron oxide nanoparticles	Hyperthermia (alternating magnetic field)	Pancreatic carcinoma cell line 181RDB-fLuc (human) subcutaneous (armpit)	(Dürr et al., 2013)]
Gold-coated iron nanoparticles (non-oxidized)	Non-oxidized iron nanoparticles	Buccal pouch carcinoma HCDB1 (hamster)	(Wu et al., 2011)
Iron oxide nanoparticles (Fe ₃ O ₄) with aminosilane coating	Hyperthermia (alternating magnetic field)	Prostate cancer	(Johannsen et al., 2007)
Iron oxide nanoparticles (Fe ₃ O ₄) with aminosilane coating	Hyperthermia (alternating magnetic field)	Glioblastoma	(Maier-Hauff et al., 2011)

1.10.3 Challenges of MNPs

1.10.3.1 High variation in size and physical aggregation of MNPs

The high variation in size and physical aggregation displayed by chemically synthesised MNPs is a concern that has been raised by many researchers. For example, Raguraman and colleague reported this concern (Raguraman and Suthindhiran, 2019). They found that synthetic MNPs agglomerated inside the cell which subsequently damage the redox system causing mortality. However, Florea et al., demonstrated high cell uptake of PEI coated MNPs in Cos1 (green monkey fibroblasts) and airway epithelial cells (calu-3) but this correlated strongly with PEI toxicity (Florea et al., 2002). Similarly, Thomas and co-workers found that PEI coated MNPs

facilitated gene transfer into the A549 lung carcinoma cells *in vitro* and into the lungs of mice but this also was highly toxic to cells (Thomas et al., 2005). This needs to be addressed if these particles are to be applied clinically (Blanco-Mantecon and O'Grady, 2006).

1.10.3.2 Toxicity of nanoparticles

A major issue that still needs to be addressed regarding MNPs in medicine is toxicity. Toxicity is largely affected by MNP dose, chemical structure, size, surface chemistry, biodegradability, pharmacokinetics, solubility, bio-distribution, structure and shape (Tran and Webster, 2010). The main tool which is used to reduce the toxicity of MNPs is modifying their surface properties (Park et al., 2006). Many of the current studies on MNP toxicity have been *in vitro* investigations, which whilst useful could be unreliable due to their simplicity. *In vivo* studies in preclinical animal models should be done to completely understand the MNP toxicity along with clinical studies in humans.

One should also treat the *in vitro* data with caution as it has been described that some of the typical cell viability assays (such as MTT and neutral red (NR) assays) are affected by the MNPs leading to false results because of MNP/dye interfaces (Monteiro-Riviere et al., 2009). Consequently, checking the toxicity of MNPs should be done using a combination of different assays.

As mentioned above MNPs have mainly been utilized in MRI applications as contrast agents. The first generation of MNPs, such as Feridex are coated with dextran and are fast removed from the blood via RES. Feridex has been used to detect tumours (primary and metastasis) in normal liver tissue, and was FDA-approved in 1993 for this application via intravenous injection. New MNPs like those described above are being developed by researchers worldwide. Some of these should become approved for clinical use in the coming years.

1.10.3.3 Controlling and guiding MNPs via an external magnetic field

Controlling MNP drug transporters to the chosen place for treatment is considered one of the major challenges faced in MNP-based therapeutics. Targeting systems which use these MNPs depend on using an external magnet located near the target tissue (Muthana et al., 2008b, Lübbecke et al., 1996, Lemke et al., 2004, Kettering et al., 2007). The magnetic field which is used by this strategy cannot penetrate a tissue depth more than 12 cm, thus the permanent magnet is not useful for targeting tissues deep in the body (Goodwin et al., 1999, Neuberger et al., 2005). As previously suggested by Shapiro, dynamically controlled magnetic fields could be utilized to deliver magnetic transporters to deep tissue targets (Shapiro, 2009). This could also be achieved

using the powerful magnets in MRI machines. A recent study from the University of Sheffield demonstrated that MRI could be used to magnetically guide magnetic cell therapies carrying the OV (HSV1716) to tumours located in the prostate and lungs of mice. This significantly improved the number of cells trafficking to tumours and resulted in a reduction in primary and metastatic tumour burden (Muthana et al., 2015a). The magnets in use today in MRI are in the 0.5 T to 3.0 T range, while the magnet that we used in this study is 0.7 T. In this PhD project a naturally occurring MNPs called magnetosomes will be used and therefore will be discussed in more detail below.

1.10.4 Magnetotactic bacteria and magnetosomes

Another type of MNPs is magnetosomes. Most of magnetotactic bacteria contain magnetosomes, which consist of magnetic iron particles providing species-specific features as shown in **Figure 1.7**. Magnetotactic bacteria (MTB) are a Gram-negative motile group that have the ability to produce magnetic nanoparticles called magnetosomes, through a controlled biomineralization process (Bazylinski and Frankel, 2004). Adopting iron in ionic state from the environment is considered one of the most unique features of the magnetotactic bacteria. These bacteria produce magnetosomes and potentially use it as a compass to navigate in the direction of the earth's magnetic field (Alphandéry, 2014). Magnetite-producing spirillum named *Aquaspirillum* (now *Magnetospirillum*) *magnetotacticum* strain MSR-1 is considered the first MTB cultivated in axenic culture (Blakemore, 1975). Study in these microorganisms was delayed for a long time because of the obstacles in isolating and cultivating different species of MTB. However, over the last 30 years, different kinds of MTB were isolated in axenic culture because of the important developments in culture approaches for different kinds of MTB, mainly since 2011 (Lefevre and Bazylinski, 2013). Moreover, the number of publications which use MTB and magnetosomes in diverse biotechnological applications has also significantly increased since 2011. Today, there are around 25 MTB species in axenic culture (Lefevre and Bazylinski, 2013). In spite of this, there are a rare species that are accessible in cell line sources, containing the American Type Culture Collection (ATCC) or the Leibniz Institute DSMZ-German Collection of Microorganisms and Cell Cultures (Deutsche Sammlung von Mikroorganismen und Zellkulturen GmbH; DSMZ).

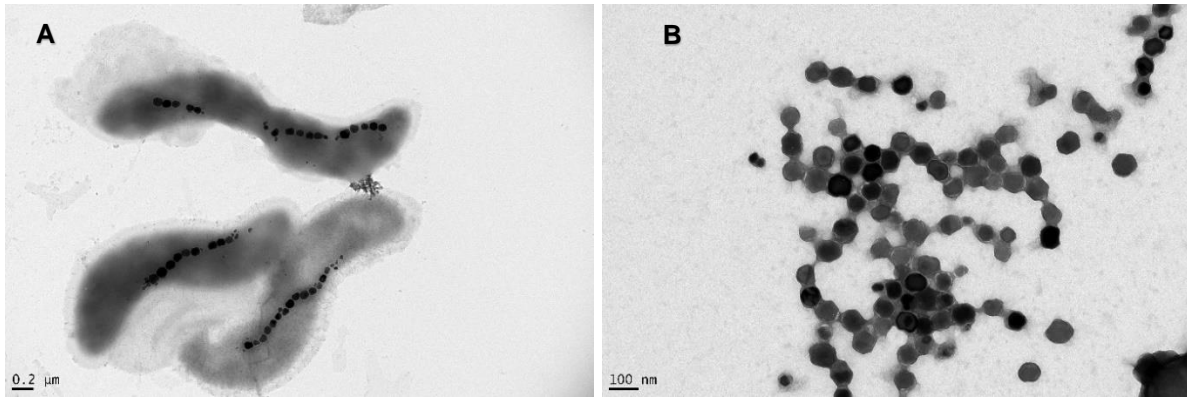


Figure 1.7: Transmission electron microscopy (TEM) images. A. Magnetotactic bacteria (*magnetospirillum magneticum* AMB-1) contain magnetosomes (black dots) **B.** Magnetosomes isolated from magnetotactic bacteria at higher magnification (Al-Janabi et al, 2015 unpublished data). Magnetosomes have a uniform morphology and are approximately 40-50nm in diameter.

Magnetosomes isolated from magnetotactic bacteria display uniform morphology and unique structure with narrow-size distribution (Lins et al., 2000, Schüler and Frankel, 1999). The *M.gryphiswaldense* strain is able to create iron oxide MNPs of cubic-octahedral shape, which have an average size range of 35-50 nm (Zeytuni et al., 2012, Greene and Komeili, 2012). Magnetosomes have a membrane lipid bilayer admixed with special proteins. For example, free fatty acids and neutral lipids; in addition to glycolipids, sulfolipids, and phospholipids which include phosphatidylserine and phosphatidylethanolamino are present on the magnetosome membrane isolated from *M. magnetotacticum* MS-1 (Gorby et al., 1988). Magnetosomes have high surface negativity on the membrane as a result of the lipid composition and the occurrence of polarizable primary amino groups (Tanaka and Matsunaga, 2000). Below is a comparison of magnetosomes to the chemically synthesised MNPs described in **Table 1.5**.

Table 1.6: Compares magnetosomes derived from *M. gryphiswaldense* with chemically synthesised MNPs (Fischer et al., 2011, Liu et al., 2010, Sun et al., 2008a).

Magnetosomes	Chemically synthesized MNPs
Regular morphology and small size distribution (25–55 nm).	Typically, measuring 1–100 nm in diameter often not uniform
An inorganic component of Fe ₃ O ₄ with high purity.	An inorganic nanoparticle core.
Stable single-magnetic-domain particles.	Single magnetic domain particles.
Biocompatible surface with negative charge and good dispersal because of polarized primary amino groups in the bilayer lipid membrane of magnetosome. Easy integration with varied bioactive molecules due to the plenty of primary amino groups on the magnetosomes surface.	Coating of surface provides good stability under physiological circumstances and permits for the functional ligand integration.
Large-scale production methods are needed	Comparatively easy to manufacture.
High biocompatibility.	Biocompatible.

The magnetic mineral crystals of magnetosomes exhibit unique magnetic and physical features that considered essential in their use in many biotechnological applications. These mineral crystals display a uniform crystal morphology reliant on the species of MTB, such as a small crystal size range, comparatively high chemical purity and limited crystallographic deficiencies (Bazylinski et al., 1995, Bazylinski et al., 1994). There are diverse crystals shapes of magnetosome among types of MTB; however, generally, one species of MTB produces crystals of a particular morphology (Bazylinski and Frankel, 2004, Balkwill et al., 1980). Currently, three shapes of magnetosome crystals were observed in MTB with only minor differences and include, roughly cubic (cuboctahedral) (Mann et al., 1984a, Mann et al., 1984b, Kiseleva et al., 2015); elongated prismatic (appear rectangular in projection) (Blakemore, 1975); and bullet or tooth-shaped (anisotropic) (Lefevre et al., 2011, Li et al., 2015, Mann et al., 1988) (**Figure 1.8**).

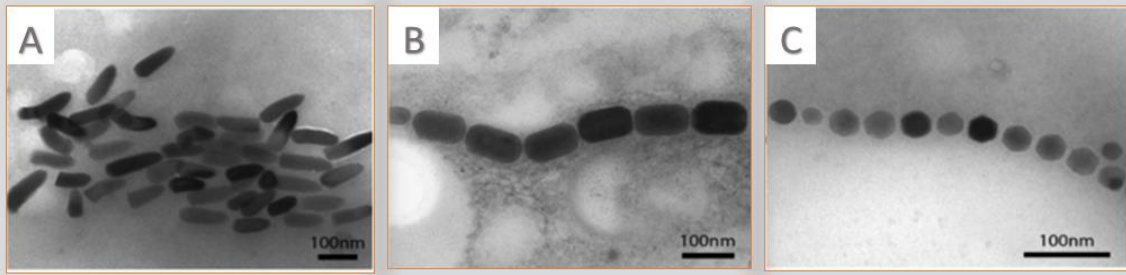


Figure 1.8: Transmission electron microscopy (TEM) images of different crystal shapes of magnetite magnetosome crystals that organise into chain(s) within magnetotactic bacteria. Magnetite magnetosomes **A.** bullet-shaped purified from magnetotactic *Nitrospirae*, **B.** prismatic purified from magnetotactic *Alphaproteobacteria*, and **C.** cubo-octahedral purified from *Aquaspirillum magnetotacticum*. Figure taken from (Vargas et al., 2018).

Magnetite magnetosome are mineralized under strict genetic and (bio) chemical control by a process called biomineralisation (Gorby et al., 1988, Komeili, 2012, Amemiya et al., 2007). MTB uses particular genes named ‘mms’ (magnetic particle membrane specific) or ‘mam’ (magnetosome membrane) genes to encode proteins that contribute to formation of magnetosome membrane, uptake of iron, magnetic crystal nucleation and gathering of the magnetosomes into chains (Murat et al., 2010, Komeili, 2012, Grunberg et al., 2004, Amemiya et al., 2007). However, particular steps of magnetosome biomineralization require further investigation and could be different reliant on the species of MTB (Komeili, 2012, Faivre and Godec, 2015).

Although, magnetosomes have some features superior to those appeared in synthetic iron particles as described above (Xie et al., 2009). The fastidious and microaerophilic growth features of MTB are considered a common problem in the production of biogenic iron particles (Yan et al., 2012, Heyen and Schuler, 2003). As cultures of MTB results in a low yield of magnetite and purification techniques of magnetosomes from cultures are showed very time-consuming compared to the production of synthetic MNPs (Xu et al., 2014). Many strategies for culturing of MTB in bioreactors have been suggested (Heyen and Schuler, 2003, Liu et al., 2010, Zhang et al., 2011, Sun et al., 2008) and commonly utilise *Magnetospirillum* strains growing in batch, fed-batch, and semi-continuous cultures (Araujo et al., 2015). For example, cultures of MTB under very low O₂ tensions or anaerobically results in much higher of magnetite yields (Heyen and Schuler, 2003). Therefore, a usual effective method in large-scale cultivation of MTB is strict control over O₂ tension during growth (Sun et al., 2008). Magnetosome production is also effected by other medium components, for example nitrogen,

carbon and iron sources and concentrations (Heyen and Schuler, 2003, Liu et al., 2010, Zhang et al., 2011). Recent study have shown that final biomass concentration is increases by lower concentrations of lactic acid in the feed of *M. gryphiswaldense* MSR-1, while cellular magnetism is increased by a high concentration. Therefore, it is important to balance the production of biomass and magnetosomes in the design of these fermentation processes (Fernández-Castané et al., 2018). It is essential to note that, these techniques are considered environmentally friendly procedures with comparatively good reproducibility, low cost, and high yield as mentioned by Xu and colleagues (Xu et al., 2014).

The mixture of these chemical/physical/magnetic features, alongside with the properties of magnetosome membrane, leads the magnetosomes to be unique and value investigation for their possible in biotechnology, nanotechnology and nanomedicine applications.

1.10.4.1 Applications of MTB and Magnetosomes

So far, whole MTB and magnetosomes have been considered in many applications, such as drug delivery, DNA and antigen recovery/detection, cell separation, food science, hyperthermia, enzyme immobilization, MRI image contrast and bioremediation (**Table 1.6&1.7**).

Table 1.7: This table shows applications of whole MTB.

Field	Application	Advantages	Disadvantages	Ref.
Drug delivery	Drug-loaded nanoliposomes attached to marinus cells for targeted tumor treatment Mc.	lysis; Uses cell's Dispenses cell own magnetotaxis	Potentially immunogenic due to outer LPS	(Felfoul et al., 2016)
Bioremediation	Wastewater treatment; Removal of heavy metals (Cd, Te, Se)	Magnetic crystal doping possible; Recovery of removed minerals	Poor growth of MTB in contaminated medium; Biomineralization may be affected	(Shimoshige et al., 2017, Zhou et al., 2017, Tanaka et al., 2016)
Energy generation	Electricity generation by cells and magnetosomes of <i>Ms. magneticum</i> AMB-1 by means of electromagnetic induction	Green energy technology	Only millivolts generated; Expensive	(Smit et al., 2018)

Sun et al., used magnetosomes from *Magnetospirillum gryphiswaldense* MSR-1 bacteria as magnetic-targeted drug carriers to establish an anti-tumour influence of doxorubicin-loaded magnetosomes in EMT-6 and HL60 cancer cell lines. Moreover, cardiac toxicity was

remarkably decreased in doxorubicin-loaded magnetosomes in a rodent tumour model of liver cancer compared with doxorubicin alone (Sun et al., 2007). Magnetosomes have gained attention as diagnostic and therapeutic agents because of their physical properties (Lee et al., 2011, Hartung et al., 2007). Their use in magnetic hyperthermia was recently considered advantageous because of their specific absorption rate (SAR), this was numerous orders of magnitude greater than the chemically synthesised MNPs that are currently used in magnetic thermotherapy (Alphandéry et al., 2012, Alphandéry et al., 2011a, Lee et al., 2011, Hartung et al., 2007, Hergt et al., 2005). Magnetosomes can therefore tolerate high heating effects when exposed to alternative magnetic field (AMF).

Table 1.8: This table shows applications of magnetosomes.

Field	Application	Functionalization Method	Advantages	Disadvantages	Ref.
Drug delivery	Delivery of antitumor drugs: doxorubicin, cytarabine, daunorubicin; delivery of gangliosides; Antitumor gene delivery	Chemical crosslinking with glutaraldehyde and genipin/PLGA; Surface adsorption of plasmids	Targeted drug delivery; Reduction of drug toxicity; Tissue specificity; Easy functionalization	Possible activity alteration; Unclear biological fate; Endotoxin test needed	(Sun et al., 2008, Cheng et al., 2016, Wang et al., 2018c)
Cell separation	Sorting of blood cells;	Binding protein expression by vector cloning; Insertion of modified binding protein into membrane	Reutilization of capture complex; High specificity separation	Difficult steps of cloning and expression; Alteration of cell viability after capture	(Yoshino et al., 2008, Takahashi et al., 2010, Grouzdev et al., 2014)
Food safety	Capture of Salmonella and Vibrio cells; Enterotoxin detection	Crosslinking of antibodies	Reutilization of capture complex; High sensitivity	Antibody specificity	(Li et al., 2010, Wu et al., 2013, Xu et al., 2014a)
MRI contrast agent	Diagnostic detection of tumors	No functionalization; Chemical coupling of targeting peptide	May also be used as therapeutic tool (by hyperthermia, drug delivery); High affinity to target cells; High detection sensitivity	Unclear biological fate; Endotoxin test needed	(Boucher et al., 2017, Xiang et al., 2017, Lee et al., 2011b)
DNA/Antigen Recovery/Detection	Capture of oligonucleotides and antibodies; Hepatitis B antigen detection	Biotinylation by chemical crosslinking with NHS	High sensitivity and recovery efficiency	Complex technology	(Ceyhan et al., 2006, Wacker et al., 2007)
Hyperthermia	Treatment of tumors	No functionalization, generally	Less significant side-effects than chemotherapy and radiotherapy; Tissue specificity; May also be used as diagnostic tool	Unclear biological fate; Endotoxin test needed	(Alphandery et al., 2017, Alphandery et al., 2011, Mannucci et al., 2018)
Enzyme immobilization	Bioremediation of organophosphate pesticides; Cellulose degradation	Enzyme expression by vector cloning	Reutilization of nanobiocatalysts; Immobilization of multiple catalysts	Difficult steps of cloning and expression; Possible loss of activity due to immobilization	(Ginet et al., 2011, Honda et al., 2015)

Magnetosome studies in the field of biomedical science are still in their infancy and the toxicity of this kind of particles has not yet been fully evaluated (Xiang et al., 2007). For example, as

these particles are derived from bacteria, there could be some immunogenicity associated with their use, however this requires further investigation. Indeed, magnetosomes that extracted from gram negative magnetotactic bacteria possess endotoxins at their surface, which need to be removed for medical applications (Le Fèvre et al., 2017). However, these particles do hold promise particularly given their small and uniform size as well as their biocompatibility.

1.11 Hypothesis and Aims

OVs are fast becoming accepted anti-cancer therapies but there is a critical need to overcome the challenges of systemic delivery if this is to become an accepted cancer treatment particularly for hard to access tumours or metastatic disease. Our overarching hypothesis is that magnetising OVs and magnetic guidance strategies will protect the viruses from inactivating immune mechanisms they encounter in circulation resulting in improved tumour targeting located in primary and metastatic sites in preclinical models of breast cancer. In doing so this will promote antitumour immunity.

To test our hypothesis, we aimed to:

Develop a stable nanomedicine whereby HSV1716 is co-assembled with magnetosomes derived from magnetotactic bacteria AMB-1. The magnetosomes will serve to protect the OV from deactivating immune responses and increase the targeting of the virus from circulation to the tumour in the presence of a magnetic field.

To achieve this our specific objectives were to:

1. Magnetise the OV 'HSV1716' with magnetosomes (MAG-OV) and characterise the physicochemical and biological properties of the nanomedicine.
2. Characterise the oncolytic potential of MAG-OV.
3. Investigate the magnetic targeting efficacy of MAG-OV in mammary tumours in the presence and absence of neutralising antibodies and assess the anti-tumour properties of our nanomedicine.

Chapter 2

Materials and Methods

2.1 Materials

2.1.1 List of reagents

Reagent	Company
1% Eosin	Sigma-Aldrich
1% Penicillin and Streptomycin	Lonzo BioWhittaker Ltd
10% Foetal Bovine Serum (FBS)	Lonzo BioWhittaker Ltd
4',6-Diamidino-2-Phenylindole, Dihydrochloride (DAPI)	Invitrogen
Absolute Ethanol	Thermo Fisher Scientific
Acetone	Thermo Fisher Scientific
Agarose	Sigma-Aldrich
Cryo-M Bed Optimal Cutting Temperature Compound (OCT)	VWR International
Dimethyl Sulfoxide (DMSO)	Sigma Aldrich
Dispase II	Gibco
DPX Mounting medium	Sigma Aldrich
Dulbecco's Modified Eagle's Medium (DMEM) Ultraglutamine, 4.5g/L glucose Lonza DMEM medium	Lonzo BioWhittaker Ltd
Eosin Y	Thermo Fisher Scientific
FcR blocking reagent, mouse	Miltenyi Biotec
Growth Factor Reduced (GFR) Matrigel	Corning
Haematoxylin Solution Gill No. 2	Sigma Aldrich
Immune-mount	Sigma-Aldrich
Iscove's Modified Dulbecco's Medium (IMDM)	Lonza
L-Glutamine (4mM)	Lonzo BioWhittaker Ltd

Normal Goat Serum	Vector Laboratories
Nuclease free water	Qiagen
Paraformaldehyde	Sigma Aldrich
Phosphate Buffered Saline	Lonzo BioWhittaker Ltd
PI	Thermo Fisher
PrecisionPlus qPCR mastermix with SYBR green and ROX	Primer Design
ProLong Gold Antifade mountant	Invitrogen
Roswell Park Memorial Institute (RPMI) mediumRPMI medium	Lonzo BioWhittaker Ltd
Super PAP pen	Thermo Fisher Scientific
TO-PRO-3	Thermo Fisher
Trypan blue	Sigma-Aldrich
Trypsin/EDTA	Sigma Aldrich
TWEEN 20	Thermo Fisher Scientific
Zombie UV Fixable Viability kit	Biolegend

2.1.2 List of materials

Material	Supplier
Coverslips	Scientific Laboratory Supplies
Fisherbrand 384-well skirted PCR plate	Thermo Fisher Scientific
Superfrost Plus Microscope Slides	Thermo Fisher Scientific
Tissue culture flasks (Nunc EasYFlask) 25cm ² ; 75cm ² ; 125cm ²	Thermo Fisher Scientific

2.1.3 List of equipment and Apparatus

Equipment and apparatus	Company
Applied Biosystems 7900 Real-time PCR machine	Applied Biosystems
Automated Cell Counter	BIO-RAD
Bench centrifuge	SANYO
Compound light microscope	Olympus
FACSCalibur	Becton Dickinson
Incubator	SANYO
Laminar airflow hood	Heraeus
Light microscopy	Leica
LSR II Flow cytometer	BD Bioscience
Micropipette	Eppendorf
MS2 meters	Bartington Instruments
NanoBrook Zeta PALS	Brookhaven instrument
Nanodrop	Thermo Scientific
Nikon A1 Confocal	Nikon
PIPETBOY	INTEGRA
Plate reader	Thermo Scientific
Refrigerator	BioCold
Sensitive balance	Sartorius
Shaking platform	Luckham
Sonicator	Bioruptor
Spectrophotometer	Varian Associates
Water bath	Grant

2.1.4 List of Primers

All primers were either designed using NCBI primers blast or previously published. Parameters used when designing primers included exon-exon junction, product length and GC ratio) (Ye et al., 2012). Primers were validated using melt-curve analysis and a standard curve was used to assess the efficiency of these primers. All of the primers were purchased from Sigma and dissolved in nuclease free water and stored at -20°C on arrival. Of note, all primers were designed by a post-doctoral research fellow in the group (Dr. Emer Murphy).

Primer Name	Primer Sequence
ATGS	Forward: 5' - TCTGGATGGGATTGCAAAATG -3' Reverse: 5' - TTTCTTCTGCAGGATATTCCATG -3'
Bcl-2	Forward: 5' -GGAAGTGAACATTTTCGGTGAC -3' Reverse: 5' -GCCTCTCCTCACGTTCCC -3'
CASP3	Forward: 5' - AAAGCACTGGAATGACATC-3' Reverse: 5' - CGCATCAATTCCACAATTTTC-3'
CASP8	Forward: 5' - CTACAGGGTCATGCTCTATC-3' Reverse: 5' - ATTTGGAGATTTCTCTTGC-3'
CXCL10	Forward: 5' -GAATTTCCCAGCATCCCAAAG-3' Reverse: 5' -TGCCTTCTGCACTCCCTTTATC-3'
FasL	Forward: 5' --ATCCCTCTGGAATGGGAAGA -3' Reverse: 5' -CCATATCTGTCCAGTAGTGC -3'
gB	Forward: 5' -TGTGTACATGTCCCGTTTTACG -3' Reverse: 5' - GCGTAGAAGCCGTCAACCT -3'
HSP90AA1	Forward: 5' - ATATCACAGGTGAGACCAAG-3' Reverse: 5' - GTGACTGACACTAAAGTCTTC-3'
HSP90B1	Forward: 5' - TTCAAAGGAAAGTGATGACC-3' Reverse: 5' - GCATCATATCATGGAAGTCG-3'

HSPA1A	Forward: 5'- AATTCCTGTGTTTGCAATG-3' Reverse: 5'- AAAATGGCCTGAGTTAAGTG-3'
ICP0	Forward: 5'-AAGCTTGGATCCGAGCCCCGCC -3' Reverse: 5'-AAGCGGTGCATGCACGGGAAGGT -3'
ICP8	Forward: 5'-GACATTACGTTACGGCCTTCGAAGCCAG -3' Reverse: 5'-GGCCGAGTTGGTGCTAAATACCATGGC -3'
IFN γ	Forward: 5'-TGCAGGTCATTCAGATGTAGCGGATA -3' Reverse: 5'-TCATGTATTGCTTTGCGTTGGACA -3'
IL-10	Forward: 5'-GCCTAACATGCTTCGAGATC-3' Reverse: 5'-CTCATGGCTTTGTAGATGCC-3'
IL-1B	Forward: 5'- GCCACCTTTTGACAGTGATGAG -3' Reverse: 5'-AGCTTCTCCACAGCCACAAT-3'
LC3B	Forward: 5'- GTGGAAGATGTCCGGCTCAT -3' Reverse: 5'- TGGTCAGGCACCAGGAACTT -3'
NF-kB	Forward: 5'-ACCTGAGTCTTCTGGACCGCTG-3' Reverse: 5'-CCAGCCTTCTCCCAAGAGTCGT-3'
TGf- B	Forward: 5'- AGCGACTCGCCAGAGTGGTTA-3' Reverse: 5'- GCAGTGTGTTATCCCTGCTGTCA-3'
TNF	Forward: 5'-CCAGGAGAAAGTCAGCCTCCT-3' Reverse: 5'-TCATACCAGGGCTTGAGCTCA-3'
VEGF	Forward: 5'-GAAGTTCATGGACGTCTACCAG Reverse: 5'-CATCTGCTATGCTGCAGGAAGCT-3'
House Keeping gene (GAPDH)	Forward: 5'- TGCACCACCAACTGCTTAGC -3' Reverse: 5'- GGCATGGACTGTGGTCATGAG -3'

2.1.5 List of commercial kits

Kit	Company
ENLITEN ATP kit	Promega
HMGB1 ELISA Kit	Shino-Test
Precision 2X q-PCR Mastermix	PrimerDesign
Precision Nanoscript 2 RT Kit	PrimerDesign
RNeasy Mini Kit	QIAGEN

2.1.6 List of solutions

Solution	Instructions
DAPI staining solution	50µg/ml DAPI in PBST
FACS buffer	DPBS with 0.5% FBS
PBST	250µL TWEEN 20 in 50ml DPBS
Tumour dissociation medium	IMDM with 0.2mg/ml collagenase type IV and 2mg/ml dispase II

2.1.7 List of software

Software	Supplier
Fiji	https://imagej.net/Fiji [184]
Flow Jo	TreeStar Inc
GraphPad Prism 7	Graph Pad Inc.
Primer Blast	National Institute of Health, USA

2.1.8 Human Materials

Human platelet-depleted waste buffy coats were supplied by the Sheffield Blood Transfusion Service. All patients donating blood gave informed consent to the Sheffield blood Transfusion Service and the University of Sheffield Ethics Committee has approved all procedures. This was carried out under ethics SMBRER 139.

Most of the chemicals utilized in this project were obtained from Sigma and Sigma Aldrich. All water that was used for this project was Ultrapure MilliQ (18M Ω cm), degassed and sparged with N₂ before use.

2.2 Methods

2.2.1 Preparation of Magnetosomes (MAG)

MAG were prepared from purified magnetotactic bacteria AMB-1 using established protocols (Staniland et al., 2007). Preparation of MAG was carried out in assistance with Ms. Zainab Taher in Chemical department at Sheffield University. Details are explained in the following sections.

2.2.1.1 Bacterial culture

The strain *magnetospirillum magneticum* AMB-1 used in this project was kindly provided by the Matsunaga group, Tokyo Institute of Agriculture and Technology, in both anaerobic and microaerobic conditions in liquid medium (Arakaki et al., 2008). This bacteria can produce internal magnetite particles with a size of 50-100nm that are cuboctahedral shaped (Arakaki et al. 2008). AMB-1 was grown in a cabinet within microaerobic conditions consisting of 1% O₂ and 99% nitrogen at 30.1 C° in liquid culture medium (see 2.2.1.2) which is specific to AMB-1 bacteria.

2.2.1.2 AMB-1 culture medium

The AMB-1 culture medium was prepared following the methodology of DSMZ 380 institute (<https://www.dsmz.de/catalogues/catalogue-microorganisms/culture-technology/list-of-media-for-microorganisms.html>).

Table 2.1 AMB-1 growth medium.

Ultrapure MilliQ water	2000ml
KH ₂ PO ₄	1.36g
L(+)-Tartaric acid	0.74g
Na-acetate	0.10g
NaNO ₃	0.24g
Resazurin	1mg
Succinic acid	0.74g

All these components were added to the water in the order provided in (**Table 2.1**). 1M NaOH was used to adjust the AMB-1 culture medium to pH 6.75 and 400ml was aliquoted into 500ml-sterilised bottles, autoclaved on a standard cycle (121 C° for 15 min at 15P) and stored in a Whitley VA 500 workstation cabinet (30⁰C and 99% nitrogen). The following day, sodium thioglycolate was added by passing first through a cellulose nitrate membrane filter (pore size 0.22um). Two days after this vitamins, minerals and 0.01M ferric quinate was added to the medium using the quantities described in **Table 2.2**. Ferric quinate is known to encourage magnetosome growth resulting in a high density of cells. The solutions in **Tables 2.3-5** were prepared as stock solutions and were pre-sterilised with a 0.22um filter prior to adding to the culture medium. The nitrilotriacetic was dissolved first then, NaOH was added to adjust the pH to 6.5 before the remaining minerals were added. The final pH was set to 7.0.

Table 2.2: Welfer's vitamins solution.

Ultrapure MilliQ water	1000 ml
Biotin	2.00mg
D-Ca-pantothenate	5.00mg
Folic acid	2.00mg
Lipoic acid	5.00mg
Nicotinic acid	5.00mg
P-Aminobenzoic acid	5.00mg
Pyridoxine-HCl	10.00mg
Riboflavin	5.00mg
Thiamine-HCl	5.00mg
Vitamin B12	0.10mg

Table 2.3: Volume of vitamins and minerals and ferric-quinat that was added to 400ml medium.

Solution	400ml of Medium
Ferric quinate (0.01M) solution (Table 2.4)	0.16ml
Na-thioglycolate	3% Wt
Welfer's mineral (Table 2.5)	1ml
Welfer's vitamins (Table 2.2)	4ml

Table 2.4: Ferric quinate 0.01M.

Ultrapure water	20ml
FeCl ₃ .6H ₂ O	0.45g
Quanic acid	0.19g

The vitamin solution was kept in the dark.

Table 2.5: Welfer's mineral solution.

Ultrapure MilliQ water	250 ml
CaCl ₂ . 2H ₂ O	0.10g
CoSO ₄ . 7 H ₂ O	0.18g
CuSO ₄ . 5H ₂ O	0.01g
FeSO ₄ . 7H ₂ O	0.10g
H ₃ BO ₃	0.01g
KAl(SO ₄) ₂ .12H ₂ O	0.02g
MgSO ₄ .7H ₂ O	3.00g
MnSO ₄ .7H ₂ O	0.50g
Na ₂ MoO ₄ .2H ₂ O	0.01g
Na ₂ SeO ₃	0.30mg
NaCl	1.00g
NiCl ₂ .6H ₂ O	0.03g
Nitilotriacetic acid	1.50g
ZnSO ₄ . 7H ₂ O	0.18g

2.2.1.3 AMB-1 inoculation

Bacteria (1ml) stocks stored at -80 C° were thawed and transferred into small glass bottles of AMB-1 culture medium (75ml) and left for one week in a Whitley VA 500 workstation cabinet (30 C° and 99% nitrogen) to reach maximum density. 75ml was decanted into 400ml glass bottles of medium and incubated for four weeks. The light scattering in UV/Visible spectrophotometer (Varian Associates) was used to check the density of cells in medium at 600nm, where 1ml of cultured bacteria was compared to 1 ml of media only. Optical density measurements were recorded every 8 hr for 72 hr then on a weekly basis until the fourth week.

2.2.1.4 Harvest and lysis of AMB-1 cells

The MAG were extracted from AMB-1 bacteria by centrifugation of culture media in 50ml falcon tubes at 4700 rpm for 45 min at 4°C. The pellet was transferred into 1.5ml eppendorf

tubes and positioned for 1 day on a strong neodymium magnetic rack (0.1-1 T) to separate them from the original medium. The pellet was resuspended in 1.5ml eppendorf tubes (10mM Tris-HCl buffer (pH 7.4), and the AMB-1 cells were sonicated for 1 hour using microprobe tip sonication (Sonics USA) to lyse the cells. After the sonication a neodymium magnet was used to separate the MAG from other cellular debris. 10mM Tris-HCl buffer (pH 7.4) was used to wash the MAG four times followed by resuspension in DPBS (pH 7.4).

2.2.1.5 Sterilization of MNPs

70% ethanol was used to sterilize the MAG. 1 ml of MAG (0.2mg/ml) were mixed with 9 ml of 70% ethanol, vortexed for 15 s and kept at RT for 30 min. The sample was centrifuged at 3800 rpm for 10 min and air-dried in a Laminar airflow hood. Sterilised water was used to re-suspend the pellet (Li et al., 2013)

2.2.1.6 Sonication of MNPs

Sonication (Bioruptor® Sonication System, Diagenode) was used to reduce MNP aggregation. Before use the MNPs were resuspended in Roswell Park Memorial Institute (RPMI) culture medium and sonicated on the highest setting for 10 min at 4°C.

2.2.2 Culturing of breast cancer cells

Breast cancer cell lines (MDA-MB-231 and MCF7) were purchased from the ECACC. MDA-MB-231 is a human caucasian breast adenocarcinoma originally derived from pleural effusion of a 51-year-old metastatic breast cancer patient. This is a triple negative breast cancer (TNBC) cell line for the oestrogen, progesterone and human epidermal growth factor HER2 receptors. MCF7 cells were originally derived from human Caucasian breast adenocarcinoma patient. These are oestrogen receptor positive. MDA-MB-231 cells were cultured in T75 flasks (Fisher Scientific®) and sub-cultured once 70-80% confluent in RPMI medium supplemented with 10% Foetal Bovine Serum (FBS) and 1% L-Glutamine (200mM in 0.85% NaCl solution). MCF7 cells were cultured in Dulbeccos Modified Eagles Medium (DMEM) ultraglutamine with 10% FBS and 5% Non-essential Amino Acids (NEAA) (Lonza®). Cultured cells were incubated at 37°C with 5% CO₂ in an incubator.

EO771 cells were obtained from Dr. Penelope Ottewell, University of Sheffield. This cell line is a spontaneously developing medullary breast adenocarcinoma derived from C57BL/6 mice (Sugiura and Stock, 1952). This is also a triple negative breast cancer (TNBC) cell line for the oestrogen, progesterone and human epidermal growth factor HER2 receptors, making it

difficult to target therapeutically (Johnstone et al., 2015). Furthermore, this tumour model naturally metastasises to the lungs in C57BL/6 mice (Johnstone et al., 2015). Cells were also cultured in Dulbecco's Modified Eagles Medium (DMEM) ultraglutamine with 10% FBS and 5% Non-essential Amino Acids (NEAA) (Lonza®). Cultured cells were incubated at 37⁰C with 5% CO₂ in an incubator.

TS-1 cells were provided by Professor Janet Joyce, Memorial Sloan Kettering Cancer Research Centre. These are HER-2 receptor positive and originally derived from the transgenic MMTV-PyMT tumours that spontaneously develop in mammary tumours. Cells were also cultured in Dulbeccos Modified Eagles Medium (DMEM) ultraglutamine with 10% FBS and 5% Non-essential Amino Acids (NEAA) (Lonza®). Cultured cells were incubated at 37⁰C with 5% CO₂ in an incubator.

2.2.3 Cell harvesting and seeding densities

When cells were at 70-80% confluency, 3ml trypsin/ETDA (170,000 U Trypsin/L and 200 mg/L Versene) was used to detach all cells from the flask. Trypsin/EDTA was neutralised in an equal volume of culture medium and then centrifuged at 600g for 5 min (Sanyo® Harrier 18/80). Cells were resuspended in culture medium and counted in trypan blue (Sigma-Aldrich®) to determine cell viability using a TC20 Automated Cell Counter (Bio-Rad®). Live cells were trypan blue negative. Cells were prepared as followed and cultured for 24 hr at 37⁰C;

1. For flow cytometry cells were seeded on to 6 well plates at 300,000 cells/well in 2ml of medium.
2. For Prussian blue assays cells were seeded into 24 well plates (Scientific Laboratory Supplies®) containing 13mm coverslips (BDH Cover glass), using a seeding density of 50,000 cells/well in a final volume of 1ml of medium.
3. For the MTT assays cells were plated at a seeding density of 1000 cells/well in a final volume of 200 µl of medium in 96 well plates.

2.2.4 Primary cells isolation

Ficoll density gradient centrifugation was used to isolate the Primary cells from blood according to (Muthana et al., 2011a, Muthana et al., 2013). 50ml falcon tubes were used to dilute 15ml of blood with 30ml of PBS. 20ml of Ficoll-Paque was overlaid with 30ml of blood/PBS and centrifuged at 1400rpm with brake off for 40 min. 4 layers (Plasma, PBMCs, Ficoll and red blood cells) were isolated and the lymphocytes located in the central creamy layer were removed and washed twice in PBS. After the centrifugation, the cell pellet was

resuspended in complete IMDM medium (supplemented with 2% human AB serum and 4mM L-Glutamine). Haemocytometer cell counting machine (Bio-Rad) was used to count the cells. After re-suspending 50 million cells in 5 ml of complete IMDM in T75 flasks and incubating for 2 hr (37°C at 5% CO₂), monocytes were attached to the flask by plastic adherence and the non-adherent lymphocytes were suspended in the entire medium.

2.2.5 Incubation of magnetic nanoparticles (MNPs) with cell lines

MAG isolated from magnetotactic bacteria (**Section 2.2.1**) were used at approximately 0.2mg/ml throughout this study. This concentration of iron has been used successfully in previous studies for cellular uptake (Mannucci et al., 2014). The culture medium was removed from cells after 24 hr of seeding onto wells and 0.2mg/ml of MAG that re-suspend in culture medium was added to each well. Following this, the plates were located on a shaking platform (low speed) (Luckham® R100 Rotatest Shaker) in an incubator at 37°C for 1 hour. A further equal volume of medium was then added to each well. After this, the plates were kept in an incubator until needed.

2.2.6 Flow cytometry (FACS) to assess MNP uptake and cell death in MDA-MB-231s

Flow cytometry was used to assess MNP uptake by tumour cells and cytotoxicity following overnight incubation of cells with MNPs. Trypsin/EDTA was used to detach the cells (**Section 2.2.6**) and the cell pellet was washed twice in 5ml PBS. The supernatant was discarded and 500µl PBS was used to re-suspend the pellet. All samples were added into flow cytometry tubes (400µl). Cell death was assessed by adding 2µl Propidium Iodide (PI) (50 mg/ml) to each sample just before analysis on the FACS Calibur (BD Biosciences). 10,000 events per sample were measured (equivalent to 10,000 cells) and FlowJo® software used to analyse cell death by generating fluorescent dot plots based on a change in fluorescence against FL3-H and MNP uptake based on changes in forward scatter (FSC-H) and side scatter (SSC-H).

2.2.7 Prussian blue staining to visualise MNP uptake

Cells seeded onto coverslips were incubated overnight with MNPs and then washed twice with 500µl PBS. PBS was removed from the wells and 200µl of acetone was added followed by incubation at 4°C for 10 min and two further washes in 500µl PBS. 200µl of 1:1 dilution of 1M Hydrochloric acid (1 M HCL) and 2% Potassium Ferranocyanide was added to each well and incubated at 37°C for 1 hour. The cells were washed again in 500µl PBS and then 200µl of 1% eosin was added to each well. Coverslips were mounted onto glass slides using immune-mount.

Light microscopy (Leica DM1000) was used to assess MNP uptake by viewing the slides at 40x magnification. Mitotic Images plus 2.0 Software was used to take the images.

2.2.8 MTT assay to assess cell viability

Seventy-two hours after incubation of cells with MNPs, 50µl of 3mg/ml MTT was added to each well and incubated at 37°C for 3 hr. The supernatant was removed and 200µl Dimethyl Sulfoxide (DMSO) was added to each well. A plate reader (Thermo Scientific® Multiskan FC) was used to measure absorbance at 540 nm; this detects differences in the dissolved purple formazan produced by viable cells. Microsoft Excel was used to analyse the results, in which the fold change over the control (no MNPs) was calculated. In this case 1 was set to the control and any results below 1 show reduced viability.

2.2.9 HSV1716 oncolytic virus

HSV1716 is one of a selectively replication competent mutants of the herpes simplex virus. The HSV1716 virus and Green fluorescent protein (GFP) expressing HSV1716 were kindly prepared by Virttu Biologics in 1.5ml aliquots at a concentration of 1×10^8 Particle Forming Units (PFU)/ml and 1×10^9 PFU/ml respectively. CMV-GFP expression cassette was inserted in the UL-43 gene to produce HSV1716 GFP. The virus stock was initially produced on 23/07/99 and was titrated by plaque forming assay to reconfirm titre in December 2012 (1×10^9 pfu/ml). The stock of virus was stored at -80 °C. The GFP reporter virus allowed detection of HSV1716 infected cells by flow cytometry and immunofluorescence.

2.2.10 Preparation of Magnetic Viral Complexes

HSV1716 virus was mixed with MNPs derived from AMB-1 bacteria. To prepare the complexes, 200ul of DPBS containing 0.22mg MAG and 1 ml of PBS containing 1×10^8 pfu OV were suspended in a final volume of 1.2 ml (0.2mg/ml MAG and 1×10^8 pfu OV). Following this, complexes were incubated for 20 min at room temperature (RT) and the tubes were inverted intermittently. Complexes resulting from virus and magnetosomes were called MAG-OV. These were stored at 4°C or used immediately.

2.2.11 Characterisation of MAG and MAG-OV complex

2.2.11.1 Transmission Electron Microscopy (TEM)

TEM was used in the Department of Biomedical Sciences (FEI Tecnai Biotwin) operated at 120kV with an Orius 1000 camera. TEM studies were carried out with the support of Chris Hill in the Department of Biomedical Science at Sheffield University.

2.2.11.1.1 TEM sample preparation

Samples of either AMB-1 purified MAG or MAG-OV complexes were centrifuged at 4700 rpm at 4°C for 45 min and the pellet transferred into 1ml eppendorf tubes resuspended in phosphate buffer. A droplet of this buffer was added onto carbon-coated copper grids for one minute and excess fluid was removed using tissue to leave a thin layer of sample over the TEM grid. Samples containing virus were also counterstained with 1% phosphotungstic stain, this is a common negative stain for viruses including HSV (Stannard et al., 1987).

2.2.11.1.2 Preparation of MAG-OV infected cells for TEM

Infected tumour cells (10^5) were fixed with 3% glutaraldehyde in 0.1M phosphate buffer (pH 7.4) overnight at 4 °C and then washed in 0.1M phosphate buffer twice at 30 min intervals. The samples were then post-fixed in 2 % aqueous osmium tetroxide for 2 hr at RT and washed in buffer as above. Sample dehydration was performed by passing the grids through a graded sequence of ethanol (75 – 100 %) and propylene oxide. Samples were inserted in araldite resin and dried at 60 °C for 48-72 hr. Slices approximately 0.5µm thick were cut and stained with 1% toluidine blue in 1% Borax. Ultrathin slices of 70-90 nm thick were attached onto 200 mesh copper grids, stained with 3% uranyl acetate in 50% ethanol and then stained with lead citrate for 25 min before examination by TEM.

2.2.11.2 MNP size determination by TEM

TEM was carried out to measure the size of MNPs; this was taken arbitrarily from prepared samples. Sizes range between approximately 50 to 200nm depending on sample composition and were measured by analysing MNPs randomly at 100 and 200 nm magnification. Image J was used to measure the length of chosen particles manually.

2.2.11.3 qNano

Particle concentration and size distribution were determined by TRPS using a qNano instrument (Izon). Calibration was performed using CPC100B calibration particles (Izon) with a modal diameter of 114 nm diluted 1/2000 (v/v) in PBS, supplemented with 0.03% (v/v) Tween-20 (PBST). Samples were diluted 1/3 (v/v) in PBST and then filtered through either a 0.2 or 0.45µm centrifugal unit. Sample and calibration samples were analysed with the same NP100 nanopore with the same settings for voltage, nanopore stretch and pressure. Settings were chosen that gave an optimum separation of particles from the background noise and a constant flow rate of particles.

2.2.11.4 Zeta potential analysis

Zeta potential is a measurement of the magnitude of the electrostatic or charge attraction/repulsion in the space separating particles, and is an essential parameter recognized to impact stability of MNPs (Nikam et al., 2014). The zeta potential was measured at RT on a NanoBrook Zeta PALS (Brookhaven instrument, NY, U.S.A) from a suspension of the sample in ddH₂O.

2.2.11.5 Magnetic susceptibility measurements (MSM)

MS2 meters (Bartington Instruments, UK) were used to measure the magnetic susceptibility of particles using Bartsoft software. MSM is a method that enables the rapid quantification (1s) of iron particles in a sample. Water was used as a blank and each sample was measured 3 times for 1s in a volume of 400 µl.

2.2.11.6 Inductively coupled plasma Atomic Emission Spectrometer (ICP-AES).

Inductively coupled plasma (ICP) is an analytical method that is carried out for chemical analysis of elements. Stimulated ions and atoms which produce electromagnetic radiation was formed by this technique at specific wavelengths that are characteristic of a specific element, therefore the concentration of metals in a sample can be measured by the strength of this emission. Spectro-Ciros-Vision Inductively Coupled Plasma Atomic Emission Spectrometer ICP-AES was utilized to calculate the quantity of Fe as a ratio of metal ions for the MNPs used in this project. About 0.3 mg of MNPs was dissolved in aqua regia (King's water a mixture of concentrated nitric and hydrochloric acids) in a molar ratio of 1:1 of nitric acid and HCL. 1ml of the MNP sample was added to 1ml of aqua regia solution and diluted in 10ml with dH₂O. The samples were sonicated for 4 hr in a water bath sonicator, Fe content (mg/l) was determined as a measure of atomic absorption.

2.2.12 Cell death and uptake of magnetic viral complexes

The OV_s HSV1716 or HSV1716-GFP were defrosted on ice for approximately 15 min. Cells seeded onto 6-Well Plates (**Section 2.2.2**) 24 hr earlier were washed with PBS and then cultured in 500 µl serum free RPMI for MDA-MB-231 cells or 500 µl serum free DMEM for MCF7 cells. After that, OV_s or MAG-OV complexes prepared as mentioned in **Section 2.2.10** at MOI 10 (1×10^8 pfu/ml) were added to the wells and incubated for 2 hr at 37°C followed by the addition of 2.5 ml of complete medium to each well. The cells and OV_s were incubated for time periods of 1, 3 and 6 days.

After culture, cells were washed with 2 ml PBS and trypsin/EDTA was used to detach the cells as in **Section 2.2.3** ready for flow cytometry. All samples were added into flow cytometry tubes (400µl). Cell death was assessed by adding 2µl of the viability dye TOPRO-3 to each sample prior to analysis on the FACS Calibur (BD biosciences). FlowJo® software was used to analyse the results and cell death was assessed by generating dot plots based on a change in fluorescence against FL-4-H. MNP uptake by cells was assessed based on changes in forward scatter (FL-1-H) and side scatter (SSC-H). In studies using the HSV1716 GFP viral infection of cells was assessed by GFP expression in the FL1-H channel.

2.2.13 Tumour spheroid experiments

Agarose, low melting point temperature was dissolved in DMEM (4.5 g/l glucose, no supplements) in the microwave followed by autoclaving the solution. 100µl warm agarose was added to each well of a 96-well plate (except the outer wells) using a multichannel pipette. After that, plates were allowed to cool and were inverted and stored at 4°C until required. Tumour cells were seeded into wells at 20×10^3 cells per well and the approximate size they grew to was 10^5 cells.

After 5-7 days post- seeding in 96 well plates, OV or magnetic viral complexes (MAG-OV) were added to the spheroids as described in **Section 2.2.12**. The spheroid size was monitored using Light microscopy (Leica DM1000) at 10x magnification and Mitotic Images plus 2.0 software was used to take images. Flow cytometry was used to assess cellular death after 6 days of infection (as mentioned in **Section 2.14**). Of note, spheroids were digested into cell suspensions using trypsin/EDTA prior to flow cytometry.

2.2.14 Measuring mRNA gene expression after OV infection

2.2.14.1 RNA extraction

Cells were infected with OV, MAG-OV and MAG alone alongside the control, untreated cells as described in **Section 2.2.12** for 24h and then scraped from the surface of the plates and centrifuged at 1400rpm for 5 min. RNA extraction was performed using the Qiagen RNeasy Mini Kit (QIAGEN). Cells were resuspended in 350µL of RLT lysis buffer and were kept on ice at all times. 70% ethanol (350 µL) was added to the lysed cells and all 700 µL was transferred to pink filter tubes placed in a 2ml collection tube and centrifuged at 8000 rpm for 15 s. RW1 buffer (700 µL) was then added and centrifuged at 8000 rpm for 15 s followed by 500ul of RPE buffer and centrifugation at 8000 rpm for 15 s. This was followed by the addition of 500 µL RPE buffer and centrifuged at 8000 rpm for 2 min before 50 µL of RNA-free water

was added and centrifuged for a further 1 min at 8000 rpm to release the RNA. The concentration of mRNA was measured using the NanoDrop Spectrophotometer ND 1000. The concentration of the RNA was standardised by diluting the sample in RNase/DNase-free water and then stored at -80°C until required.

2.2.14.2 Complementary DNA (cDNA) Synthesis

High-Capacity cDNA Reverse Transcription Kit was used to prepare the cDNA for q-PCR. All RNA samples were normalized to the same concentration according to the following calculation

$$(\text{RNA concentration desired} / \text{sample concentration}) \times \text{desired volume of RNA}$$

The 2X RT Master Mix was prepared according to the manufacturer's instructions as shown in **Table 2.6** for each reaction.

Table 2.6: Components of 2X RT Mastermix

Reagent	Volume (μL)
10X RT buffer	2.0
25X dNTP Mix (100mM)	0.8
10X RT Random Primer	2.0
MultiScribe Reverse Transcriptase	1.0
Nuclease-free H ₂ O	4.2

10μL of 2X RT Master Mix was added to 10 μL of RNA samples. The thermal cycler machine, setting as described in (**Table 2.7**), was used to synthesize cDNA from RNA samples.

Table 2.7: Thermocycler parameters for generation of cDNA

Step	Time	Temperature
Step 1	10 Min	25°C
Step 2	120 Min	37°C
Step 3	5 Min	85°C
Step 4	Hold	4°C

2.2.14.3 Real-Time Quantitative Polymerase Chain Reaction (RT-qPCR)

Real-time q-PCR was used to determine levels of mRNA expression of the genes using the prepared cDNA (**Section 2.20.3**). The 2X q-PCR Mastermix was prepared according to (**Table 2.8**).

Table 2.8: Components of 2X qPCR Mastermix.

Reagent	Volume (ul)
SYBR green Mastermix	5
Nuclease-free H ₂ O	3
Forward Primer	0.5
Reverse Primer	0.5
cDNA	1

SYBR green mastermix, nuclease-free H₂O, forward and reverse primers were added to each well of the 384 well qPCR plate at a total volume of 9µl. Following this, 1µl of cDNA was added to the specified wells followed by centrifugation of the qPCR plate for 2 min at 2000rpm. Applied Biosystems 7900 machine was used to run the qPCR plate using the following cycles (**Table 2.9**).

Table 2.9: q-PCR Conditions

Total Cycles	Reaction Step	Cycle length	Temperature
x1 cycle	Enzyme Activation	10 min	95°C
x50 cycles	Denaturation	15 sec	95°C
	Data Collection	1 min	60°C

The data produced was analysed using $2^{-\Delta\Delta C_t}$ method of relative quantification. Melt-curve analysis was carried out for all primers. Good primers should have one single peak, revealing of one reaction product as shown in **Figure 2.1**.

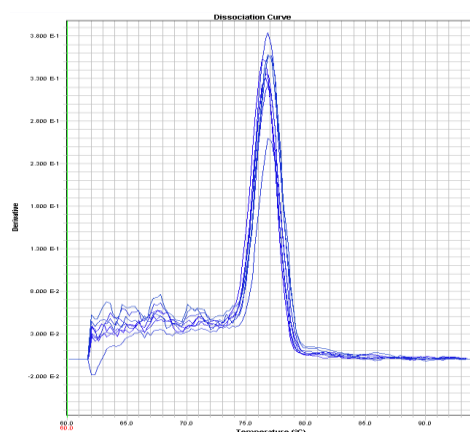


Figure 2.1: shows an example melt curve from a good primer pairs have a single peak. Samples were heated from 60°C to 95°C to create a melt-curve by using qPCR.

2.2.15 Cytokine Protein Level Expression Analysis with Cytokine Bead Array (CBA)

Cells were infected with OV, MAG-OV and MAG alone alongside the control, untreated cells as described in **Section 2.2.12**. After 24h supernatants were collected from each well. CBA was then performed to assess the expression levels of a series of cytokines. These human flex sets were obtained from BD Biosciences and included: IP-10, IL-6, IL-8, TNF, IL-10, IL-1B, IFN-Y and VEGF.

Flow team performed CBA assay. Each BD™ CBA Flex Set contained two vials of Standard and one vial each of Capture Bead and PE Detection Reagent. The formularization of the

Capture Bead and PE Detection Reagent components was carried out to a 50x concentration to confirm product performance when multiplexed. Lyophilisation of The Standard component was also performed and then transferred to a 15 ml polypropylene tube for re-formation. When reconstituted in 4.0 ml Assay Diluent, the standard contained a protein concentration of 10,000 pg/ml. Importantly, the lyophilized standard and other components were stored at 4°C to protect the capture beads and PE Detection Reagent from sustained light exposure. An Attune Autosampler was used to read the samples.

2.2.16 Virus neutralization

Neutralization experiments were performed to determine if MAG could protect OV from neutralizing Antibodies. Sheep anti-HSV-1 antiserum was used to neutralise the OV. This antibody was kindly prepared by Virttu Biologics by four consecutive monthly injections of 1×10^6 PFU HSV1716. To prepare the mixture of OV+NAb or MAG-OV+NAb, 1×10^7 PFU of OV or MAG-OV were incubated with 100-fold dilution of antiserum for 18 h at 4°C (Conner et al., 2005), alongside the controls (no antibody control and no virus control). Combinations (OV+NAb or MAG-OV+NAb) were then transferred to the wells containing monolayers of MDA-MB-231 cells and incubated for 24 hr at 37° C. Flow cytometry was performed to measure cell viability as mentioned in **Section 2.2.12**.

2.2.17 HMGB1 ELISA

The supernatants of infected and uninfected control cells (MDA-MB-231 cells and MCF7) cells were collected and cellular debris removed by centrifugation at 6200 rpm for 5 min. Secreted extracellular HMGB1 in the supernatants was measured with a HMGB1 ELISA Kit II (Shino-Test, Kanagawa, Japan) according to the manufacturer's protocol outlined for the normal sensitivity format of the assay. In brief, 10 µL of supernatant and 100 µL of sample diluent was added to immobilized anti-HMGB1 antibody on the well and incubated for 20-24 hr at 37°C to allow HMGB1 to specifically bind to the antibody. Peroxidase (POD)-conjugated secondary antibody was then added to the sample well. Microplate spectrophotometer was used to read the plates at a wavelength of 450 nm.

2.2.18 ATP assay

The supernatants of infected cells and uninfected control cells were first collected and debris removed by centrifugation at 6200 rpm for 5 min. ENLITEN ATP assay (Promega, Madison, WI, USA) was performed to measure the Secreted extracellular ATP in the supernatants according to the manufacturer's protocol. In brief, 100 µL of supernatant was

added to the 100 μ L of rL/L reagent (ATP reagent). Then, Turner Biosystems luminometer (TD-20/20; Promega) was used to read the plates at a wavelength of 560 nm.

2.2.19 Immunocytochemistry

The expression of calreticulin and appearance of HSV1716 within the cells were measured by immunocytochemistry. Cells (200,000/well) were seeded on small coverslips placed in 24 well plates and cultured overnight with complete medium as mentioned in **Section 2.2.5**. The following day, cells were infected with OV, MAG-OV and MAG alone alongside the control, untreated cells for 24h. The next day, cells were washed 3 times with PBST and fixed by adding 300 μ l of 2% paraformaldehyde (PFA) for 15min (37⁰C at 5% CO₂). After washing, 5% Goat serum and 10% Murine FcR blocking solution in PBST was added for 30 min at RT to block the cells from non-specific binding. Primary Ab -rabbit anti human calreticulin was diluted 1:100 (Abcam, Cambridge, UK) or sheep antiHSV1716 diluted 1:500 (Virtuu Biologics, Glasgow, UK) were added for 1hr at RT then washed 3 times with PBST. This was followed by incubation with e FITC (fluorescein isothiocyanate)-conjugated goat polyclonal antibody diluted 1:100 and appropriate secondary antibodies, diluted at 1:400 in PBST, for 30min at RT then washed 3 times with PBST. 50ng/ml DAPI solution was added for 2 min and then washed another three times with PBST. Finally, coverslips were removed from the wells and 1 drop of ProLong Gold Antifade mountant was added before attaching to glass slides. Slides were then kept in the dark for 1 day and imaged using the Nikon A1 confocal microscope.

2.2.20 *IN VIVO*

2.2.20.1 Murine model of breast cancer

C57BL/6 female mice were purchased from Envigo at 6-8 weeks old and housed in the University of Sheffield Biological Services Unit and cared for according to the University of Sheffield code of ethics and Home Office regulations. All work was carried out under personal licence number is 1806F7C1E and Home office project licence PPL70/8670.

Mice were allowed to acclimatise for 1 week after arrival from the supplier. Mice were injected into the nipple with 5x10⁵ EO771-Luc cells using the following protocol. Inhalant isoflurane (IsoFlo) was used to anaesthetise mice. They were then shaved around the whole abdominal area to expose both nipples (inguinal group) and Hibiscrub was used to disinfect the skin. Following this, 5x10⁵ EO771 cells (which were collected from flasks during their exponential growth phase) in 20 μ l PBS containing 33% matrigel/66% PBS/1% trypan blue) were injected into the nipple using an insulin syringe. Mice were monitored daily and weighed every three

days. Tumour volume was measured using callipers and also recorded every three days using the following equation:

$$\text{Tumour volume (mm}^3\text{)} = \frac{W^2 \times L}{2}$$

For the bioluminescence test, mice were injected with 100 μL of d-Luciferin subcutaneously for 5 Min. Then, a non-invasive *in vivo* imaging system (IVIS 200 System, Xenogen) was used to image mice under isoflurane anaesthesia delivered via a nose cone. Each group of mice included in this study consisted of $n=8$ mice/group. The number of animals were justified by a power calculations using the following equation:

$$n = \frac{\log 0.05}{\log 0.7} = 8.4.$$

Once the tumours reached $\sim 150\text{-}200\text{mm}^3$ mice received the following treatments intravenously (i.v.).

1. **Control:** Mice were injected three times i.v. (0, 5, 10 days) with 100ul PBS.
2. **MAG:** Mice were injected three times i.v. (0, 5, 10 days) with 100ul MAG (10ul MAG + 90ul PBS).
3. **OV:** These mice were injected three times i.v. (0, 5, 10 days) with 100ul HSV1716 (10ul OV at 10^6 pfu + 90ul PBS).
4. **MAG-OV without magnet:** Mice were injected three times i.v. (0, 5, 10 days) with 100ul magnetised HSV1716 (12ul MAG-OV at 10^6 pfu + 88ul PBS).
5. **MAG-OV+ magnet:** Mice were injected three times i.v. (0, 5, 10 days) with 100ul magnetised HSV1716 (12ul MAG-OV at 10^6 pfu + 88ul PBS) in the presence of an external permanent magnetic array secured above the tumour (0.7 T) for 30 min.

Once the tumours reached $\sim 1500\text{mm}^3$ mice were culled by cervical dislocation, and the organs and tumours removed and stored in liquid nitrogen for post-mortem analysis. Of note, the magnet design, assembly and length of time placed above the tumour, were optimised by a post-doctoral research fellow in the group (Dr Priya Patel).

2.2.20.2 HSV1716 *in vivo* neutralisation experiment

Mice were injected into the nipple with 5×10^5 EO771 cells as mentioned in **Section 2.2.20.1**. Once the tumours reached $\sim 150\text{-}200\text{mm}^3$ mice received the following intravenously. The following groups were included in this study with $n=3$ mice/group.

- 1. Control:** Mice were injected three times i.v. (0, 5, 10 days) with vehicle (PBS) (in a volume no more than 0.2 ml).
- 2. OV+ NAb (see section 2.2.19):** Mice were injected three times i.v. (0, 5, 10 days) with 100ul HSV1716 (10ul OV at 10^6 pfu + NAb + 90ul PBS).
- 3. MAG-OV+ NAb (see section 2.2.19) + magnet:** Mice were injected three times i.v. (0, 5, 10 days) with 100ul magnetised HSV1716 (12ul MAG-OV at 10^6 pfu + NAb + 88ul PBS) in the presence of an external magnetic field for 30 min.

Once the tumours reached ~1500mm³ mice were culled by cervical dislocation, and the organs and tumour were removed and stored in liquid nitrogen for post-mortem analysis.

2.2.20.3 Tissue preparation of samples for post-mortem analysis

Immediately following removal from the mice, tumours were divided into two parts. One of them was first dissected into small chunks before placing in cryobuffer (90% FCS with 10% DMSO) and frozen in liquid nitrogen until used for flow cytometry, RNA extraction for qPCR or Nanostring technology.

The other half of the tumours were embedded in Optimal cutting temperature (OCT) and frozen at -80°C in preparation for cryosectioning. Frozen sections (14µM thick) were cut for immunofluorescence staining.

2.2.20.4 Dissociation of EO771 cells tumours

Ice-cold DPBS containing 2% FCS (FACS buffer) was prepared prior to thawing tumour chunks and washing 3 times with DPBS. Tumour chunks were then incubated with 5ml enzymatic dissociation solution containing 0.2 mg/ml collagenase, 2 mg/ml dispase and 1.25ug/ml DNase I in serum-free Iscove's Modified Dulbecco's Medium (IMDM), for 30 min using a rotator in a warm room (37°C). Following this, 10% FBS was added to neutralize the enzymes within the medium and the dispersed specimen was passed through a 40-70µm nylon filter. Once filtered, the cell suspension was then centrifuged at 4500 rpm for 5 min, and the cell pellet was washed 3 times in 500µL DPBS for flow cytometry (see 2.2.20.5) or RNA extraction for qPCR or Nanostring technology (see 2.2.20.7)

2.2.20.5 Preparation of tumour cells for flow cytometry

Tumour chunks were dissociated as mentioned in section 2.2.20.4. The cell pellet was re-suspended in the correctly diluted primary antibody (Ab) and Zombie UV viability dye (1µL in 100µL) and incubated for 45-60 min on ice. 500µL of FACS buffer (50ml DPBS with 25µL

FCS) was then used to wash the samples twice to remove excess unbound antibody and the cell suspension was then centrifuged again in a microcentrifuge at 4500 rpm for 5 min. Finally, samples were re-suspended in 300ul of FACS buffer (1% FBS/PBS solution) and transferred to flow cytometry tubes (400µl). Flow cytometry data was analysed using the BD LSR II flow cytometer. Data files were further processed using FlowJo Software. **Table 2.10** shows the antibodies used to analyse immune cell infiltration into the tumours.

Table 2.10: Antibodies of analysing immune cells infiltration into the tumours

Laser	Filter	Fluorochrome	Markers	Purpose
UV 355nm	450/40	Live/Dead Blue	Viability	Exclude Dead cells
	530/30			
Violet 405nm	450/40	BV421	F4/80	Macrophages cells marker
	530/30	BV510	CD4	T helper marker
Blue 488nm	530/30	GFP	GFP	
	575/26	PE	CD8	Cytotoxic T cells marker
	610/20			
	660/20			
	695/40	PercP-5.5	Ly-6G	Neutrophils cells marker
	780/60	PECy7	CD11b	Myeloid cells marker
Red 633nm	660/20	APC	CD3	Generic T cell marker
	730/45	AF 700	LY-6C	Monocyte cells marker
	780/60	APC/Cy7	NK-1.1	NK cells

A number of different controls were included to help determine if fluorescence was a false positive signal.

1-Compensation control: 100ul PBS+ 1drop negative beads+1drop positive beads (Thermo Fisher Scientific / Cat no: A10344/ USA) +1ul of antibody of interest (each antibody of interest was in a separate tube)

2-FMO (Fluorochrome Minus One): 100ul of the cell suspension + All Abs used in this experiment minus one Ab.

3-SCC (Single Cell Control): 100ul of the cell suspension+ 1ul of only one Ab.

4-Untained: only cells.

As multiple fluorophores were used in this study (**Table 2.11**), fluorescent minus one (FMO) controls were used to detect if fluorescence was emitted because of false positive signals or because of real antibody binding. FMO controls contain all Abs used in this experiment minus

one Ab to determine fluorescent spectral overlap from all the other fluorophores, before measuring the fluorescence of the antibody of interest. Flow cytometry users prefer to use FMO controls because of their hallmark to detect background between all fluorophores (Herzenberg et al., 2006).

Table 2.11: Details of antibodies and controls used in flow cytometry experiments.

Samples	Compensation control	FMO (Fluorochrome Minus One)	SCC (Single Cell Control)
Unstained control	Negative beads		Cells
GFP	Negative beads + positive beads + anti mouse antibody	Cells + all Ab – GFP	Cells + GFP
Viability	Cells+ Zombie UV dye	Cells + all Ab - Zombie UV dye	Cells+ Zombie UV dye
F4/80	Negative beads + positive beads + F4/80 Ab	Cells + all Ab - F4/80 Ab	Cells+ F4/80 Ab
CD4	Negative beads + positive beads + CD4 Ab	Cells + all Ab – CD4 Ab	Cells+ CD4 Ab
CD8	Negative beads + positive beads + CD8 Ab	Cells + all Ab – CD8 Ab	Cells+ CD8 Ab
CD11B	Negative beads + positive beads + CD11B Ab	Cells + all Ab – CD11B Ab	Cells+ CD11B Ab
LY-6G	Negative beads + positive beads + LY-6G Ab	Cells + all Ab – LY-6G Ab	Cells+ LY-6G Ab
CD3	Negative beads + positive beads + CD3 Ab	Cells + all Ab – CD3 Ab	Cells+ CD3 Ab
LY-6C	Negative beads + positive beads + LY-6C Ab	Cells + all Ab – LY-6C Ab	Cells+ LY-6C Ab
NK1.1	Negative beads + positive beads + NK1.1	Cells + all Ab – NK1.1	Cells+ NK1.1

2.2.20.6 Immunofluorescent staining of tumours

Tumours sections were fixed with ice cold acetone for 10 min at RT and then rehydrated with PBST for 1 min. A dark humidified chamber was used for all incubations to prevent fluorescent antibodies from reacting with light. Tissue was surrounded using a Super PAP barrier pen. Following this, 5% Goat serum and 10% Murine FcR blocking solution made in PBST was added for 30 min at RT to block the tissue from non-specific binding. Tissue was then incubated with primary antibodies (**Table 2.12**), for 1hr at RT and then washed 3 times with PBST. Appropriate secondary antibodies (diluted 1:400 in PBST) were then added for 30 min at RT and the tissue was washed 3 times with PBST. Tissue was stained with 50ng/ml DAPI solution for 2 min and then washed another three times with PBST. Finally, before adding coverslips, tissue was mounted with 1 drop of ProLong Gold Antifade mountant. Slides were then kept in the dark for 1 day and analysed using a Nikon A1 confocal microscope. The 40x objective lens was used for imaging and a selection of at least 5 fields of view (FOV) were captured per tumour. Fiji (Fiji Is Just ImageJ), accessed via <http://fiji.sc/Downloads>, as previously published (J. Schindelin et al. 2012) was used to analyse the images.

Table 2.12: Antibodies used in immunofluorescent staining experiment.

Primary Ab	Cat no	Supplier	Conjugate	Dilution	Secondary	Dilution	Laser	Magnification
Calreticulin	505207	Biolegend	Unconj	1 in 100	Anti-rab AF647	1 in 400	647	20x/40x
CD3	20-0031-U100	BD Pharmingen	APC	1 in 200	NA	NA	647	40x
CD31	102515	Biolegend	AF647	1 in 100	NA	NA	647	40x
CD4	100425	Biolegend	AF488	1 in 50	NA	NA	488	40x
CD4	100425	Biolegend	PE	1 in 100	NA	NA	555	40x
CD8	100707	Biolegend	PE	1 in 100	NA	NA	555	40x
F4/80	MCA497A488	AbD Serotec	AF488	1 in 25	NA	NA	488	40x
GFP	ab290	Abcam	Unconj	1 in 1000	Ant-Sheep AF488	1 in 400	488	20x/40x
IFN γ	505809	Biolegend	APC	1 in 100	NA	NA	647	40x
NK-1.1	108723	Biolegend	APC/CY7	1 in 100	NA	NA	647	40x
PD1	135215	Biolegend	PE/CY7	1 in 100	NA	NA	647	40x

2.2.20.7 Haematoxylin and Eosin staining

Tumours sections were fixed in acetone (methanol 50:50 mix (kept in freezer) or methanol only) for 10-20 min. Sections were then washed 2 times in PBS and placed in Gill's Haematoxylin solution for 1 min and washed in tap water for 5 min until the water ran clear. Slides were placed in 70% ethanol for 3 min then 90% ethanol for a further 2 min. Following this sections were placed in eosin (2g eosin dissolved in 400ml 95% ethanol) for 1 min before rinsing slides in 100% ethanol for 5 min. Slides were then mounted using DPX mounting medium. Aperio ScanScope CS with a 40x objective lens was used to scan the slides.

2.2.20.8 NanoString gene expression analyses.

Gene expression profile in EO771 cells tumour samples were carried out at the John van Geest Cancer Research Centre in College of Science and Technology at Nottingham Trent University as part of a collaborative study and analysed using murine pan-cancer immune profiling panel,

which consist of 750 immune related genes, 20 housekeeping genes. All the RNA samples were quality controlled using Nanodrop 8000 and 150ng of total RNA from each samples were used for setting up nanostring probe hybridisation overnight (20hrs) at 65°C (each reaction mixture contains 5ul of RNA solution (150ng), 8ul of reporter probe and 2ul of capture probe). After overnight hybridization, excess probes were removed using nCounter Prep Station and magnetic beads and hybridised mRNA/probe were immobilised on a streptavidin-coated cartridge. The processed cartridge subsequently scanned using an nCounter digital analyser platform for generation of the raw data with a high-resolution scan (555 fov). Raw data were processed with nSolver Analysis Software (V.4.0), imaging quality control (QC), mRNA positive control QC and normalisation QC checked and all the samples were with the quality parameters of nanoString gene expression assays. Differential expression, pathway scoring and cell type scoring was performed using nSolver advance analysis module V. 2.0.115. Normalization of the data was performed using geNorm algorithm for the selection of best housekeeping genes. Genes which showed ≥ 2 , fold change in their expression with a BY (benjamini yekutieli) P value ≤ 0.05 were considered significantly different between the groups.

2.2.21 Statistical analysis

All statistical analysis was performed using GraphPad Prism (GraphPad Inc, San Diego, CA, USA). Data are expressed as mean and SEM. Statistics were analysed utilizing the suitable statistical test and post-test as described in the figure legends. Statistically, a p value of $p < 0.05$ was deemed significant.

Chapter 3

Characterisation of MAG-OV

3.1 Introduction

Cancer nanotechnology is a relatively new branch of medicine that is currently going through intense phases of development for cancer imaging, molecular and cellular diagnosis and for targeted therapies (Gharpure et al., 2015). The potential of MNPs for application in drug delivery and for the diagnosis of tumours is established (Kim et al., 1999, Kataoka et al., 2000). The development of multifunctional MNPs for the delivery of both drugs and MRI contrast agents for malignancies is now possible for tumour theranostics (Torchilin, 2006, Kim et al., 2008, Peer et al., 2007). In addition, MNPs offer many opportunities, that allow for the combination of magnetic resonance imaging (MRI) as contrast agents and active delivery of chemotherapeutics in one nanocarrier system, representing a novel strategy in nanomedicine (Nasongkla et al., 2006). MNPs are therefore attractive for the navigation of drugs into tissues from circulation in response to application of a magnetic field. The magnetic targeting of drugs results in an increased concentration of the drug within the tissue/organ of interest and consequently reduces the side effects such as toxicities as a result of systemic drug delivery. Superparamagnetic iron oxide (SPIO) have magnetic properties which can be used for MRI as a contrast agent and for the detection and characterization of tumours within the body. The magnetic properties of SPIOs has also been used to magnetically guide drugs to a specific tissue. This has led to the development of MNPs that can be used not only as MRI contrast agent but their ability to respond to magnetic field enables magnetic hyperthermia and magnetic drug targeting to diseased tissue (Senyei et al., 1978, Neuberger et al., 2005). Previous studies have shown that conjugation of MNPs with anticancer agents e.g. doxorubicin (DOX) and methotrexate (MTX) resulted in an increase in the accumulation of the drug in HeLa cells and B-cells by applying an external magnetic force (Samra et al., 2013). They also found that Sixteen to 22% more killing effect was observed on HeLa cells than in B cells. Clinical studies using chemotherapeutics coated with MNPs have also been performed in cancer patients. The first clinical trial in humans using MNPs linked to doxorubicin were reported in 14 patients with advanced solid liver cancer. The authors found that the MNPs accumulated in the targeted tissue and were safe and not toxic (Lubbe et al., 1996). This type of magnetic targeting could therefore provide an opportunity to use less of a potentially toxic drug but still obtain higher drug concentration at the tissue of interest.

MAG are becoming increasingly recognized as important tools in cancer treatment. These particles have the potential to 1) target therapy to the tumour site due to the magnetic core 2) improve binding to the target by displaying receptors or recognition molecules 3) kill tumours

if they carry a therapeutic payload. Moreover, the MAG can be imaged using conventional MRI enabling the therapy to be tracked in real-time. A study by Mahmoudi and colleagues showed that MAG derived from magnetotactic bacteria *Magnetospirillum magneticum* strain AMB-1 could be used to label and image pluripotent stem cell (iPSC)-derived cardiomyocytes (iCMs) for the regeneration of the injured myocardium in mice. The MAG-labelled iCMs were injected into the infarcted area of the murine heart and imaged by MRI. They showed that MAG were robust biological contrast agents to track iCMs in mice. More importantly, they were cleared within one week of injection whereas SPIONs remain over 2 weeks (Mahmoudi et al., 2016). MAG, may therefore be an excellent alternative. MNPs also provide the opportunity to track therapeutics with imaging modalities, which is not possible with current cancer treatments. Furthermore, biocompatibility, chemical stability and magnetic properties are considered very important for diagnostic application (Almstätter et al., 2015). It is, therefore, important to further understand the physicochemical characterisation of these particles.

MAG have also been used to deliver anticancer medicines doxorubicin (DOX) in H22 cell-bearing mice (Sun et al., 2011). They found that the tumour suppression rates following administration of DOX-loaded Bacterial MAG (DBMs), DOX, and Bacterial magnetosomes (BMs) were 86.8%, 78.6%, and 4.3%, respectively. DBMs, DOX, and BMs revealed mortality rates of 20%, 80%, and 0%, respectively. Pathological examination of hearts displayed that DBMs revealed a much lower cardiac toxicity compared with DOX.

Oncolytic virotherapy is an emerging treatment modality that uses replication-competent viruses to destroy cancers whilst leaving healthy cells unharmed. Success of using these viruses has relied on direct intratumoural injection, however to target tumours deep in the body or metastasis it is necessary to deliver virus in circulation. So far, systemic delivery of OV has been hampered by low intra-tumoural titres due to strong anti-viral host immune responses and sequestration by the liver and spleen resulting in poor tumour targeting (Ferguson et al., 2012). We propose to use magnet targeting like that described above for improving the targeting of OV to tumours after systemic delivery. A recent study showed that MNPs (PEI-Mag2 or SO-Mag6-11.5) could be used to form stable complexes with OV by self-assembly (Almstätter et al., 2015b). This relies on electrostatic interaction of negatively charged viral particles and positively charged MNPs. They found that the virus dose required for 50 % cell growth inhibition/oncolysis (IC₅₀) values of the MNP-VP complexes in 7.5 % FCS under magnetic field-guided infection were 1.6- and 2.5-fold lower for VSV, and 11.8- and 27.4-fold lower for

Ad, respectively, than those of the virus alone in McA and RDB cells, confirming the higher oncolytic activity of the MNP-VP complexes. Understanding the oncolytic potential and the cell death mechanisms of OV is a rapidly evolving field. For the purposes of this work, we performed experiments to investigate the effects of MAG-OV in breast cancer 2D and 3D tumours spheroids and compared this to OV. Oncolytic HSV1716 has previously been shown to reduce viability of tumour spheroids (SF188, KNS42, DIPG) 72 and 96 hr post-infection (Cockle et al., 2017).

The aim of this chapter was to magnetise the OV 'HSV1716' using MAG derived from magnetotactic bacteria and characterise the physicochemical and biological properties of the final complex (MAG-OV). The specific aims are to:

1. Determine the physicochemical properties and toxicity of the bacterial derived magnetosomes (MAG) in breast cancer cell lines.
2. Prepare the MAG-OV and measure the physicochemical properties.
3. Measuring the Oncolytic potential of magnetic viral complexes on breast cancer cells.

3.2 Results

3.2.1 Characterization of bacterial derived MNPs

The properties and physicochemical characteristics of these particles was assessed. We used AMB-1 derived MAG purified using established protocols (Staniland et al., 2007). In brief, AMB-1 was grown in a cabinet within microaerobic conditions consisting of 1% O₂ and 99% nitrogen at 30.1 C° in liquid culture medium (see Section 2.2.1.2) which is specific to AMB-1 bacteria. The lysed AMB-1 cells were sonicated for 1 hour using microprobe tip sonication (Sonics USA). After the sonication a neodymium magnet was used to separate the MAG from other cellular debris. 10mM Tris-HCl buffer (pH 7.4) was used to wash the MAG four times followed by resuspension in DPBS (pH 7.4). The properties of the purified MAG are shown in **Table 3.1**. The MAG were typically small in diameter ($46 \pm 5\text{nm}$) as assessed by TEM. The electrokinetic potential (ζ) was also assessed to determine the charge of the particles. MAG displayed a negative electrokinetic potential (ζ) ($-9 \pm 2.3\text{ mV}$) on the membrane most likely a result of the lipid composition and the occurrence of polarizable primary amino groups (Tanaka and Matsunaga, 2000) this was measured using NanoBrook Zeta PALS (**Table 3.1**). This means that MAG tend to coagulate or flocculate, possibly leading to poor physical stability. Magnetic susceptibility is a measure of the magnetic properties of the particles which will be important when considering their targeting potential in response to a magnetic field. This is

measured in System International (SI) units as a function of iron mass (mgFe). MAG displayed high magnetic susceptibility (8.164×10^{-5} SI) and the iron content of the MAG was (0.17mg/l).

Table 3.1: The physicochemical properties of MAG purified from magnetospirillum magneticum AMB-1. Data are derived from N=3 independent experiments.

Samples	Diameter (nm)	Electrokinetic potential (mv)	Magnetic susceptibility (SI)	Iron content (mg/l)
MAG	46 ± 5	-9 ± 2.3	8.164×10^{-5}	0.17 ± 0.5

The morphological characteristics and size distribution of the MNPs was determined using high-resolution transmission electron microscopy (HRTEM). The diameter of MAG was typically (46 ± 5 nm). qNano does not measure below 50 nm and so results data is based on TEM images. Interestingly, MAG have a much more uniform diameter compared to synthetic MNPs (Almstätter et al., 2015a) where there is a significant variation in the diameter between individual particles in the same sample. TEM images of magnetotactic bacteria and purified MAG are shown in **Figure 3.1**. Next, we assessed the uptake of the MAG by tumour cells.

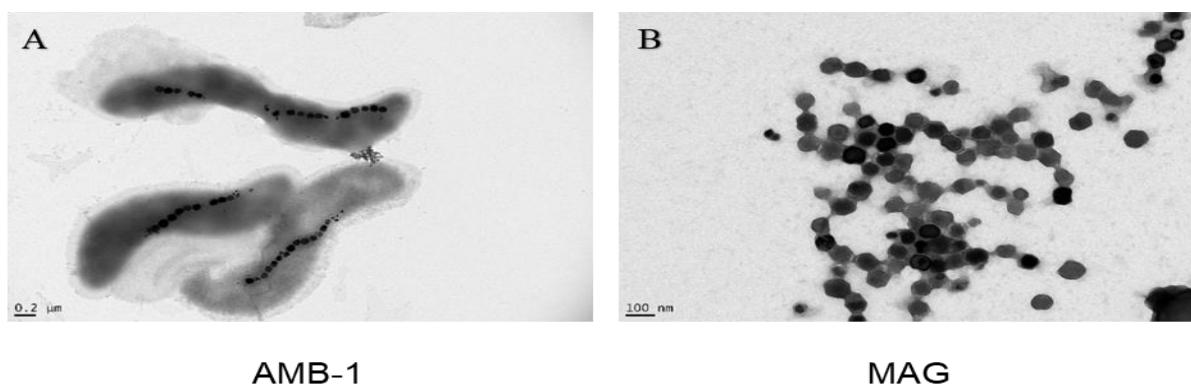


Figure 3.1: High-resolution Transmission electron microscopy of magnetotactic bacteria and purified MAG. **A.** TEM images of AMB-1 magnetotactic bacteria, grown in micro-anaerobic conditions in 1% O₂ gas and 99% nitrogen at 30.1 C° in liquid culture medium which is specific to AMB-1 bacteria (scale bar-0.2um). **B.** MAG purified from AMB-1 were sonicated prior to TEM and mounted onto carbon-coated copper grids. The MAG displayed a typical cuboidal crystal shape with uniform size of ~46nm diameter (scale bar-100nm). Images were taken on a TEM operated at 120kV with an Orius 1000 camera.

3.2.2 Breast cancer cell internalisation of MNPs

MDA-MB-231 is a triple negative breast cancer (TNBC) cell line; patients with TNBC are resistant to chemotherapy and most hormonal therapies so have limited treatment options (Lee et al., 2011). This cell line has been used in our studies with an aim to develop new treatments

for this patient group. In the first instance, MDA-MB-231 cells were incubated with MAG at a concentration of 0.2 mg/ml for 24h. This concentration was selected based on previous studies carried out by Mannucci and coworkers, they showed that HT-29 cells were able to effectively internalise MAG at concentration 0.2 mg/ml for 24h among the different concentrations tested (ranging from 0.2 to 1 mg/ml) using Prussian Blue staining (Mannucci et al., 2014). The degree of MAG uptake into cells was assessed by flow cytometry where a change in granularity of the cells because of taking up the MAG was detected based on changes in the side scatter. This was also confirmed by immunostaining the iron particles within the cell using the gold standard stain for iron 'Prussian blue' (Muthana et al., 2008a).

As shown in **Figure 3.2A**, MDA-MB-231 cells were able to effectively internalise MAG $\sim 43\% \pm 4$ ($P \leq 0.01$) compared to the control untreated cells (0 %). To confirm intracellular MAG uptake, MDA-MB-231 cells were grown on coverslips and incubated with MAG (0.2 mg/ml) for 24 hr. After this, cells were fixed in 200 μ l of acetone at 4°C for 10 min and stained with Prussian blue to detect iron and counterstained with eosin to define the cytoplasm (Brace et al., 2009, Arcangeli et al., 1980). Coverslips were mounted onto microscope slides and light microscopy was used to take images. As shown in **Figure 3.2B** MAG were internalised by the MDA-MB-231 cell line and multiple particles were present within the cytoplasm of cells. It was difficult to quantify the number particles/cell, as the signal from the Prussian blue stain was very strong. Convinced that MAG entered the cells, next we investigated cell viability after uptake.

MTT test was also used to estimate the viability of cells in longer-term cultures of the MNPs. This colorimetric test estimates the decrease of yellow 3-(4,5-dimethylthiazol-2-yl)-2,5-diphenyl tetrazolium bromide (MTT) via mitochondrial succinate dehydrogenase. While a decrease of MTT can only happen in metabolically active cells, the level of activity is a measurement of cell viability. MDA-MB-231 cells were incubated with MAG at a concentration of 0.23 mg/ml for 72 hr. After that, MTT reagent was added to each well followed by incubation for a further 3 hr. Cell death/viability was measured spectrophotometrically at 570nm. As shown in **Figure 3.2B**, and in concurrence with the flow cytometry data, there was no significant effect on cell viability for MAG compared to the control.

Together these data suggest that the MDA-MB-231s efficiently take up bacterially-derived MAG without any significant toxicity to the cells.

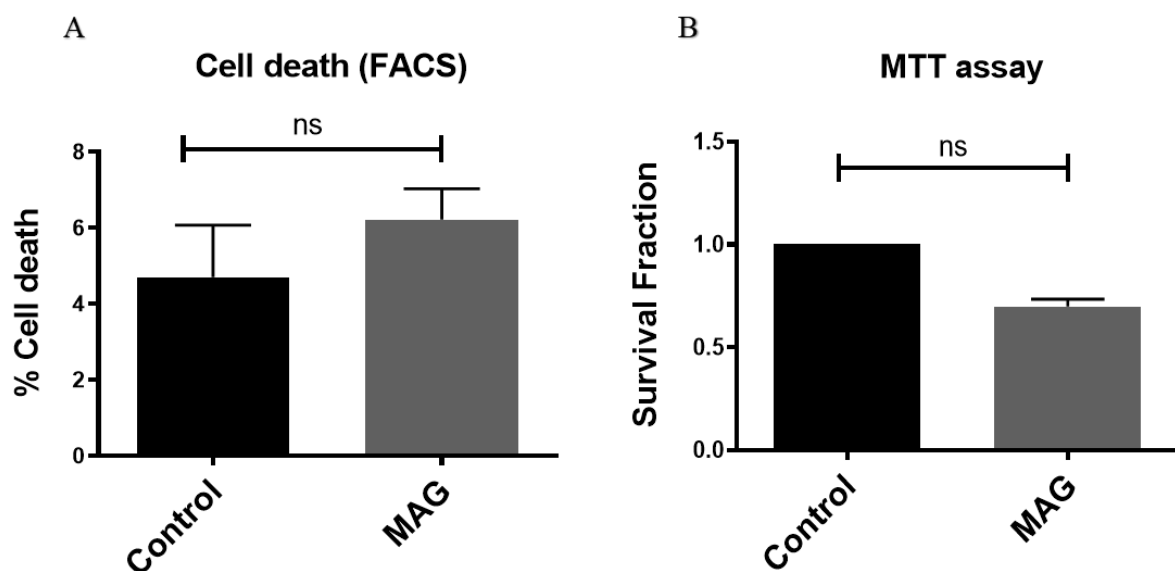


Figure 3.3: MDA-MB-231 remain viable after incubation with MAG. MDA-MB-231 cells were incubated with purified MAG for 24 hr. Cells were collected and flow cytometry as used to evaluate cell death by the addition of PI immediately prior to analysis. **A.** Cell death (PI+ cells) in the presence of MAG was not significant when compared to the control. **B.** MTT assay also revealed no significant change in cell viability in the presence of MAG. Of note, data are the Mean \pm SEM (n=3) and statistical analysis was assessed using the T test.

3.2.4 Characterization of MAG-OV

Here we set out to prepare and characterise MAG-OV complexes. 200ul of DPBS containing 0.22mg MAG and 1 mL of PBS containing 1×10^8 pfu OV were suspended in a final volume

of 1.2 ml (0.2mg/ml MAG and 1×10^8 pfu OV). Following this, complexes were incubated for 20 min at RT. This is shown as a schematic in **Figure 3.5**.

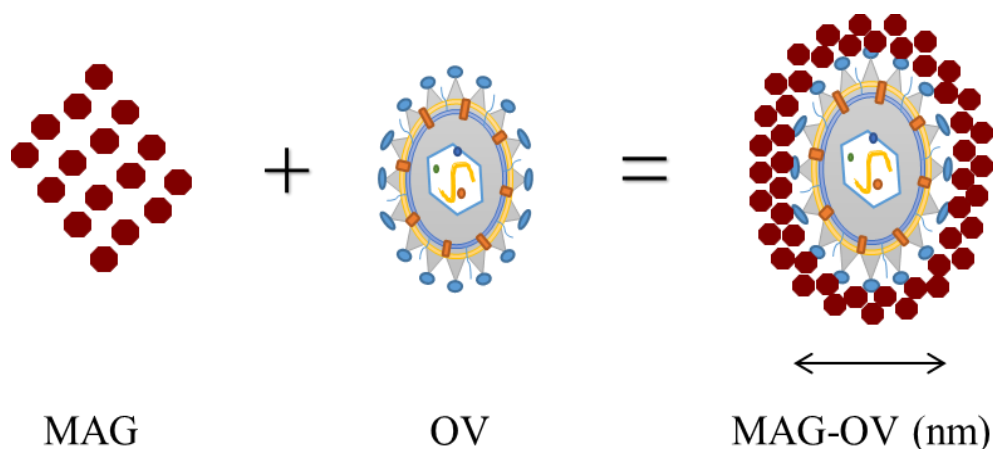


Figure 3.4: Diagram of the self-assembly of MAG and OV. To prepare the complexes, 200ul of DPBS containing 0.22mg MAG and 1 ml of PBS containing 1×10^8 pfu OV were suspended in a final volume of 1.2 ml (0.2mg/ml MAG and 1×10^8 pfu OV). Following this, complexes were incubated for 20 min at RT. These were stored at 4°C or used immediately.

We first measured the charge of the magnetic viral complexes using NanoBrook Zeta PALS. Co-assembly of MAG with OV (MAG-OV) resulted in a net negative charge (MAG-OV $\zeta = -11 \pm 5$ mV). Of note, a net negative charge was detected with free OV ($\zeta = -13 \pm 2.1$ mV). The magnetic susceptibility of the MAG-OV complexes were slightly lower compared to respective unbound MAG (MAG-OV=5.438e-5 SI) as shown in **Table 3.2**. As expected, MAG-OV was larger compared to the OV and free MAG (MAG-OV Diameter = 160 ± 20 nm) see **Table 3.2** and **Figure 3.5**.

Table 3.2: The physicochemical properties of the OV and MAG-OV. N=3

Samples	Diameter (nm)	Electrokinetic potential (mv)	Magnetic susceptibility (SI)
OV	60 ± 10	-13 ± 2.1	-
MAG-OV	160 ± 20	-11 ± 5	5.438e-5

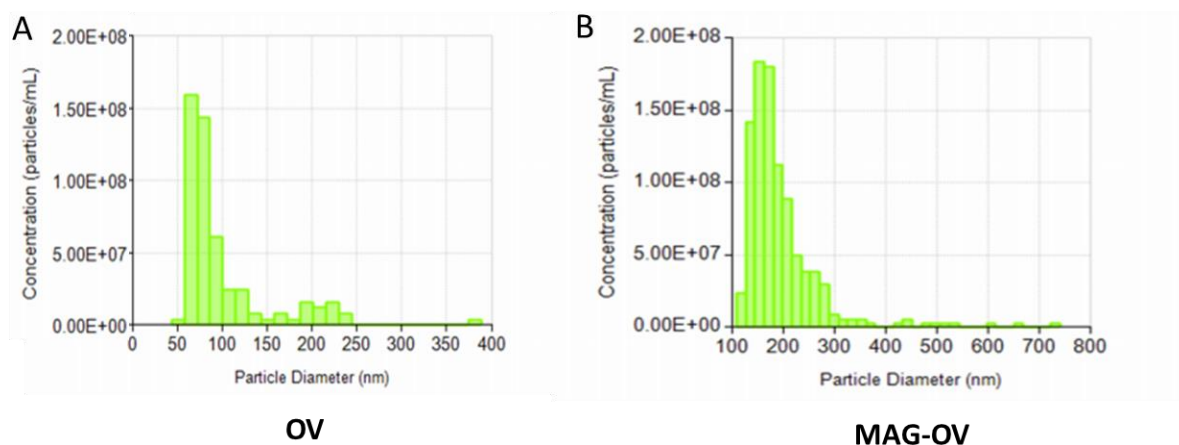


Figure 3.5: The size distribution of the OV and MAG-OV. The size distribution of OV and MAG-OV were determined by Tunable Resistive Pulse Sensing (TRPS) using a qNano instrument (Izon). Graphs show representative diameter data of **A.** OV **B.** MAG-OV. This is experiment was performed N=1 in triplicate.

Typically, TEM images revealed that multiple MAG surrounded a single virus and this tended to form clusters of the complex (**Figure 3.6**). We were unable to detect any uncoated virus in the samples. The same MAG-OV complex was imaged by TEM after 72h storage at 4⁰C to determine if the complexes were stable. This data showed that the complexes were still intact (**Figure 3.6**).

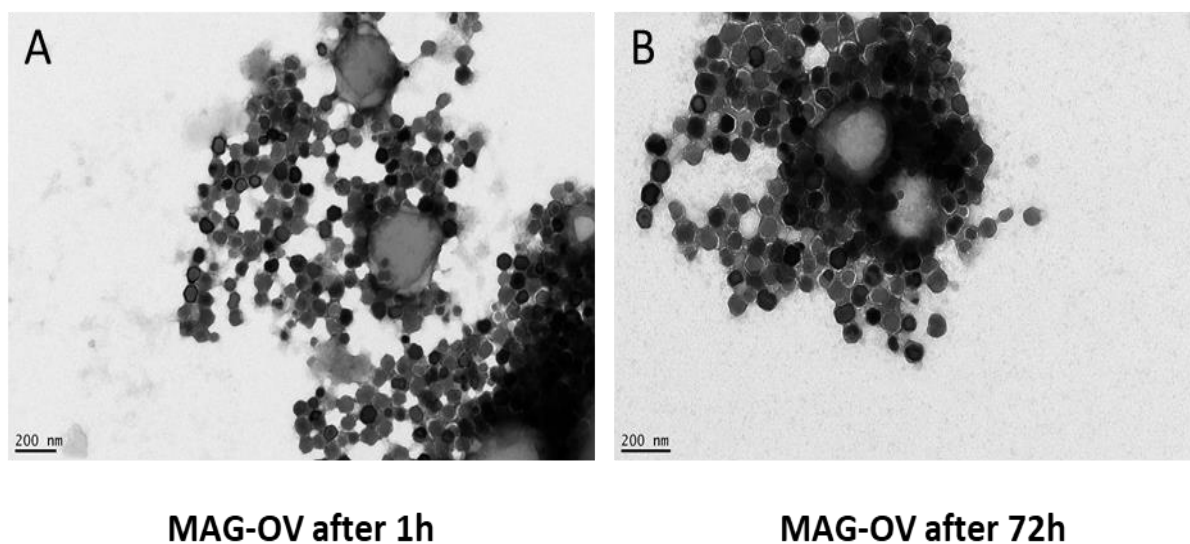


Figure 3.6: TEM images showing stability of MAG-OV over time. Samples containing virus were counterstained with 1% phosphotungstic stain, this is a common negative stain for viruses including HSV. Images were taken on a TEM operated at 120kV with an Orius 1000 camera. **A.** Representative image of MAG-OV after 1h of incubation and **B.** After 72h, to show the stability of complexes. The scale bars are 200 nm.

3.2.5 Transmission electron microscopy of MAG-OV cell internalisation.

TEM was also performed to investigate the intracellular localization of MAG-OV. Infected tumour cells (10^5) were prepared as described in (section 2.2.14.1.2). **Figure 3.7** shows images of MAG-OV internalisation in MDA-MB-231 cells. MAG-OV were observed to cluster in the cytoplasm or in the vesicles of the cell (e.g. Endosomes). Interestingly, free OV were seen throughout the cytoplasm and MAG were located within the endosomes. This suggests that once inside the cell the OV is able to free itself from the MAG. Therefore, in the next section we investigated the oncolytic potential of MAG-OV.

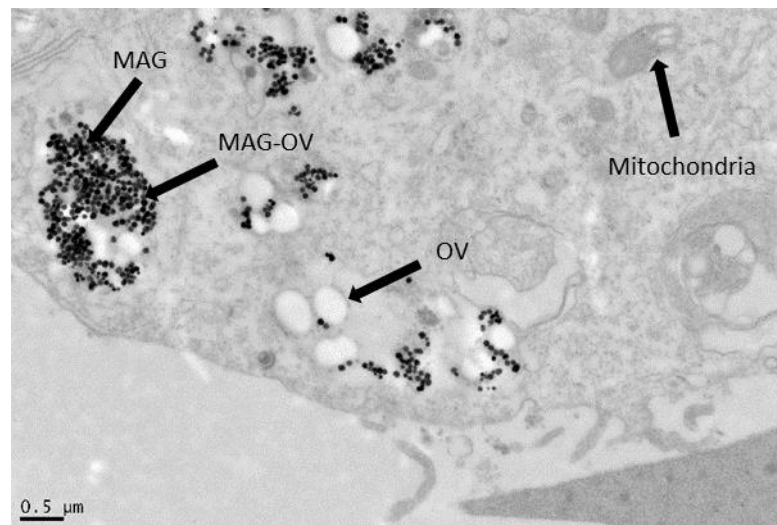


Figure 3.7: TEM images of MAG-OV inside MDA-MB-231 cells. Representative image of MAG-OV in the cytoplasm or in the endosomes of MDA-MB-231 cells. Arrows show MAG within the cytoplasmic vesicles. Free OV can be seen throughout the cytoplasm. Images were taken on a TEM operated at 120kV with an Orius 1000 camera. The scale bars are 0.5 μ m.

3.2.6 MAG-OV induce MDA-MB-231 cell oncolysis

MDA-MB-231 cells were seeded into 6-well plates (3×10^5 cells/well) and after 24 hr, cells were infected with either the OV on its own or MAG-OV at MOI 10 (selected based on previous studies in our lab), MAG and non-infected cells were used as controls. For these studies we used the reporter virus HSV1716-GFP so that the GFP could be used to confirm virus infection. After 1, 3 and 6 days of culture with the viruses, plates were harvested and flow cytometry was used to analyze the cells. The level of viral infection was measured as the percentage of GFP (+)/Topro-3(-) cells. In these studies, TOPRO3 was used as a viability dye where dead/dying cells take up the dye but live cells exclude it. As shown in **Figure 3.8**, MAG-OV was able to infect the tumour cells as efficiently as the naked OV with no differences between these groups after 24h of culture. GFP expression was markedly reduced by day 6 of culture in all the treatments groups compared to the control and MAG groups (**Figure 3.8**).

This decrease in GFP expression was most likely because of cell death and indeed statistically significant cell death was observed with both MAG-OV and OV, compared to the control group at day 3 and 6 (**Figure 3.9**). As expected, cell death increased over time with maximum death measured at day 6 of culture. As shown in **Figure 3.9**, MAG-OV was not significant at 1, 3 and 6 days of culture compared to virus alone.

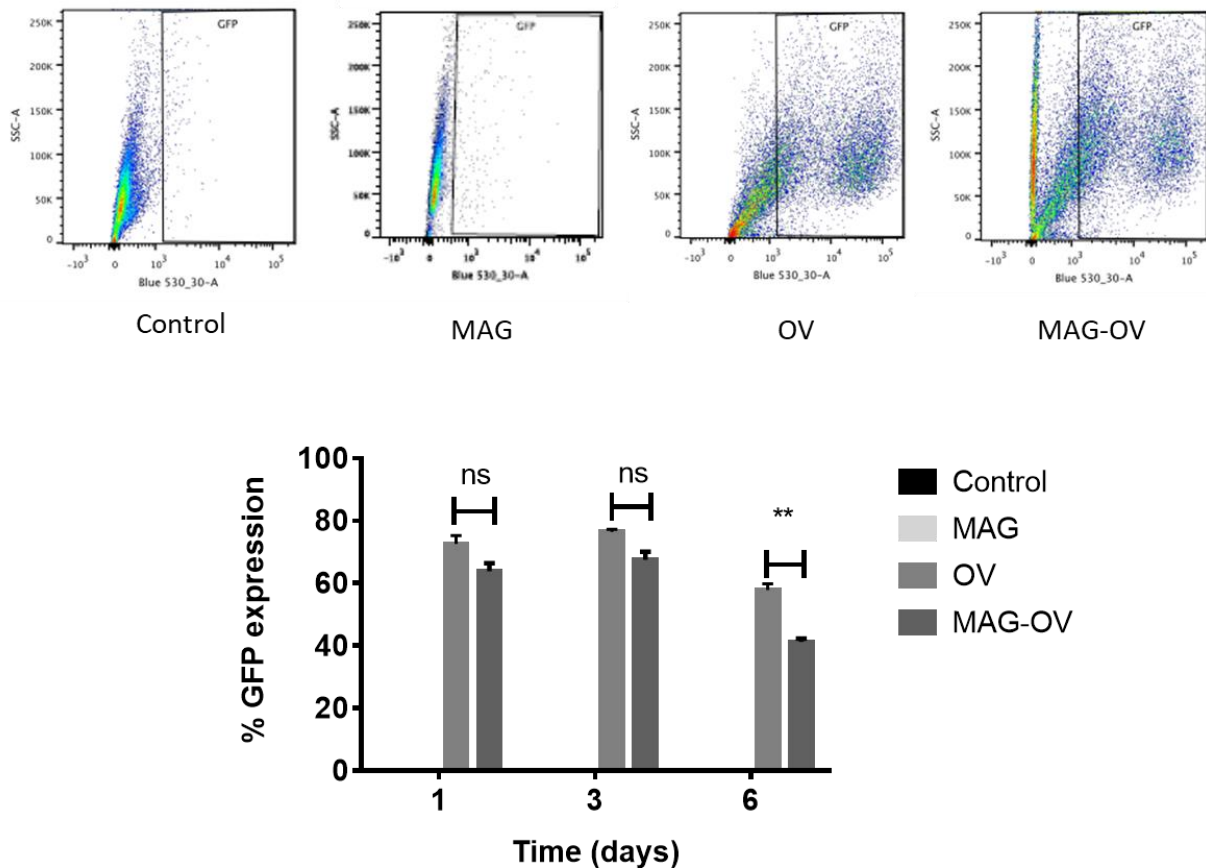


Figure 3.8: MAG-OV induce MDA-MB-231 cell oncolysis. Representative fluorescent dot plots of GFP expression following 24h incubation of MBA-MB-231 cells with OV, MAG-OV (at MOI 10), MAG and untreated control cells. Cells were harvested and immediately before analysis on a flow cytometer (machine type LSRII) 2ul of TOPRO-3 was added to each sample. GFP expression was measured in FL-1 (488nm). GFP infection was also assessed on day 3 and 6 post-infection. Of note, all dead cells were gated out of the GFP analysis. Data are the mean \pm SEM of n=3 independent experiments and statistical analysis was assessed using the two-way Anova test with multiple comparisons. **p<0.01.

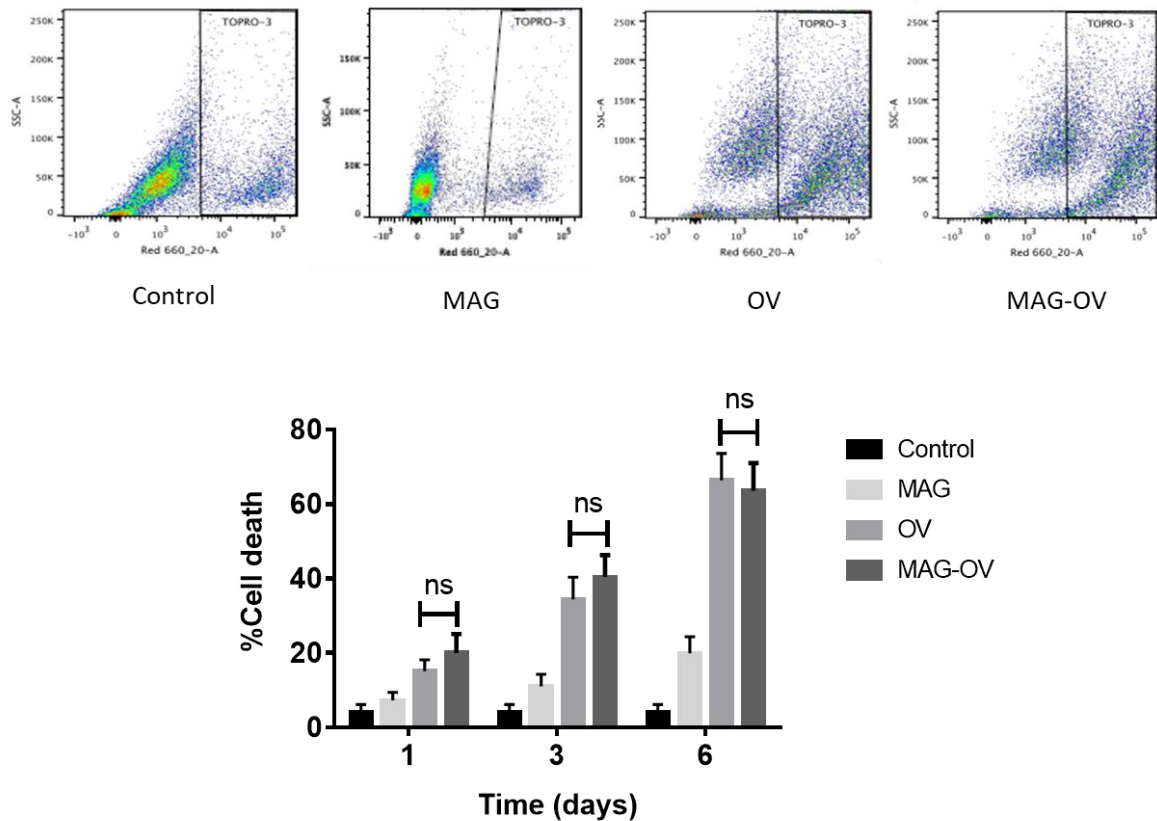


Figure 3.9: MAG-OV induce MDA-MB-231 cell oncolysis. Representative dot plots of cell death following 24h incubation of MDA-MB-231 cells with OV, MAG-OV (at MOI 10), MAG and untreated control cells. Cells were harvested and immediately before analysis on a flow cytometer (LSRII) 2ul of TOPRO-3 was added to each sample. TOPRO-3 was measured in the FL-4 (640nm). Cell death was also assessed on day 3 and 6 post-infection. Of note, data are the mean \pm SEM of n=3 independent experiments and statistical analysis was assessed using the two-way Anova test with multiple comparisons.

3.2.7 MAG-OV induce MCF7 cell oncolysis

Here the oncolytic ability of OV and MAG-OV on another breast carcinoma cell line, MCF7 (originally derived from human Caucasian breast adenocarcinoma patient), was assessed. 3×10^5 cells were seeded into 6-well plates and infected with OV and MAG-OV at MOI 10, MAG and non-infected cells were used as controls. Cells were incubated for different periods (1 day, 3 days and 6 days) and analysed by flow cytometry. Cell death was measured as Topro-3(+) cells; virus uptake in living cells was measured as GFP (+)/Topro-3 (-) cells. After infection (1, 3 and 6 days). There was no significant difference between the OV and MAG-OV infection (**Figure 3.10**). On the other hand, statistically significant levels of cell death were observed with MAG-OV and OV compared to controls (**Figure 3.11**). Moreover, MAG-OV cell death levels were similar to virus naked cell death at all-time points (1, 3 and 6 days).

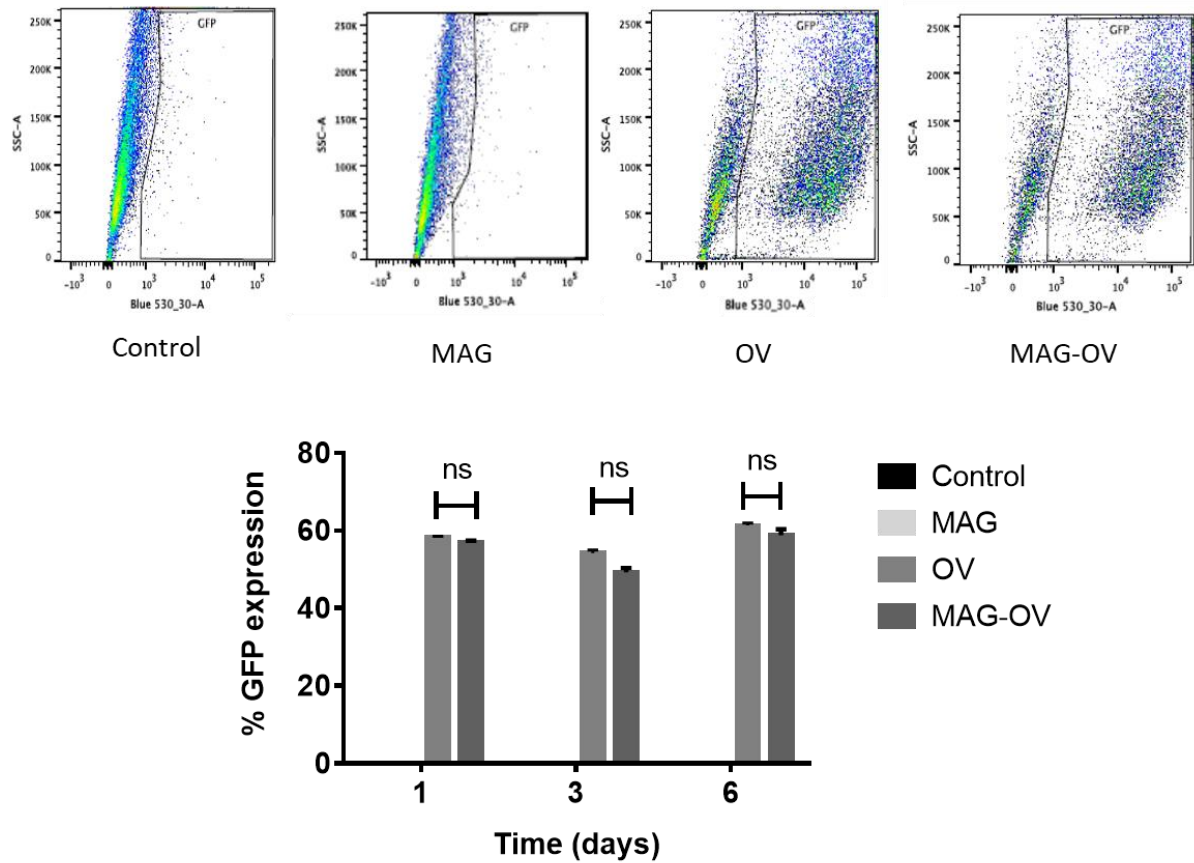


Figure 3.10: MAG-OV induce MCF7 cell oncolysis. Representative fluorescent dot plots of GFP expression following 24h incubation of MCF7 cells with OV, MAG-OV (at MOI 10), MAG and untreated control cells. Cells were harvested and immediately before analysis on a flow cytometer (LSR, II) 2ul of TOPRO-3 was added to each sample. GFP expression was measured in FL-1 (488nm). GFP infection was also assessed on day 3 and 6 post-infection. Of note, all dead cells were gated out of the GFP analysis. Data are the mean \pm SEM of n=3 independent experiments and statistical analysis was assessed using the two-way Anova test with multiple comparisons.

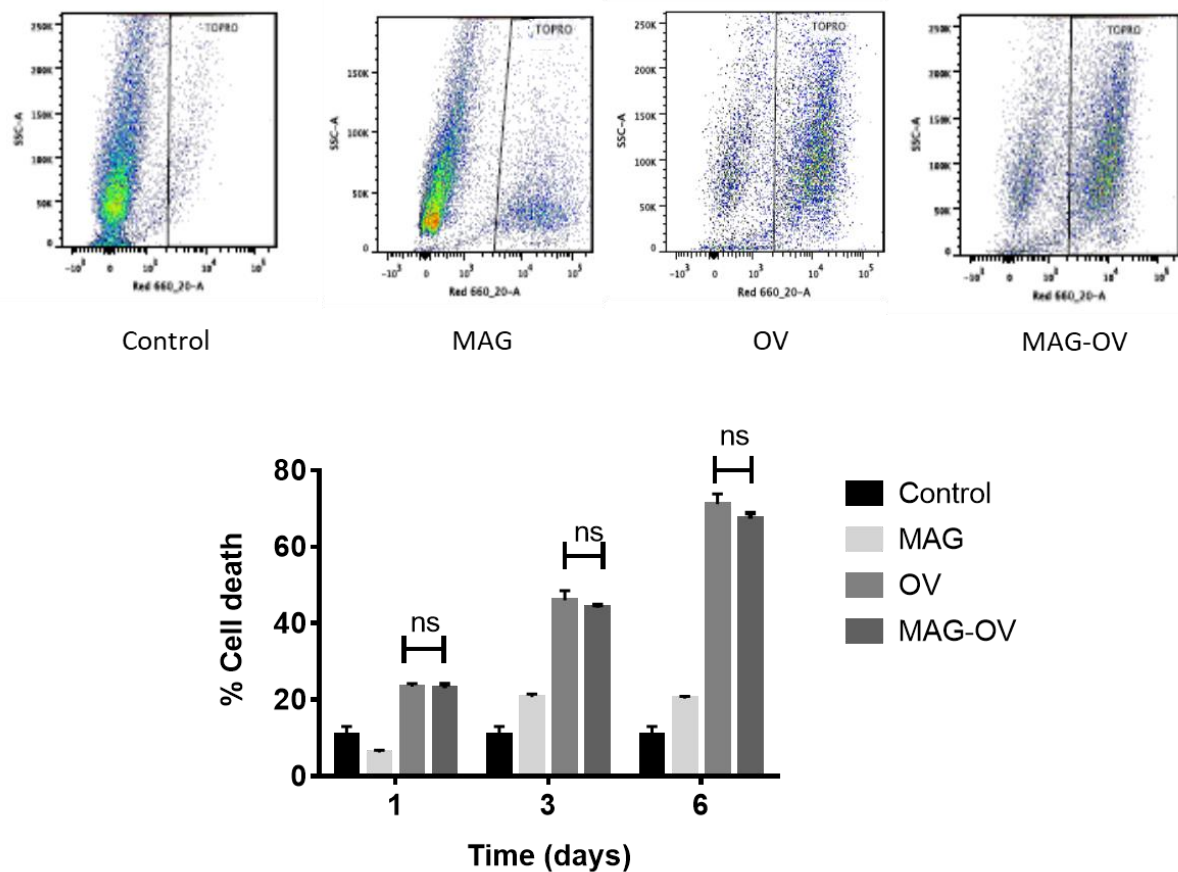


Figure 3.11: MAG-OV induce MCF7 cell oncolysis. Representative dot plots of cell death following 24h incubation of MCF7 cells with OV, MAG-OV (at MOI 10), MAG and untreated control cells. Cells were harvested and immediately before analysis on a flow cytometer, 2ul of TOPRO-3 was added to each sample. TOPRO-3 was measured in the FL-4 (640nm). Cell death was also assessed on day 3 and 6 post-infection. Of note, Data are the mean \pm SEM of n=3 autonomous trials and statistical analysis was assessed using the two-way Anova test with multiple comparisons.

3.2.8 MAG-OV induced tumour spheroid cell death

2D cell cultures contrasts significantly with 3D cultures in nutrient access, cell-cell interaction and cellular mechanics (Edmondson et al., 2014). Spheroids were prepared as described in **Section 2.2.16**. The use of 3D spheroids has the benefit of having established oxygen-exhausted central zones surrounded by a well-oxygenated region, mimicking small micro-metastasis (Muthana et al., 2011a). One of the most hallmark uses of 3D cell cultures is the ability to replicate some of the same behaviour of *in vivo* conditions. Therefore, we performed experiments to investigate the effects of MAG-OV in breast cancer 3D tumours spheroids. Tumour spheroids were prepared with the human cancer cell lines MDA-MB-231 and MCF7 cells (2×10^4 cells seeded onto 2% agarose-coated 96-well plates). Five days later (day 5), spheroids were infected with OV and MAG-OV at MOI 10 and incubated for a further 6 days;

non-infected spheroids were used as controls. In these studies, light microscopy images were taken after 6 days of infection, to image changes in the shape of spheroids. We observed that MAG-OV elicited as much damage to the MDA-MB-231s (**Figure 3.12A**) and MCF7 spheroids cells as the OV group (**Figure 3.13A**). Spheroids were harvested and washed after 3 days of infection and cell viability of enzymatically-dispersed spheroids was analysed by flow cytometry. As expected the OV and MAG-OV groups showed significant cell death compared to the control spheroids in both MDA-MB-231 and MCF7s (**Figure 3.12B & Figure 3.13B**).

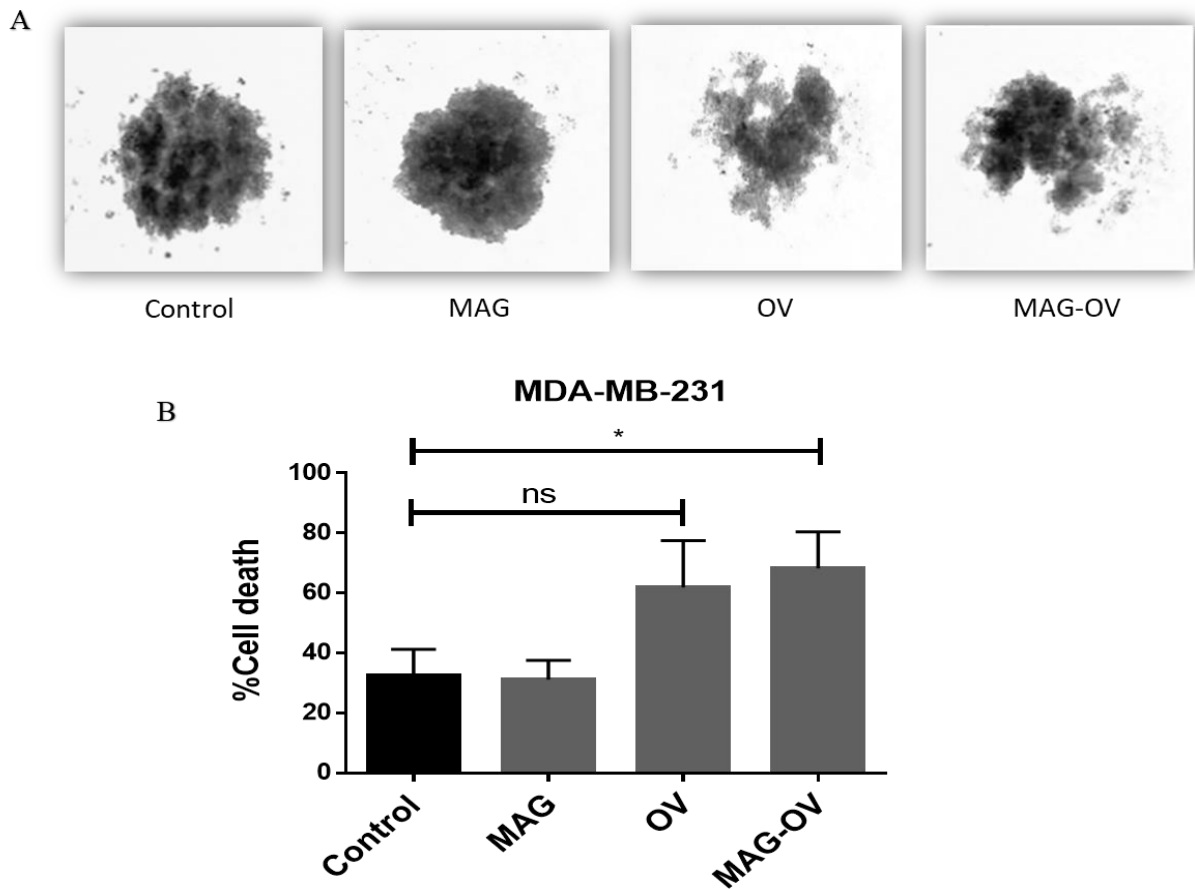


Figure 3.12: MAG-OV infects and kills MDA-MB-231 spheroids. Tumour cells were seeded into wells of a 96 well plate, that contained agarose dissolved in DMEM, at 20×10^3 cells per well and the approximate size they grow to was 10^5 cells. After 5-7 days of seeding OV or magnetic viral complexes (MAG-OV) were added to the spheroids as described in **section 2.2.15**. **A.** shows MAG-OV and OV increased the necrotic core of MDA-MB-231 spheroids. Images were taken by light microscopy 6 days' post infection. This was taken at 10x Magnification. **B.** Infection with OV and MAG-OV induced tumour spheroid cell death. Representative fluorescent dot plots of dispersed MDA-MB-231 Spheroids. TOPRO3+ cells were measured by flow cytometry 3 days' post-infection. The percentage of cell death is shown (TOPRO-3+). While no significant changes in viability were detected between OV and MAG-OV, both virus groups induced significant cell death compared to the control untreated spheroids. Data are the mean \pm SEM of $n=3$ independent experiments and statistical analysis was assessed using the one-way Anova test with multiple comparisons. * $p<0.05$.

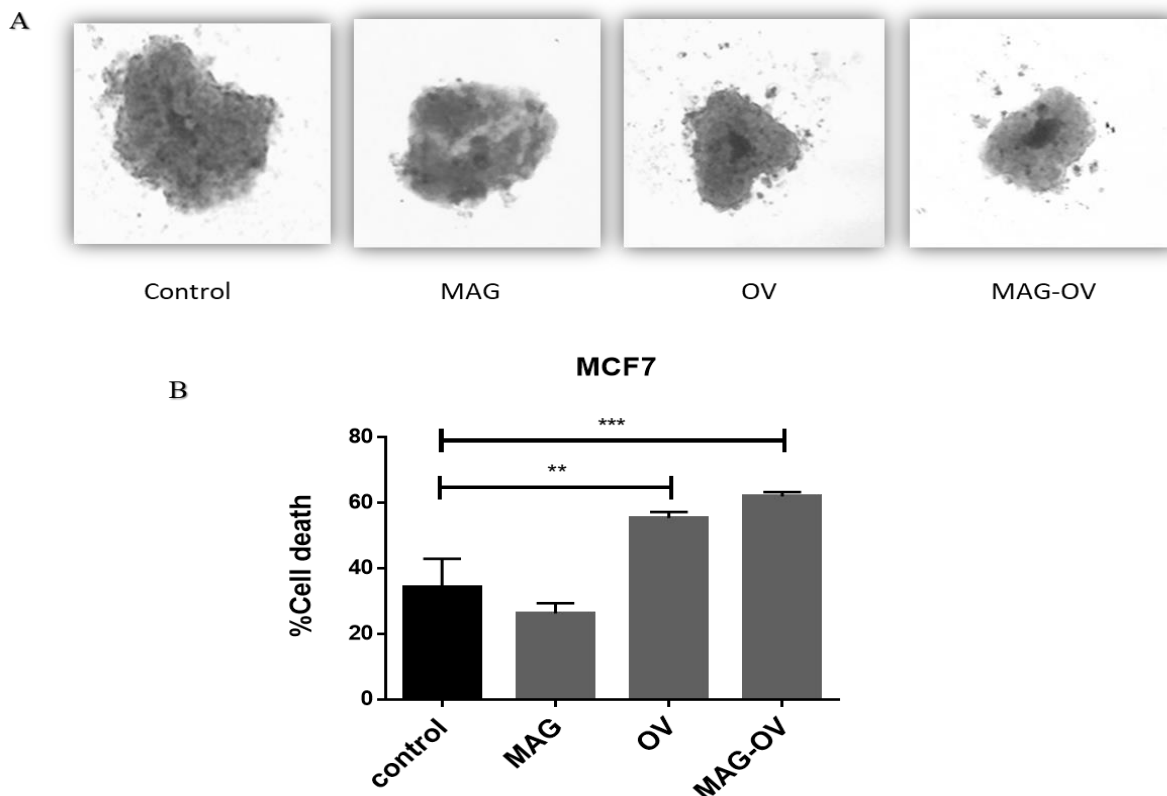


Figure 3.13: MAG-OV infects and kills MCF7 spheroids. Tumour cells were seeded into wells, that contain agarose dissolved in DMEM, at 20×10^3 cells per well and the approximate size they grow to was 10^5 cells. After 5-7 days of seeding the cells in 96 wells plate, OV or magnetic viral complexes (MAG-OV) were added to the spheroids as described in section 2.2.15. **A.** MAG-OV and OV increase the necrotic core of MCF7 spheroids. Images were taken by light microscopy 6 days' post infection. This was taken at 10x Magnification. **B.** Infection with OV and MAG-OV induces tumour spheroid cell death. Representative fluorescent dot plots of 3D MCF7 Spheroids. TOPRO3+ cells were measured by flow cytometry 3 days' post-infection. The percentage of cell death (TOPRO-3+). While no important changes in viability were detected between OV and MAG-OV, both virus groups induced significant cell death compared to the control untreated cells. Data are the mean \pm SEM of n=3 independent experiments and statistical analysis was assessed using the one-way Anova test with multiple comparisons. **p<0.01 ***p<0.001.

3.3 Discussion

3.3.1 Characterisation of MAG

The physio-chemical characteristics of MAG was investigated. MAG have an advantage in that the particles have a small size distribution and their size can be better managed during production, resulting in more uniform particles with average size of 46 ± 5 (Byrne et al., 2011). This offers an advantage over chemically synthesised particles that are often irregular and not uniform in size. Recently, studies have also confirmed that MAG purified from *Magnetospirillum gryphiswaldense* MSR-1 displayed uniform arrangement of particles whereas MNPs were clustered (Raguraman and Suthindhiran, 2019). They also found that the MAG have higher crystallinity than synthetic MNPs and this is related to the biomineralization

property of MTB in producing MAG. The high variation in size and physical aggregation displayed by chemically synthesised MNPs is a concern that has been raised by many researchers. For example, Raguraman and colleague reported this concern (Raguraman and Suthindhiran, 2019). They found that synthetic MNPs agglomerated inside the cell which subsequently damage the redox system causing mortality. However, Florea et al., demonstrated high cell uptake of PEI coated MNPs in Cos1 (green monkey fibroblasts) and airway epithelial cells (calu-3) but this correlated strongly with PEI toxicity (Florea et al., 2002). Similarly, Thomas and co-workers found that PEI coated MNPs facilitated gene transfer into the A549 lung carcinoma cells *in vitro* and into the lungs of mice but this also was highly toxic to cells (Thomas et al., 2005). This needs to be addressed if these particles are to be applied clinically (Blanco-Mantecon and O'Grady, 2006). It is clear that MNP needs to be sufficiently small (10–50 nm) for biomedical applications (Issa et al., 2013). This will have numerous benefits as outlined below:

1. Small MNPs will be more stable and aggregate less if their magnetic interaction is decreased.
2. Small MNPs can stay in the circulation after injection and pass through the capillary systems of organs and tissues avoiding vessel embolism.
3. Small MNPs have a high saturation magnetisation that leads to control the movement of the particles in the blood by moderate external magnetic field.
4. Being very small, the particles can avoid precipitation due to gravitation forces.
5. Small MNPs will have small dipolar interactions, because the dipole-dipole interactions rely on the radius of the particle. This will minimize particle aggregation.

This study shows that MAG display higher magnetic susceptibility ($8.164e-5$ SI), suggesting MAG are more likely to be attracted to a magnetic field. This is important, as the goal of this study is to apply a magnetic guidance strategy to target our complexes to tumours. Interestingly, the electrokinetic potential of the MAG was negative (-9 ± 2.3 mV) (**Table 3.1**). Studies have also shown that the zeta potential of MAG in the colloidal state was stable and negatively charged (-17.4 mV), showing they were well dispersed (Raguraman and Suthindhiran, 2019). This negative charge is because of the presence of lipid membrane around MAG (Sun et al., 2011).

3.3.2 MAG internalisation and viability by breast cancer cells

In the first instance bacterially derived MAG to be internalized by breast cancer cells was investigated. MAG was taken up successfully and this was confirmed using two approaches. Flow cytometry was used to assess changes in cell size and granularity after uptake and Prussian blue staining to visualize the occurrence of iron within the cells. MAG uptake by cells was not detected efficiently by flow cytometry (**Figure 3.1**). This may be due to the MAG size (MAG ~46 nm) thus after uptake of smaller MAG perhaps flow cytometry could not detect the changes in cell granularity. However, from the Prussian blue images it was clear that MAG were abundant in the cells (**Figure 3.1**). MAG were not toxic to breast cancer cells (**Figure 3.2**). Other studies have also confirmed that MAG are not toxic to tumour cells. For example, using the MTT assay MAG uptake had no toxicity effects on HT-29 (human colon adenocarcinoma grade II cell line) cells compared to untreated cells (Mannucci et al., 2014). In agreement with our study, Alphantery and colleagues demonstrated MAG (1 mg/ml) uptake by MDA-MB-231 cells resulted in improved cell viability compared to chemically synthesised super paramagnetic iron oxide particles (SPIOs) coated with PEG or citrate ions (Alphantery et al., 2011). The latter were more toxic to cells (20%) after 72 h. Moreover, the antitumour activity of the MAG after hyperthermia treatment was also demonstrated to be superior to SPIOs in a breast tumour xenograft following exposure to an alternative magnetic field (Alphantery et al., 2011). This suggests that MAG are more responsive to a magnetic field. Raguraman and colleague also shown that MAG are not toxic and do not cause any potential risk to the environment compared to chemically synthesised MNPs in different models such as human red blood cells, macrophage cell lines (RAW 264.7), onion root tips (*Allium cepa*), *Artemia salina* (*A. salina*) and zebrafish embryo (*Danio rerio*). For example, MAG showed 13.4% cytotoxicity at 250 µg/ml whereas the cytotoxicity induced by chemically synthesised MNPs was 36.01% for the same concentration in a macrophage (RAW 264.7) cell line (Raguraman and Suthindhiran, 2019).

It would have been useful to quantify MAG uptake by MDA-MB-231 by fluorescence uptake using flow cytometry rather than relying on a change in cell size. This could be achieved by fluorescently labelling the MAG (e.g. fluorescent dyes or infrared probes). A previous report demonstrated that MAG can be labelled with rhodamine B in order to be fluorescent with absorption and emission peaks (Alphantery et al., 2017). They have added the rhodamine B in the growth medium of magnetotactic bacteria in addition to the iron source whilst the magnetotactic bacteria are growing. We are currently attempting to do this in the laboratory so

we can visualise uptake by tumour cells *in vitro* and *in vivo* but have found the rhodamine label is not expressed. We are currently experimenting with different fluorescent labels such as lipophilic membrane stains (DiL and DiD). This is considered a more accurate method for determining MAG uptake but caution must be taken as this can change the size of the particles (Kircher et al., 2003, Medarova et al., 2007).

From the Prussian blue staining and the TEM images it was evident that MAG tended to aggregate (**Figure 3.1&3.2B**). To overcome this the MAG were sonicated to reduce the aggregation. This is a common method that is used in the preparation of MNPs (Kouassi et al., 2005). In this study, the MAG were sonicated for 10 min, whereas in other studies, sonication had been used for up to 3 hr to reduce aggregation (Hao et al., 2012). Further optimization of the sonication protocol is necessary and this is currently under investigation in our laboratory. Other steps taken to improve MAG uptake into cells included placing the cells and MAG on an orbital shaker during the incubation step. This was carried out by a Masters student in the laboratory that was under my supervision. Here we found that most MAG were internalised within 1 hour of incubation with the cells, we also established that no further uptake was evident after 24 hr. The data for this experiment was not included as the experiment was only performed with N=1 and therefore requires further investigation. However, incubating the particles for 1 hour and removing the shaker could improve the speed and efficiency of future experiments. This is in contrast to previous studies where shaking and longer time points were necessary for effective MNP internalisation (Haritha et al., 2015).

3.3.3 Characterisation of magnetic viral complexes

MAG possess lipids on their surface that render the particles negatively charged (Sun et al, 2008). Since the MAG display a negative electrokinetic potential we did not expect the self-assembly with the OV. However, this was not the case as MAG and OV formed complexes (MAG-OV) and this was evident by TEM (**Figure 3.6**). Creating the magnetic viral complexes using synthetic MNPs relies on the positive electrokinetic potential of the MNP so that complex formation depends on electrostatic interactions with negatively charged viral particles (OV)(Almstätter et al., 2015a). Almstatter et al., showed that core-shell type iron oxide MNPs gathered with vesicular stomatitis virus (VSV) or adenovirus (Almstätter et al., 2015). Their complexes were between 500-900 nm in diameter and by TEM it was evident that MNP-OV complexes formed but the MNPs were not very defined and formed aggregates, whereby the MNPs appeared to be on top of each other making the TEM images unclear. This probably results from magnetic di-pole-dipole interactions between the MNPs. We used a similar

approach in this study, however MAG-OV were smaller in size and exhibited a lot less aggregation than the MNP-OV showed in the Almstatter study (Almstatter et al., 2015a). MAG-OV have a negative electrokinetic potential and retained their magnetic susceptibility (**Table 3.2**). This complex formation is most likely a result of MAG possessing polarizable primary amino groups, enabling self-assembly based on the homo-bifunctional cross linking agents for example aliphatic binary aldehyde, diisothiocyanates, diisocyanates, di(succinimido) aliphatic esters, and their derivatives (Sun et al., 2011). However, hydrophobicity may also cause them to stay together as both of them contain hydrophobic proteins on their membrane.

3.3.4 Oncolytic potential of magnetic viral complexes on breast cancer cells

Uptake of the MAG-OV complexes was determined using flow cytometry and TEM. These complexes were efficient in infecting MDA-MB-231 and MCF7 cells after 24 h of culture displaying very similar viral GFP expression as in the OV only group (**Figure 3.8, Figure 3.10**).

The localisation of the MAG-OV complexes after cell uptake was confirmed by TEM. Typically, the MAG-OV complexes were captured in endosomes (**Figure 3.7**), whilst any unconjugated or free MAG were grouped in the cytoplasm and only very few were detected in the endosomes (**Figure 3.7**). Infection by HSV is usually via receptors on the cell surface so that admission of virus can be permitted; this process requires the complex interaction of a number of viral and cellular membrane components (Spear and Longnecker, 2003, Spear, 2004). There are 5 glycoproteins of viral membrane, gD, gB and the heterodimer including gH and gL (gH/gL) that are necessary for HSV-1 access into cells (Conner et al., 2008) and gC that is important for binding (Spear, 2004). HSV utilise numerous receptors for access into cells such as members of the tumour necrosis factor (TNF) receptor family; nectin-1 and nectin-2, Herpesvirus entry mediator (HVEM), heparan sulphate (HS) chains on cell surface proteoglycans as well as two members of the immunoglobulin superfamily linked to the poliovirus receptor (**Figure 3.14**). It is becoming increasingly clear that herpes viruses can enter cells by exploiting the endocytic pathways, although the mechanisms remain poorly defined (Clement et al., 2006). Whilst it is not known which receptors HSV1716 utilises to enter MDA-MB-231 cells, from the TEM images we guess that the MNP-OV/MAG-OV complex uptake was not receptor mediated, and most probably via endocytosis.

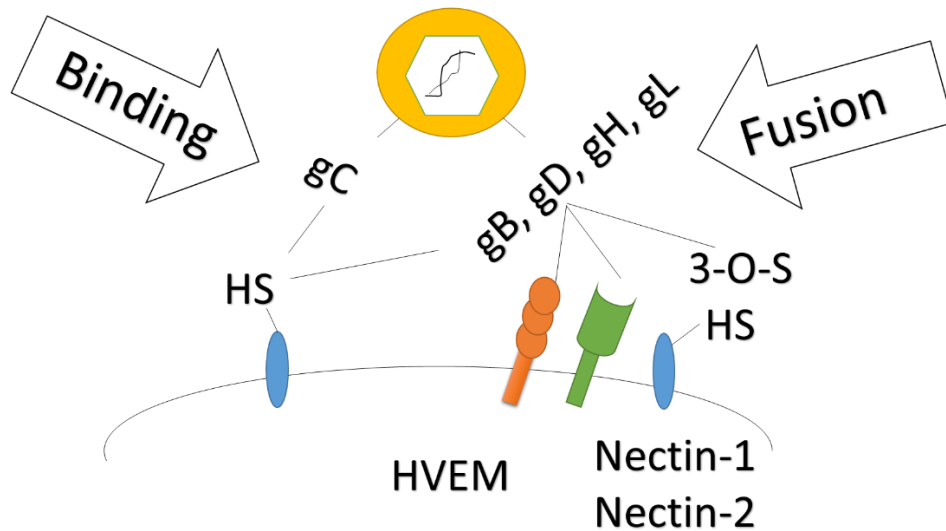


Figure 3.14: Viral and cellular membrane components that contribute to HSV1716 entry. There are 5 glycoproteins of viral membrane (gB, gC, gD, gH and gL) that are necessary for HSV-1 access into cells. Virus can start binding to the cell surface through gB or gC to heparan sulphate (HS) chains that are located on cell surface proteoglycans. This triggers fusion of the viral envelope with a cell membrane by binding gD to one of its cell surface receptors that includes members of the tumour necrosis factor (TNF) receptor family; nectin-1 and nectin-2, Herpesvirus entry mediator (HVEM), heparan sulphate chains on cell surface proteoglycans as well as two members of the immunoglobulin superfamily linked to the poliovirus receptor in addition to the action of the of gB and gH-gL heterodimers.

After confirming that the MAG-OV complexes were able to infect breast cancer cells we then investigated their ability to induce oncolysis. Complexes induced time-dependent cell death in line with the OV therapy on its own (**Figure 3.9, Figure 3.11**). No significant change in cell toxicity was detected between the MAG-OV and free OV.

Next, we tested the oncolytic potential of MAG-OV in 3D spheroid cultures. This provides an opportunity to investigate the influence of MAG-OV in a more sophisticated model that is physiologically relevant than 2D culture (Edmondson et al., 2014). One of the hallmark uses of 3D cell cultures is the ability to replicate some of the same behaviour of *in vivo* conditions, albeit not completely and they are still a very simplistic model. To investigate the effects of MAG-OV in breast cancer 3D tumours spheroids, we performed some preliminary experiments where the virus was allowed to infiltrate into multicellular 3D spheroids. The main objective was to determine if the coated virus in MAG-OV influenced 1) delivery of the virus 2) viral induced cell death. A previous study showed that initial damage of a glioblastoma biopsy spheroid *in vitro* by oncolytic HSV-1-based vector (G207) was characterized by a ruffling of the spheroid surface (Huszthy et al., 2008). Microscopy was used to observe changes in spheroid shape on day 6 of infection. In these studies, MAG-OV or OV was added to MDA-

MB-231 and MCF7 spheroids. We observed ruffled edges and a flattened morphology, indicating damage and cell death of the three-dimensional spheroid structure on day 6 of infection with both OV and MAG-OV treatment compared to untreated spheroids and MAG only. Interestingly, MAG-OV damaged the spheroid of MDA-MB-231s and MCF7 cells as efficiently as OV (**Figure 3.12A, Figure 3.13A**). Reassuringly, flow cytometry of enzymatically dispersed spheroids showed considerable cell death post infection with both OV and MAG-OV (**Figure 3.12B & 3.13B**) compared to control and MAG only group ($p \leq 0.01$ and $p \leq 0.01$, respectively). Together this suggests that MAG-OV is as efficient as OV on its own with respect to infectivity and cell death in both monolayer and 3D cultures. Huszthy *et al* have also shown that G207 could damage spheroids obtained from glioblastoma multiforme GBM1 (95% of the spheroids lysed after 10 days of infection) (Huszthy et al., 2009). Therefore, this kind of cell cultures could help reduce animal numbers in the long run. As an alternative, it would be interesting to take fluorescent images to show GFP in the hypoxic necrotic areas in future and include other cell types for example fibroblast, endothelial cells and see how MAG-OV changes other cell types in the TME.

In summary, this chapter shows that MAG-OV can be assembled without having any impact on the oncolytic potential of the virus. MAG are more small and uniform in size and form complexes with OV in such a way that the virus does not change its properties. The complexes are still nm in size and can infect and kill tumour cells. The following chapter will focus on the oncolytic potential of MAG-OV and the cell death mechanisms.

Chapter 4
Oncolytic potential of MAG-OV

4.1 Introduction

Results from the previous chapter show that OV can form a complex with MAG derived from magnetotactic bacteria. The physicochemical characteristics of MAG-OV and the ability to infect and kill human breast carcinoma cell in 2D and 3D culture was also demonstrated. In this chapter, the replication potential and cell death mechanisms of the virus will be assessed.

4.1.1 HSV1716 entry into tumour cells

In tumour cells, entry of HSV1716 to the cell by fusion of the virus envelope with the plasma membrane, leads to release of the viral nucleocapsid into the cytoplasm of the cell. After the capsid binds to the nuclear pore the genome is then released into the nucleus where all the steps of transcription, replication of viral DNA and assembly of progeny nuclear capsid take place (**Figure 4.1**). HSV viral replication genes are ICP0 – immediate early (Smith et al., 2011), ICP8 – early (Gao and Knipe, 1989) and gB – late (Singh et al., 2012) and these can be used to detect viral replication. After entry into the host, ICP0 is immediately expressed. ICP0 is able to avoid the hosts initial immune response when degradation of various immune activating proteins takes place, including ND10 associated proteins, because it has ubiquitin ligase activity (Lanfranca et al., 2014). Initiating HSV mRNA synthesis and marking the very beginning of virus replication is then controlled by ICP0. Before virus replication, the main function of ICP8, which is a single-stranded DNA binding protein, is to mediate the synthesis of viral DNA upon co-localisation with other proteins, including UL30, UL42 and UL9 (Uprichard and Knipe, 2003). gB is then able to control virus replication and cell entry upon successful viral DNA synthesis. HSV viral capsids can enter the nuclear membrane in the presence of gB. Previous studies demonstrated that using a gB knockout HSV mutant resulted in unsuccessful virus entry into the nucleus of keratinocytes (HaCaT), the virus mainly localised on the cell surface and cytoplasm, as a result glycoproteins gB and gH are necessary for the fusion between the virion envelope and the outer nuclear membrane (Farnsworth et al., 2007). In this chapter the replication of OV will be assessed to ensure that the MAG do not interfere with this process.

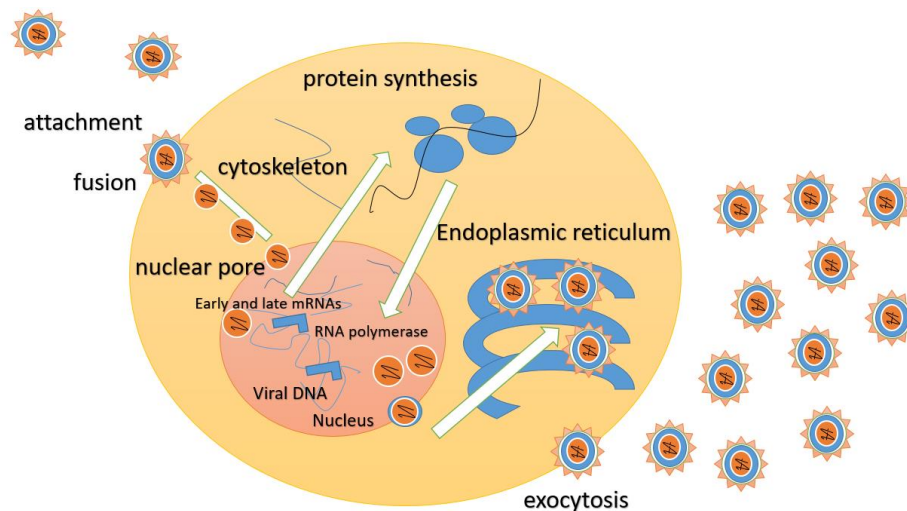


Figure 4.1: A simplified illustration of HSV1716 replication. HSV1716 enters tumour cells by fusion of the virus envelope with the plasma membrane, leads to release of the viral nucleocapsid into the cytoplasm of the cell. After the capsid bind to the nuclear pore the genome is then released into the nucleus where all the steps of transcription, replication of viral DNA and assembly of progeny nuclear capsid take place.

4.1.2 HSV1716 mechanisms of cell death and influence on the TME

The direct oncolysis of cancer cells by OV involves a mixture of apoptosis, necrosis, and autophagic cell death, often with one mechanism being predominant for a particular OV (see chapter one for details). For example, vaccinia virus has been shown to induce different cell death mechanisms including apoptosis, necrosis and autophagy in different human ovarian carcinoma cell lines including A2780, A2780CP, SKOV3ip1, IGROV1, TOV21G, and OVCAR-4 (Whilding et al., 2013). On the other hand, adenovirus has been shown to induce classical apoptosis in human cell lines such as A549 and A2182 lung cancers (Hall et al., 1998). There is some evidence in the literature that HSV-1716 induces necrosis or p53-independent apoptosis in human ovarian cancer cells (Coukos et al., 2000). Nevertheless, there remains inadequate information on these mechanisms of cell death in malignant tumour cells following infection with OV.

Immunogenic cell death (ICD) is a type of cell death that involves the adaptive arm of the immune system. ICD can activate anti-tumour immunity (Melcher et al., 2011b, Prestwich et al., 2008). This process leads to the production of key signals that alert APCs like dendritic cells (DCs). These include danger signals as well as tumour-associated antigens (TAAs), both required for DCs to trigger adaptive immune responses against cancer (Tang et al., 2012). The danger signals include damage-associated molecular pattern (DAMP) and pathogen-associated molecular pattern (PAMP) molecules derived from the OVs. Ground-breaking research by

Lindenmann and Klein almost half a century ago was the first to demonstrate increased immunogenicity of tumour cell antigens following influenza virus infection. In this study A2G mice were shown to be immunized against the Ehrlich ascites tumour following intraperitoneal injections of homogenized and lyophilized tumour cells which had been infected with oncolytic strains of influenza virus (Lindenmann and Klein, 1967). However, the mechanisms responsible for this immunogenicity were not understood.

Studies have shown that some viruses produce ICD associated with the release of DAMPs. For example, a recent study demonstrated that DAMPS are produced by squamous cell carcinoma (SCC) cells after infection with HSV-1 RH2. In this study HSV-1 RH2 also resulted in extracellular release of high mobility group protein B1 (HMGB1) and adenosine triphosphate (ATP), and translocation of calreticulin (CRT) to the cell membrane (Takasu et al., 2016). These are all indicators of ICD. In addition, Coxsackievirus B3 virus infection induced ICD in human non-small cell lung cancer cells (NSCLC; A549, H1299, and H460), including cell surface CRT and release of ATP as well as HMGB1 (Miyamoto et al., 2012). However, there are no published studies investigating cell death mechanisms and ICD by HSV1716 in breast cancer cells specifically and so this chapter aims to explore these mechanisms as part of its therapeutic efficacy.

The benefit of the natural inflammatory response to virus infection and immune responses to OV are considered the main steps of viral immunotherapy (Vacchelli et al., 2013). A previous study demonstrated that HSV1716 induces an inflammatory response in a murine syngeneic model of ovarian carcinoma. This study showed that intratumoral injection of HSV1716 resulted in upregulation of IFN- γ and CXCL10 (Benencia et al., 2005). CXCL10 is one of the proinflammatory chemokines that plays a role in activate T lymphocytes (Th1), NK cells, inflammatory dendritic cells, most macrophages and B cells (Liu et al., 2011b). Intratumoral injection of the third generation oHSV, G47 Δ -mIL12, significantly changed the microenvironment of glioblastoma stem cell (GSC)-derived intracerebral tumours. In this study, they showed G47 Δ -mIL12 downregulated VEGF expression and upregulated IP-10 (CXCL10) (Cheema et al., 2013).

4.1.3 Pre-existing immunity to HSV1716

The major with problem systemic delivery of OV is pre-existing immunity, because of the nature of many of the OV used in medicine, many of us have already been exposed during childhood and development (Ferguson et al., 2012). As claimed by a new report from the World

Health Organization, Herpes simplex virus type 1 (HSV-1) has infected approximately 67% of the global population (more than 3.7 billion people under the age of 50). Therefore, many strategies have been developed to help overcome this and provide protection to the virus when in circulation. Trojan Horse delivery is one of the strategies used to protect OV from neutralising antibodies. An example, of this approach is using cells which are derived from the model organism, then infected with the OV *ex vivo* and then injected systemically (Ferguson et al., 2012). At the University of Sheffield, macrophages (infected with either adenovirus or HSV1716) were shown to protect the virus from neutralising antibodies when administered systemically (Muthana et al., 2015b, Muthana et al., 2011b). Nanomedicine approaches have also been developed for protecting OVs in circulation. For example, a previous study demonstrated that oncolytic adenovirus Ad520 could be protected against the inhibitory effects of serum or a neutralizing antibody *in vitro* when it was protected by PEI-Mag2 (fluorinated surfactant ZONYL FSA (lithium 3-[2-(perfluoroalkyl)ethylthio]propionate) combined with 25-kDa branched polyethylenimine (PEI-25Br)) or PB-Mag1 (the fluorinated surfactant ZONYL FSE (ammonium bis[2-(perfluoroalkyl)ethyl]phosphate) combined with the cationic polymer polybrene (PB)) nanoparticles (Tresilwised et al., 2012b). Furthermore, aptamers (oligonucleotide or peptide molecules that bind to a specific target molecule) have been shown to protect vesicular stomatitis virus (VSV) from neutralising antibodies by blocking the Fab fragments of antibodies or binding to the virus. In this study, they showed that viral infectivity increased significantly (by more than 70%) in the presence of neutralizing antibodies in Vero cells (Muharemagic et al., 2014).

The hypothesis tested in this chapter is that MAG will protect OV in our MAG-OV complex providing a protective shield from neutralising antibodies they may encounter in circulation.

To test this first, we wanted to ensure that the OV in the MAG-OV complex could infect, replicate and kill breast cancer cells as effectively as OV alone. Secondly, the ability of the MAG to shield the virus from neutralising antibodies to HSV was assessed *in vitro*. The specific aim of the work described in this chapter was, therefore, to characterise the oncolytic potential of MAG-OV - with particular reference to:

1. Oncolytic potential of MAG-OV (including apoptosis, necrosis, autophagy and ICD).
2. Changes in the tumour microenvironment following MAG-OV: Pro-Inflammatory vs. Anti- Inflammatory Cytokines.
3. Viral neutralisation of MAG-OV.

4.2 Results

4.2.1 MAG-OV induces tumour cell oncolysis

To confirm OV uptake, MDA-MB-231 cells were grown on coverslips and incubated with either HSV1716-GFP (OV) on its own or MAG-OV at MOI 10 and MAG alone along with non-infected cells as controls for 24 hr. After this, cells were fixed and stained with sheep antibody to detect HSV1716 (Conner et al., 2005). Moreover, 50ng/ml DAPI solution was added for 2 min to define the nucleus. Coverslips were mounted onto the microscope slides and a Nikon A1 confocal microscope was used to take images. As shown in **Figure 4.2** OV and MAG-OV were able to infect MDA-MB-231 cells, where HSV1716 was detected within the cytoplasm of most cells.

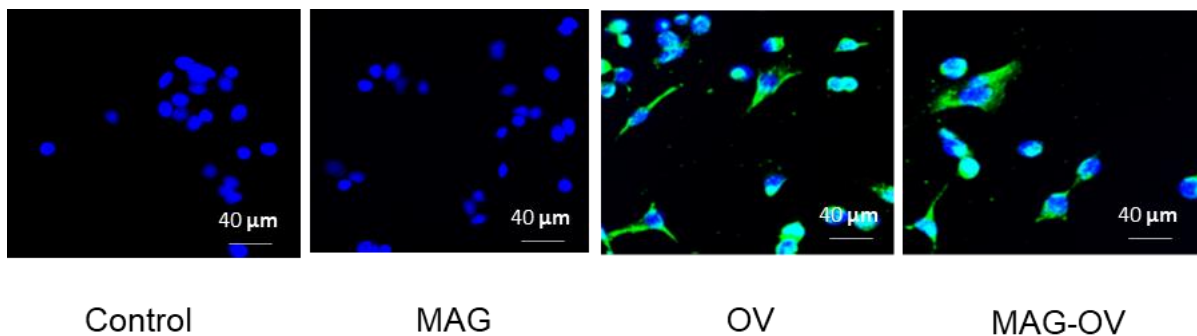


Figure 4.2: MAG-OV infected MDA-MB-231 cells. MDA-MB-231 cells were incubated with OV (MOI 10), MAG-OV (MOI 10) or MAG (0.2 mg/mL) for 24 h. Cells were fixed and stained with sheep antibody to detect HSV1716 and (4',6-diamidino-2-phenylindole) (DAPI) and then analysed under a confocal laser-scanning microscope. Scale bar = 40µm. Data are representative images from a single experiment. However, the experiment was repeated n=3 and showed the same result.

In the last chapter MAG-OV were shown to infect and kill human breast carcinoma cell lines. Above we have confirmed uptake of MAG-OV was as effective as OV alone. Next, we assessed if MAG-OV was as effective in a panel of human and murine breast cancer cell lines. To analyse the oncolytic potential human MCF7 & MDA-MB-231 and murine EO771 and TS1 cells were seeded into 6-well plates (3×10^5 cells/well) and after 24 hr, cells were infected with either the OV on its own or as MAG-OV at MOI 10 and MAG alone (0.2 mg/ml) with non-infected cells used as controls. HSV1716-GFP was used as a reporter virus to visualise virus infectivity. After 6 days of culture, plates were harvested and flow cytometry was used to analyse the cells. In these studies, TOPRO3 was used as a viability dye where dead/dying cells take up the dye but live cells exclude it. As shown in **Figure 4.3**, MAG-OV were able to destroy the tumour cells as efficiently as the naked OV with no differences between these groups after 6 days of culture.

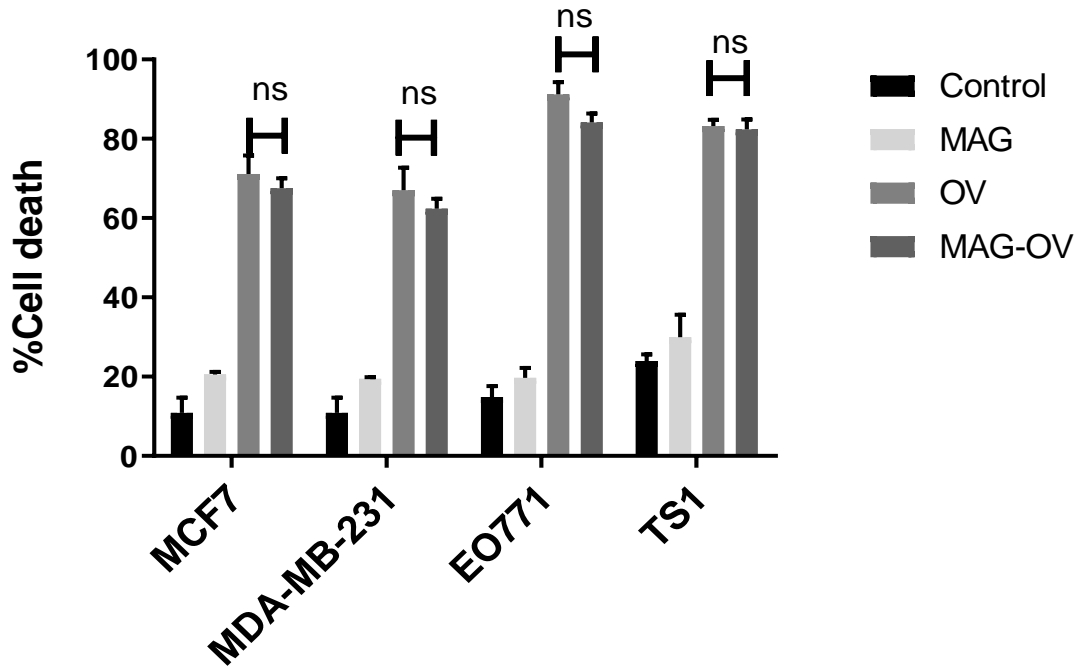


Figure 4.3: OV and MAG-OV induce oncolysis in a panel of human and murine breast cancer cell lines. Cells were infected with OV, MAG-OV (at MOI 10) or MAG with non-infected cells used as controls. After 6 days of infection, cells were harvested and immediately before analysis on a flow cytometer 2ul of TOPRO-3 was added to each sample. TOPRO-3 was measured in the FL-4 (640nm). Of note, Data are the mean \pm SEM of $n=3$ independent experiments and statistical analysis was assessed using the two-way Anova test with multiple comparisons.

4.2.2 Viral replication genes

Given that MAG-OV induced tumour cell death, next we wanted to determine if the virus was able to replicate post-infection. MDA-MB-231 and MCF7 cells were seeded into 6 well plates at 3×10^6 cells per well. Cells were then infected with OV, MAG-OV at MOI 10 and MAG (0.2 mg/ml) alone with untreated cells as controls and cultured for 24h. Expression of viral replication genes was determined by qPCR. RNA was extracted after 24h of infection and used to synthesise cDNA. Viral replication genes included; ICP0 – immediate early, ICP8 – early and gB – late genes (Singh et al., 2012). Virus successfully replicated within the cells, as shown by the significant increase in viral mRNA expression of both OV ($P \leq 0.0001$) and MAG-OV ($P \leq 0.0001$) when compared to the control in MDA-MB-231 cell lines (**Figure 4.4A**). In the MCF7 cells, viral mRNA expression was also significant with OV (ICP0: $p \leq 0.01$, ICP8: $p \leq 0.001$, gB: $p \leq 0.001$) and MAG-OV (ICP0: $p \leq 0.01$, ICP8: $p \leq 0.05$, gB: $p \leq 0.001$) compared to the control (**Figure 4.4B**).

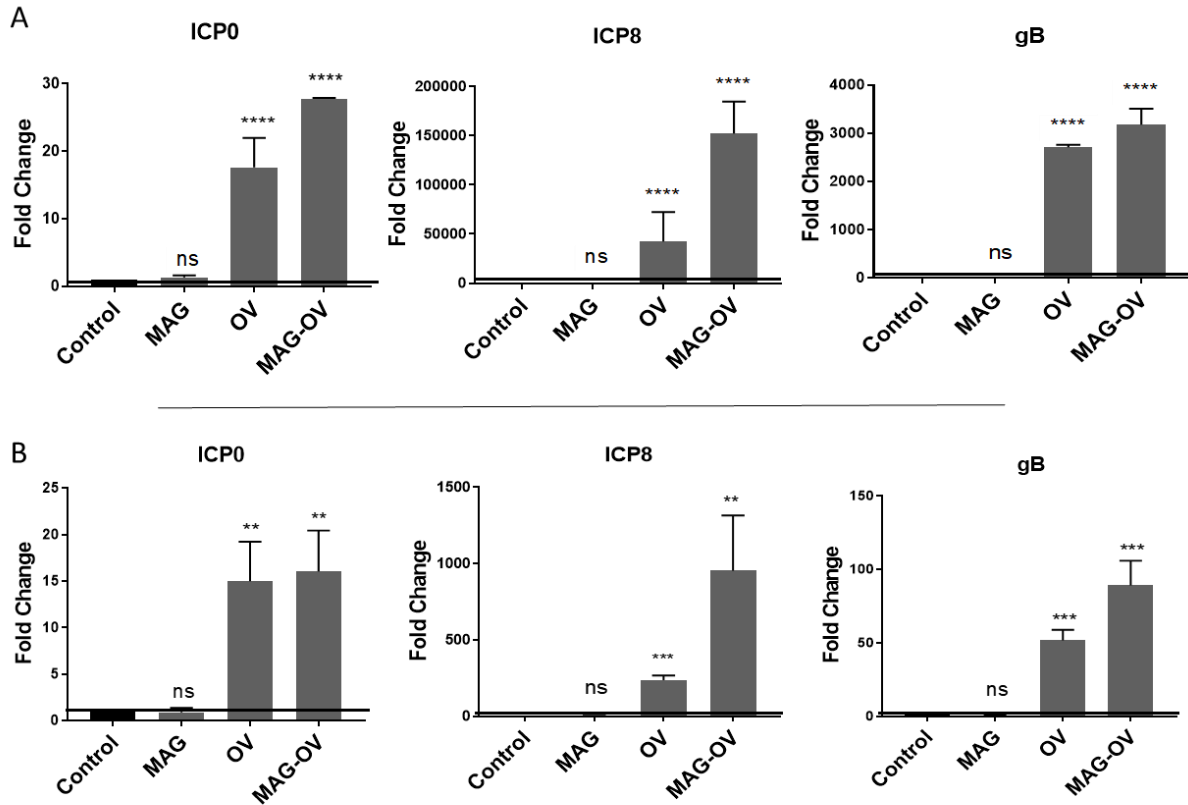


Figure 4.4: MAG-OV undergoes viral replication in breast cancer cells. Breast cancer cells were infected with OV, MAG-OV at MOI 10 and MAG alone with untreated cells as controls. Viral replication genes were assessed by qPCR after 24h of infection. **A.** Significant increase in mRNA expression of ICP0, ICP8 and gB of both OV ($P \leq 0.0001$) and MAG-OV ($P \leq 0.0001$) in MDA-MB-231 cells compared to the control. **B.** Viral mRNA expression is also significant with OV (ICP0: $P \leq 0.01$, ICP8: $P \leq 0.001$, gB: $P \leq 0.001$) and MAG-OV (ICP0: $P \leq 0.01$, ICP8: $P \leq 0.05$, gB: $P \leq 0.001$) in MCF7 cells compared to the control. The expression levels were calculated relative to the untreated cells (control) using the $2^{-\Delta\Delta CT}$ method after the data was normalised to the housekeeping gene, *GAPDH*. The data is presented as *Mean* \pm *SEM* for $n=3$, independent experiments and statistical analysis was assessed using the one-way Anova test with multiple comparisons. ** $p < 0.01$; *** $p < 0.001$; **** $p < 0.0001$.

4.2.3 Cell Death Mechanisms

Next, we wanted to assess the potential mechanisms of HSV1716 mediated cell death. Cell death genes were selected that marked the critical death pathways and were found to be upregulated following HSV1716 infection by a post-doctoral researcher in the laboratory (Dr Emer Atkinson, unpublished observations). These included; Caspase 3, Caspase 8– Apoptosis genes, ATG5, LC3B – Pro-autophagy genes, Bcl-2- anti-apoptotic gene, FasL- pro-apoptotic gene and HSP90AA1, HSP90B1, HSPA1A – Heat shock Proteins genes. Breast cancer cells MDA-MB-231 (**Figure 4.5A**) and MCF7 (**Figure 4.5B**) cells were infected with OV, MAG-OV at MOI 10 and MAG alone with untreated cells as controls and cultured for 24h. Viral infection appeared to induce a significant increase in Caspase 3, Caspase 8, LC3B, FASL and

HSPA1A, mRNA expression (**Figure 4.5**) when compared to the control with both OV and MAG-OV treatment in both cell lines. ATGS was unaffected but HSP90AA1, HSP90B1 and Bcl-2 displayed a significant decrease in expression with both OV and MAG-OV infection. These genes are necessary for cancer cell survival and proliferation (Haase and Fitze, 2016).

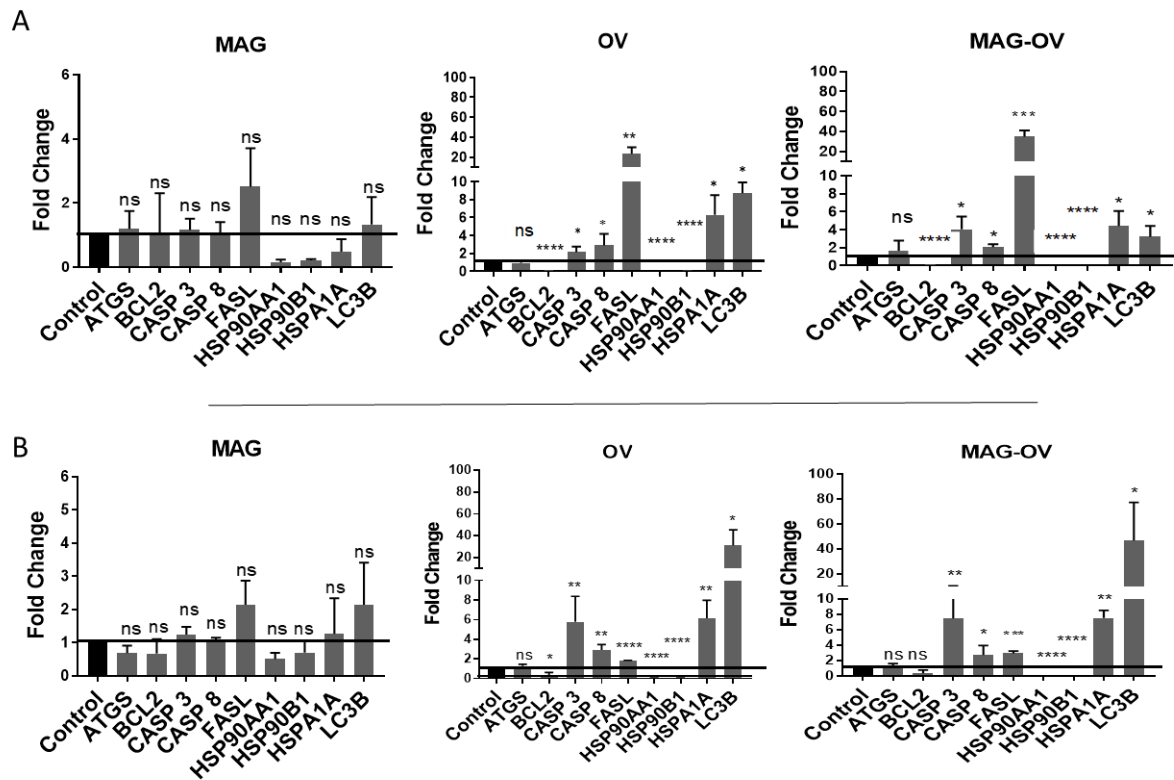


Figure 4.5: Increased expression of cell death markers following MAG-OV infection. Cell death mechanisms were investigated after 24h of infection of breast cancer cells MDA-MB-231 and MCF7 with OV, MAG-OV at MOI 10 and MAG alone with untreated cells as controls. **A.** A significant increase in mRNA expression of HSPA1A, Caspase 3, Caspase 8, LC3B and FASL in both OV and MAG-OV treated MDA-MB-231 cells compared to the control. **B.** mRNA expression of HSPA1A, Caspase3, Caspase8, LC3B and FASL is also significant with both OV and MAG-OV in MCF7 cells. The expression levels were calculated relative to the untreated cells using the $2^{-\Delta\Delta CT}$ method after the data was normalised to the housekeeping gene, *GAPDH*. The data is presented as Mean \pm SEM for n=3, independent experiments and statistical analysis was assessed using the one-way Anova test with multiple comparisons. *p<0.05; **p<0.01; ***p<0.001; ****p<0.0001.

4.2.4 Immunogenic cell death

As mentioned earlier, many studies have shown that some viruses induce ICD associated with the release of DAMPs such as ATP and HMGB1 and/or those translocated to the cell surface such as calreticulin (CRT) (Takasu et al., 2016). Therefore, the release of ATP and HMGB1 following MAG-OV infection was measured in breast cancer cells. MDA-MB-231 and MCF7 cells were seeded into 6 well plates then infected with OV, MAG-OV at MOI 10 and MAG

alone with untreated cells as controls and cultured for 24h. ENLITEN ATP assay (Promega, Madison, WI, USA) was used to measure the secreted extracellular ATP in the cell culture supernatants according to the manufacturer’s protocol, using a Turner Biosystems luminometer (TD-20/20; Promega). Extracellular ATP levels were significantly increased in both OV and MAG-OV when compared with control and MAG alone (**Figure 4.6**). This suggests that HSV1716-infected breast cancer cells lead to cell membrane damage and release of ATP. Secreted extracellular HMGB1 in the supernatants was measured with a HMGB1 ELISA Kit II (Shino-Test, Kanagawa, Japan) according to the manufacturer’s protocol outlined for the normal sensitivity format of the assay. Extracellular HMGB1 levels also significantly increased after a 24h incubation in both OV and MAG-OV treated groups when compared with control and MAG alone (**Figure 4.6**).

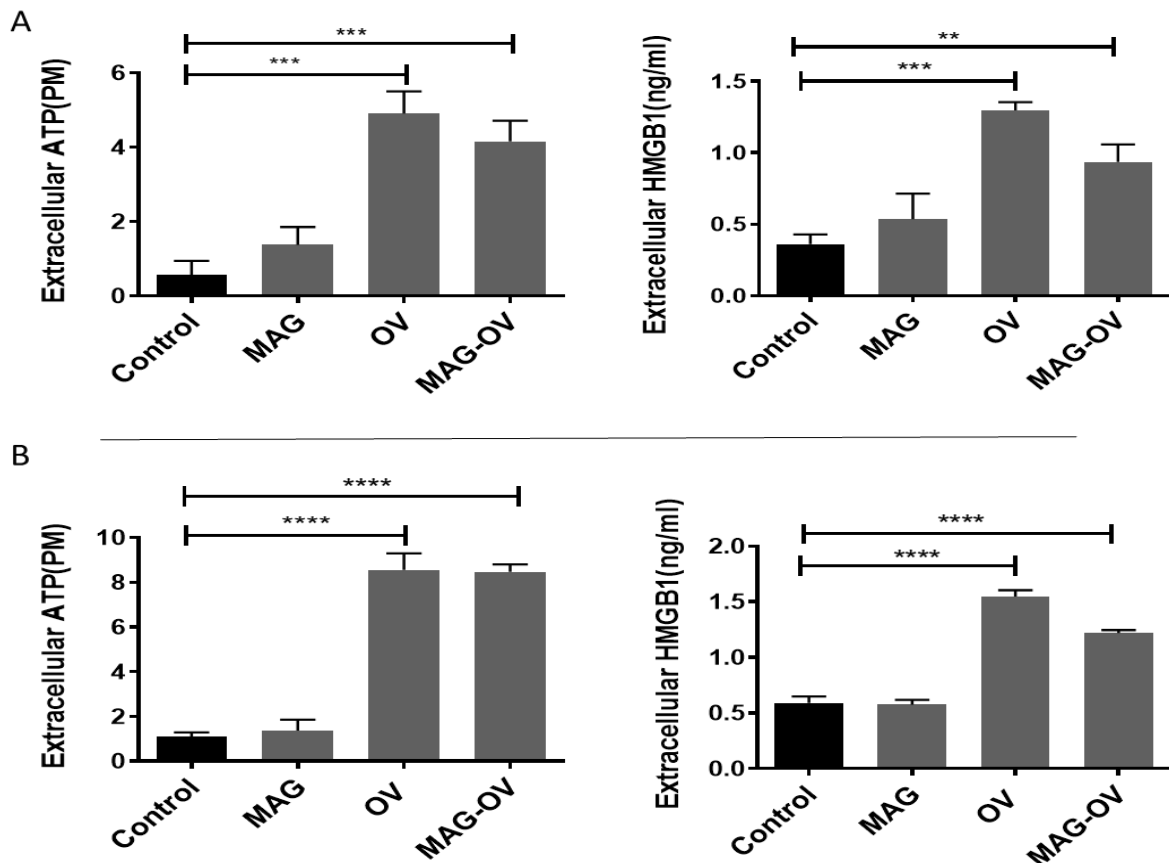


Figure 4.6: Extracellular levels of immunogenic cell death markers ATP and HMGB1 in human breast cancer cells. MDA-MB-231 and MCF7 cells were infected with OV, MAG-OV at MOI 10 and MAG alone with untreated cells as controls for 24 h, **A.** Shows Significant increase in Extracellular levels of HMGB1 and ATP of both OV and MAG-OV in MDA-MB-231 cells compared to the control while **B.** in supernatants of MCF7 cells. Data are the mean ± SEM of n=3 independent experiments and statistical analysis was assessed using the one-way Anova test with multiple comparisons. **p<0.01; ***p<0.001; ****p<0.0001.

Calreticulin (CRT) is a DAMP that is normally located in the lumen of the endoplasmic reticulum. Immunogenic apoptosis leads to translocation of CRT to the surface of dying cells as an eat-me indicator for professional phagocytes (Obeid et al., 2006, Gold et al., 2010, Voll et al., 1997). The expression of CRT following HSV1716 infection was measured by immunocytochemistry. Cells were seeded on a small coverslip and infected with OV, MAG-OV at MOI 10 and MAG alone alongside the control (untreated cells) for 24h and were stained with rabbit anti human CRT diluted 1:100 (Abcam, Cambridge, UK). Cells were then stained with DAPI. CRT was distributed sparsely in the cytoplasm before infection (Green colour). Nevertheless, its expression increased and distribution changed to accumulate at the plasma membrane 24 h after infection in response to both OV and MAG-OV in MDA-MB-231 (**Figure 4.7A**) and MCF7 (**Figure 4.7B**) cells.

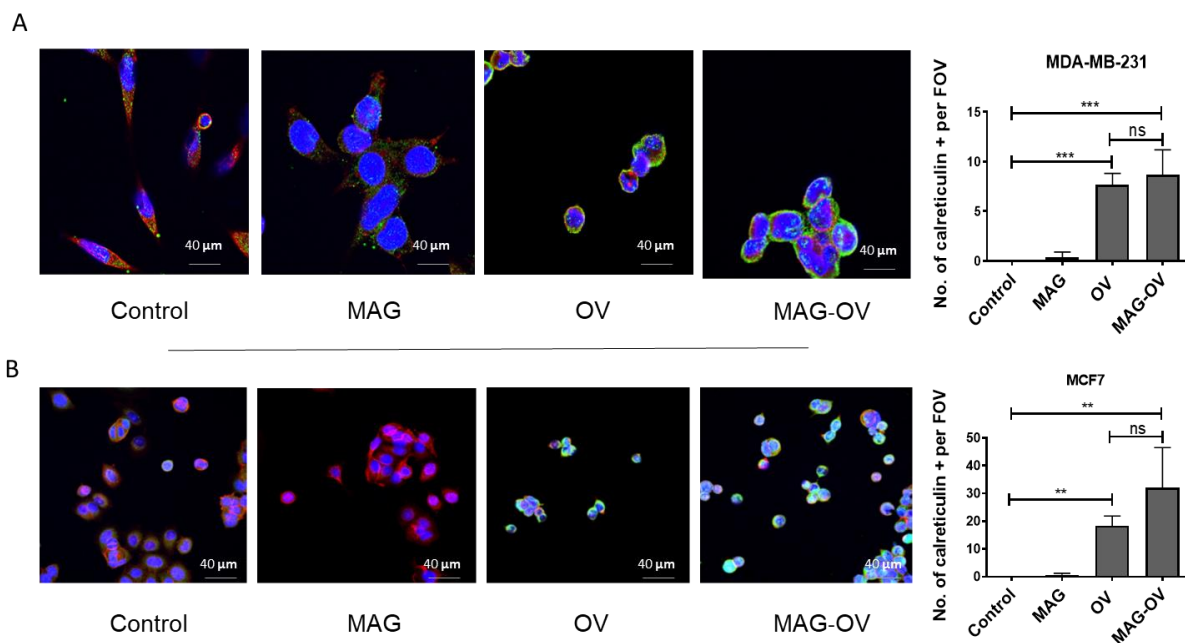


Figure 4.7: Increased expression of calreticulin (CRT) on the cell surface of human breast cancer cells following MAG-OV infection. MDA-MB-231 and MCF7 cells were infected by MAG, OV or MAG-OV at a MOI 10 for 24 h. **A.** Expression of CRT on the cell surface of MDA-MB-231 cells increased with OV and MAG-OV infection (Green colour). **B.** Expression of CRT on the cell surface of MCF7 cells increased with OV and MAG-OV infection. Cells were fixed and stained with an anti-CRT antibody (Green colour), F-actin staining with Phalloidin (red colour) and (4',6-diamidino-2-phenylindole) (DAPI:Blue)) and analysed under a confocal laser-scanning microscope. All data are representative of a single experiments that repeated N=3. Scale bar= 40µm.

4.2.5 MAG-OV induces changes in Pro-Inflammatory cytokines and Anti-Inflammatory cytokines

As mentioned above, both OV and MAG-OV successfully entered and replicated inside breast cancer cells, at the same time inducing ICD. Next, we assessed whether tumour cell death in response to OV infection influenced the tumour microenvironment using a panel of pro-inflammatory and anti-inflammatory markers. This included pro-inflammatory cytokines (IL-1B, TNF, CXCL10 and INF γ) and anti-inflammatory cytokines (IL-10, TGF-B, NF-KB and VEGF). A previous study demonstrated that HSV1716 induces an inflammatory response in a murine syngeneic model of ovarian carcinoma. This study showed that intratumoral injection of HSV-1716 resulted in upregulation of IFN- γ and CXCL10 in the tumour (Benencia et al., 2005). Furthermore, Vesicular stomatitis virus (VSV) have been shown to up-regulate pro-inflammatory genes in CT-26 tumours 24 hr after infection. In this study, VSV upregulated most pro-inflammatory genes including TNF, CXCL10 and IL-6 *in vivo* (Breitbach et al., 2007a).

Therefore, we assessed the effects of MAG-OV on the production of both pro- and anti-inflammatory genes in human breast cancer cells. The level of mRNA expression of these genes was measured in MDA-MB-231 and MCF7 cells infected with the OV, MAG-OV and MAG alone by qPCR. All samples were normalized to the untreated control cells. **(Figure 4.8)** shows fold change expression of mRNA levels. The expression of TNF were upregulated in both MDA-MB-231 **(Figure 4.8A)** and MCF7 **(Figure 4.8B)** cells treated with OV or MAG-OV compared to the untreated cells. Moreover, the expression of CXCL10 was upregulated in MCF7 cells **(Figure 4.8B)** while unchanged in MDA-MB-231 **(Figure 4.8A)** cells treated with OV or MAG-OV compared to the untreated cells. Furthermore, the expression IL-1B, NF-KB and VEGF were significantly downregulated in both MDA-MB-231 and MCF7 cells treated with OV or MAG-OV compared to the untreated cells.

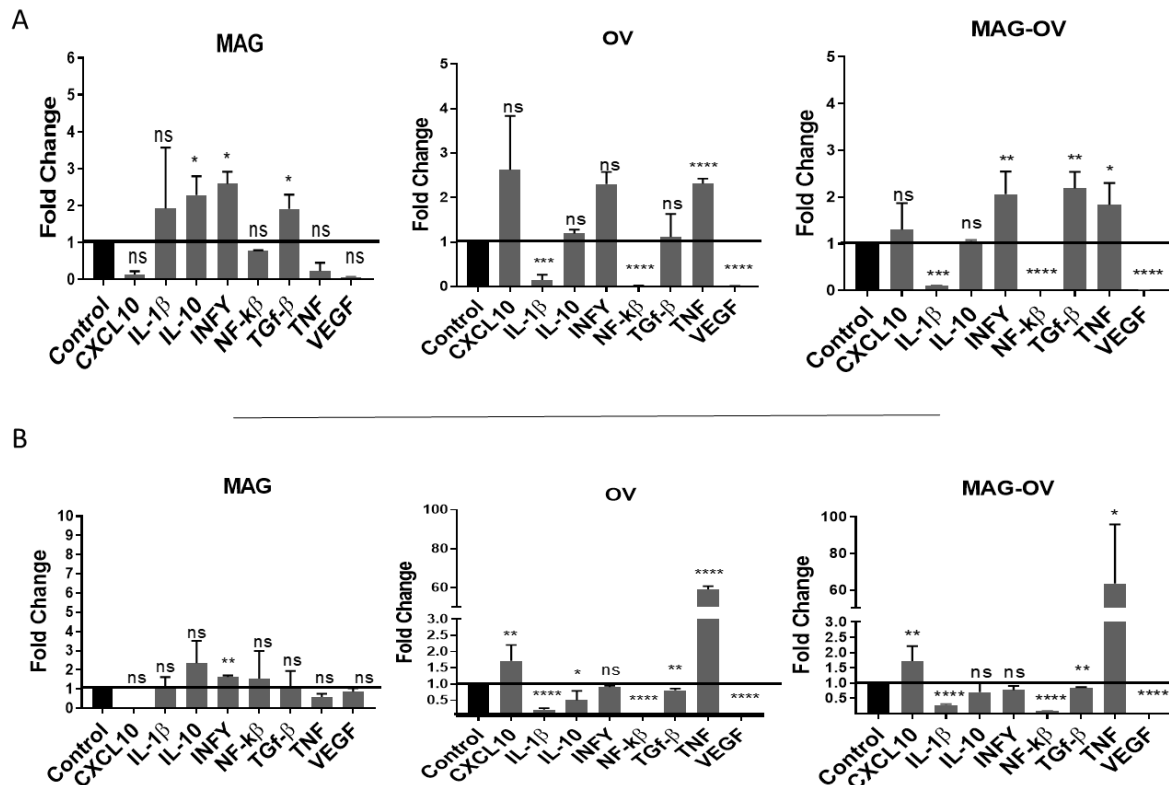


Figure 4.8: MAG-OV induces pro-Inflammatory cytokine mRNA expression in human breast cancer cells. mRNA expression of pro-Inflammatory and anti-inflammatory cytokines was measured in MDA-MB-231 and MCF7 cells infected with the OV, MAG-OV and MAG alone for 24h by qPCR. **A.** Shows significant downregulation in mRNA expression of IL-1 β , NF- κ β and VEGF and upregulation in TNF and INF γ in both OV and MAG-OV in MDA-MB-231 cells compared to the control. **B.** Shows significant downregulation in mRNA expression of IL-1 β , NF- κ β and VEGF and upregulation in TNF only of both OV and MAG-OV in MCF7 cells. The expression levels were calculated relative to the untreated cells using the $2^{-\Delta\Delta CT}$ method after the data was normalised to the housekeeping gene, GAPDH. The data is presented as Mean \pm SEM for n=3 independent experiments and statistical analysis was assessed using the one-way Anova test with multiple comparisons. *p<0.05; **p<0.01; ***p<0.001; ****p<0.0001.

Cytokines expression was also assessed at the protein level using a cytokine bead array (CBA). MDA-MB-231 and MCF7 cells were treated with OV & MAG-OV at MOI 10 and Mag alone with untreated cells as controls. Supernatants were collected 24h after culture and clarified by filtration. An Attune Autosampler was used to read the samples (**Figure 4.9**), this displays cytokine levels analysed including CXCL10, IL-1 β , IL-6, IL-8, IL-10, INF γ , TNF and VEGF. The expression of CXCL10, IL-6, IL-8, IL10 and VEGF were significantly downregulated in both MDA-MB-231 (**Figure 4.9A**) and MCF7 (**Figure 4.9B**) cells treated with OV or MAG-OV compared to the untreated cells. Like with the mRNA expression IL-10 in MCF7 cells was not affected in all the treatment groups. Unlike the mRNA expression IL-1 β , INF γ and TNF

were not affected at the secreted protein level in both MDA-MB-231 and MCF7 cells treated with OV or MAG-OV compared to the untreated cells.

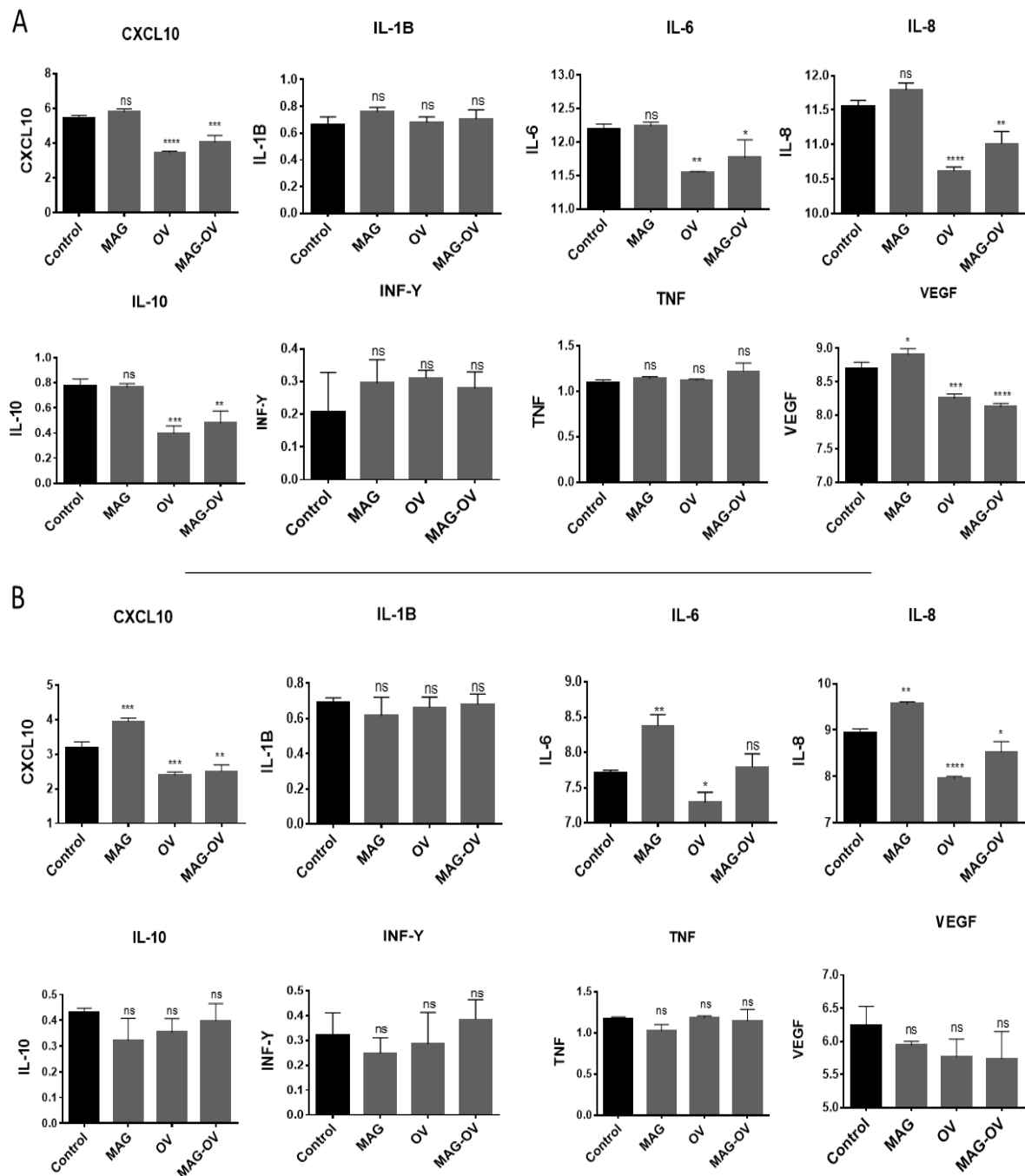


Figure 4.9: MAG-OV induces pro-Inflammatory cytokines protein expression in human breast cancer cells. The protein levels of pro-inflammatory and anti-inflammatory cytokines were analysed after 24h of cells infection with the OV, MAG-OV and MAG alone using a cytokine bead array (CBA). **A.** Significant downregulation in protein levels of CXCL10, IL-6, IL-8, IL-10 and VEGF in both OV and MAG-OV in MDA-MB-231 cells compared to the control. **B.** Significant downregulation in protein levels of CXCL10, IL-8 and VEGF in both OV and MAG-OV in MCF7 cells. Data are the mean \pm SEM of n=3 independent experiments and statistical analysis was assessed using the one-way Anova test with multiple comparisons. *p<0.05; **p<0.01; ***p<0.001; ****p<0.0001.

4.2.6 Primary cells infection

The ability of cells to migrate into tissues naturally has led them to be appropriate cell delivery targets for OV. This has been demonstrated for immune cells for example macrophages (Muthana et al., 2015b). Therefore, we tried to measure the uptake of MAG-OV with primary cells found in circulation. Ficoll density gradient centrifugation was used to isolate the Primary cells from blood according to (Muthana et al., 2011a, Muthana et al., 2013). Mononuclear cells were infected with either the OV on its own or MAG-OV, at MOI 1, MAG (0.2mg/ml) and non-infected cells were used as controls. For these studies, we used the reporter virus HSV1716-GFP so that the GFP could be used to confirm virus infection. As shown in **Figure 4.10**, MAG-OV was able to marginally infect the primary cells as efficiently as the naked OV with no differences between these groups after 6 hr of culture. However, we found that MAG-OV and OV alone tended more to infect monocytes than other mononuclear cells (**Figure 4.10B**). Suggesting that monocytes could be used to improve delivery of our complex *in vivo*.

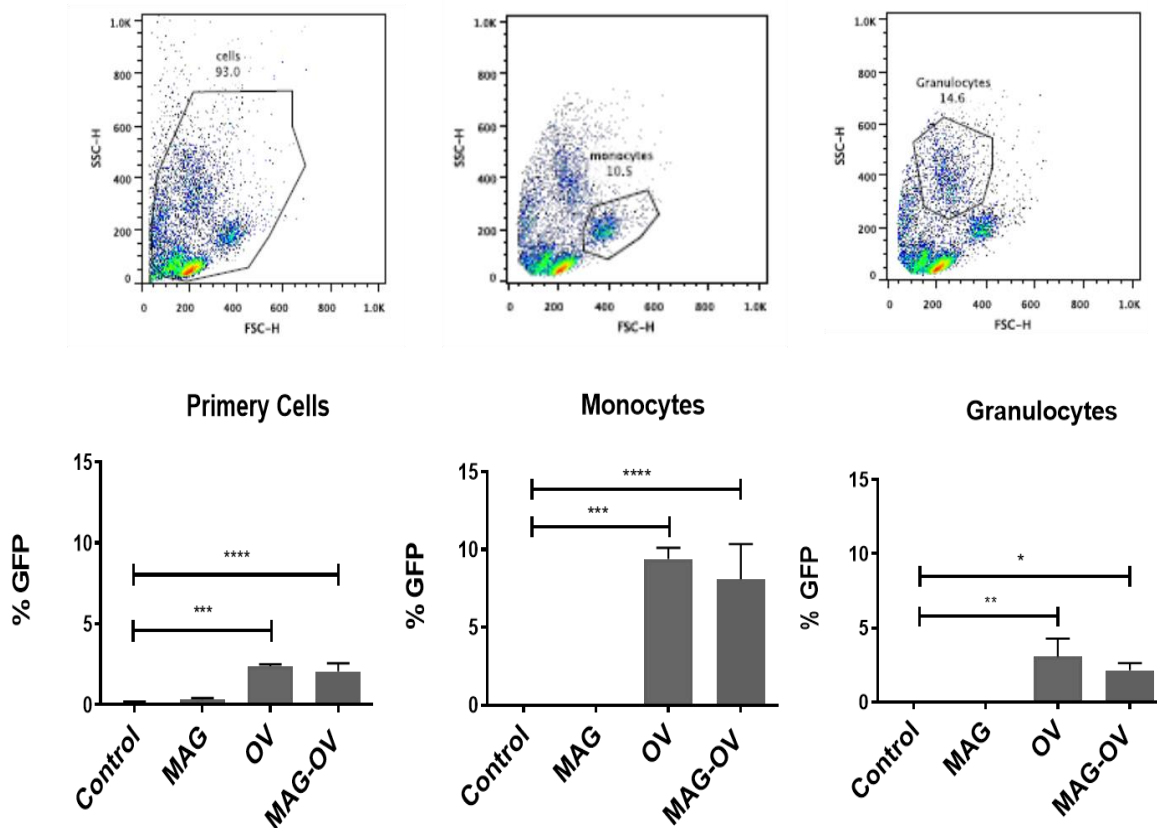


Figure 4.10: MAG-OV infected primary cells. Primary cells were incubated with OV (MOI 1), MAG-OV (MOI 1) or MAG (0.2 mg/ml) for 6 h. MAG-OV was able to infect the primary cells as efficiently as the naked OV with no differences between these groups after 6 hr of culture. MAG-OV and OV alone tended more to infect monocytes than other mononuclear cells. Data are the mean \pm SEM of n=3 independent experiments and statistical analysis was assessed using the one-way Anova test with multiple comparisons. *p<0.05; **p<0.01; ***p<0.001; ****p<0.0001.

4.2.7 Viral neutralisation

Systemic delivery of OV results in low intra-tumoural titres due to pre-existing immunity that has established because of exposure to the virus, previous immunization, or prior oncolytic viral therapy (Ferguson et al., 2012). Neutralisation experiments were performed to determine if MAG could protect OV from neutralizing Ab in the MAG-OV complex. Sheep anti-HSV-1 antiserum was used to neutralise the OV. This neutralising antibody (NAb) was kindly prepared by Virttu Biologics by four consecutive monthly injections of 1×10^6 PFU HSV1716 (Conner et al., 2005). 100-fold dilution of sheep Ab obtained after the fourth injection and 1×10^7 PFU of OV or MAG-OV were incubated in culture medium for 18 hr at 4°C, alongside the controls, no antibody control and no virus control. As shown in **Figure 4.11A**, cells incubated with OV+Nab expressed significantly less GFP after 24h of culture compared to MAG-OV+ NAb. This decrease in GFP expression is most likely because of OV neutralisation and indeed statistically significant less cell death was observed with OV+NAb compared to the MAG-OV+ NAb after 24h of culture (**Figure 4.11B**).

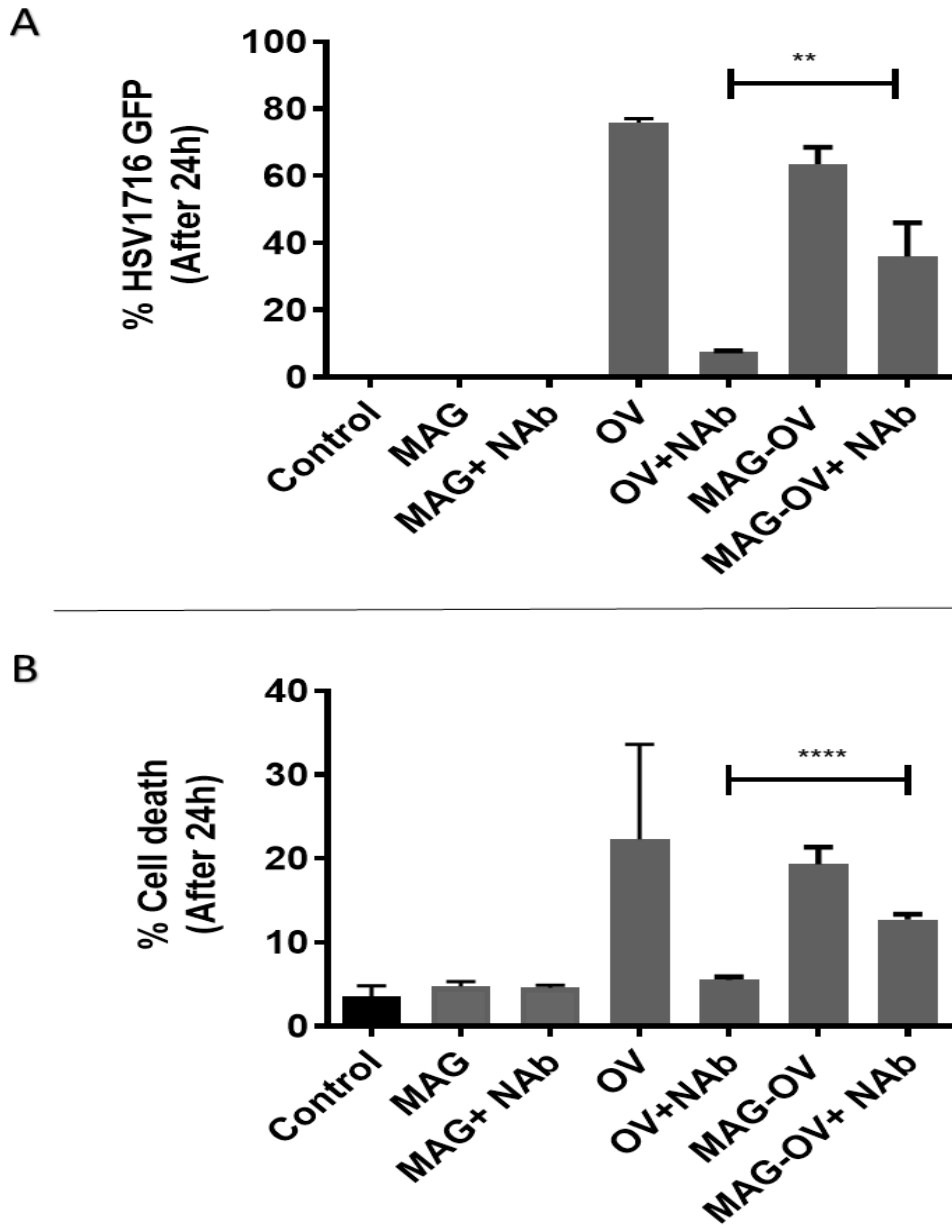


Figure 4.11: MAG-OV is protected from anti-HSV neutralising antibodies and induces MDA-MB-231 oncolysis. **A.** GFP expression following 24h incubation of MDA-MB-231 cells with OV, MAG-OV or MAG (at MOI 10) in the presence or absence of neutralising antibody.. **B.** The oncolytic potential of MAG-OV in the presence of NAb in MDA-MB-231 cells. Data are the mean \pm SEM of n=3 independent experiments and statistical analysis was assessed using the one-way Anova test with multiple comparisons. **p<0.01; ****p<0.0001.

4.3 Discussion

In this chapter, infection of the MAG-OV complex was determined by immunostaining. These complexes were equally efficient in infecting MDA-MB-231 cells after 24 h of culture displaying very similar viral GFP expression as the OV alone (**Figure 4.2**). Already, previous studies showed that the FDA approved HSV1 virus T-Vec induced 13.6 and 64.4% cell death

after 24 and 48 h post infection respectively at MOI 1 in a human breast adenocarcinoma cell line (MDA-MB-231)(Tan et al., 2015). Here we have extended the panel of established cell lines to include human and murine cells (MCF7, MDA-MB-231, EO771 and TS1 cells) and compared the oncolytic potential of HSV1716 alone (OV) or in the MAG-OV complex. MAG-OV induced cell death in line with the OV therapy on its own (**Figure 4.3**) in both species. No significant change in cell toxicity was detected between the MAG-OV and free OV in all breast cancer cells. This data is reassuring and suggest that coating the OV with MAG does not affect the oncolytic potential of HSV1716. It also suggests that murine cells can be used for our future *in vivo* studies. This is advantageous and will allow immune parameters to be assessed following administration of our MAG-OV to tumour-bearing immunocompetent mice. There has been some speculation in the literature regarding HSV1716 in the 4T1 mouse model. Toda and co-workers demonstrated a small decrease in primary tumour size in the 4T1 mouse mammary carcinoma model. They suggested this absence of efficacy was due to poor replication of HSV1716 within the 4T1 tumours as measured by the plaque assay (Toda et al., 1999, Toda et al., 1998). It is not clear why this occurs, yet the block is not at the point of viral entry, like in B16 melanoma cells (Miller et al., 2001), as HSV-1 is able to infect 4T1 cells. More studies would be required to exactly understand why HSV-1 has a reduced capability to replicate in murine tumour cells and this should be investigated in the future.

After we showed that MAG-OV was able to infect breast cancer. We therefore tested viral replication genes; ICP0 – immediate early (Smith et al., 2011), ICP8 – early (Gao and Knipe, 1989) and gB – late (Singh et al., 2012) after 24h of cell infection. As shown in **Figure 4.4**, all genes were upregulated following infection with OV and MAG-OV with the ICP8-early-stage and gB-late-stage displaying the greatest fold change increase at the mRNA level. This suggests that MAG surrounding the OV do not affect viral replication and the OV was able to complete its life cycle following cell infection. Indeed, from the TEM images in **Figure 3.7** once the MAG-OV was inside the cell the MAG were shed and free OV was visible, this most likely enables the OV to replicate. This is in keeping with previous studies which showed shielding the oncolytic adenovirus Ad520 with silica-modified particles decorated with 25-kDa branched polyethylenimine(SO-Mag2) nanoparticles resulted in a significant increase in the replication of adenoviral DNA in tumour xenografts from 181RDB-fLuc human pancreatic carcinoma cells stably expressing firefly luciferase (Tresilwised et al., 2012). They showed that the magnetofection group displayed a significant increase ($p < 0.05$) in the expression of adenoviral DNA (hexon gene) compared with the group that received virus alone by using

regular PCR analysis. This is also in agreement with previous studies where Ad520-PEI-Mag2 complexes resulted in an increase in vitro of adenoviral DNA replication exposed by Southern blot analysis, and an enhancement in infectious progeny virus particles compared with the naked virus (Tresilwised et al., 2010b).

Next, an appreciation of the potential mechanisms of how MAG-OV induces cell death was investigated. Caspases are linked to apoptosis and viruses are known typically to activate apoptosis via caspase 8 and caspase 3 (Felt et al., 2015). Nguyen and Blaho have shown that HSV infection triggers apoptosis during the early stages of viral infection leading to immediate early viral gene expression. They found caspase 3 contributed to apoptosis induction. However, anti-apoptotic genes such as Bcl-2 and NF- κ B, which inhibit apoptosis, are produced during the later time-points post infection, leading to early and late viral gene expression. Consequently, this provide a balance between the pro- and anti-apoptotic factors during HSV infection (Nguyen and Blaho, 2009). Here we found that viral infection (OV and MAG-OV) appeared to induce a significant increase in Caspase 3, Caspase 8, FASL and HSPA1A gene expression when compared to the control in both MDA-MB-231 and MCF7 cells (**Figure 4.5**). While Bcl-2 and NF- κ B were significantly decreased following both OV and MAG-OV infection (**Figure 4.5, Figure 4.8**). Our data was taken at one-time point (24h) and therefore we cannot predict if changes in cell death markers occur over time. We assume that HSV1716 was able to induce apoptosis by downregulating anti-apoptotic factors and the data of high expression of heat shock protein 'HSPA1A' gene suggest immunogenic apoptotic cell death. HSV-2 infection was previously shown to cause apoptosis with the activation of Caspase 7 and Caspase 3 in mammary gland tumour cells (Ag et al., 2010). Another study reported that HSP70 and cleaved caspase 3 increased when HSV-1 ICP 0 mutant and wild-type HSV-1 were injected into mouse TUBO tumours (Workenhe et al., 2014). Together this suggests that both HSV-1 and HSV-2 treated tumours were able to induce apoptosis and induction of heat shock protein e.g. high expression of HSP-70 suggest immunogenic apoptotic cell death.

OV are also known to induce autophagy. For example, Santana et al., showed that HSV-1 is able to induce autophagy by increasing the GFP-LC3 and endogenous LC3 lipidation, and initiates autophagosomes in human neuroblastoma cells (Santana et al., 2012). Another study reported that LC3B lipidation increased when HSV-1 and a wild-type strain of HSV-2 infected SIRC (Statens Seruminstitut Rabbit Cornea) corneal cell line, suggesting both HSV types affect autophagy (Petrovski et al., 2014). Here we found that viral infection appeared to induce a significant increase in LC3B gene expression when compared to the control at both OV and

MAG-OV in both MDA-MB-231 and MCF7 cells (**Figure 4.5**). Suggesting that HSV1716 can induce apoptosis and autophagy in a coordinated fashion. In contrast, a previous study reported that HSV-1 ICP0 null oncolytic virus KM100 alone at MOI 10 was unable to increase the protein level of caspase 3 and LC3B in TUBO cells after different point time, while both mitoxantrone (MTX) and KM100 + MTX showed significant increase in levels of caspase 3 and LC3B (Workenhe et al., 2013). However, the level of caspase 3 and LC3B in this study were measured using Western blotting (protein level), whilst in our study this was measured using qPCR (gene level). Furthermore, ATG5 was unaffected in our study but the cancer cell survival and proliferation genes HSP90AA1, HSP90B1 and Bcl-2 displayed a significant decrease in both the OV and MAG-OV groups. Overall, our study suggests that there are multiple cell death mechanisms activated following infection with either OV or MAG-OV. It would be interesting to measure the protein level of these markers with our MAG-OV in future and experiment with different time points.

Immunogenic cell death (ICD) is one of the cell death types that includes the adaptive arm of the immune system (Melcher et al., 2011, Prestwich et al., 2008). The goal of ICD for dying tumour cells to induce the paracrine activation of dendritic cells and consequential priming of cytotoxic effectors, is the release of the extracellular ATP and HMGB1 along with the accumulation of CRT (Angelova et al., 2014, Kepp et al., 2011). Therefore, the release of ATP and HMGB1 following MAG-OV infection was measured in infected breast cancer cells. We found that extracellular ATP levels and HMGB1 levels were significantly increased at both OV and MAG-OV when compared with control and MAG alone (**Figure 4.6**). We also noticed the expression of CRT around the plasma membrane significantly increased with both OV and MAGOV, whereas untreated cells presented the diffuse distribution of CRT (**Figure 4.7**). MAG-OV infection was able to produce DAMPs from breast cancer cells as effectively as OV alone. Similarly, Coxsackievirus B3 virus infection induced the *in vitro* ICD of human non-small cell lung cancer cells, including cell surface CRT expression and release of ATP as well as HMGB1 (Miyamoto et al., 2012). Another report revealed that LG 261 glioma cells treated with Newcastle disease virus induced ICD, and expressed CRT and secreted HMGB1, but not ATP, and moreover improved the antigenicity of the cells resulted in an increase in infiltration of IFN- γ (+) T cells (Koks et al., 2015). Furthermore, an *in vitro* study showed that HSV-1 ICP0 mutant (the entire ICP0 coding region has been removed) and wild-type HSV-1 did not increase the level of HMGB1 in culture, however serum HMGB1 levels, HSP70 and cleaved

caspase 3 were increased when these viruses were injected into mouse tumours (Workenhe et al., 2014).

Next, we attempted to understand the impact of HSV1716 on the surrounding environment. Increasing the expression of cytokines generated upon OV infection, can result in activating the immune system towards the tumour cells that were infected with virus (Breitbach et al., 2016, Singh et al., 2012). In order to assess whether OV or MAG-OV influenced the tumour microenvironment, a panel of pro-inflammatory and anti-inflammatory cytokines were measured using qPCR and cytokine bead array (CBA). As we expected, there was not a big difference between OV and MAG-OV in both MDA-MB-231 and MCF7 cells. In our findings related to the gene expression data, the expression of TNF were upregulated in both MDA-MB-231 (**Figure 4.8A**) and MCF7 (**Figure 4.8B**) cells treated with OV or MAG-OV compared to the untreated cells. Moreover, the expression of CXCL10 was upregulated in MCF7 cells (**Figure 4.8B**) while unchanged in MDA-MB-231 (**Figure 4.8A**) cells treated with OV or MAG-OV compared to the untreated cells. At the protein level, CXCL10 and TNF was not in agreement with gene data. As the protein level of CXCL10 was significantly downregulated and the protein level of TNF were not affected in both cell lines treated with OV or MAG-OV (**Figure 4.9**). The protein level of INF γ showed a trend towards being upregulated in both MDA-MB-231 and MCF7 cells treated with MAG-OV compared to the untreated cells (**Figure 4.9**). However, this change was not significant. A previous study showed that HSV1716 resulted in the upregulation of IFN- γ and CXCL10 in ovarian cancer (Benencia et al., 2005). Another study found increasing the expression of the TNF in the tumour and surrounding tissue from a HSV vector backbone resulted in an increase in the ability of tumour cell killing in the presence of ganciclovir (GCV) (Moriuchi et al., 1998). Suggesting that OV or MAG-OV influenced the tumour microenvironment by increasing the level of pro-inflammatory cytokines. On the other hand, the gene level of anti-inflammatory cytokines IL-1B, NF-KB and VEGF were decreased in both MDA-MB-231 and MCF7 cells treated with OV or MAG-OV compared to the untreated cells. In general, the literature does support a decrease in VEGF levels (Breitbach et al., 2007b, Breitbach et al., 2011b). Previous study revealed that intratumoral injection of the third generation oHSV, G47 Δ -mIL12, significantly altered the tumour microenvironment of GSC-derived intracerebral tumours. In this study, they have shown G47 Δ -mIL12 downregulated VEGF expression and upregulated CXCL10 (Cheema et al., 2013). VEGF is a pro-angiogenic marker and is important to carcinogenesis. In many solid tumors, high expression of VEGF have been associated with poor clinical consequence (Dent,

2009). The reduction of VEGF with HSV1716 therefore has the potential to inhibit angiogenesis.

At the protein level, the expression of IL-6, IL-8, IL10 and VEGF were also significantly downregulated in both MDA-MB-231 and MCF7 cells treated with OV or MAG-OV compared to the untreated cells except the expression of IL-10 in MCF7 cells was not changed (**Figure 4.9**). The cytokine bead array (CBA) was used to measure the extracellular level of these proteins therefore we assume that the intracellular proteins level have been changed. It would have useful to also assess intracellular protein expression with western blots. Also assessing protein expression over more than a single timepoint would have been useful in case protein secretion was missed.

OV neutralisation following systemic delivery is a major hindrance to success of this therapy for tumours that are inaccessible (**Figure 1.7**). *In vivo* studies have already shown OVs are cleared after a few days following infection of mice bearing gliomas (Andreansky et al., 1997, Mineta et al., 1994). In addition, Extracellular Enveloped Virus (EEV) (one of the morphologically distinct infectious forms of virions that produced by the prototype of the poxvirus family) can avoid both complement and neutralising antibodies by protecting itself in an envelope derived from host cells (Ichihashi, 1996, Law et al., 2002, Smith et al., 1997, Vanderplassen et al., 1998). This envelope is formed when the outer intracellular enveloped virus (IEV) membrane fuses with the plasma membrane. In this thesis, we hypothesised that MAG would protect the virus from neutralisation. As shown in **Figure 4.10**, MAG-OV+ NAb were able to infect the tumour cells as efficiently as the MAG-OV after 24h of culture. Cells incubated with OV+Nab expressed significantly less GFP after 24h of culture compared to MAG-OV+ NAb. This decrease in GFP expression is most likely because of OV neutralisation and indeed statistically significant reduced cell death was observed with OV+Nab compared to the MAG-OV+ NAb after 24h of culture (**Figure 4.10**). Suggesting that MAG-OV could minimise the interaction of HSV1716 with neutralising Ab because of MAG protecting the virus. Studies available in the literature examining the neutralisation of HSV1716 are limited. However, there are many attempts to overcome the problem of virus neutralisation. For example, Muthana et al., have tried to protect the virus from neutralisation using cell carriers, in this study magnetic resonance targeting using MRI was used to steer magnetically labelled macrophages carrying Ad-CMV-GFP into primary and metastatic tumour sites (lungs) in mice (Muthana et al., 2015b). A previous study attempted to overcome the problem of virus neutralization by using Nanomedicine approaches. They found that oncolytic adenovirus

Ad520 can be protected against the inhibitory effects of serum or a neutralising antibody *in vitro* when it was protected with PEI-Mag2 or PB-Mag1 nanoparticles (Tresilwised et al., 2012a)

In this study we used sheep serum but it would be interesting to use other inhibitory effects to neutralize the HSV1716, such as using human serum derived from donors who have high, medium or little/no HSV antibodies to assess MAG-OV neutralisation.

Taken together these data suggest that MAG-OV is able to enter and replicate inside breast cancer cells, at the same time inducing tumour cell death as good as OV alone but with the addition of protecting the virus from neutralising Ab. Nevertheless, this inference is based on *in vitro* data. Therefore, the next chapter will study whether MAG will improve targeting of OV in the presence of external magnetic field gradients and examine whether our complex can stimulate immune effector cells in an *in vivo* model.

Chapter 5

Targeting delivery and immunotherapy of MAG-OV in tumour-bearing mice using an external magnetic field

5.1 Introduction

There are numerous studies documenting the targeted delivery of MNPs in tumour-bearing mice using an external magnetic field to guide the particles to the tumour (Kyrtatos et al., 2009, Arbab et al., 2004, Riegler et al., 2010, Landázuri et al., 2013, Riegler et al., 2013). A previous study showed that HAI-178-FMNPs, an anti- α -subunit of ATP synthase antibody, (HAI-178) monoclonal antibody-conjugated fluorescent MNPs, could be injected intravenously into gastric cancer-bearing nude mice under the application of an external alternating magnetic field with 63 kHz and 7 kA/m for 4 min (Wang et al., 2014a). This resulted in reducing tumour growth compared to the control group (treated with saline), suggesting that HAI-178-FMNPs has a therapeutic function for gastric cancer *in vivo*. Moreover, the copolymer of reducible polyamidoamine (rPAA) self-assembled with superparamagnetic iron oxide nanoparticles (SPIONs) was used to deliver doxorubicin (DOX) in mice in a xenograft of the MDA-MB-231 tumour cells through i.v. injection and inhibited tumour growth efficiently. Here they used a magnet that was left on the tumour for 1.5 h following injection (Chen et al., 2014).

Furthermore, a recent study showed that using MNPs with an OV offered high cellular uptake within a minute and was considered a key advantage for the non-invasive targeting of OVs *in vivo*. In this study, Almstätter et al. used a selected core-shell type iron oxide MNPs in combination with either adenovirus (Ad) or vesicular stomatitis virus (VSV) intratumourally in orthotopic hepatocellular carcinoma (HCC) bearing rats in the presence of a magnet placed on the surface of the tumour nodule opposite to the injection site (Almstätter et al., 2015). They found that MNP-VP complex accumulated in the tumour at the side of where the magnet was placed. In addition, VSV titre and non-heme iron content of SO-Mag-VSV complex-injected tumours increased compared to naked VSV-injected tumours (30 min post infection).

Whilst direct intratumoural administration is possible for accessible tumours and has the potential to attain high concentrations of MNPs without the complications of systemic toxicity, this can also lead to undertreated regions in the tumour, thus allowing untreated tumour areas to progress (Hilger et al., 2005, van Landeghem et al., 2009). Importantly, intratumoural administration will not be useful for targeting small metastatic tumour growths or inaccessible tumours. Intravenous injection would be a better alternative as this would generally reach tumours adequately, even small tumours (Hainfeld et al., 2011, Hainfeld et al., 2013) and is less invasive than direct tumour injection. Furthermore, the distribution of intravenous injection is more comprehensive than the punctate distribution from direct intratumoural injections (Hilger et al., 2002, Huang and Hainfeld, 2013). Previous work has shown that

polyethyleneimine-modified iron oxide nanoparticles could be injected intravenously into mice with brain tumours under the application of an external magnetic field (50 mT) (Chertok et al., 2010). This resulted in selective accumulation and retention in GBM (brain) tumours in comparison to control animals, which did not undergo magnetic targeting. Further, studies at the University of Sheffield have shown that macrophages loaded with MNPs could be injected systemically into mice with prostate tumours and attracted from the circulation to the implanted tumour (on the flank) in mice using a 0.5T external magnetic placed directly above the tumour (Muthana et al., 2008a).

A recent study by Khierkah and co-workers showed that magnetic targeting of drugs could be used to treat intramedullary spinal cord tumours of the central nervous system. They used biocompatible iron oxide magnetite (Fe_3O_4) conjugated to doxorubicin. The iron particles were coated with gold and electrostatic interactions were used to attach the chemotherapy to the MNPs (DOX-MNP). They used a rat model whereby human glioblastoma multiforme tumour cells were implanted into the thoracic spine parenchyma. At the same time, they also implanted a 1 cm, 0.01 Tesla neodymium magnet sub-dermally overlying the tumour cell injection site to create a magnetic field at the tumour site. MNP-DOX nanoparticles were then introduced into the lumbar intrathecal space once the tumour was established and guided by the implanted magnet to the tumour site (Kheirkhah et al., 2018). Whilst exciting, surgically implanting the magnet could have serious adverse effects and result in complications from the surgery. In addition, this magnet was in place throughout the whole time of the experiment and it is unclear if this may have affected the animals.

Wang and co-workers showed that magnetic targeting of MAG + near infrared (NIR) could be used to treat hepatoma 22 (H22) cells injected subcutaneously into the right flank region of mice. They used MAG extracted from *Magnetospirillum magneticum* strain AMB-1 with NIR light stimulated photothermal therapy (PTT) with nanomaterials. The rectangular-pyramid frustum pole of the C-shaped magnet were placed on the tumour for 4 hr following injection of the purified MAG (4.0 mg/ml) intravenously. They found that all the tumours of mice in MAG + MF + NIR group completely disappeared. Suggesting that magnetic targeting could be used to increase the therapeutic efficiency of PPT with MAG after intravenous injection (Wang et al., 2018a).

OVs are extremely immunogenic and stimulate both innate and/or adaptive immune responses, in addition to the hallmark of the direct oncolytic effect (Takasu et al., 2016). As a result, OV's

are considered to be a cancer immunotherapy. Stimulating the immune system using HSV1716 to destruct the tumour has been studied in a syngeneic murine intracranial melanoma model (Miller and Fraser, 2000). In addition to reducing tumour growth infiltration of CD4+ T cells and macrophages, as well as CD8+ T cells, B cells, NK cells and microglia cells into the tumour, were examined after viral infection. Specifically, CD4+ T cells and macrophages were increased after viral administration (Miller and Fraser, 2000). Furthermore, HSV (G207) therapy of mouse CT26 colon adenocarcinoma tumours inhibited the growth of contralateral tumours as well as a second challenge of tumour cells in immune-competent mice (Toda et al., 1999). This study suggested that HSV increased mouse survival as a result of infiltrating cytotoxic T-cells.

Therefore, we will study both the magnetic targeting potential of our MAG-OV complex as well as the virus's ability to induce anti-tumour effects in mammary tumours. A detailed investigation of the immune activity of our MAG-OV is essential due to the combination of using an OV and bacterial-derived MAG. As mentioned earlier, MAG have the potential to activate the immune system particularly if the bacterial derived proteins are not stripped from the MAG, so it is important to determine if this activates the immune system and if this could result in adverse effects.

In addition to investigating the anti-tumour efficiency of MAG-OV, we will also determine whether MAG can protect OV from neutralizing Ab in an *in vivo* immunocompetent mouse model. We have used an immunocompetent mouse model whereby C57/BL6 mice were injected into the nipple with the luciferase labelled breast cancer cell line EO771-Luc. This cell line is a spontaneously developing medullary breast adenocarcinoma derived from C57BL/6 mice (Sugiura and Stock, 1952). This is also a triple negative breast cancer (TNBC) cell line for the oestrogen, progesterone and human epidermal growth factor HER2 receptors, making it difficult to target therapeutically (Johnstone et al., 2015). Furthermore, this tumour model naturally metastasises to the lungs in C57BL/6 mice (Johnstone et al., 2015). As the cell line is luciferase labelled, bioluminescence imaging using the IVIS was used to monitor tumour growth and metastasis.

The specific objectives of the study were to characterise the targeting of MAG-OV *in vivo* using external field gradients - with particular reference to:

1. Tumour targeting and therapeutic efficacy of MAG-OV in the E0771 mammary carcinoma model.
2. Stimulation of immune effector cells by MAG-OV.
3. MAG-OV protection from neutralising antibodies.

5.2 The antitumour efficacy of MAG-OV in the E0771 mammary carcinoma model

5.2.1 *In vivo* study Design

C57BL/6 female mice were purchased from Envigo at 6-8 weeks old and housed in the University of Sheffield Biological Services Unit and cared for according to the University of Sheffield code of ethics and Home Office regulations. All work was carried out under personal licence number is 1806F7C1E and Home office project licence PPL70/8670.

Mice were injected into the nipple with 5×10^5 EO771-Luc cells, and monitored daily, and weighed every three days. Tumour volume was measured using callipers and also recorded every three days. Each group of mice included in this study consisted of n=6-9 mice/group because some of mice have not developed tumours. Once the tumours reached $\sim 150\text{-}200\text{mm}^3$ mice received the following treatments intravenously (i.v.), see (**Figure 5.1**) for a schematic of the study.

1. **Control:** Mice were injected three times i.v. (0, 5, 10 days) with 100ul PBS.
2. **MAG:** Mice were injected three times i.v. (0, 5, 10 days) with 100ul MAG (10ul MAG + 90ul PBS).
3. **OV:** These mice were injected three times i.v. (0, 5, 10 days) with 100ul HSV1716 (10ul OV at 10^7 pfu + 90ul PBS).
4. **MAG-OV without magnet:** Mice were injected three times i.v. (0, 5, 10 days) with 100ul magnetised HSV1716 (12ul MAG-OV at 10^7 pfu + 88ul PBS).
5. **MAG-OV+ magnet:** Mice were injected three times i.v. (0, 5, 10 days) with 100ul magnetised HSV1716 (12ul MAG-OV at 10^7 pfu + 88ul PBS) in the presence of an external permanent magnetic array secured above the tumour (0.7 T) for 30 min.

Once the tumours reached $\sim 1500\text{mm}^3$ mice were culled by cervical dislocation, and the organs and tumour were removed and stored in liquid nitrogen for post-mortem analysis. Of note, the magnet design, assembly and length of time placed above the tumour, were optimised by a post-doctoral research fellow in the group (Dr Priya Patel).

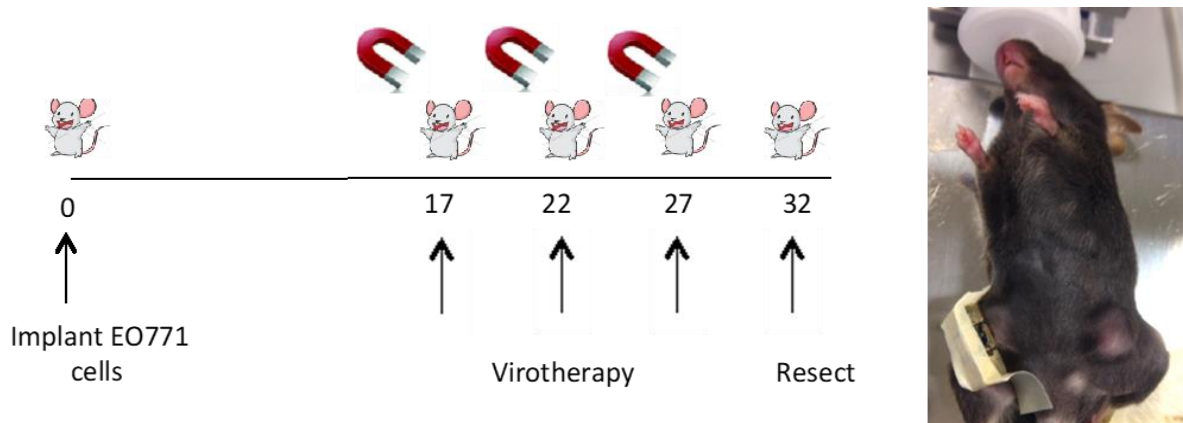


Figure 5.1: Treatment scheme in C57BL/6 female mice with a mammary carcinoma. Mice were injected into the nipple with 5×10^5 EO771-Luc cells. Each group of mice included in this study consisted of $n=6-9$ mice/group. Once the tumours reached $\sim 150-200 \text{ mm}^3$ mice were injected three times i.v. (0, 5, 10 days) with 100ul of PBS, MAG, OV and with and without MAG-OV. Once the tumours reached $\sim 1500 \text{ mm}^3$ mice were culled by cervical dislocation, and the organs and tumour were removed and stored in liquid nitrogen for post-mortem analysis.

5.2.2 Magnetic guidance of MAG-OV shrinks primary mammary tumours and promotes survival

In this *in vivo* experiment, we used an external magnet to guide MAG-OV from circulation into primary mammary tumours. Mice were intravenously treated with three doses of MAG, OV, MAG-OV without magnet (MAG-OV WM), MAG-OV with magnet (MAG-OV+M) or PBS as a control and monitored over time. There was no change in body weight in all treatment groups compared to the PBS treated mice in the 2 weeks post therapy (**Figure 5.2A**). However, a significant change in average tumour volume was observed in mice receiving MAG-OV with magnet compared to the mice receiving PBS on day 12 after treatment ($p = 0.0002$). In addition, a significant change in average tumour volume was observed in mice receiving OV compared to the mice receiving PBS on day 12 after treatment ($p = 0.0036$). While no significant change was observed in mice receiving MAG or MAG-OV without magnet compared to the mice receiving PBS. In theory, the MAG-OV without magnet should be the same as OV- not seeing any effect suggests that either the MAG are not letting the virus have its effect or without the magnetic guidance perhaps the two are separating and not enough is getting to the tumour. This requires further investigation. In addition, the average tumour volume was significantly smaller in the MAG-OV+M -treated group than in the OV group at day 15 after treatment ($p = 0.0062$), (**Figure 5.2B**). This indicates that magnetic targeting is improving the efficacy of this treatment. Furthermore, **Figure 5.2C** shows most of the mice in MAG-OV+M group resulted in a significant increase in survival compared to the others groups. For the bioluminescence

imaging (BLI), mice were injected with 100 μL of d-Luciferin subcutaneously for 10 Min. Then, a non-invasive in vivo imaging system (IVIS 200 System, Xenogen) was used to image mice. Based on the detection and quantitation of the photons produced by the oxidation of luciferin by luciferase enzymes. Bioluminescence imaging of mice receiving MAG-OV+M on day 12 of treatment showed this marked reduction in the size of the primary tumour, (**Figure 5.2D**). For all the following experiments and the rest of this chapter MAG-OV+M (in the presence of the magnetic field) will be referred to as MAG-OV.

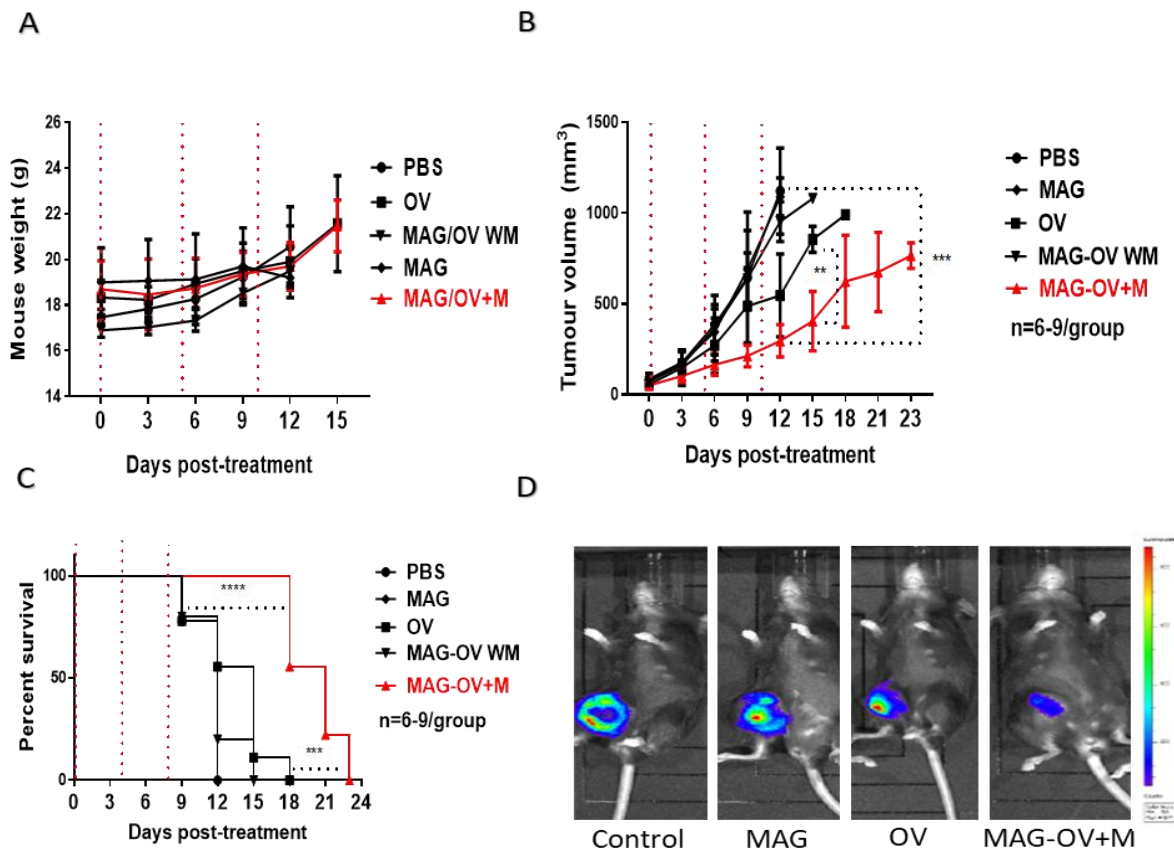


Figure 5.2: Magnetic targeting of MAG-OV shrinks primary mammary tumours. EO771 tumour-bearing mice were monitored daily for tumour growth with calipers and weighed every three days. **A.** No change in body weight was recorded for treated animals compared to untreated mice for up to 2 weeks post-therapy. **B.** A significant change in average tumour volume was observed in mice receiving MAG-OV in the presence of a magnet (red line: MAG-OV+M) compared to the mice receiving PBS on day 12 after treatment. **C.** Moreover, MAG-OV+M treated mice demonstrated a significant increase in survival compared to the others groups. **D.** For the BLI, mice were injected with 100 μL of d-Luciferin subcutaneously for 10 Min. Then, a non-invasive in vivo imaging system (IVIS 200 System, Xenogen) was used to image mice. Based on the detection and quantitation of the photons produced by the oxidation of luciferin by luciferase enzymes. BLI of mice receiving OV therapy or MAG-OV+M on day 12 of treatment showed this marked reduction of the primary tumour. Of note, data are the Mean \pm SEM (n=6-9) and statistical analysis was assessed using one-way Anova test with multiple comparisons for tumour volume and survival curve for mice survival. **p<0.01; ***p<0.001; ****p<0.0001.

5.2.3 Increased MAG-OV in primary breast tumours following magnetic guidance

As shown above, MAG-OV+M was the most effective therapy for reducing tumour volume. Next, we wanted to confirm the presence of the HSV1716 within the tumours. This was performed using two approaches flow cytometry and immunofluorescence and at two timepoints (3 days and at end of the experiment). For the former, cells were analysed on a flow cytometer to detect the HSV1716-GFP. Tumour chunks were dissociated as described in **Section 2.2.23.4**. Samples were re-suspended in 300ul of FACS buffer (1%FBS/PBS solution) and transferred to flow cytometry tubes. A cell viability dye was added to all the samples to gate out debris and dead cells. Flow cytometry data was analysed using the BD LSR II flow cytometer and GFP expression was measured in FL-1 (488nm). A significant increase in the percentage of HSV1716-GFP was observed in MAG-OV compared to the PBS group after 3 days of infection (MAG-OV 6% vs PBS 0%) (**Figure 5.3A**). Moreover, a significant increase in the percentage of HSV1716-GFP was observed in MAG-OV compared to all other groups at the end of the experiment (MAG-OV 13% vs. PBS 0 %) as shown in **Figure 5.3B**. One of the difficulties with the flow cytometry experiment is that the samples contained so much debris and dead cells that the data may not be truly representative. It is not clear whether this was due to how the samples were processed or because of the necrotic nature of the mammary tumours. Therefore, to further confirm the presence of HSV1716-GFP, immunofluorescent staining of tumours was performed in sections that were frozen immediately following removal. Tumours were first embedded in OCT before freezing and sectioned using a cryostat (14µm thick sections). After this, cells were fixed and stained with a sheep antibody to detect HSV1716 (Conner et al., 2005). Moreover, 50ng/ml DAPI solution was added for 2 min to define the nucleus. Coverslips were mounted onto the microscope slides and a Nikon A1 confocal microscope was used to take images. HSV1716 positive cells were counted by using Fiji (Fiji Is Just ImageJ), as previously published (Schindelin et al., 2012). The number of nuclei per FOV needed to be assessed, so cell counts could be normalised to the total number of cells in the FOV. As shown in **Figure 5.3C**, MAG-OV resulted in the greatest expression of HSV1716 compared to OV alone (MAG-OV 70.2% vs. OV 14.8% $P= 0.0027$). No virus was detected in the control or MAG treated mice.

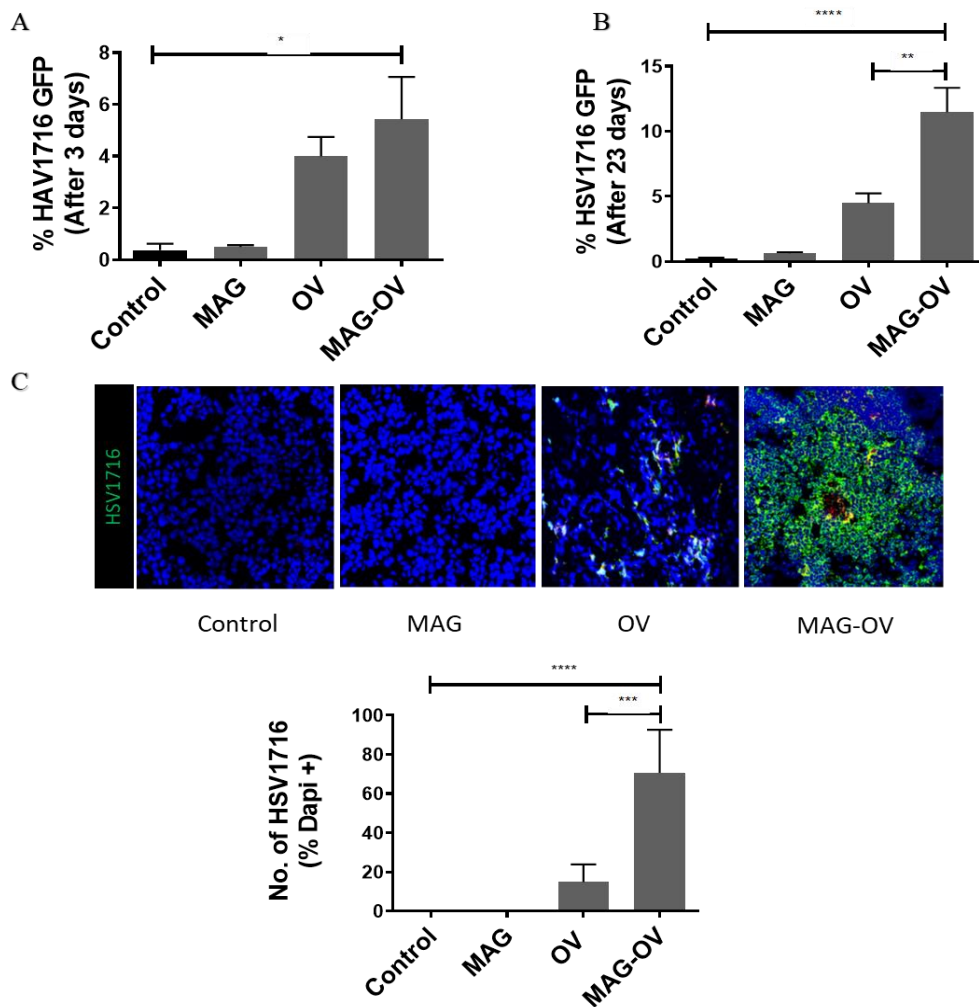


Figure 5.3: Increased systemic targeting of MAG-OV to mammary tumours in the presence of an external magnetic field. Dissociated tumour chunks were analysed on a flow cytometer to detect HSV1716-GFP. GFP expression was measured in FL-1 (488nm) on a LSRII flow cytometer. **A.** A significant increase in percentage of HSV1716-GFP was observed in MAG-OV compared to the all other groups after 3 days of infection. **B.** The presence of the HSV1716 was also measurable at the end of the experiment (day 23). **C.** Immunofluorescence staining of tumours was also used to detect the HSV1716-GFP. MAG-OV was able to infect EO771 cells significantly more compared to the OV alone and the other groups. A Nikon A1 confocal microscope was used to take images. The density of HSV1716 was calculated by dividing the total number of HSV1716 positive cells by the number of DAPI+ events in each specified region and multiplying by 100. Of note, data are the Mean \pm SEM (n=5) and statistical analysis was assessed using the one-way Anova test with multiple comparisons. *p<0.05; **p<0.01; ***p<0.001; ****p<0.0001.

5.2.4 Increased MAG-OV viral replication following magnetic guidance

Expression of viral replication genes was determined by qPCR in mammary tumour removed from mice post-treatment. RNA was extracted after tumour digestion and used to synthesise cDNA. Viral replication genes ICP0 – immediate early, ICP8 – early and gB – late genes (Singh et al., 2012), were evaluated. Virus successfully replicated within the tumour microenvironment, as shown by the significant increase in all the viral mRNA genes (ICP0,

ICP8 and gB) in the MAG-OV treated mice compared to the OV and control groups (**Figure 5.4**). This suggests that magnetic guidance enabled virus to replicate more efficiently than the other treatment groups. mRNA expression of ICP8 was also significant with OV groups compared to the control (**Figure 5.4**). Suggesting that OV was able to complete their life cycle within EO771 tumour cells.

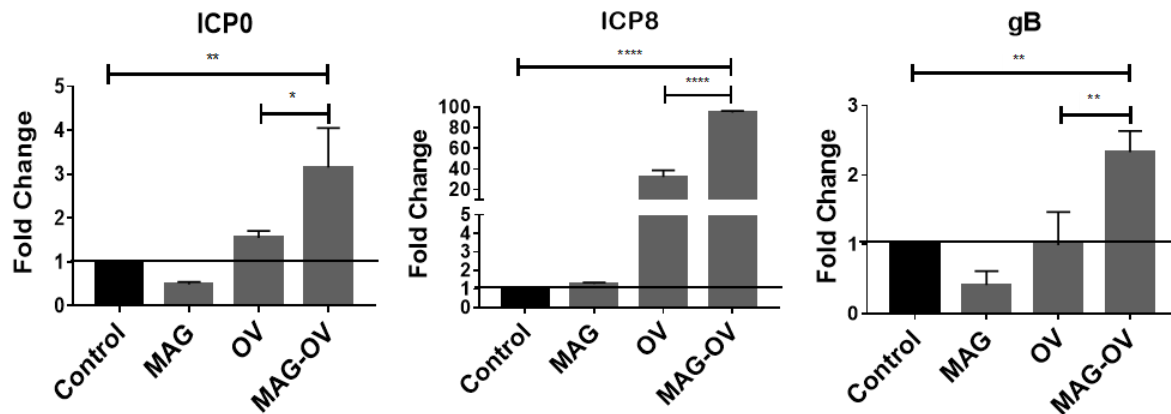


Figure 5.4: Increased viral replication of MAG-OV in mammary tumours in the presence of an external magnetic field. RNA was isolated from mammary tumours post-treatment and analysed using qPCR. Virus successfully replicated within the cells, as shown by the significant increase in viral mRNA expression of ICP0, ICP8 and gB in the MAG-OV treated mice when compared to the OV and control groups. The expression levels were calculated relative to the untreated cells using the $2^{-\Delta\Delta CT}$ method after the data was normalised to the housekeeping gene, *GAPDH*. Of note, data are the Mean \pm SEM (n=3) and statistical analysis was assessed using the one-way Anova test with multiple comparisons. *p<0.05; **p<0.01; ***p<0.001; ****p<0.0001.

5.2.5 MAG-OV induces anti-tumour properties following magnetic guidance

The anti-tumour effect of MAG-OV was detected by measuring a number of changes within tumour microenvironment including tumour vascularity, necrosis, the expression of calreticulin (CRT) and pulmonary metastasis. Targeting the tumour vasculature using OV is an attractive strategy in cancer therapy. OV including vaccinia and vesicular stomatitis virus can intrinsically target tumour vasculature leading to vessel disruption (Toro Bejarano and Merchan, 2015). Tumour vascularity post-treatment was assessed by calculating the number of CD31+ve cells per field of view (FOV) using immunofluorescent staining. CD31 is a standard marker of blood vessels and used to assess vascularity in tumours (Muthana et al., 2015b). MAG-OV treated tumours showed a trend of being less vascularised than the other treatments groups (**Figure 5.5A**). However, this change was not significant.

Necrosis is a type of cell death caused by external factors such as viruses (Yu et al., 2015). Necrosis was assessed by calculating the percentage of necrotic areas in the whole tumour section by Haematoxylin and Eosin staining. As shown in **Figure 5.5B**, tumours treated with MAG-OV in the presence of a magnet were significantly more necrotic than those treated with PBS (MAG-OV 61.3% vs PBS 21%). While tumours treated with naked OV or MAG showed no significant change compared to those treated with PBS (OV 43.2% and MAG 18.3% vs. PBS 21%). This was also confirmed by flow cytometric analysis of the percentage of live cells, where tumours treated with MAG-OV were significantly less than those treated with PBS, (**Figure 5.5C**).

Furthermore, CRT is a DAMP that is normally located in the lumen of the endoplasmic reticulum. Immunogenic apoptosis leads to translocation of CRT to the surface of dying cells as an eat-me indicator for professional phagocytes (Obeid et al., 2006, Gold et al., 2010, Voll et al., 1997). The expression of calreticulin was measured by using immunofluorescence staining. **Figure 5.5D** shows that the number of calreticulin positive cells (and Dapi+ve) increased significantly in tumours treated with MAG-OV than those treated with PBS or OV.

In C57BL/6 mice, EO771 cells implanted into the mammary fat pads metastasise to the lungs (Johnstone et al., 2015). Therefore, pulmonary metastasis was measured using Haematoxylin and Eosin staining. Lungs were prepared as described in **Section 2.2.23.6**. Pulmonary metastases were identified by microscopy and could be seen as tumour nodules greater than 10 mm in diameter (Kaseda et al., 2016). Many metastases were detected in the lungs of mice injected with PBS or MAG alone at day 12 of treatment because of the large size of their primary tumours. However, the number of pulmonary metastasis was significantly reduced in mice that received MAG-OV compared to those treated with PBS (**Figure 5.5E**).

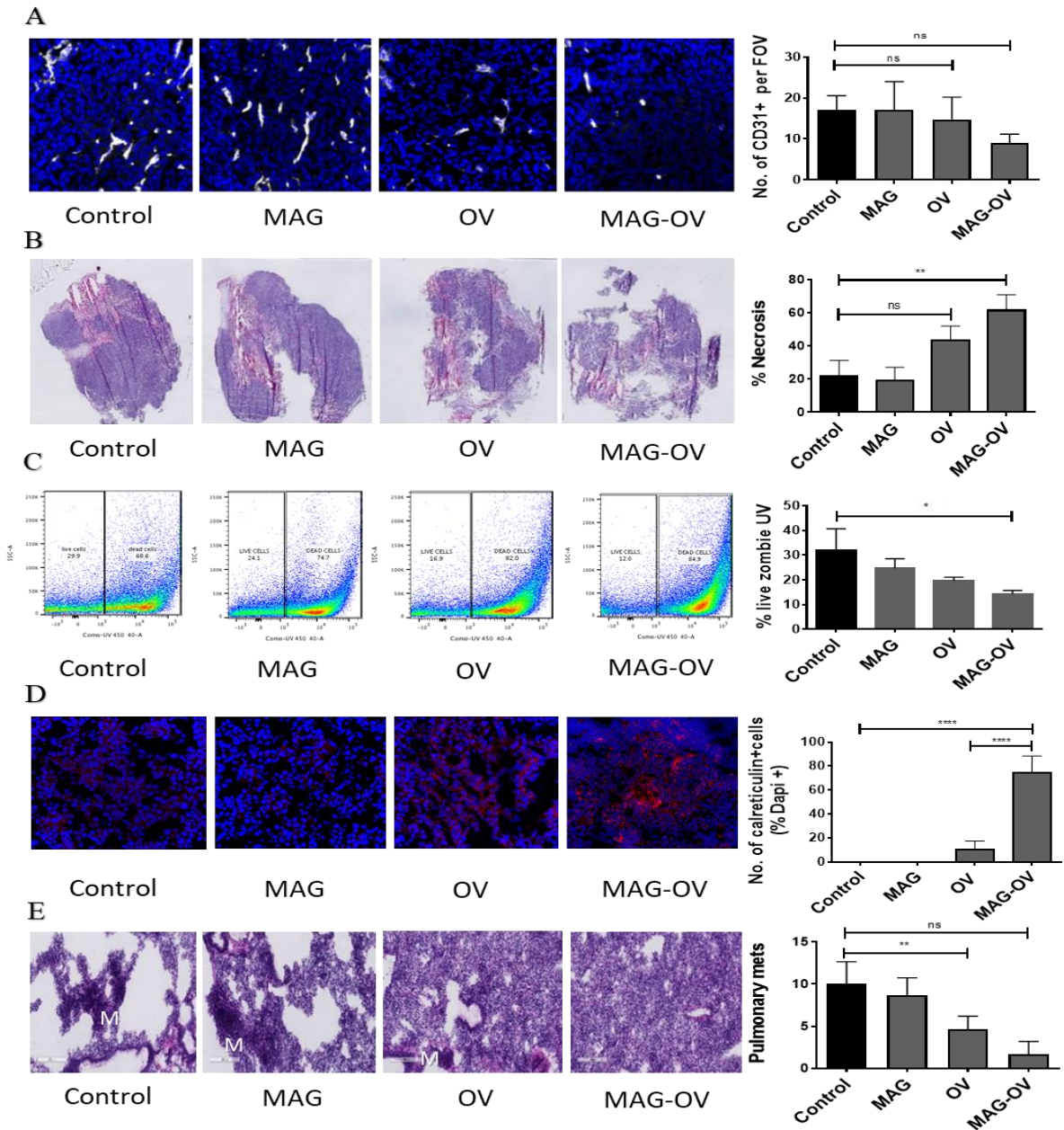


Figure 5.5: MAG-OV increases tumour necrosis and immunogenic cell death. A. Immunofluorescence staining of CD31+ve cells per Field of view (FOV) showed MAG-OV treated tumours were less vascularised than the PBS-treated tumours (scale bar = 40 μ m). However, this change was not significant. **B.** Haematoxylin and eosin staining (scale bar = 200 μ m) indicated that tumours treated with MAG-OV were significantly more necrotic than those treated with PBS. **C.** This was also confirmed by flow cytometry analysis of live cells using the Zombie UV viability dye, where tumours treated with MAG-OV were significantly less viable than those treated with PBS. **D.** Immunofluorescence staining analysis of CRT showed that the number of CRT^{+ve} cells (& Dapi^{+ve}) increased significantly in tumours treated with MAG-OV than those treated with PBS or OV lone (scale bar = 40 μ m), the density of CRT^{+ve} cells was calculated by dividing the total number of CRT^{+ve} cells by the number of DAPI+ events in each specified region and multiplying by 100. **E.** The number of pulmonary metastasis was significantly reduced in mice that received MAG-OV compared to those treated with PBS (scale bar = 200 μ m). Of note, data are the mean \pm SEM (n=3-5) and statistical analysis was assessed using the one-way Anova test with multiple comparisons. *p<0.05; **p<0.01; ***p<0.001; ****p<0.0001.

5.2.6 MAG-OV treated tumours induce anti-tumour immunity: NanoString analysis

Prior studies have revealed that, during oncolytic virotherapy, cellular immune mechanisms act jointly with virally mediated tumour damage (Thomas and Fraser, 2003, Miller and Fraser, 2003, Miller and Fraser, 2000). Therefore, to define the effect of MAG-OV targeting in the presence of a magnetic field on the immune pathways, RNA was isolated from tumours of treated mice (**Section 2.2.17.1**). This was analysed using the NanoString murine pan-cancer immune profiling panel, which consist of 750 immune related genes and 20 housekeeping genes. This work was carried out at the John van Geest Cancer Research Centre in College of Science and Technology at Nottingham Trent University in collaboration with Professor Graham Pockley and Jayakumar Vadakekolathu. All the RNA samples were quality controlled using Nanodrop 8000 and 150ng of total RNA from each sample was used for setting up the NanoString analysis. All the data processing was carried out by Mr Jayakumar Vadakekolathu in Nottingham. **Figure 5.6** shows volcano plots of gene expression in MAG, OV or MAG-OV treated tumours compared to the PBS treated group. Interestingly, in the MAG only treated group (MAG) >27 genes were up-regulated (e.g. Ctsw, Cmah, C1s1) and 10 genes downregulated (e.g. Trp53, Cxcl12). Whilst, the MAG only group did not induce any therapeutic changes, this change in gene expression highlights that some consideration should be given when using MAG and this will be discussed later. As expected, the OV treated group resulted in up regulation of >35 genes compared to the PBS treated group. In the MAG-OV treated tumours, genes related to innate and adaptive immune responses (e.g. Cxcl2, Thbs1, Ifitm1, Cxcr2, Ccl3, Cd14, Ccr1, Icos and Clu), T-cell function (CTL-A4, Ccl3, Xcl1, Icos), NK Cell Functions (Ccl3), Macrophage Functions (Thbs1), Dendritic Cell Functions (Ccr1), Interferon (Runx3) as well as apoptosis (Gzmb, Osm, Gzma, Clu and Runx3) were differentially upregulated. These genes are outlined in **Table 5.1**. For simplicity the table only focuses on the MAG-OV vs. PBS treatment groups.

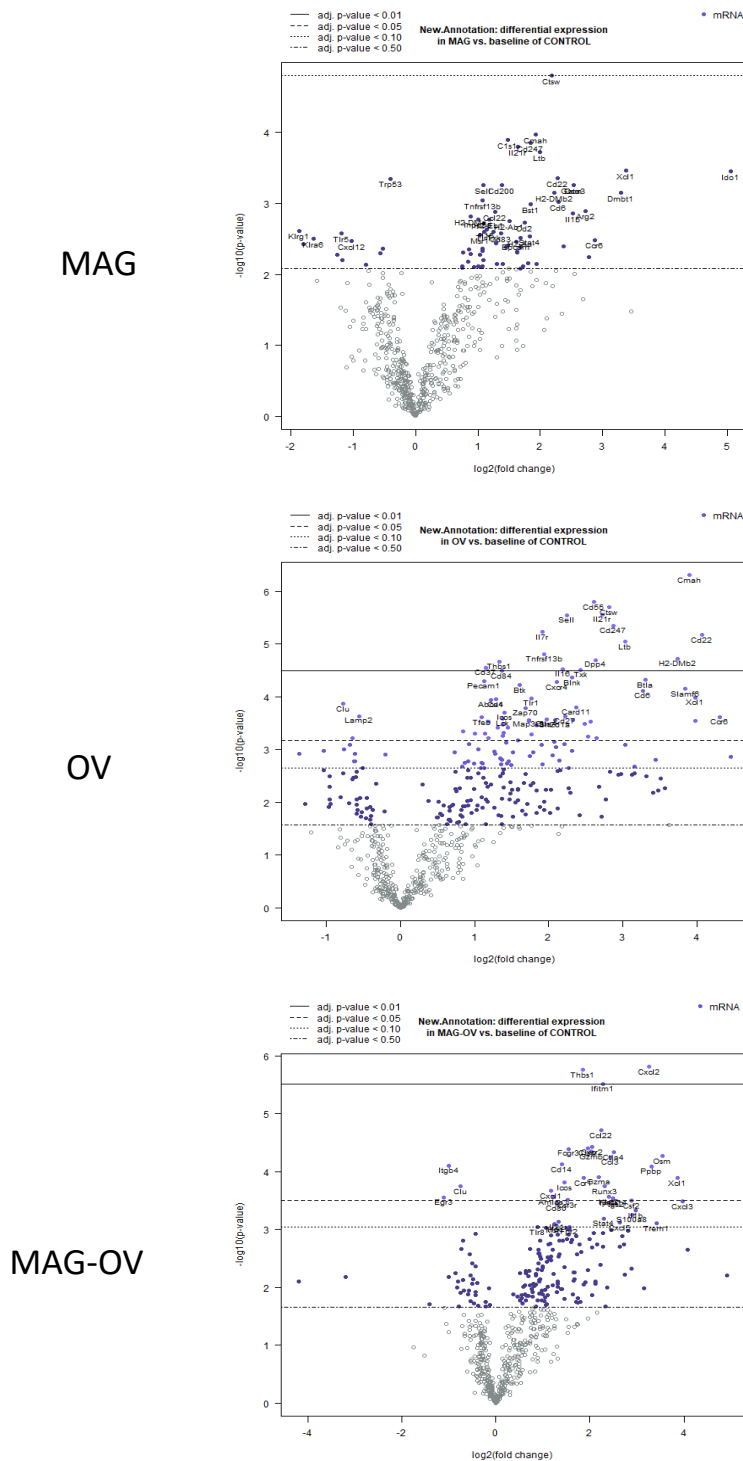


Figure 5.6: Volcano plots show MAG-OV increases expression of genes related to an immune response. To define the effect of MAG-OV on genes related to immunity, RNA was isolated from tumours and analysed using the NanoString murine pan-cancer immune profiling panel. Volcano plots show genes that were up regulated (+) or downregulated (-). The volcano plots show gene expression in MAG, OV or MAG-OV treated tumours compared to PBS treated tumours (n=3).

Table 5.1: Top 20 genes differentially regulated in MAG-OV treated tumours. Genes related to innate and adaptive immune responses (Cxcl2, Thbs1, Ifitm1, Cxcr2, Ccl3, Cd14, Ccr1, Icos and Clu), T-cell function (Ctla4, Ccl3, Xcl1, Icos), NK Cell Functions (Ccl3), Macrophage Functions (Thbs1) as well as apoptosis (Gzmb, Osm, Gzma, Clu and Runx3) are indicated (n=3) with fold change in expression over the control (PBS) and the pathways or gene sets. Data was processed and analysed using nSolver Analysis Software, using the Advanced Analysis module.

Gene	Log2 fold change	Gene. Sets
Cxcl2-mRNA	3.26	Adaptive, Chemokines & Receptors, Cytokines & Receptors, Inflammation, Innate, Leukocyte Functions
Thbs1-mRNA	1.85	Adaptive, Cell Cycle, Inflammation, Macrophage Functions
Ifitm1-mRNA	2.27	CD molecules, Innate, Interferon
Ccl22-mRNA	2.24	Chemokines & Receptors, Cytokines & Receptors, Humoral, Inflammation
Cxcr2-mRNA	2.04	Adaptive, CD molecules, Chemokines & Receptors, Cytokines & Receptors, Inflammation, Innate, Interleukins
Ctsw-mRNA	1.95	CD molecules
Fcgr3-mRNA	1.55	Antigen Processing, CD molecules, MHC, Transporter Functions
Gzmb-mRNA	2.02	Apoptosis, T-Cell Functions
Ctla4-mRNA	2.51	B-Cell Functions, CD molecules, T-Cell Functions
Osm-mRNA	3.54	Apoptosis, Cytokines & Receptors
Ccl3-mRNA	2.44	Adaptive, Chemokines & Receptors, Cytokines & Receptors, Humoral, Inflammation, NK Cell Functions, T-Cell Functions, Transporter Functions
Cd14-mRNA	1.4	CD molecules, Cytokines & Receptors, Inflammation, Innate, Pathogen Response, Transporter Functions
Itgb4-mRNA	-0.997	Adhesion, CD molecules
Ppbp-mRNA	3.31	Chemokines & Receptors
Gzma-mRNA	2.19	Apoptosis
Ccr1-mRNA	1.87	Adaptive, CD molecules, Chemokines & Receptors, Cytokines & Receptors, Dendritic Cell Functions, Inflammation, Innate, Leukocyte Functions, Transporter Functions
Xcl1-mRNA	3.86	Chemokines & Receptors, Cytokines & Receptors, Inflammation, Innate, T-Cell Functions
Icos-mRNA	1.45	CD molecules, T-Cell Functions
Clu-mRNA	-0.745	Apoptosis, Cancer Progression, Innate
Runx3-mRNA	2.32	Apoptosis, Cell Cycle, Interferon

Next, we carried out analysis of the different tumour infiltrating immune cells. A heat map shows infiltrating immune cells in PBS, MAG, OV or MAG-OV treated tumours. In the heat maps orange indicates high cell expression and blue indicates low cell expression (**Figure 5.7**). Cell type scoring and pathway scoring was performed using nSolver advance analysis module

V. 2.0.115. This software compares all the different immune cell types and creates scores relative to each other. The majority of the immune related cell types in the panel were upregulated in MAG-OV treated tumours. **Figure 5.7** shows that the T cells (cytotoxic CD8), NK cells, neutrophils and macrophages increased significantly in tumours treated with MAG-OV than those treated with PBS. T cells, CD8 T cells and Treg cells were also increased in tumours treated with MAG-OV than those treated with PBS. However, this change was not significant. On the other hand, CD4 vs. T cells were downregulated in tumours treated with MAG-OV than those treated with PBS.

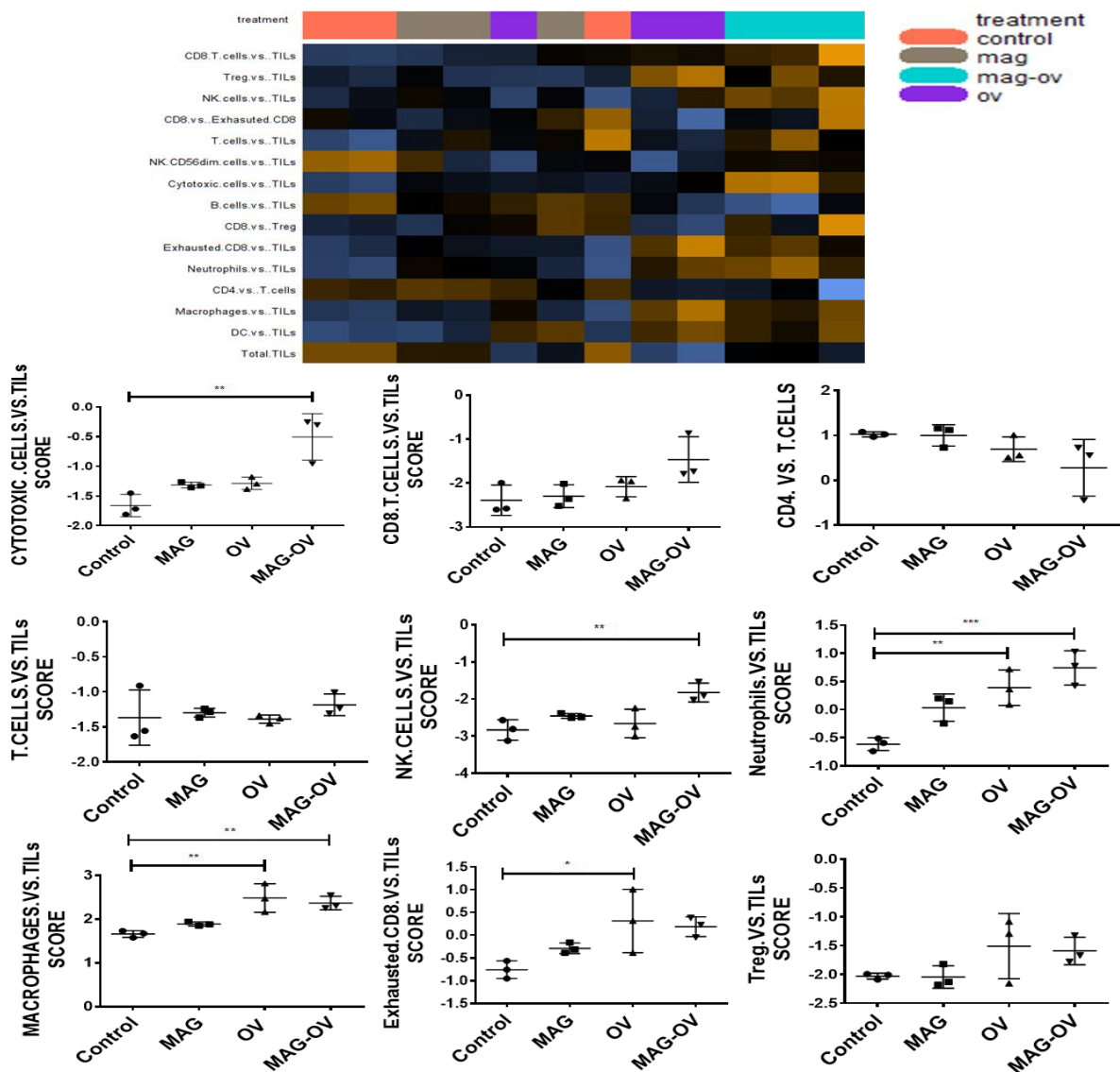


Figure 5.7: MAG-OV upregulates tumour infiltrating immune cells. nSolver 4.0 Analysis Software was used to prepare the heat map to show tumour infiltrating immune cells in PBS, MAG, OV or MAG-OV treated tumours. Orange indicates high cell expression and blue indicates low cell expression. The majority of the immune related genes in the panel were upregulated in MAG-OV treated tumours. Of note, data are the Mean \pm SEM (n=3) and statistical analysis was assessed using the one-way Anova test with multiple comparisons. * $p < 0.05$; ** $p < 0.01$; *** $p < 0.001$.

Furthermore, we carried out an immune pathway analysis of the genes in the PBS, MAG, OV or MAG-OV treated tumours. Notably, we detected a significant increase in expression of a range of immune-pathway genes in MAG-OV treated tumours than those treated with PBS (Figure 5.8). These pathways include innate and adaptive immunity, T-cell function, NK cell function, chemokines and receptors, cytokines and receptors, inflammation, TLR, leukocyte function, macrophage function pathway, transporter function, senescence y, dendritic cell function, basic cell function, cell cycle, apoptosis and pathogen response, many of which have previously been linked to immune activation by OV_s (Miller and Fraser, 2003, Thomas and Fraser, 2003, Miller and Fraser, 2000).

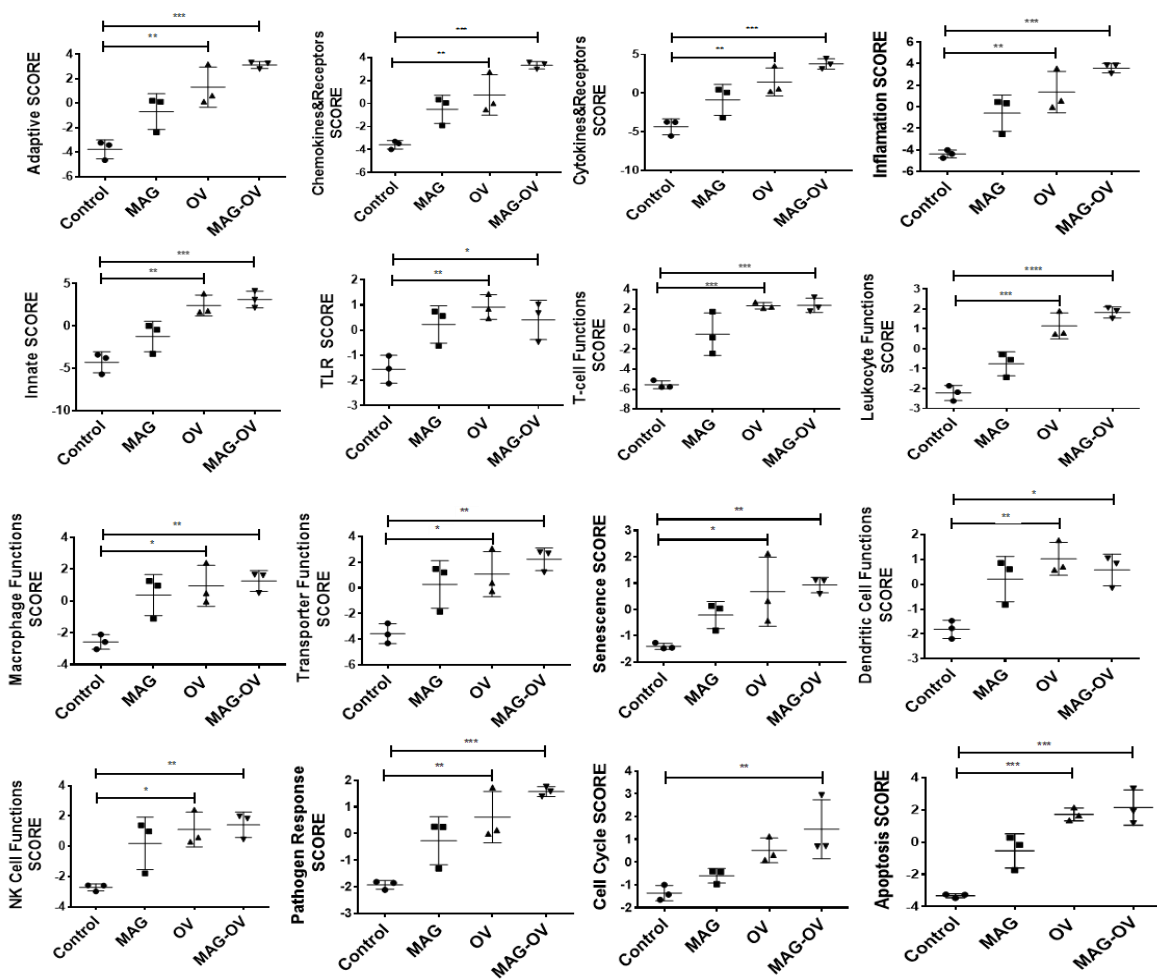


Figure 5.8: Magnetic targeting of MAG-OV upregulated the expression of a range of immune-pathway genes. A significant increase in expression of a range of immune-pathway related genes in MAG-OV treated tumours than those treated with PBS including adaptive innate pathway, T-cell function pathway, NK cell function pathway, chemokine and receptor pathway, cytokine and receptor pathway, inflammation pathway, TLR pathway, leukocyte function pathway, macrophage function pathway, transporter function pathway, senescence pathway, dendritic cell function pathway, basic cell function pathway, cell cycle pathway, apoptosis pathway and pathogen response pathway. Of note, data are the Mean \pm SEM (n=3) and statistical analysis was assessed using the one-way Anova test with multiple comparisons. *p<0.05; **p<0.01; ***p<0.001.

5.2.7 Magnetic targeting of MAG-OV increased immune cell infiltrates – Flow cytometry

To confirm the data of the NanoString technology, flow cytometry was used to measure the recruitment of immune cells into tumours. Tumour chunks were dissociated as described in **Section 2.2.23.4**. Cells were collected and flow cytometry was used to evaluate the percentage of CD3, CD4, CD8, NK1.1, LY6G and CD11B immune cell markers. The percentage of T cells (CD3⁺), cytotoxic T cells (CD3⁺/CD8⁺), Neutrophils (CD11B⁺/LY6G⁺) and NK cells (NK1.1) were significantly increased in tumours treated with MAG-OV compared to those treated with PBS (**Figure 5.9**). In contrast, the percentage of T helper cells (CD3⁺/CD4⁺) decreased in these treated tumours. However, this change was not significant (**Figure 5.9**). The receptor expression of immune cell surface markers, as measured by FACS, mirrors the gene expression data measured by NanoString.

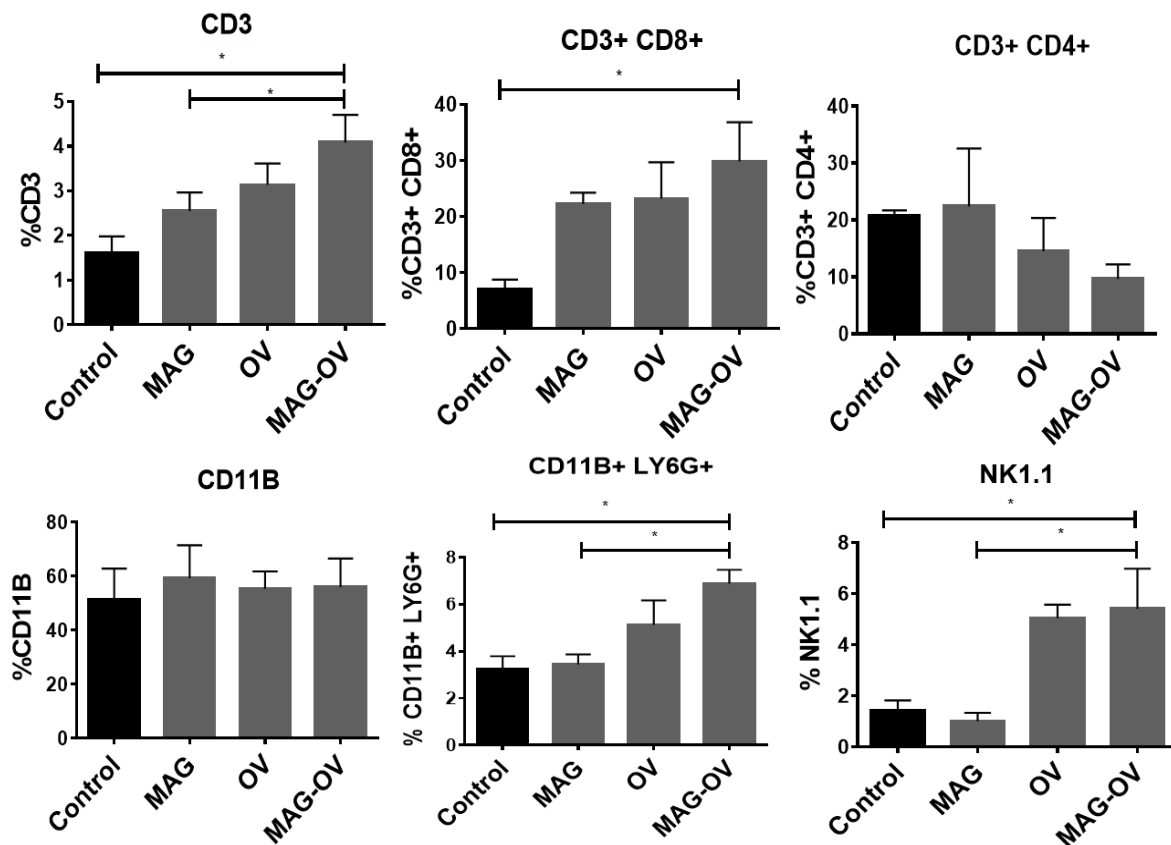


Figure 5.9: Magnetic targeting of MAG-OV upregulated infiltration of immune cells into tumours. Dissociated tumour chunks were collected and flow cytometry was used to evaluate the percentage of CD3, CD4, CD8, NK1.1, LY6G and CD11B. The percentage of CD3⁺, CD3⁺/CD8⁺, CD11B⁺/LY6G⁺ and NK1.1 significantly increased in tumours treated with MAG-OV compared to those treated with PBS. In contrast, the percentage of CD3⁺/CD4⁺ decreased in these treated tumours. A cell viability dye (Zombie UV dye) was included to gate out any cellular debris. Data was run on the LSRII and analysed using FlowJo. Data are the Mean \pm SEM (n=5 mice per group) and statistical analysis was assessed using the one-way Anova test with multiple comparisons. *p<0.05.

5.2.8 Magnetic targeting of MAG-OV increased immune cell infiltrates: Immunofluorescence

Immunofluorescent staining was also used to evaluate the number of CD3, CD8, CD4, F4/80 and NK1.1 expression within the tumours. Tumours were first embedded in optimal cutting temperature (OCT) before freezing, sectioned using the cryostat (14µm thick sections), fixed with ice cold acetone for 10 min at RT and then rehydrated with PBST for 1 min. Sections were then stained with anti-CD3, CD4, CD8, F4/80, NK1.1 and (4',6-diamidino-2-phenylindole) (DAPI) and analysed using a confocal laser-scanning microscope. The number of CD3⁺ (%Dapi+), CD3⁺/CD8⁺ (%Dapi+) and CD3⁺/CD4⁺ (%Dapi+) were significantly increased in tumours treated with MAG-OV compared to those treated with PBS or OV only, (**Figure 5.10A**). Moreover, F4/80⁺ (%Dapi+) and NK1.1 (%Dapi+) were also significantly increased in tumours treated with MAG-OV compared to those treated with PBS or naked OV (**Figure 5.10B&C**). Of note, in **Figure 5.10B**, F4/80 was co-labelled with the endothelial cell marker 'CD31'. This showed that macrophages within the TME were located throughout the tumour with some around the vascular areas in mice treated with virus, whereas in the control mice, most macrophages were in the perivascular areas. This is an interesting topic that warrants further investigation, particularly given that perivascular macrophages are thought to have a pro-tumour phenotype in breast cancer (Hughes et al., 2015).

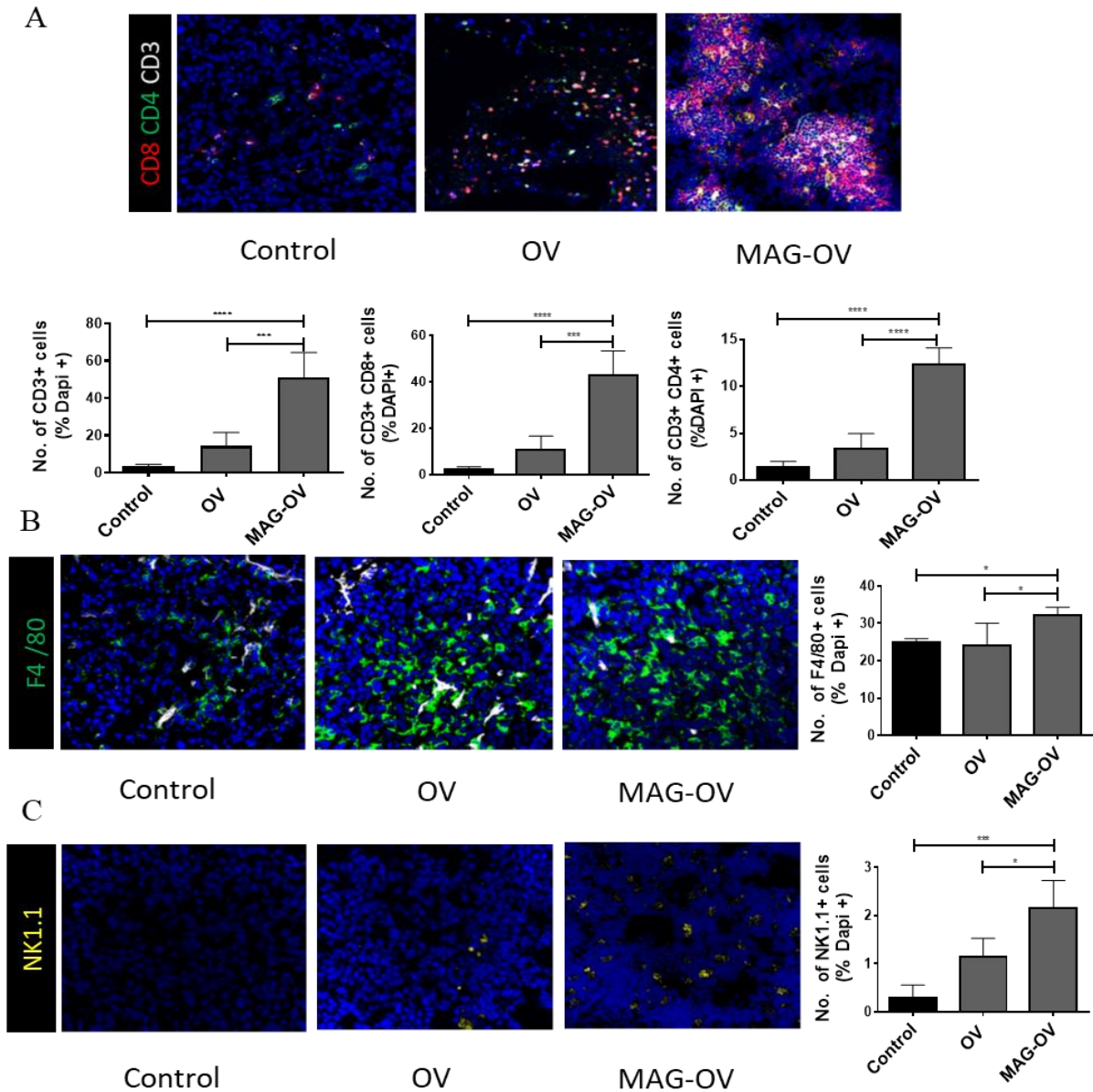


Figure 5.10: Magnetic targeting of MAG-OV increases antitumour immunity. Tumour sections were stained with anti-CD3, anti-CD4, anti-CD8, anti-F4/80, anti-NK1.1 and DAPI (4',6-diamidino-2-phenylindole) and then analysed under a confocal laser-scanning microscope. Three images from two slides (6 total) from each mouse. The density of positive cells was calculated by dividing the total number of positive cells by the number of DAPI+ events in each specified region and multiplying by 100. **A.** CD3⁺ (%Dapi+), CD3⁺/CD8⁺ (%Dapi+), CD3⁺/CD4⁺ (%Dapi+), **B.** F4/80⁺ (%Dapi+) and CD31⁺ **C.** NK1.1 (%Dapi+) were significantly increased in tumours treated with MAG-OV compared to those treated with PBS or naked OV. Of note, data are the Mean \pm SEM (n=5) and statistical analysis was assessed using the one-way Anova test with multiple comparisons. Scale bar= 40 μ m. *p<0.05; ***p<0.001; ****p<0.0001.

5.2.9 Magnetic targeting of MAG-OV increases T cell activation

Given that CD8⁺ T cells were recruited into tumours following MAG-OV treatment next the activation status of these T cells was determined. IFN- γ production by immune cells is considered the hallmark of an active immune response and IFN- γ is released by activated CD8⁺ T cells (Showalter et al., 2017). This is also linked to Programmed Death 1 (PD1) expression by activated T cells (Westin et al., 2014). Therefore, T cell activation was assessed by measuring the number of CD8⁺/IFN- γ ⁺ (%Dapi⁺) and CD8⁺/PD1⁺ (%Dapi⁺) expressing cells by immunofluorescence staining. Sections were co-stained with antibodies to anti-CD8, IFN- γ , PD1 and DAPI and then analysed under a confocal laser-scanning microscope. As shown in **Figure 5.11A-C** the number of CD8⁺/IFN- γ ⁺ (%Dapi⁺) and CD8⁺/PD1⁺ (%Dapi⁺) were significantly increased in tumours treated with MAG-OV compared to those treated with PBS or naked OV (CD8⁺/IFN- γ ⁺ (%Dapi⁺) $P= 0.0008$, CD8⁺/PD1⁺ (%Dapi⁺) $P= 0.0002$). Whilst the T cells were recruited and activated, the increased expression of PD1 suggests that the cells may encounter checkpoint suppression, as we know these tumours express PD-L1 (Crosby et al., 2018). This could be why we see tumour re-growth after the 3rd treatment and our therapy would benefit from combination with checkpoint inhibitors. This will be discussed later.

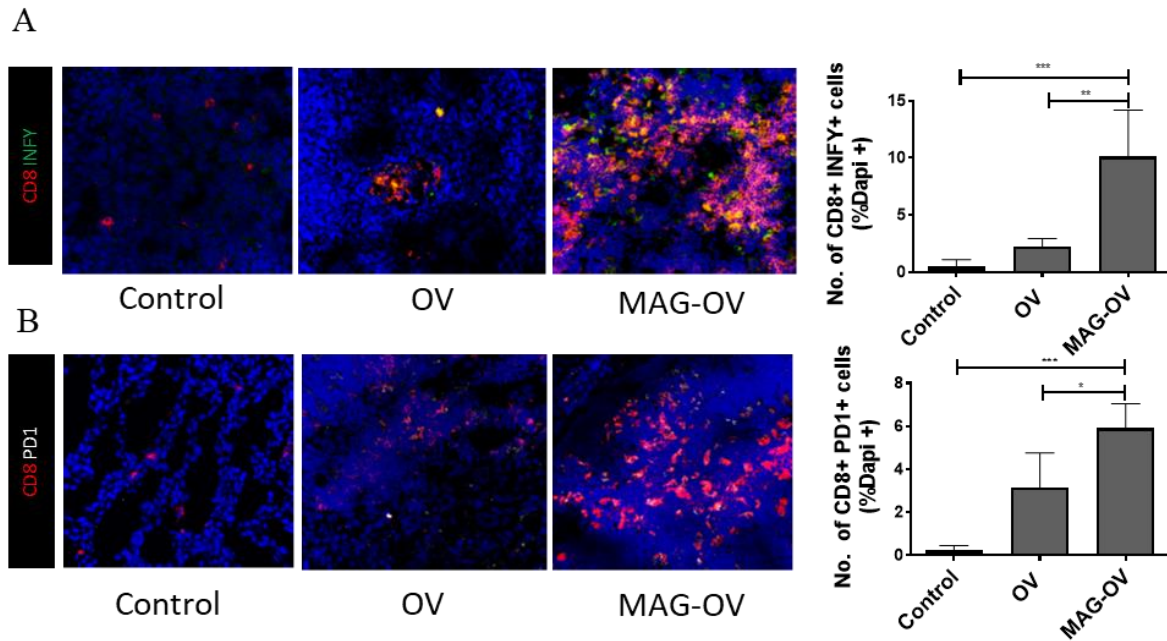


Figure 5.11: MAG-OV activated T cells to express interferon and PD1. Sections were stained with antibodies to anti-CD8, IFN- γ , PD1, and (4', 6-diamidino-2-phenylindole) (DAPI) and then analysed under a confocal laser-scanning microscope. The number of **A.** CD8⁺ /IFN- γ ⁺ (% DAPI+) and **B.** CD8⁺/PD1⁺ (% DAPI+) were significantly increased in tumours treated with MAG-OV compared to those treated with PBS or naked OV. The density of positive cells was calculated by dividing the total number of positive cells by the number of DAPI+ events in each specified region and multiplying by 100. Of note, Data are the Mean \pm SEM (n=5) and statistical analysis was assessed using the one-way Anova test with multiple comparisons. Scale bar= 40 μ m and a magnet was used with MAG-OV. *p<0.05; **p<0.01; ***p<0.001.

5.3 Magnetising HSV1716 protect the virus from neutralisation

5.3.1 *In vivo* study design

Next, we wanted to determine if MAG served to protect the OV from neutralising antibodies as was revealed for the *in vitro* neutralisation experiments in **Section 4.2.6**. Systemic delivery of OV results in low intra-tumoural titres due to pre-existing immunity that has been established because of prior exposure to the virus, previous immunisation, or prior oncolytic viral therapy (Ferguson et al., 2012). Therefore, *in vivo* neutralisation experiments were performed to determine if MAG could protect OV from neutralising Ab (NAb) *in vivo*. Sheep anti-HSV-1 antiserum was used to neutralise the OV. This antibody was kindly prepared by Virttu Biologics as described in **section 2.2.19**. Mice were injected into the nipple with 5×10^5 EO771 cells as described in **section 2.2.23.1**. Once the tumours reached ~ 150 - 200 mm^3 mice received the following intravenously:

1. **Control:** Mice were injected three times i.v. (0, 5, 10 days) with vehicle (PBS) (in a volume no more than 0.2 ml).
2. **OV+ NAb (see section 2.2.19):** Mice were injected three times i.v. (0, 5, 10 days) with 100ul HSV1716 (10ul OV at 10^6 pfu + NAb + 90ul PBS).
3. **MAG-OV+ NAb (see section 2.2.19) + magnet:** Mice were injected three times i.v. (0, 5, 10 days) with 100ul magnetised HSV1716 (12ul MAG-OV at 10^6 pfu + NAb + 88ul PBS) in the presence of an external magnetic field for 30 min.

The group included in this study consisted of n=3 mice/group. Once the tumours reached $\sim 1500\text{mm}^3$ mice were culled by cervical dislocation, and the organs and tumour were removed and stored in liquid nitrogen for post-mortem analysis.

5.3.2 MAG-OV protects HSV1716 from neutralising antibodies

To see if the virus reached the tumour and infected cells within the tumour, GFP expression in dissociated tumours was assessed by flow cytometry. As shown in **Figure 5.12A**, tumours treated with MAG-OV+NAb expressed more GFP after three days of infection compared to tumours treated with OV+NAb (MAG-OV+NAb 5% and OV+NAb 2%). This decrease in GFP expression in tumours treated with OV+NAb is most likely because of OV neutralisation. Moreover, the average tumour volume was significantly smaller in the MAG-OV+NAb with magnet -treated group than in the OV+NAb or PBS ($P= 0.0191$) group at day 12 after treatment (**Figure 5.12B**). Furthermore, **Figure 5.12C** shows all mice in MAG-OV+NAb treated group resulted in an increase in survival compared to the OV+NAb or PBS group. From **Figure 5.12**, it is clear that the OV is not able to have any therapeutic effect in the presence of the NAb. Together this data suggests that MAG have the potential to protect HSV1716 from neutralising antibodies in circulation.

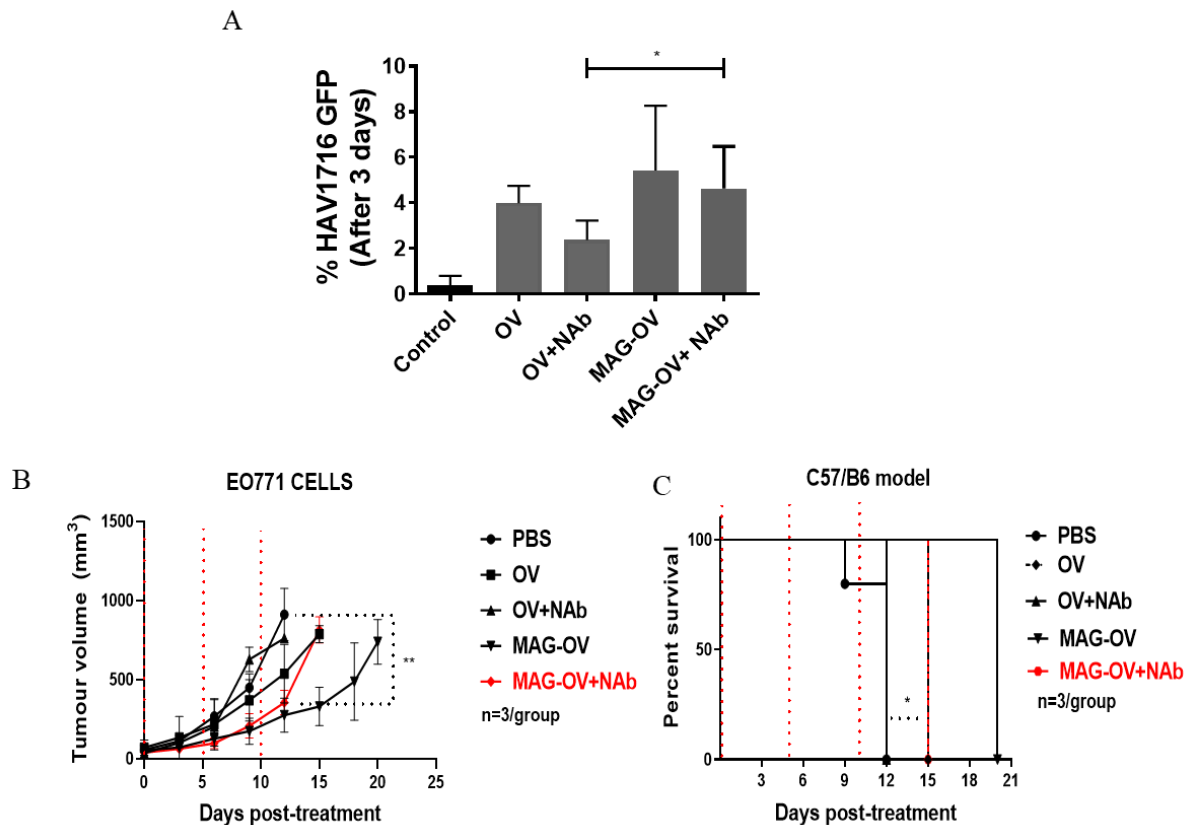


Figure 5.12: MAG-OV is protected from neutralising antibodies. *In vivo* neutralisation experiments were performed to determine if MAG could protect OV from NAb. Sheep anti-HSV-1 antiserum was used to neutralise the OV. 1×10^7 PFU of OV or MAG-OV were incubated with 100-fold dilution of antiserum for 18 h at 4°C prior to the experiment. Mice implanted with EO771 cells were monitored daily and weighed every three days after treatment. Tumour volume was measured using calipers and also recorded every three days. **A.** Tumours treated with MAG-OV+NAb expressed significantly more GFP after three days of infection compared to tumours treated with OV+NAb ($p=0.0260$) as assessed by flow cytometry on an LSRII. **B.** The average tumour volume was significantly smaller in the MAG-OV+NAb treated group than in the OV+NAb or PBS group at day 12 after treatment. **C.** Mice in the MAG-OV+NAb treated group responded to the treatment and resulted in an increase in survival compared to the OV+NAb or PBS group. Of note, data are the Mean \pm SEM ($n=3$ mice/group) and statistical analysis was assessed using one-way Anova test with multiple comparisons for tumour volume and survival curve for mice survival. * $p<0.05$; ** $p<0.01$.

5.4 Discussion

The main goal of OV treatment would be to selectively target and infect tumour cells whilst sparing healthy tissues and organs. Therefore, guiding and confining the OV into the tumours in circulation is important. A previous study showed that oncolytic adenovirus Ad520 co-incubated with MNPs (Ad-SO-Mag2) was able to inhibit human pancreatic tumour (181RDB-fLuc) growth in mice more than naked Ad in both short (3 days) and long-term (25 days) treatments in the presence of NeoDelta magnets (NE155, IBS Magnet, Berlin, Germany) for 30 min immediately after intratumoural injection (Tresilwised et al., 2012a). The same group

also reported that intratumoural injection of Ad in combination with the Core/shell type iron oxide MNPs (PEIMag2) displayed a stronger oncolytic effect than naked adenovirus in a murine xenograft model of daunorubicin-resistant human pancreatic carcinoma cells (Tresilwised et al., 2010a). Together these studies support our study and suggest that OV can be magnetised (all studies including ours relied on electrostatic interactions) and can be guided to a tumour using a magnetic field. Of note, all the above studies relied on direct injection of the magnetised viruses into the tumour and the presence of an external magnet really only served for retention of the therapy within the tumour rather than its delivery. Whereas in this study, MAG associated with HSV1716 has been used to target MAG-OV from circulation to mammary tumours in mice. MAG-OV was injected intravenously in the presence of an external permanent magnetic secured above the tumour (0.7 T) for 30 min. The magnet design, assembly and length of time placed above the tumour, were optimised by a post-doctoral research fellow in the group (Dr Priya Patel). Tumour targeting and therapeutic efficacy of MAG-OV as well as stimulation of immune effector cells by this complex and MAG-OV protection from neutralising antibodies have been studied. To our knowledge, this is the first study to report delivery of magnetised OV from circulation into tumours using bacterially-derived MAG.

5.4.1 Magnetic guidance of MAG-OV shrinks primary mammary tumours and promotes survival

The efficiency of magnetically guiding MAG-OV into mammary tumours in mice was demonstrated in the above results (**Figure 5.2**) where a significant change in average tumour volume, increased mouse survival and a reduction in pulmonary metastasis was observed compared to the others treatment groups. This therapy was more effective than when the OV was administered intravenously. However, whilst the tumour growth was retarded once the administration of HSV1716 ceased, the tumours started to regrow. Muthana et al., demonstrated that prostate tumour-bearing mice received HSV1716-shielded by macrophages (monocyte-derived macrophage (MDM) + OV) resulted in marked reduction of the primary tumour than those that received naked OV in the presence of a magnetic field, (Muthana et al., 2015b). In this study, they did not see the same level of tumour regrowth, however they used an immunocompromised mouse model where the adaptive immune system was not present and therefore may not have contributed to clearance of the virus.

We have shown that MAG-OV magnetic guidance into tumours is effective but does not completely eradicate tumour growth once the therapy has ceased. This means that the therapy

is not so effective alone and should be combined with other cancer treatments or that the virus would need to be given continuously. Others have also reported that intratumoural injection of recombinant non-pathogenic poliovirus (PVSRIPO) into B6-ovalbumin (OVA) melanoma model wasn't able to completely eradicate tumour growth once the therapy ceased (Brown et al., 2017). It would be interesting to try prolonged use of our complex, as there are studies, which says that actually the presence of NAb is not a problem. For example, Melcher have shown that piggybacking of the dsRNA, non-genetically modified OV reovirus on the monocytes could overcome neutralisation and provide access tumours in patients in the brain or liver following systemic injection (Melcher, 2019). Perhaps we could target monocytes by coating our MNPs with a ligand that binds to monocytes in circulation. Already in our laboratory this is being attempted with agents like CCL2. CCL2 bind to the CCR2 receptor on monocytes and the CCL2/CCR2 combination is important for monocyte recruitment into tumours (Lim et al., 2016). In addition, it would be interesting to combine our complex with another cancer treatment. As prior studies have shown that combining the oncolytic Rhabdovirus Maraba-MG1 with Paclitaxel, one of the most common chemotherapeutics used to treat patients with breast cancer, could improve efficacy in all of the breast cancer models they tested, including EMT6, 4T1 and E0771 (Bourgeois-Daigneault et al., 2016).

We already know HSV1716 increases the mean survival time of mice and reduces the burden of 4T1 tumour metastasis in the lungs (Thomas and Fraser, 2003). However, this is the first time we have seen efficacy of HSV1716 in the EO771 model of cancer. From our observation, the virus on its own is not particularly effective compared to the untreated group. However, by using an external magnetic field this improves the anti-tumour efficacy of the virus most likely because the virus is reaching the tumour in greater numbers. In the 4T1 study, 5.4×10^5 pfu of HSV1716 was injected intratumourly in two or three places with a total volume of 20 μ l, while in our study 100ul of HSV1716 at 10^7 pfu was injected into circulation. It is true we have given a much higher dose in our study but as a result we have avoided direct tumour injection, which comes with significant risk and is not always possible in the metastatic setting. Furthermore, studies from our lab have shown that different strains of mice respond differently to HSV1716. This research was carried out by a postdoctoral researcher in the group who noticed that Balb/C mice (used for the 4T1 model) were unable to tolerate the same dose of HSV1716 (1×10^7 pfu/ml) as the C57BL/6 mice used in this study. Moreover, the FVB strain whilst more tolerant than Balb/C mice still required a lower dose than the C57BL/6 strain (**Table 5.2**). This difference in maximum tolerated dose could be attributed to the strains host immune system as C57BL/6

mice display a classically Th2 type immune response, whereas Balb/c and FVB mice naturally display Th1 type immunity. Th1 immunity is important for the removal of intracellular pathogens, whereas Th2 immunity plays a role in the clearance of infectious parasites. Such characteristics may explain the differences in dose tolerability in response to HSV1716. Hiroyuki and colleagues showed the effects of different immune responses in C57BL/6 and Balb/c mice, in response to sepsis. The results indicated that due to the naturally impaired macrophage activity in Balb/c mice, tolerability to viral infection was lower than C57BL/6 mice, this led to the activation of systemic inflammation to viral antigens and the mice experienced multiple organ failure and shock, which could explain data the generated in **Table 5.2** (Hiroyuki et al., 2004). It is interesting that different mouse models respond differently to HSV1716 and perhaps patients will also respond differently and this should definitely be considered in future clinical application of oncolytic virotherapy. As we did not see any difference with MAG-OV without magnet and OV alone and chose to assess MAG-OV with magnet in the rest of chapter as mentioned above (in **section 5.2.2**).

Table 5.2: Different mouse stains respond differently to HSV1716. Dr Faith Howard carried out this research.

Strain	Treatment (pfu/ml)	Adverse effects	Outcomes	Conclusion
BALB/c	1x10 ⁷	Severe adverse effects (hunched, swollen, piloerection, death)	Animal needed to be culled immediately and dose lowered	BALB/c's did not tolerate 1x10 ⁷ pfu/ml at first treatment and barely tolerated 1x10 ⁶ pfu/ml. Therefore, 1x10 ⁵ pfu/ml is the optimal dose.
	1x10 ⁶	Severe adverse effects (hunched, swollen)	Animal needed to be culled immediately and dose lowered	
	1x10 ⁵	No adverse effects witness	Animal survived	
FVB	1x10 ⁷	Severe adverse effects (hunched, swollen, piloerection, death)	Animal needed to be culled immediately and dose lowered	FVB did not tolerate 1x10 ⁷ pfu/ml at first treatment, however less severe adverse effects were observed at 1x10 ⁶ pfu/ml. 1x10 ⁶ pfu/ml is tolerated and can be used in FVB strains.
	1x10 ⁶	Adverse effects, appearance od discomfort (but did not exceed severity limit)	Animal recovered	
	1x10 ⁵	No adverse effects witness	Animal survived	
C57	1x10 ⁷	No adverse effects witness	Animal survived	No adverse effects were seen throughout all treatments. C75 mice will tolerate 1x10 ⁷ pfu/ml and can be used for later experiments.
	1x10 ⁶	No adverse effects witness	Animal survived	
	1x10 ⁵	No adverse effects witness	Animal survived	

5.4.2 Increased MAG-OV targeting in primary breast tumours following magnetic guidance

We found a significant increase in the percentage of HSV1716-GFP in the MAG-OV with magnet treatment group compared to the all other groups after day 3 of treatment and also at the end of the experiment (day 23) using flow cytometry and immunofluorescence staining (**Figure 5.3A&B**). Suggesting that MAG under the guidance of the external magnet could deliver the virus to the tumour. In our study, we used a magnet (0.7 T) to target the mammary tumour and whilst this is a relatively weak magnetic field, the magnetic was placed directly above the tumour due to its superficial location. A stronger magnet may have improved the targeting. However, these are often heavier compared to the size of the mouse and most studies reported in mice use weaker magnets. For example, Chao et al. established that growing tumours could be shrunk significantly in mice with hepatocellular carcinomas using doxorubicin-coupled MNPs and an external magnetic devices of 0.5 T applied on the tumour

(for 2 hrs) to achieve local enhancement (Chao et al., 2012b). Another study showed that an Ad vector tagged with MNPs (Ad-mag) using a biotinylated adenovirus vector with a streptavidin-conjugated MNP localised to the head of a mouse embryo following injection into the ventricle of the embryo in the presence of a weak neodymium–iron–boron magnet (260 mT) placed closed to the head (Hashimoto and Hisano, 2011).

In our study only the primary tumours were targeted with MAG-OV, however metastasis is the major cause of breast cancer mortality (Scully et al., 2012). Therefore, it would be more appropriate to target breast tumours in common metastatic sites (e.g. brain, lungs, bone). However, as these are tumours located deep in the body a weak external magnetic field would not successfully target the therapy. As an alternative, it would be interesting to use the powerful magnetic gradients of MRI scanners to guiding our MAG-OV *in vivo*. Our laboratory has already demonstrated that the powerful magnets present in MRI machines could guide magnetised macrophages loaded with HSV1716 and iron oxide MNPs to tumours in the prostate and lungs of mice. The number of macrophages gathering within tumours was amplified using this strategy, resulting in tumour shrinkage (Muthana et al., 2015b). Cell therapy is complicated and very personalised thus by eliminating the cells and magnetising the virus directly makes this approach more amenable and suited to all patients. The data from this PhD have been used to successfully secure funding from CRUK to develop magnetised HSV1716 for targeting metastatic breast cancer using MRI.

5.4.3 Increased MAG-OV viral replication following magnetic guidance

To confirm that the reduction in tumour size in the MAG-OV treatment group (**Figure 5.2B**), was in response to HSV1716 the mRNA expression of viral replication genes within EO771 tumour cells was measured using qPCR. Interestingly, we found mRNA expression of these genes in the tumour tissue was significantly higher in the MAG-OV group than in the OV only and control groups (**Figure 5.4**). Suggesting that the MAG did not prevent viral replication and the OV was able to complete its life cycle within EO771 tumour cells. This result was in agreement with previous study that found a significant increase ($p < 0.05$) in the expression of adenoviral DNA (hexon gene) in the tumour tissue in the magnetofection group compared with the group that received virus alone using regular PCR analysis (Tresilwised et al., 2012a). Also, another study showed that infectious progeny virus particles of Ad520-PEIMag2 complex was increased compared with the virus alone (Tresilwised et al., 2010a). In contrast, a previous study showed that HSV1716 was only temporarily able to reduce the progress of primary tumours in 4T1 mouse mammary carcinoma model; mainly this absence of efficacy was

because of poor replication of HSV1716 in 4T1 tumours as measured by the plaque assay (Toda et al., 1998, Toda et al., 1999). Further studies would be needed to accurately understand why HSV-1 has a reduced capability to replicate in this tumour cell line, while it can successfully replicate in EO771 tumour cells.

There is always concern that manipulation of OV may influence viral properties such as host cell recognition, virus growth and oncolytic activity mainly by reducing replication rates (Campbell and Gromeier, 2005). However, Tresilwised et al., have shown that shielding the oncolytic adenovirus Ad520 with SO-Mag2 nanoparticles resulted in a significant increase the replication of adenoviral DNA in the tumour xenografts, mainly in the short-term treatments (Tresilwised et al., 2012a). We also found that by magnetising HSV1716 we see improved viral replication (**Figure 5.4**).

5.4.4 MAG-OV induces anti-tumour immunity following magnetic guidance

Previous studies showed that HSV could directly infect tumour endothelium *in vivo* and significantly decrease the mean vessel density in preclinical tumour models of ovarian, glioma, and rhabdomyosarcoma (Benencia et al., 2005, Huszthy et al., 2009). We used immunofluorescence staining to assess tumour vascularity and measured the No. of CD31+ cells per FOV. As expected magnetic guidance of MAG-OV treated tumour cells were less vascularised than the PBS-treated tumours (**Figure 5.5A**). This result agreed with our *in vitro* study where we found expression of VEGF was significantly downregulated in both MDA-MB-231 and MCF7 cells treated with OV and MAG-OV compared to the untreated cells (**section 4.8**). VEGF is one of the most potent vascular permeability factors and is important in tumour angiogenesis (Adams et al., 2000), reducing VEGF and vessel numbers is one of the mechanisms by which OV target tumours. Prior studies revealed that intratumoral injection of the third generation oHSV, G47 Δ -mIL12, significantly changed the tumour microenvironment of GSC-derived intracerebral tumours (Cheema et al., 2013). They revealed that G47 Δ -mIL12 downregulated VEGF expression and upregulated CXCL10.

Necrosis is a type of cell death caused by external factors such as infection and toxins. OVs induce cell death by many mechanisms including necrosis (Wang et al., 2014b). Muthana et al, demonstrated that tumours from prostate tumour-bearing mice that received HSV1716-carrying macrophages (monocyte-derived macrophage (MDM) + OV) were significantly more necrotic than those that received naked OV (Muthana et al., 2015b). Therefore, tumour necrosis was measured after MAG-OV magnetic targeting and was found to be significantly more

necrotic than those treated with PBS (**Figure 5.5B**). This was also confirmed by flow cytometric analysis, where tumours treated with MAG-OV were significantly less viable than those treated with PBS (**Figure 5.5C**). This result was also in agreement with our *in vitro* studies in the earlier chapters where cell death was observed and this was accompanied with the expression of TNF in both MDA-MB-231 and MCF7 cells treated with OV or MAG-OV compared to the untreated cells. Proinflammatory cytokines including TNF- α is released in response to cell necrosis (Fadok et al., 2001). Suggesting that MAG-OV therapy could successfully promote tissue necrosis and cell death.

The expression of calreticulin was also measured using immunofluorescence staining. We found that the number of calreticulin⁺ cells increased significantly in tumours treated with MAG-OV than those treated with PBS or OV alone (**Figure 5.5D**). This data agreed with our *in vitro* study that found CRT accumulated at the plasma membrane 24 h after infection with OV or MAG-OV compared to the untreated cells (**Section 4.6**). Infection of human non-small cell lung cancer cells with the Coxsackievirus B3 OV resulted in inducing ICD and led to the expression of abundant cell surface CRT (Miyamoto et al., 2012). Also, another study showed that oncolytic HSV-1 RH2 induced the translocation of CRT to the cell membrane of the mouse squamous cell carcinoma cell line SCCVII (Takasu et al., 2016). They suggested that HSV induce ICD in this cell line.

One limitation of the data presented in this chapter is that the *in vivo* studies only focused on CRT expression. HMGB1 and ATP levels were not measured in the *in vivo* studies, as in the *in vitro* studies described in Chapter 4. In our *in vitro* studies, we assayed secreted HMGB1 and ATP in the cell culture supernatants according to the manufacturer's protocol; however, we cannot do this in the tumour. It would be interesting to measure the level of HMGB1 and ATP in the serum sample from each mouse. Recently, serum HMGB1 levels in mice treated with lipopolysaccharides (LPS) and/or ATP or LPS and high - fat diet to induce NLRP3 inflammasome activation have been measured using the HMGB1 ELISA kit (Wang et al., 2018b).

5.4.5 MAG-OV treated tumours induce expression of immune-related genes

Nanostring analysis revealed that magnetically guided MAG-OV induced a number of immune-related pathways. Genes related to innate and adaptive immune responses (Cxcl2, Thbs1, Ifitm1, Cxcr2, Ccl3, Cd14, Ccr1, Icos and Clu), T-cell function (CTLA4, Ccl3, Xcl1, Icos), NK cell Functions (Ccl3), macrophage functions (Thbs1), dendritic cell functions (Ccr1),

Interferon (Runx3) as well as apoptosis (Gzmb, Osm, Gzma, Clu and Runx3) were elevated after treatment with magnetically targeted MAG-OV. This suggests that MAG-OV treatment could elevate the majority of the immune-related genes in the NanoString immune profiling panel. OV's are known to activate the immune system. A study by Zamarin et al., showed that injection of Newcastle disease virus (NDV) into the bilateral flanks of B16-F10 melanoma-bearing mice upregulated the majority of the immune-related genes we describe including those related to T-cell function, DC function and type I IFN (Zamarin et al., 2017). Some researchers have engineered OV so that they can be more immunogenic via the expression of genes that recruit or activate immune cells. For example, the recruitment of antigen-presenting cells (APCs) by production of granulocyte macrophage colony-stimulating factor (GM-CSF) expressing HSV and vaccinia virus has been demonstrated (Breitbach et al., 2011b, Andtbacka et al., 2015). Indeed the FDA approved T-VEC (genetically modified HSV1 designed to produce GM-CSF) demonstrated antitumour immunity, where tumour gene expression data from the Phase 1b clinical trial resulted in elevated CD8a and IFN- γ mRNA in advanced melanoma patients (Ribas et al., 2018). Our data confirmed that MAG-OV not only induces tumour necrosis, ICD but also activated antitumour immunity.

Interestingly in the MAG only treated group (MAG) >27 genes were up-regulated (e.g. Ctsw, Cmah, C1s1) and 10 genes down-regulated (e.g. Trp53, Cxcl12). Whilst, the MAG only group did not induce any therapeutic changes some of these genes such as Xcl1, Ido1, IL21r and Ctsw have been linked to Chemokines & Receptors, Cytokines & Receptors, Inflammation, Innate and T-Cell Function pathways suggesting that the MAG may have immunogenic properties. We used stringent wash steps to purify our MAG (>10 washes) but perhaps this is not adequate. A previous study suggested that intravenous injection of 40mg/kg of bacterial MAG into rats revealed absence of immunotoxicity (Sun et al., 2010b). They found that no difference in the number of white blood cells and lymphocytes to those in untreated rats. However, they mentioned that 'it is not yet clear whether purified MAG contain antigens or pyrogens. Therefore, some consideration should be given when using MAG. Because, the MAG are derived from bacteria and contain biological impurities, such as bacterial proteins, nucleic acids and polysaccharides this could lead to immunotoxicity. This will need to be considered in great detail before using MAG in the clinical setting. As previously suggested the MAG membrane could be stripped to remove bacterial endotoxins by detergent treatment (Xie et al., 2009). We have also not measured the endotoxin levels in our preparations and this is something we plan to do in the future (Wong et al., 2016).

5.4.6 MAG-OV recruits immune cells into the tumour microenvironment

HSV therapy of CT-26 tumours inhibited the growth of contralateral tumours or of a second challenge of tumour cells in immune-competent mice (Toda et al., 1999, Toda et al., 1998, Toda et al., 2002). This suggests that anti-tumour immune responses have developed after the virotherapy. HSV1716 therapy of primary 4T1 mammary tumours with lacking RAG2, CD4, CD8, and NK cells is ineffective in immune-competent mice, suggesting a role for the T cell infiltrate in attacking the tumour (Thomas and Fraser, 2003). Another report by Miller and Fraser confirmed the importance of T cells following OV therapy. They showed that cyclophosphamide administration (before and during HSV1716 administration) in SCID mice with brain tumours in an experimental model of metastatic melanoma was also ineffective (Miller and Fraser, 2000).

We used, flow cytometry to measure the percentage of immune cell infiltration after MAG-OV infection. Consistent with our tumour gene expression data, flow cytometry data showed that the percentage of CD3, CD3+ CD8+, CD11B+ LY6G+ and NK1.1 significantly increased in tumours treated with MAG-OV compared to those treated with PBS (**Figure 5.9**), with reduction in the percentage of CD3+ CD4+ cells, albeit the latter was not significant. This was also confirmed by immunofluorescence staining. The data suggest that MAG-OV increased the infiltration of immune cells and is in agreement with Thomas and Fraser, who demonstrated that HSV1716 therapy of 4T1 tumours increased the percentage of CD4+ and CD8+ T cells in immune competent mice (Thomas and Fraser, 2003).

Given that MAG-OV increased the percentage of CD3+ CD8+ cells, it was important to measure their activation status within the tumours. As IFN- γ can be released by activated CD8+ T cells in a typical response (Showalter et al., 2017) and PD1 is expressed by activated T cells (Westin et al., 2014) we therefore measured the expression of both IFN- γ and PD1 to evaluate T cell activation after MAG-OV therapy. Our data suggested that following MAG-OV targeting into tumours, cytotoxic T cells (CD8+) had elevated IFN- γ and PD1 expression compared to mice treated with PBS or naked OV (**Figure 5.11**). This data implies that MAG-OV induces T cell activation. This increase in the number of T cells expressing PD-1 after MAG-OV infection offered a possible explanation as to why our complex did not show complete tumour remissions. Perhaps the increase in PD-1 resulted in checkpoint inhibition of the activated T cells via checkpoint inhibition (Pfannenstiel et al., 2019). Likewise, it has been suggested that T cells expressing PD-1 in the presence of tumours positive for PD-L1 may negatively influence the antitumour activity of single-agent T-VEC (Ribas et al., 2018). It

would be interesting to combine MAG-OV therapy with anti-programmed death protein 1 (PD-1) or anti-PD-L1 antibody therapy to overcome some of these limitations. As long-lasting antitumour responses in patients with a variety of cancers with PD-1 or anti-PD-L1 antibodies therapy has been demonstrated (Sharma and Allison, 2015). Recently, it was suggested that HSV-1 and PD-1 blockade combination therapy could be a successful treatment strategy for childhood soft tissue sarcoma. They found a significant increase in the number of CD4+ and CD8+ T cells but not with the CD4+CD25+Foxp3+ regulatory T cell populations in M3-9-M (MHC I high) tumour models that received combination therapy (intratumoral HSV1716 injection followed by intraperitoneal injection of anti-PD-1) (Chen et al., 2017).

5.4.7 MAG-OV protection from neutralising antibodies

Many strategies have been used before to protect viruses from inactivating immune mechanisms they encounter in circulation resulting in improved tumour targeting following systemic delivery. Our *in vitro* experiments have shown that adding neutralising Ab to the naked HSV1716 resulted in significant inhibition of oncolytic activity. While the oncolytic potential of MAG-OV was not changed when adding the neutralising Ab because of the MAG shielding of the virus. Neutralisation experiments were performed to determine if MAG could protect OV from neutralizing Ab *in vivo* following injection into the circulation. Interestingly, we found that the average tumour volume was significantly smaller in the MAG-OV+NAb treated group than in the OV+NAb or PBS group at day 12 after treatment (**Figure 5.12A**). Further, most of the mice in MAG-OV+NAb treated group responded to the treatment survived for longer compared to the others groups (**Figure 5.12B**). This also correlated with an increase in GFP expressing virus in the MAG-OV treated group. This suggests that MAG-OV could minimize the interaction of HSV1716 with neutralising Ab because of magnetosome shielding. The use of magnetised HSV provides an opportunity to not only guide the virus to the tumour in the presence of a magnetic field but to also protect from immune attack whilst in the bloodstream. The limitation of this experiment is that only n=3 mice were used in each treatment group. Moreover, it would be interesting to use other inhibitory mechanisms to neutralise HSV1716, such as using human serum containing neutralising antibodies to HSV instead of the sheep antibody.

In summary, we have shown that MAG-OV can be guided to mouse mammary tumours using an external magnetic field and this reduces tumour growth, tumour blood vessels and increases tumour cell death whilst activating anti-tumour immunity.

Chapter 6

Summary of main outcomes and general conclusion

6.1 Summary of main outcomes and general conclusion

So far, systemic delivery of OV has been obstructed by low intra-tumoural titres due to strong anti-viral host immune responses and sequestration by the liver and spleen resulting in poor tumour targeting (Ferguson et al., 2012). Several studies have proposed to use different ways for improving the targeting of OV to tumours. This is the first study using bacterial derived MAG to target viruses to tumours after systemic delivery and evaluate the anti-tumour immune response. In chapter 3, We showed that MAG are small and uniform in size compared to synthetic MNPs used by other researchers (Almstätter et al., 2015a). This is agreement with a recent study that also confirmed that MAG purified from *Magnetospirillum gryphiswaldense* MSR-1 displayed uniform arrangement of particles whereas MNPs were clustered (Raguraman and Suthindhiran, 2019).

Interestingly, the electrokinetic potential of the MAG was negative (-9 ± 2.3 mV) (**Table 3.1**). Since the MAG display a negative electrokinetic potential we did not expect the self-assembly with the OV. As Almstatter et al., showed that creating the magnetic viral complexes using synthetic MNPs relies on the positive electrokinetic potential of the MNP so that complex formation depends on electrostatic interactions with negatively charged viral particles (OV) (Almstätter et al., 2015a). However, our complex formation is most likely a result of MAG possessing polarisable primary amino groups, enabling self-assembly based on the homobifunctional cross linking agents for example aliphatic binary aldehyde, diisothiocyanates, diisocyanates, di(succinimido) aliphatic esters, and their derivatives (Sun et al., 2008). Using TEM and flow cytometry, we found that they form complexes with OV without having any impact on the oncolytic potential of the virus. The complexes were also still 'nm' in size and could infect and kill tumour cells. Afterward, we examined the oncolytic potential of MAG-OV in 3D spheroid cultures. We showed that MAG-OV can damage the spheroid of MDA-MB-231s and MCF7 cells as good as OV alone (**Figure 3.12A, Figure 3.13A**). We observed ruffled edges and a flattened morphology, indicating damaging and cell death of the three-dimensional spheroid structure on day 6 of infection with both OV and MAG-OV treatment compared to untreated spheroids and MAG only. This suggests that MAG-OV is as efficient as OV on its own with respect to infectivity and cell death in both monolayer and 3D cultures.

In chapter 4, the replication potential and cell death mechanisms of the virus were assessed. MAG-OV was able to enter and replicate inside breast cancer cells, at the same time inducing tumour cell death as good as OV alone. We also showed that OV and MAG-OV in both MDA-

MB-231 and MCF7 cells appeared to induce a significant increase in Caspase 3, Caspase 8, FASL and HSPA1A gene expression when compared to the control (**Figure 4.5**). While Bcl-2 and NF- κ B were significantly decreased (**Figure 4.5, Figure 4.8**). We assume that HSV1716 was able to induce apoptosis by downregulating anti-apoptotic factors and the data of high expression of heat shock protein 'HSPA1A' gene suggest immunogenic apoptotic cell death. Viral infection appeared also to induce a significant increase in LC3B gene expression when compared to the control at both OV and MAG-OV in both MDA-MB-231 and MCF7 cells (**Figure 4.5**). This suggests that HSV1716 can induce apoptosis, necrosis and autophagy in a coordinated fashion. Immunogenic cell death (ICD) following MAG-OV infection was also measured in infected breast cancer cells. We showed that extracellular ATP levels and HMGB1 levels were significantly increased at both OV and MAG-OV when compared with control and MAG alone (**Figure 4.6**). We also noticed the expression of CRT around the plasma membrane significantly increased with both OV and MAGOV, whereas untreated cells presented the diffuse distribution of CRT (**Figure 4.7**). This suggests that MAG-OV infection was able to produce DAMPs from breast cancer cells as effectively as OV alone.

Next, we attempted to understand the impact of HSV1716 on the surrounding environment. qPCR and cytokine bead array (CBA) were used to measure a panel of pro-inflammatory and anti-inflammatory cytokines. The expression of CXCL10, IFN γ and TNF were upregulated in both MDA-MB-231 and MCF7 cells treated with OV or MAG-OV compared to the untreated cells (**Figure 4.8**). On the other hand, the level of anti-inflammatory cytokines IL-1B, NF-KB and VEGF were decreased. Suggesting that OV or MAG-OV influenced the tumour microenvironment by increasing the level of pro-inflammatory cytokines.

We also hypothesised that MAG would protect the virus from neutralisation. So next we tried to test the efficacy of our complex in the presence of neutralizing Ab *in vitro*. We showed that cells incubated with OV+Nab expressed significantly less GFP after 24h of culture compared to MAG-OV+ NAb. This decrease in GFP expression is most likely because of OV neutralisation and indeed statistically significant reduced cell death was observed with OV+Nab compared to the MAG-OV+ NAb after 24h of culture (**Figure 4.10**). Suggesting that MAG-OV could minimize the interaction of HSV1716 with neutralising Ab because of MAG protecting the virus.

In chapter 5, we attempted to understand whether MAG will improve targeting of OV in the presence of external magnetic field gradients and examine whether our complex could stimulate immune effector cells in an *in vivo* model. All the previous studies relied on direct injection of the magnetised viruses into the tumour and the presence of an external magnet really only served for retention of the therapy within the tumour rather than its delivery. Whereas in this study, MAG associated with HSV1716 was used to target MAG-OV from circulation to mammary tumours in mice. We showed that MAG-OV resulted in a significant change in average tumour volume, increased mouse survival and a reduction in pulmonary metastasis compared to the others treatment groups. We have shown that MAG-OV guidance into tumours is effective but does not completely eradicate tumour growth once the therapy has ceased. This means that the therapy is not so effective alone and should be combined with other cancer treatments or that the virus would need to be given continuously. This is the first time we have seen efficacy of HSV1716 in the EO771 model of cancer. From our observation, the virus on its own is not particularly effective compared to the untreated group. However, by using an external magnetic field this improves the anti-tumour efficacy of the virus most likely because the virus is reaching the tumour in greater numbers.

Interestingly, we found a significant increase in the percentage of HSV1716-GFP in the MAG-OV with magnet treatment group compared to the all other groups after day 3 of treatment and also at the end of the experiment (day 23) using flow cytometry and immunofluorescence staining (**Figure 5.3A&B**). Suggesting that MAG under the guidance of the external magnet could deliver the virus to the tumour. To confirm that the reduction in tumour size of MAG-OV treatment group observed in **Figure 5.2B**, was in response to HSV1716 replication the mRNA expression of viral replication genes within EO771 tumour cells were measured using qPCR. Moreover, we found mRNA expression of these genes in the tumour tissue was significantly higher in the MAG-OV group than in the OV only and control groups (**Figure 5.4**). Suggesting that the MAG did not prevent viral replication and the OV was able to complete its life cycle within EO771 tumour cells. In doing this, MAG-OV also increased tumour necrosis and immunogenic cell death. Interestingly, the number of pulmonary metastasis was significantly reduced in mice that received MAG-OV compared to those treated with PBS (**Figure 5.5E**). The number of pulmonary metastasis was also reduced in mice that received MAG-OV compared to those treated with OV alone, but this change was not significant. Suggesting that MAG-OV therapy of the primary tumour could reduce the number of metastases in the lungs.

The study then addressed whether MAG-OV could induce anti-tumour immunity. Nanostring, flow cytometry and immunofluorescence staining analysis revealed that magnetically guided MAG-OV significantly increased the number of T cells and myeloid cells. The data suggest that MAG-OV increased the infiltration of immune cells. Then, it was important to measure the activation status of CD3⁺ CD8⁺ cells. Therefore, we tried to measure the expression of both IFN- γ and PD1 to assess T cell activation after MAG-OV therapy. Our data suggested that Cytotoxic T cells (CD8⁺) had elevated IFN- γ and PD1 expression following MAG-OV targeting into tumours compared to mice treated with PBS or naked OV (**Figure 5.11**). This data suggests that MAG-OV induces T cell activation and this is important for inducing anti-tumour immunity.

Finally, we aimed to determine whether MAG was able to protect OV against neutralising Ab *in vivo* following injection into the circulation. Interestingly, we showed that a significant change in average tumour volume was observed in mice receiving MAG-OV+NAb with magnet compared to the mice receiving OV+NAb or PBS on day 12 after treatment (**Figure 5.12A**). **Figure 5.12B** showed most of the mice in the MAG-OV+NAb group resulted in a significant increase in survival compared to the others groups. This was also associated with an increase in GFP expressing virus in the MAG-OV treated group. This data suggests that MAG-OV could reduce the interaction of OV with neutralising Ab because of the shielding provided by the MAG.

This study represents a novel therapeutic approach for delivering OV to tumours in circulation whilst protecting the virus from unwanted immune attack. Not only does this overcome the challenge of systemic delivery of OVs it also provides an opportunity for many cancer types to be treated particularly those cancers that are not responsive to conventional therapies or the new exciting immunotherapies (e.g. checkpoint inhibitors) due to the low abundance of immune cells within the tumour. This particularly applies to breast cancers which are thought to be immunologically 'cold'. MAG-OV provides the opportunity to re-programme the tumour microenvironment to be immunologically 'hot' (have more activated T cells) and therefore responsive to immunotherapies. The combination of MAG-OV with such immunotherapies is exciting and will no doubt be explored in the future.

6.2 Limitations of studies

One of the limitations of this study is that cultures of MTB often took weeks to grow and resulted in a low yield of magnetite that limited the number of experiments that could be

performed. Therefore, it would be important to use different strategies for cultivation of MTB in the future. The use of bioreactors is an attractive alternative and could produce much higher magnetite yields. A previous study showed that magnetosome production of the marine magnetotactic vibrio *Magnetovibrio blakemorei* strain MV-1 could improve using statistics-based experimental factorial design (Silva et al., 2013). They obtained maximum magnetite yields of 64.3 mg/liter in batch cultures and 26 mg/liter in a bioreactor. Recent study also showed that the growth and magnetosome production of the of *Magnetospirillum gryphiswaldense* MSR-1 could optimize using simple pH-stat fed-batch fermentation strategy (Fernández-Castané et al., 2018). The highest biomass concentration, which was an optical density at 565 nm of 15.5 (equivalent to 4.2 g DCW·L⁻¹), and the highest cellular iron content, which was 33.1 mg iron·g⁻¹ DCW, were obtained.

Another limitation to this study is that we relied on a change in cell size to confirm uptake of the MAG by the cells. The uptake and accumulation of MAG within mammalian cells has not been well studied. Cypriano et al., recently showed that following magnetosome uptake by HeLa cells the magnetosomes were either inside or outside the cell's endosomes (suggesting different routes of internalisation) and that they persisted in culture for 120 h without any structural or chemical change. Furthermore, no toxicity to the HeLa cells was observed. This was carried out using transmission electron microscopy and high spatial resolution nano-analysis techniques (Cypriano et al., 2019). We did use TEM and detected MAG both in the cytoplasm and in the vesicles of the cell (e.g. endosomes). However, it would have been interesting to both quantify and visualise MAG uptake by MDA-MB-231 by fluorescence uptake using flow cytometry and immunofluorescence microscopy and to track this over time. This could be achieved by fluorescently labelling the MAG (e.g. fluorescent dyes or infrared probes) and carrying out time-lapse microscopy. It would also have been interesting to determine what the fate of the MAG and virus was after cell uptake. By labelling the MAG we could have performed co-localisation studies using antibodies to cytoplasmic components such as the endosomes and lysosomes and high-resolution confocal microscopy. A post-doctoral researcher (Dr Faith Howard) in our group has recently demonstrated that the MAG can be labelled with DiD (lipophilic carbocyanine DiD) and detected by both flow cytometry and immune fluorescence.

Another important consideration for biomedical application is the level of endotoxins on MAG. Since these are extracted from gram negative magnetotactic bacteria they are likely to possess

endotoxins at their surface. To reduce endotoxins the MAG were washed extensively however, it would be useful to quantify remaining endotoxins using the Limulus amoebocyte lysate (LAL) assay but due to the time limitation, it was not possible to achieve during this study but is currently being investigated by other group members.

Another limitation of this study is that the interactions between the OV and MAG were not quantified in this study. For example, the concentration of bound virus. Quantification of bound virus and unbound virus could be estimated via titration of the supernatant containing free virus using a plaque assay. This can then be compared to the MAG-OV after magnetic selection.

In the neutralisation studies we used sheep serum to inhibit the oncolytic activity of HSV1716. Other approaches could be used such as using human serum derived from blood of patients or health volunteers. A comparison of serum with high, medium or little/no HSV antibodies could be compared to assess MAG-OV neutralisation. Using breast cancer patient derived serum could provide valuable information on the clinical applicability of this approach.

6.3 Future work

In future, it would be useful to create a stable MAG-OV complex using new conjugation techniques, such as antibodies or chemical linkers. Already in our group research using Genipin, a chemical compound found in gardenia fruit extract. This is an excellent natural cross-linker for proteins, collagen, gelatin and chitosan. Others are looking into antibodies on the surface of the OV (e.g. HSV-1 gB Antibodies) and creating virus-antibody-magnetosome linkers. Here it is important to select an antibody that does not interfere with viral infection or replication. This would help in the development of a stable complex that has the potential for long-term storage and would be attractive to the pharmaceutical industry. It would also be interesting to experiment with magnetosomes from different strain of MTB, particularly those with different shapes. It could be that MAG of different shapes lead to better binding with the virus.

In addition, this study only used the Eo771 model of mammary carcinoma. It would be useful to administer our magnetic viral complexes in other breast cancer models (e.g. TS-1 derived from polyoma middle T antigen (PyMT) mice) (Tan, 2014) or a humanised model of breast cancer (Arendt, 2016). Using breast cancer models that reflect the different subtypes of breast cancer could provide information on response to this therapy. As metastasis is the major cause of breast cancer mortality (Scully et al., 2012). Targeting breast tumours in common metastatic

sites (e.g. brain, lungs, and bone) should be considered in the future. For example, intracardiac injection of (E0771/Pa) results in bone metastases in C57BL/6 mice within 2 weeks (Hiraga and Ninomiya, 2018). Whilst this route of administration enable colonisation studies at specific sites without complications of primary tumour growth, it is an artificial route of administration that requires the implantation of large tumour cell numbers.

Finally, combining MAG-OV therapy with anti-programmed death protein 1 (PD-1) or anti-PD-L1) antibody therapy would be also interesting. Particularly, given that we showed a significant increase in the number of T cells expressing PD-1 after MAG-OV infection. The presence of checkpoint inhibitors within the tumour will lead to inactivation of the T cells and this offers a possible explanation as to why our complex did not show complete tumour inhibition. Using MAG-OV to recruit T cells and turn a tumour from ‘cold’ to ‘hot’, followed by checkpoint inhibitors could ultimately lead to a new clinical approach for treating breast cancer.

References

- ACHARD, C., SURENDRAN, A., WEDGE, M.-E., UNGERECHTS, G., BELL, J. & ILKOW, C. S. 2018. Lighting a Fire in the Tumor Microenvironment Using Oncolytic Immunotherapy. *EBioMedicine*, 31, 17-24.
- ADAIR, R. A., ROULSTONE, V., SCOTT, K. J., MORGAN, R., NUOVO, G. J., FULLER, M., BEIRNE, D., WEST, E. J., JENNINGS, V. A., ROSE, A., KYULA, J., FRASER, S., DAVE, R., ANTHONY, D. A., MERRICK, A., PRESTWICH, R., ALDOURI, A., DONNELLY, O., PANDHA, H., COFFEY, M., SELBY, P., VILE, R., TOOGOOD, G., HARRINGTON, K. & MELCHER, A. A. 2012. Cell carriage, delivery, and selective replication of an oncolytic virus in tumor in patients. *Sci Transl Med*, 4, 138ra77.
- ADAMS, J., CARDER, P. J., DOWNEY, S., FORBES, M. A., MACLENNAN, K., ALLGAR, V., KAUFMAN, S., HALLAM, S., BICKNELL, R., WALKER, J. J., CAIRNDUFF, F., SELBY, P. J., PERREN, T. J., LANSDOWN, M. & BANKS, R. E. 2000. Vascular Endothelial Growth Factor (VEGF) in Breast Cancer: Comparison of Plasma, Serum, and Tissue VEGF and Microvessel Density and Effects of Tamoxifen. *Cancer Research*, 60, 2898-2905.
- AG, C., LAING, J. & AURELIAN, L. 2010. *The HSV-2 mutant DeltaPK induces melanoma oncolysis through nonredundant death programs and associated with autophagy and pyroptosis proteins.* *Colunga AG, Laing JM, Aurelian L. Gene Ther.* 2010 Mar;17(3):315-27.
- ALEXANDER, D. & LEIB, D. A. 2008. Xenophagy in herpes simplex virus replication and pathogenesis. *Autophagy*, 4, 101-103.
- ALEXANDER, D. E., WARD, S. L., MIZUSHIMA, N., LEVINE, B. & LEIB, D. A. 2007. Analysis of the Role of Autophagy in Replication of Herpes Simplex Virus in Cell Culture. 81, 12128-12134.
- ALEXIOU, C., ARNOLD, W., KLEIN, R. J., PARAK, F. G., HULIN, P., BERGEMANN, C., ERHARDT, W., WAGENPFEIL, S. & LÜBBE, A. S. 2000. Locoregional Cancer Treatment with Magnetic Drug Targeting. *Cancer Research*, 60, 6641-6648.
- ALMSTÄTTER, I., MYKHAYLYK, O., SETTLES, M., ALTOMONTE, J., AICHLER, M., WALCH, A., RUMMENY, E. J., EBERT, O., PLANK, C. & BRAREN, R. 2015a. Characterization of Magnetic Viral Complexes for Targeted Delivery in Oncology. *Theranostics*, 5, 667-685.
- ALPHANDÉRY, E., ABI HAIDAR, D., SEKSEK, O., THOREAU, M., TRAUTMANN, A., BERCOVICI, N., GAZEAU, F., GUYOT, F. & CHEBBI, I. 2017. Nanoprobe Synthesized by Magnetotactic Bacteria, Detecting Fluorescence Variations under Dissociation of Rhodamine B from Magnetosomes following Temperature, pH Changes, or the Application of Radiation. *ACS Applied Materials & Interfaces*, 9, 36561-36572.
- ALPHANDÉRY, E., FAURE, S., SEKSEK, O., GUYOT, F. & CHEBBI, I. 2011. Chains of Magnetosomes Extracted from AMB-1 Magnetotactic Bacteria for Application in Alternative Magnetic Field Cancer Therapy. *ACS Nano*, 5, 6279-6296.
- AMEMIYA, Y., ARAKAKI, A., STANILAND, S. S., TANAKA, T. & MATSUNAGA, T. 2007. Controlled formation of magnetite crystal by partial oxidation of ferrous hydroxide in the presence of recombinant magnetotactic bacterial protein Mms6. *Biomaterials*, 28, 5381-9.
- AMIDI, M., MASTROBATTISTA, E., JISKOOT, W. & HENNINK, W. E. 2010. Chitosan-based delivery systems for protein therapeutics and antigens. *Advanced Drug Delivery Reviews*, 62, 59-82.
- ANDREANSKY, S., SOROCEANU, L., FLOTTE, E. R., CHOU, J., MARKERT, J. M., GILLESPIE, G. Y., ROIZMAN, B. & WHITLEY, R. J. 1997. Evaluation of Genetically Engineered Herpes Simplex Viruses as Oncolytic Agents for Human Malignant Brain Tumors. *Cancer Research*, 57, 1502.
- ANDTBACKA, R. H. I., KAUFMAN, H. L., COLLICHIO, F., AMATRUDA, T., SENZER, N., CHESNEY, J., DELMAN, K. A., SPITLER, L. E., PUZANOV, I., AGARWALA, S. S., MILHEM, M., CRANMER, L., CURTI, B., LEWIS, K., ROSS, M., GUTHRIE, T., LINETTE, G. P., DANIELS, G. A., HARRINGTON, K., MIDDLETON, M. R., MILLER, W. H., ZAGER, J. S., YE, Y., YAO, B., LI, A., DOLEMAN, S., VANDERWALDE, A., GANSERT, J. & COFFIN, R. S. 2015. Talimogene Laherparepvec Improves

- Durable Response Rate in Patients With Advanced Melanoma. *Journal of Clinical Oncology*, 33, 2780-2788.
- ANGELOVA, A. L., GREKOVA, S. P., HELLER, A., KUHLMANN, O., SOYKA, E., GIESE, T., APRAHAMIAN, M., BOUR, G., RUFFER, S., CZIEPLUCH, C., DAEFFLER, L., ROMMELAERE, J., WERNER, J., RAYKOV, Z. & GIESE, N. A. 2014. Complementary induction of immunogenic cell death by oncolytic parvovirus H-1PV and gemcitabine in pancreatic cancer. *J Virol*, 88, 5263-76.
- ARAKAKI, A., NAKAZAWA, H., NEMOTO, M., MORI, T. & MATSUNAGA, T. 2008. Formation of magnetite by bacteria and its application. *Journal of The Royal Society Interface*, 5, 977-999.
- ARAUJO, A. C., ABREU, F., SILVA, K. T., BAZYLINSKI, D. A. & LINS, U. 2015. Magnetotactic bacteria as potential sources of bioproducts. *Mar Drugs*, 13, 389-430.
- ARBAB, A. S., JORDAN, E. K., WILSON, L. B., YOCUM, G. T., LEWIS, B. K. & FRANK, J. A. 2004. In vivo trafficking and targeted delivery of magnetically labeled stem cells. *Hum Gene Ther*, 15, 351-60.
- ARCANGELI, G., BARNI, E., CIVIDALLI, A., MAURO, F., MORELLI, D., NERVI, C. & TABOCCHINI, A. 1980. Effectiveness of microwave hyperthermia combined with ionizing radiation: Clinical results on neck node metastases. *International Journal of Radiation Oncology* Biology* Physics*, 6, 143-148.
- ARENDT, L. M. 2016. Modeling Breast Tumor Development with a Humanized Mouse Model. *Methods Mol Biol*, 1458, 247-59.
- ARIAS, J. L., REDDY, L. H. & COUVREUR, P. 2012. Fe₃O₄/chitosan nanocomposite for magnetic drug targeting to cancer. *Journal of Materials Chemistry*, 22, 7622-7632.
- AUBERT, M. & BLAHO, J. A. 2001. Modulation of apoptosis during herpes simplex virus infection in human cells. *Microbes Infect*, 3, 859-66.
- AUBERT, M., O'TOOLE, J. & BLAHO, J. A. 1999. Induction and prevention of apoptosis in human HEp-2 cells by herpes simplex virus type 1. *J Virol*, 73, 10359-70.
- AUBERT, M., POMERANZ, L. E. & BLAHO, J. A. 2007. Herpes simplex virus blocks apoptosis by precluding mitochondrial cytochrome c release independent of caspase activation in infected human epithelial cells. *Apoptosis : an international journal on programmed cell death*, 12, 19-35.
- BALKWILL, D. L., MARATEA, D. & BLAKEMORE, R. P. 1980. Ultrastructure of a magnetotactic spirillum. *J Bacteriol*, 141, 1399-408.
- BALLIF, B. A. & BLENIS, J. 2001. Molecular mechanisms mediating mammalian mitogen-activated protein kinase (MAPK) kinase (MEK)-MAPK cell survival signals. *Cell Growth Differ*, 12, 397-408.
- BARTLETT, D. L., LIU, Z., SATHAIAH, M., RAVINDRANATHAN, R., GUO, Z., HE, Y. & GUO, Z. S. 2013. Oncolytic viruses as therapeutic cancer vaccines. *Mol Cancer*, 12, 103.
- BATTERSON, W. & ROIZMAN, B. 1983. Characterization of the herpes simplex virion-associated factor responsible for the induction of alpha genes. 46, 371-377.
- BAZYLINSKI, D. A. & FRANKEL, R. B. 2004. Magnetosome formation in prokaryotes. *Nat Rev Microbiol*, 2, 217-30.
- BAZYLINSKI, D. A., FRANKEL, R. B., HEYWOOD, B. R., MANN, S., KING, J. W., DONAGHAY, P. L. & HANSON, A. K. 1995. Controlled Biomineralization of Magnetite (Fe₃O₄) and Greigite (Fe₃S₄) in a Magnetotactic Bacterium. *Appl Environ Microbiol*, 61, 3232-9.
- BAZYLINSKI, D. A., GARRATT-REED, A. J. & FRANKEL, R. B. 1994. Electron microscopic studies of magnetosomes in magnetotactic bacteria. *Microsc Res Tech*, 27, 389-401.
- BENENCIA, F., COURRÈGES, M. C., CONEJO-GARCÍA, J. R., MOHAMED-HADLEY, A., ZHANG, L., BUCKANOVICH, R. J., CARROLL, R., FRASER, N. & COUKOS, G. 2005. HSV oncolytic therapy upregulates interferon-inducible chemokines and recruits immune effector cells in ovarian cancer. *Molecular Therapy*, 12, 789-802.

- BENENCIA, F., COURREGES, M. C., FRASER, N. W. & COUKOS, G. 2008. Herpes virus oncolytic therapy reverses tumor immune dysfunction and facilitates tumor antigen presentation. *Cancer Biol Ther*, 7, 1194-205.
- BLAKEMORE, R. 1975. Magnetotactic bacteria. *Science*, 190, 377-9.
- BLANCO-MANTECON, M. & O'GRADY, K. 2006. Interaction and size effects in magnetic nanoparticles. *Journal of magnetism and magnetic materials*, 296, 124-133.
- BOLOGNA-MOLINA, R., MOSQUEDA-TAYLOR, A., MOLINA-FRECHERO, N., MORI-ESTEVEZ, A.-D. & SÁNCHEZ-ACUÑA, G. 2012. Comparison of the value of PCNA and Ki-67 as markers of cell proliferation in ameloblastic tumors. *Medicina oral, patología oral y cirugía bucal*, 18, e174-e179.
- BOURGEOIS-DAIGNEAULT, M.-C., ST-GERMAIN, L. E., ROY, D. G., PELIN, A., AITKEN, A. S., ARULANANDAM, R., FALLS, T., GARCIA, V., DIALLO, J.-S. & BELL, J. C. J. B. C. R. 2016. Combination of Paclitaxel and MG1 oncolytic virus as a successful strategy for breast cancer treatment. 18, 83.
- BRACE, C. L. 2009. Radiofrequency and microwave ablation of the liver, lung, kidney, and bone: what are the differences? *Current problems in diagnostic radiology*, 38, 135-143.
- BRACE, C. L., HINSHAW, J. L., LAESEKE, P. F., SAMPSON, L. A. & LEE JR, F. T. 2009. Pulmonary Thermal Ablation: Comparison of Radiofrequency and Microwave Devices by Using Gross Pathologic and CT Findings in a Swine Model 1. *Radiology*, 251, 705-711.
- BREITBACH, C. J., BURKE, J., JONKER, D., STEPHENSON, J., HAAS, A. R., CHOW, L. Q., NIEVA, J., HWANG, T. H., MOON, A., PATT, R., PELUSIO, A., LE BOEUF, F., BURNS, J., EVGIN, L., DE SILVA, N., CVANCIC, S., ROBERTSON, T., JE, J. E., LEE, Y. S., PARATO, K., DIALLO, J. S., FENSTER, A., DANESHMAND, M., BELL, J. C. & KIRN, D. H. 2011a. Intravenous delivery of a multi-mechanistic cancer-targeted oncolytic poxvirus in humans. *Nature*, 477, 99-102.
- BREITBACH, C. J., BURKE, J., JONKER, D., STEPHENSON, J., HAAS, A. R., CHOW, L. Q. M., NIEVA, J., HWANG, T.-H., MOON, A., PATT, R., PELUSIO, A., LE BOEUF, F., BURNS, J., EVGIN, L., DE SILVA, N., CVANCIC, S., ROBERTSON, T., JE, J.-E., LEE, Y.-S., PARATO, K., DIALLO, J.-S., FENSTER, A., DANESHMAND, M., BELL, J. C. & KIRN, D. H. 2011b. Intravenous delivery of a multi-mechanistic cancer-targeted oncolytic poxvirus in humans. *Nature*, 477, 99.
- BREITBACH, C. J., LICHTY, B. D. & BELL, J. C. 2016. Oncolytic Viruses: Therapeutics With an Identity Crisis. *EBioMedicine*, 9, 31-36.
- BREITBACH, C. J., PATERSON, J. M., LEMAY, C. G., FALLS, T. J., MCGUIRE, A., PARATO, K. A., STOJDL, D. F., DANESHMAND, M., SPETH, K., KIRN, D., MCCART, J. A., ATKINS, H. & BELL, J. C. 2007a. Targeted inflammation during oncolytic virus therapy severely compromises tumor blood flow. *Mol Ther*, 15, 1686-93.
- BREITBACH, C. J., PATERSON, J. M., LEMAY, C. G., FALLS, T. J., MCGUIRE, A., PARATO, K. A., STOJDL, D. F., DANESHMAND, M., SPETH, K., KIRN, D., MCCART, J. A., ATKINS, H. & BELL, J. C. 2007b. Targeted Inflammation During Oncolytic Virus Therapy Severely Compromises Tumor Blood Flow. *Molecular Therapy*, 15, 1686-1693.
- BRIDLE, B. W., STEPHENSON, K. B., BOUDREAU, J. E., KOSHY, S., KAZDHAN, N., PULLENAYEGUM, E., BRUNELLIERE, J., BRAMSON, J. L., LICHTY, B. D. & WAN, Y. 2010. Potentiating cancer immunotherapy using an oncolytic virus. *Mol Ther*, 18, 1430-9.
- BROCATO, T., DOGRA, P., KOAY, E. J., DAY, A., CHUANG, Y.-L., WANG, Z. & CRISTINI, V. 2014. Understanding Drug Resistance in Breast Cancer with Mathematical Oncology. *Current breast cancer reports*, 6, 110-120.
- BROWN, M. C., HOLL, E. K., BOCZKOWSKI, D., DOBRIKOVA, E., MOSAHEB, M., CHANDRAMOHAN, V., BIGNER, D. D., GROMEIER, M. & NAIR, S. K. 2017. Cancer immunotherapy with recombinant poliovirus induces IFN-dominant activation of dendritic cells and tumor antigen-specific CTLs. *Science translational medicine*, 9, eaan4220.
- BROWN, S. M., MACLEAN, A. R., MCKIE, E. A. & HARLAND, J. 1997. The herpes simplex virus virulence factor ICP34.5 and the cellular protein MyD116 complex with proliferating cell nuclear

- antigen through the 63-amino-acid domain conserved in ICP34.5, MyD116, and GADD34. 71, 9442-9449.
- BRUNERS, P., BRAUNSCHWEIG, T., HODENIUS, M., PIETSCH, H., PENZKOFER, T., BAUMANN, M., GÜNTHER, R., SCHMITZ-RODE, T. & MAHNKEN, A. 2010. Thermoablation of Malignant Kidney Tumors Using Magnetic Nanoparticles: An In Vivo Feasibility Study in a Rabbit Model. *CardioVascular and Interventional Radiology*, 33, 127-134.
- BUYUKHATIPOGLU, K. & CLYNE, A. M. 2011. Superparamagnetic iron oxide nanoparticles change endothelial cell morphology and mechanics via reactive oxygen species formation. *Journal of Biomedical Materials Research Part A*, 96A, 186-195.
- BYRNE, J., TELLING, N., COKER, V., PATTRICK, R., VAN DER LAAN, G., ARENHOLZ, E., TUNA, F. & LLOYD, J. 2011. Control of nanoparticle size, reactivity and magnetic properties during the bioproduction of magnetite by *Geobacter sulfurreducens*. *Nanotechnology*, 22, 455709.
- CAMPADELLI-FIUME, G., AMASIO, M., AVITABILE, E., CERRETANI, A., FORGHIERI, C., GIANNI, T. & MENOTTI, L. 2007. The multipartite system that mediates entry of herpes simplex virus into the cell. *Rev Med Virol*, 17, 313-26.
- CAMPBELL, S. A. & GROMEIER, M. 2005. Oncolytic viruses for cancer therapy I. Cell-external factors: virus entry and receptor interaction. *Onkologie*, 28, 144-9.
- CARMICHAEL, J. C., YOKOTA, H., CRAVEN, R. C., SCHMITT, A. & WILLS, J. W. 2018. The HSV-1 mechanisms of cell-to-cell spread and fusion are critically dependent on host PTP1B. *PLOS Pathogens*, 14, e1007054.
- CHAMPIAT, S., LAMBOTTE, O., BARREAU, E., BELKHIR, R., BERDELOU, A., CARBONNEL, F., CAUQUIL, C., CHANSON, P., COLLINS, M., DURRBACH, A., EDERHY, S., FEUILLET, S., FRANCOIS, H., LAZAROVICI, J., LE PAVEC, J., DE MARTIN, E., MATEUS, C., MICHOT, J. M., SAMUEL, D., SORIA, J. C., ROBERT, C., EGGERMONT, A. & MARABELLE, A. 2016. Management of immune checkpoint blockade dysimmune toxicities: a collaborative position paper. *Ann Oncol*, 27, 559-74.
- CHAO, X., ZHANG, Z., GUO, L., ZHU, J., PENG, M., VERMORKEN, A. J. M., VAN DE VEN, W. J. M., CHEN, C. & CUI, Y. 2012a. A Novel Magnetic Nanoparticle Drug Carrier for Enhanced Cancer Chemotherapy. *PLoS ONE*, 7, e40388.
- CHAO, X., ZHANG, Z., GUO, L., ZHU, J., PENG, M., VERMORKEN, A. J. M., VAN DE VEN, W. J. M., CHEN, C. & CUI, Y. 2012b. A novel magnetic nanoparticle drug carrier for enhanced cancer chemotherapy. *PLoS one*, 7, e40388-e40388.
- CHEEMA, T. A., WAKIMOTO, H., FECCI, P. E., NING, J., KURODA, T., JEYARETNA, D. S., MARTUZA, R. L. & RABKIN, S. D. 2013. Multifaceted oncolytic virus therapy for glioblastoma in an immunocompetent cancer stem cell model.
- CHEN, C.-Y., WANG, P.-Y., HUTZEN, B., SPRAGUE, L., SWAIN, H. M., LOVE, J. K., STANEK, J. R., BOON, L., CONNER, J. & CRIPE, T. P. 2017. Cooperation of Oncolytic Herpes Virotherapy and PD-1 Blockade in Murine Rhabdomyosarcoma Models. *Scientific reports*, 7, 2396-2396.
- CHEN, D. S. & MELLMAN, I. 2013. Oncology meets immunology: the cancer-immunity cycle. *Immunity*, 39, 1-10.
- CHEN, J., SHI, M., LIU, P., KO, A., ZHONG, W., LIAO, W. & XING, M. M. 2014. Reducible polyamidoamine-magnetic iron oxide self-assembled nanoparticles for doxorubicin delivery. *Biomaterials*, 35, 1240-8.
- CHEN, K., HUANG, Y.-H. & CHEN, J.-L. 2013. Understanding and targeting cancer stem cells: therapeutic implications and challenges. *Acta pharmacologica Sinica*, 34, 732-740.
- CHERTOK, B., DAVID, A. E. & YANG, V. C. 2010. Polyethyleneimine-modified iron oxide nanoparticles for brain tumor drug delivery using magnetic targeting and intra-carotid administration. *Biomaterials*, 31, 6317-24.
- CHOI, A. H., O'LEARY, M. P., FONG, Y. & CHEN, N. G. 2016. From Benchtop to Bedside: A Review of Oncolytic Virotherapy. *Biomedicines*, 4.

- CONFORTINI, C. C. & KRONG, B. 2015. Breast cancer in the global south and the limitations of a biomedical framing: a critical review of the literature. *Health Policy and Planning*, 30, 1350-1361.
- CONNER, J., RIXON, F. J. & BROWN, S. M. 2005. Herpes simplex virus type 1 strain HSV1716 grown in baby hamster kidney cells has altered tropism for nonpermissive Chinese hamster ovary cells compared to HSV1716 grown in vero cells. *J Virol*, 79, 9970-81.
- COUKOS, G., MAKRIGIANNAKIS, A., KANG, E. H., RUBIN, S. C., ALBELDA, S. M. & MOLNAR-KIMBER, K. L. 2000. Oncolytic Herpes Simplex Virus-1 Lacking ICP34.5 Induces p53-independent Death and Is Efficacious against Chemotherapy-resistant Ovarian Cancer. 6, 3342-3353.
- CROSBY, E. J., WEI, J., YANG, X. Y., LEI, G., WANG, T., LIU, C. X., AGARWAL, P., KORMAN, A. J., MORSE, M. A., GOUIN, K., KNOTT, S. R. V., LYERLY, H. K. & HARTMAN, Z. C. 2018. Complimentary mechanisms of dual checkpoint blockade expand unique T-cell repertoires and activate adaptive anti-tumor immunity in triple-negative breast tumors. *Oncoimmunology*, 7, e1421891.
- CYPRIANO, J., WERCKMANN, J., VARGAS, G., LOPES DOS SANTOS, A., SILVA, K. T., LEÃO, P., ALMEIDA, F. P., BAZYLINSKI, D. A., FARINA, M., LINS, U. & ABREU, F. 2019. Uptake and persistence of bacterial magnetite magnetosomes in a mammalian cell line: Implications for medical and biotechnological applications. *PLOS ONE*, 14, e0215657.
- DADFAR, S. M. A., ROEMHILD, K., DRUDE, N., WESTPHAL, S., KNUCHEL, R., KIESSLING, F. & LAMMERS, T. 2019. *Iron oxide nanoparticles: Diagnostic, therapeutic and theranostic applications*.
- DANSON, S., WOLL, P., EDWARDS, J., BLYTH, K., FISHER, P., ROMAN, J., SIMPSON, K., SPAVIN, R., LEARMONTH, K. & CONNER, J. 2017. *366PD Oncolytic herpesvirus therapy for mesothelioma: A phase I/IIa trial of intrapleural administration of HSV1716 (NCT01721018)*.
- DAVIES, E. & HISCOX, S. 2011. New therapeutic approaches in breast cancer. *Maturitas*, 68, 121-8.
- DAVIES, H., BIGNELL, G. R., COX, C., STEPHENS, P., EDKINS, S., CLEGG, S., TEAGUE, J., WOFFENDIN, H., GARNETT, M. J., BOTTOMLEY, W., DAVIS, N., DICKS, E., EWING, R., FLOYD, Y., GRAY, K., HALL, S., HAWES, R., HUGHES, J., KOSMIDOU, V., MENZIES, A., MOULD, C., PARKER, A., STEVENS, C., WATT, S., HOOPER, S., WILSON, R., JAYATILAKE, H., GUSTERSON, B. A., COOPER, C., SHIPLEY, J., HARGRAVE, D., PRITCHARD-JONES, K., MAITLAND, N., CHENEVIX-TRENCH, G., RIGGINS, G. J., BIGNER, D. D., PALMIERI, G., COSSU, A., FLANAGAN, A., NICHOLSON, A., HO, J. W., LEUNG, S. Y., YUEN, S. T., WEBER, B. L., SEIGLER, H. F., DARROW, T. L., PATERSON, H., MARAIS, R., MARSHALL, C. J., WOOSTER, R., STRATTON, M. R. & FUTREAL, P. A. 2002. Mutations of the BRAF gene in human cancer. *Nature*, 417, 949-54.
- DENARDO, S. J., DENARDO, G. L., NATARAJAN, A., MIERS, L. A., FOREMAN, A. R., GRUETTNER, C., ADAMSON, G. N. & IVKOV, R. 2007. Thermal Dosimetry Predictive of Efficacy of ¹¹¹In-ChL6 Nanoparticle AMF-Induced Thermoablative Therapy for Human Breast Cancer in Mice. *Journal of Nuclear Medicine*, 48, 437-444.
- DENT, S. F. 2009. The role of VEGF in triple-negative breast cancer: where do we go from here? *Annals of Oncology*, 20, 1615-1617.
- DETTA, A., HARLAND, J., HANIF, I., BROWN, S. M. & CRUICKSHANK, G. 2003. Proliferative activity and in vitro replication of HSV1716 in human metastatic brain tumours. 5, 681-689.
- DIAS, A. M. G. C., HUSSAIN, A., MARCOS, A. S. & ROQUE, A. C. A. 2011. A biotechnological perspective on the application of iron oxide magnetic colloids modified with polysaccharides. *Biotechnology Advances*, 29, 142-155.
- DINE, J., GORDON, R., SHAMES, Y., KASLER, M. K. & BARTON-BURKE, M. 2017. Immune Checkpoint Inhibitors: An Innovation in Immunotherapy for the Treatment and Management of Patients with Cancer. *Asia Pac J Oncol Nurs*, 4, 127-135.
- DORONIN, K., TOH, K., KUPPUSWAMY, M., WARD, P., TOLLEFSON, A. E. & WOLD, W. S. 2000. Tumor-specific, replication-competent adenovirus vectors overexpressing the adenovirus death protein. *Journal of virology*, 74, 6147-6155.

- DÜRR, S., JANKO, C., LYER, S., TRIPAL, P., SCHWARZ, M., ZALOGA, J., TIETZE, R. & ALEXIOU, C. 2013. Magnetic nanoparticles for cancer therapy. *Nanotechnology Reviews*.
- EDMONDSON, R., BROGLIE, J. J., ADCOCK, A. F. & YANG, L. 2014. Three-dimensional cell culture systems and their applications in drug discovery and cell-based biosensors. *Assay Drug Dev Technol*, 12, 207-18.
- EISSA, I. R., BUSTOS-VILLALOBOS, I., ICHINOSE, T., MATSUMURA, S., NAOE, Y., MIYAJIMA, N., MORIMOTO, D., MUKOYAMA, N., ZHIWEN, W., TANAKA, M., HASEGAWA, H., SUMIGAMA, S., ALEKSIC, B., KODERA, Y. & KASUYA, H. 2018. The Current Status and Future Prospects of Oncolytic Viruses in Clinical Trials against Melanoma, Glioma, Pancreatic, and Breast Cancers. *Cancers (Basel)*, 10.
- EMENS, L. A., ASCIERTO, P. A., DARCY, P. K., DEMARIA, S., EGGERMONT, A. M. M., REDMOND, W. L., SELIGER, B. & MARINCOLA, F. M. 2017. Cancer immunotherapy: Opportunities and challenges in the rapidly evolving clinical landscape. *Eur J Cancer*, 81, 116-129.
- FADOK, V. A., BRATTON, D. L., GUTHRIE, L. & HENSON, P. M. 2001. Differential Effects of Apoptotic Versus Lysed Cells on Macrophage Production of Cytokines: Role of Proteases. *The Journal of Immunology*, 166, 6847-6854.
- FAIVRE, D. & GODEC, T. U. 2015. From bacteria to mollusks: the principles underlying the biomineralization of iron oxide materials. *Angew Chem Int Ed Engl*, 54, 4728-47.
- FARNSWORTH, A., WISNER, T. W., WEBB, M., ROLLER, R., COHEN, G., EISENBERG, R. & JOHNSON, D. C. 2007. Herpes simplex virus glycoproteins gB and gH function in fusion between the virion envelope and the outer nuclear membrane. 104, 10187-10192.
- FELT, S. A., MOERDYK-SCHAUWECKER, M. J. & GRDZELISHVILI, V. Z. 2015. Induction of apoptosis in pancreatic cancer cells by vesicular stomatitis virus. *Virology*, 474, 163-173.
- FENWICK, M. L. & WALKER, M. J. 1978. Suppression of the synthesis of cellular macromolecules by herpes simplex virus. *J Gen Virol*, 41, 37-51.
- FERGUSON, M. S., LEMOINE, N. R. & WANG, Y. 2012. Systemic Delivery of Oncolytic Viruses: Hopes and Hurdles. *Advances in Virology*, 2012, 14.
- FERNÁNDEZ-CASTANÉ, A., LI, H., THOMAS, O. R. T. & OVERTON, T. W. 2018. Development of a simple intensified fermentation strategy for growth of *Magnetospirillum gryphiswaldense* MSR-1: Physiological responses to changing environmental conditions. *New Biotechnology*, 46, 22-30.
- FISHER, K. 2006. Striking out at disseminated metastases: the systemic delivery of oncolytic viruses. *Curr Opin Mol Ther*, 8, 301-13.
- FREYTAG, S. O., ROGULSKI, K. R., PAIELLI, D. L., GILBERT, J. D. & KIM, J. H. 1998. A novel three-pronged approach to kill cancer cells selectively: concomitant viral, double suicide gene, and radiotherapy. *Hum Gene Ther*, 9, 1323-33.
- FUGE, O., VASDEV, N., ALLCHORNE, P. & GREEN, J. S. 2015. Immunotherapy for bladder cancer. *Research and reports in urology*, 7, 65-79.
- GALANIS, E., HARTMANN, L. C., CLIBY, W. A., LONG, H. J., PEETHAMBARAM, P. P., BARRETTE, B. A., KAUR, J. S., HALUSKA, P. J., JR., ADERCA, I., ZOLLMAN, P. J., SLOAN, J. A., KEENEY, G., ATHERTON, P. J., PODRATZ, K. C., DOWDY, S. C., STANHOPE, C. R., WILSON, T. O., FEDERSPIEL, M. J., PENG, K. W. & RUSSELL, S. J. 2010. Phase I trial of intraperitoneal administration of an oncolytic measles virus strain engineered to express carcinoembryonic antigen for recurrent ovarian cancer. *Cancer Res*, 70, 875-82.
- GAO, J., WARD, J. F., PETTAWAY, C. A., SHI, L. Z., SUBUDHI, S. K., VENCE, L. M., ZHAO, H., CHEN, J., CHEN, H., EFSTATHIOU, E., TRONCOSO, P., ALLISON, J. P., LOGOTHETIS, C. J., WISTUBA, II, SEPULVEDA, M. A., SUN, J., WARGO, J., BLANDO, J. & SHARMA, P. 2017. VISTA is an inhibitory immune checkpoint that is increased after ipilimumab therapy in patients with prostate cancer. *Nat Med*, 23, 551-555.
- GARBER, K. 2006. China approves world's first oncolytic virus therapy for cancer treatment. *J Natl Cancer Inst*, 98, 298-300.

- GARLAND, S. M., HERNANDEZ-AVILA, M., WHEELER, C. M., PEREZ, G., HARPER, D. M., LEODOLTER, S., TANG, G. W., FERRIS, D. G., STEBEN, M., BRYAN, J., TADDEO, F. J., RAILKAR, R., ESSER, M. T., SINGS, H. L., NELSON, M., BOSLEGO, J., SATTLER, C., BARR, E. & KOUTSKY, L. A. 2007. Quadrivalent vaccine against human papillomavirus to prevent anogenital diseases. *N Engl J Med*, 356, 1928-43.
- GHARPURE, K. M., WU, S. Y., LI, C., LOPEZ-BERESTEIN, G. & SOOD, A. K. 2015. Nanotechnology: future of oncotherapy. *Clinical Cancer Research*, 21, 3121-3130.
- GOLD, L. I., EGGLETON, P., SWEETWYNE, M. T., VAN DUYN, L. B., GREIVES, M. R., NAYLOR, S. M., MICHALAK, M. & MURPHY-ULLRICH, J. E. 2010. Calreticulin: non-endoplasmic reticulum functions in physiology and disease. *Faseb j*, 24, 665-83.
- GOLDHIRSCH, A., INGLE, J. N., GELBER, R. D., COATES, A. S., THURLIMANN, B. & SENN, H. J. 2009. Thresholds for therapies: highlights of the St Gallen International Expert Consensus on the primary therapy of early breast cancer 2009. *Ann Oncol*, 20, 1319-29.
- GOLDUFSKY, J., SIVENDRAN, S., HARCHARIK, S., PAN, M., BERNARDO, S., STERN, R., FRIEDLANDER, P., RUBY, C., SAENGER, Y. & KAUFMAN, H. 2013. Oncolytic virus therapy for cancer. *Oncolytic Virother*, 2, 31-46.
- GOODWIN, S., PETERSON, C., HOH, C. & BITTNER, C. 1999. Targeting and retention of magnetic targeted carriers (MTCs) enhancing intra-arterial chemotherapy. *Journal of Magnetism and Magnetic Materials*, 194, 132-139.
- GORBY, Y. A., BEVERIDGE, T. J. & BLAKEMORE, R. P. 1988. Characterization of the bacterial magnetosome membrane. *J Bacteriol*, 170, 834-41.
- GREENE, S. E. & KOMEILI, A. 2012. Biogenesis and subcellular organization of the magnetosome organelles of magnetotactic bacteria. *Current Opinion in Cell Biology*, 24, 490-495.
- GRIFFITHS, L., BINLEY, K., IQBALL, S., KAN, O., MAXWELL, P., RATCLIFFE, P., LEWIS, C., HARRIS, A., KINGSMAN, S. & NAYLOR, S. 2000. The macrophage-a novel system to deliver gene therapy to pathological hypoxia. *Gene therapy*, 7, 255-262.
- GRUNBERG, K., MULLER, E. C., OTTO, A., RESZKA, R., LINDER, D., KUBE, M., REINHARDT, R. & SCHULER, D. 2004. Biochemical and proteomic analysis of the magnetosome membrane in *Magnetospirillum gryphiswaldense*. *Appl Environ Microbiol*, 70, 1040-50.
- GUPTA, A., DE FELICE, K. M., LOFTUS, E. V., JR. & KHANNA, S. 2015. Systematic review: colitis associated with anti-CTLA-4 therapy. *Aliment Pharmacol Ther*, 42, 406-17.
- HAASE, M. & FITZE, G. 2016. HSP90AB1: Helping the good and the bad. *Gene*, 575, 171-186.
- HAINFELD, J. F., O'CONNOR, M. J., SLATKIN, D. N., DILMANIAN, F. A. & SMILOWITZ, H. M. 2013. Abstract 4438: Gold nanoparticle imaging and radiotherapy of brain tumors in mice. 73, 4438-4438.
- HAINFELD, J. F., O'CONNOR, M. J., DILMANIAN, F. A., SLATKIN, D. N., ADAMS, D. J. & SMILOWITZ, H. M. 2011. Micro-CT enables microlocalisation and quantification of Her2-targeted gold nanoparticles within tumour regions. *The British Journal of Radiology*, 84, 526-533.
- HALL, A. R., DIX, B. R., O'CARROLL, S. J. & BRAITHWAITE, A. W. 1998. p53-dependent cell death/apoptosis is required for a productive adenovirus infection. *Nat Med*, 4, 1068-72.
- HAO, Y., SONG, S., YANG, X., XING, J. & CHEN, J. 2012. Magnetic gold nanoparticles: synthesis, characterization and its application in the delivery of FITC into KG-1 cells. *Journal of nanoscience and nanotechnology*, 12, 7716-7722.
- HARITHA, V., MESHARAM, H. M. & RAO, A. B. 2015. Lipase Immobilized on Magnetic Nanoparticles: A New Tool for Synthesis of Disulphide Compounds. *Green and Sustainable Chemistry*, 5, 25.
- HARLAND, J., DUNN, P., CAMERON, E., CONNER, J. & BROWN, S. M. J. J. O. N. 2003. The herpes simplex virus (HSV) protein ICP34.5 is a virion component that forms a DNA-binding complex with proliferating cell nuclear antigen and HSV replication proteins. 9, 477-488.
- HASHIMOTO, M. & HISANO, Y. 2011. Directional gene-transfer into the brain by an adenoviral vector tagged with magnetic nanoparticles. *J Neurosci Methods*, 194, 316-20.

- HEO, J., REID, T., RUO, L., BREITBACH, C. J., ROSE, S., BLOOMSTON, M., CHO, M., LIM, H. Y., CHUNG, H. C., KIM, C. W., BURKE, J., LENCIONI, R., HICKMAN, T., MOON, A., LEE, Y. S., KIM, M. K., DANESHMAND, M., DUBOIS, K., LONGPRE, L., NGO, M., ROONEY, C., BELL, J. C., RHEE, B.-G., PATT, R., HWANG, T.-H. & KIRN, D. H. 2013a. Randomized dose-finding clinical trial of oncolytic immunotherapeutic vaccinia JX-594 in liver cancer. *Nat Med*, 19, 329-336.
- HEO, J., REID, T., RUO, L., BREITBACH, C. J., ROSE, S., BLOOMSTON, M., CHO, M., LIM, H. Y., CHUNG, H. C., KIM, C. W., BURKE, J., LENCIONI, R., HICKMAN, T., MOON, A., LEE, Y. S., KIM, M. K., DANESHMAND, M., DUBOIS, K., LONGPRE, L., NGO, M., ROONEY, C., BELL, J. C., RHEE, B. G., PATT, R., HWANG, T. H. & KIRN, D. H. 2013b. Randomized dose-finding clinical trial of oncolytic immunotherapeutic vaccinia JX-594 in liver cancer. *Nat Med*, 19, 329-36.
- HERVAULT, A. & THANH, N. N. T. K. 2014. Magnetic nanoparticle-based therapeutic agents for thermo-chemotherapy treatment of cancer. *Nanoscale*, 6, 11553-11573.
- HERZENBERG, L. A., TUNG, J., MOORE, W. A., HERZENBERG, L. A. & PARKS, D. R. 2006. Interpreting flow cytometry data: a guide for the perplexed. *Nat Immunol*, 7, 681-5.
- HEYEN, U. & SCHULER, D. 2003. Growth and magnetosome formation by microaerophilic Magnetospirillum strains in an oxygen-controlled fermentor. *Appl Microbiol Biotechnol*, 61, 536-44.
- HILGER, I., HERGT, R. & KAISER, W. A. 2005. Use of magnetic nanoparticle heating in the treatment of breast cancer. *IEE Proceedings - Nanobiotechnology*, 152, 33-39.
- HILGER, I. P., HIERGEIST, R. P., HERGT, R. P., WINNEFELD, K. P., SCHUBERT, H. P. & KAISER, W. A. M. 2002. Thermal Ablation of Tumors Using Magnetic Nanoparticles: An In Vivo Feasibility Study. *Investigative Radiology*, 37, 580-586.
- HODI, F. S., O'DAY, S. J., MCDERMOTT, D. F., WEBER, R. W., SOSMAN, J. A., HAANEN, J. B., GONZALEZ, R., ROBERT, C., SCHADENDORF, D., HASSEL, J. C., AKERLEY, W., VAN DEN EERTWEGH, A. J., LUTZKY, J., LORIGAN, P., VAUBEL, J. M., LINETTE, G. P., HOGG, D., OTTENSMEIER, C. H., LEBBE, C., PESCHEL, C., QUIRT, I., CLARK, J. I., WOLCHOK, J. D., WEBER, J. S., TIAN, J., YELLIN, M. J., NICHOL, G. M., HOOS, A. & URBA, W. J. 2010. Improved survival with ipilimumab in patients with metastatic melanoma. *N Engl J Med*, 363, 711-23.
- HOLL, E. K., BROWN, M. C., BOCZKOWSKI, D., MCNAMARA, M. A., GEORGE, D. J., BIGNER, D. D., GROMEIER, M. & NAIR, S. K. 2016. Recombinant oncolytic poliovirus, PVSRIPO, has potent cytotoxic and innate inflammatory effects, mediating therapy in human breast and prostate cancer xenograft models. *Oncotarget*, 7, 79828-79841.
- HOSHINO, R., CHATANI, Y., YAMORI, T., TSURUO, T., OKA, H., YOSHIDA, O., SHIMADA, Y., ARI-I, S., WADA, H., FUJIMOTO, J. & KOHNO, M. 1999. Constitutive activation of the 41-/43-kDa mitogen-activated protein kinase signaling pathway in human tumors. *Oncogene*, 18, 813-22.
- HOWELLS, A., MARELLI, G., LEMOINE, N. R. & WANG, Y. 2017. Oncolytic Viruses-Interaction of Virus and Tumor Cells in the Battle to Eliminate Cancer. *Frontiers in oncology*, 7, 195-195.
- HUANG, H. S. & HAINFELD, J. F. 2013. Intravenous magnetic nanoparticle cancer hyperthermia. *International Journal of Nanomedicine*, 8, 2521-2532.
- HUGHES, R., QIAN, B. Z., ROWAN, C., MUTHANA, M., KEKLIKOGLOU, I., OLSON, O. C., TAZZYMAN, S., DANSON, S., ADDISON, C., CLEMONS, M., GONZALEZ-ANGULO, A. M., JOYCE, J. A., DE PALMA, M., POLLARD, J. W. & LEWIS, C. E. 2015. Perivascular M2 Macrophages Stimulate Tumor Relapse after Chemotherapy. *Cancer Res*, 75, 3479-91.
- HUGHES, T., COFFIN, R. S., LILLEY, C. E., PONCE, R. & KAUFMAN, H. L. 2014. Critical analysis of an oncolytic herpesvirus encoding granulocyte-macrophage colony stimulating factor for the treatment of malignant melanoma. *Oncolytic virotherapy*, 3, 11-20.
- HUSZTHY, P., IMMERSVOLL, H., WANG, J., GOPLIN, D., MILETIC, H., EIDE, G. & BJERKVIG, R. 2009. Cellular effects of oncolytic viral therapy on the glioblastoma microenvironment.

- HUSZTHY, P. C., GOPLEN, D., THORSEN, F., IMMERVOLL, H., WANG, J., GUTERMANN, A., MILETIC, H. & BJERKVIG, R. 2008. Oncolytic herpes simplex virus type-1 therapy in a highly infiltrative animal model of human glioblastoma. *Clin Cancer Res*, 14, 1571-80.
- IANKOV, I. D., BLECHACZ, B., LIU, C., SCHMECKPEPER, J. D., TARARA, J. E., FEDERSPIEL, M. J., CAPLICE, N. & RUSSELL, S. J. 2007. Infected cell carriers: a new strategy for systemic delivery of oncolytic measles viruses in cancer virotherapy. *Mol Ther*, 15, 114-22.
- ILETT, E. J., PRESTWICH, R. J., KOTTKE, T., ERRINGTON, F., THOMPSON, J. M., HARRINGTON, K. J., PANDHA, H. S., COFFEY, M., SELBY, P. J., VILE, R. G. & MELCHER, A. A. 2009. Dendritic cells and T cells deliver oncolytic reovirus for tumour killing despite pre-existing anti-viral immunity. *Gene therapy*, 16, 689-699.
- ISSA, B., OBAIDAT, I. M., ALBISS, B. A. & HAIK, Y. 2013. Magnetic Nanoparticles: Surface Effects and Properties Related to Biomedicine Applications. *International Journal of Molecular Sciences*, 14, 21266-21305.
- JENNINGS, V. A., ILETT, E. J., SCOTT, K. J., WEST, E. J., VILE, R., PANDHA, H., HARRINGTON, K., YOUNG, A., HALL, G. D., COFFEY, M., SELBY, P., ERRINGTON-MAIS, F. & MELCHER, A. A. 2014. Lymphokine-activated killer and dendritic cell carriage enhances oncolytic reovirus therapy for ovarian cancer by overcoming antibody neutralization in ascites. *International Journal of Cancer*, 134, 1091-1101.
- JOHANNSEN, M., GNEVECKOW, U., THIESEN, B., TAYMOORIAN, K., CHO, C. H., WALDÖFNER, N., SCHOLZ, R., JORDAN, A., LOENING, S. A. & WUST, P. 2007. Thermotherapy of Prostate Cancer Using Magnetic Nanoparticles: Feasibility, Imaging, and Three-Dimensional Temperature Distribution. *European Urology*, 52, 1653-1662.
- JOHNSTONE, C. N., SMITH, Y. E., CAO, Y., BURROWS, A. D., CROSS, R. S., LING, X., REDVERS, R. P., DOHERTY, J. P., ECKHARDT, B. L., NATOLI, A. L., RESTALL, C. M., LUCAS, E., PEARSON, H. B., DEB, S., BRITT, K. L., RIZZITELLI, A., LI, J., HARMEY, J. H., POULIOT, N. & ANDERSON, R. L. 2015. Functional and molecular characterisation of EO771.LMB tumours, a new C57BL/6-mouse-derived model of spontaneously metastatic mammary cancer. *Dis Model Mech*, 8, 237-51.
- JUGOVIC, P., HILL, A. M., TOMAZIN, R., PLOEGH, H. & JOHNSON, D. C. 1998. Inhibition of Major Histocompatibility Complex Class I Antigen Presentation in Pig and Primate Cells by Herpes Simplex Virus Type 1 and 2 ICP47. *Journal of Virology*, 72, 5076-5084.
- KAMI, D., TAKEDA, S., ITAKURA, Y., GOJO, S., WATANABE, M. & TOYODA, M. 2011. Application of Magnetic Nanoparticles to Gene Delivery. *International Journal of Molecular Sciences*, 12, 3705-3722.
- KANTOFF, P. W., HIGANO, C. S., SHORE, N. D., BERGER, E. R., SMALL, E. J., PENSON, D. F., REDFERN, C. H., FERRARI, A. C., DREICER, R., SIMS, R. B., XU, Y., FROHLICH, M. W. & SCHELLHAMMER, P. F. 2010. Sipuleucel-T immunotherapy for castration-resistant prostate cancer. *N Engl J Med*, 363, 411-22.
- KARAPANAGIOTOU, E. M., ROULSTONE, V., TWIGGER, K., BALL, M., TANAY, M., NUTTING, C., NEWBOLD, K., GORE, M. E., LARKIN, J., SYRIGOS, K. N., COFFEY, M., THOMPSON, B., METTINGER, K., VILE, R. G., PANDHA, H. S., HALL, G. D., MELCHER, A. A., CHESTER, J. & HARRINGTON, K. J. 2012. Phase I/II Trial of Carboplatin and Paclitaxel Chemotherapy in Combination with Intravenous Oncolytic Reovirus in Patients with Advanced Malignancies. *Clinical Cancer Research*, 18, 2080-2089.
- KARASNEH, G. A. & SHUKLA, D. 2011. Herpes simplex virus infects most cell types in vitro: clues to its success. *Virology journal*, 8, 481-481.
- KASEDA, K., WATANABE, K.-I., SAKAMAKI, H. & KAZAMA, A. 2016. Solitary pulmonary metastasis from occult papillary thyroid carcinoma. *Thoracic cancer*, 7, 261-263.
- KATAOKA, K., MATSUMOTO, T., YOKOYAMA, M., OKANO, T., SAKURAI, Y., FUKUSHIMA, S., OKAMOTO, K. & KWON, G. S. 2000. Doxorubicin-loaded poly(ethylene glycol)-poly(beta-

- benzyl-L-aspartate) copolymer micelles: their pharmaceutical characteristics and biological significance. *J Control Release*, 64, 143-53.
- KAUR, B., CHIOCCA, E. A. & CRIPE, T. P. 2012a. Oncolytic HSV-1 Virotherapy: Clinical Experience and Opportunities for Progress. *Current pharmaceutical biotechnology*, 13, 1842-1851.
- KAUR, B., CHIOCCA, E. A. & CRIPE, T. P. 2012b. Oncolytic HSV-1 Virotherapy: Clinical Experience and Opportunities for Progress. *Curr Pharm Biotechnol*, 13, 1842-51.
- KELLY, B. J., FRAEFEL, C., CUNNINGHAM, A. L. & DIEFENBACH, R. J. 2009. Functional roles of the tegument proteins of herpes simplex virus type 1. *Virus Research*, 145, 173-186.
- KEPP, O., GALLUZZI, L., MARTINS, I., SCHLEMMER, F., ADJEMIAN, S., MICHAUD, M., SUKKURWALA, A. Q., MENGER, L., ZITVOGEL, L. & KROEMER, G. 2011. Molecular determinants of immunogenic cell death elicited by anticancer chemotherapy. *Cancer Metastasis Rev*, 30, 61-9.
- KETTERING, M., WINTER, J., ZEISBERGER, M., BREMER-STRECK, S., OEHRING, H., BERGEMANN, C., ALEXIOU, C., HERGT, R., HALBHUBER, K. J., KAISER, W. A. & HILGER, I. 2007. Magnetic nanoparticles as bimodal tools in magnetically induced labelling and magnetic heating of tumour cells: an in vitro study. *Nanotechnology*, 18, 175101.
- KHEIRKHAH, P., DENYER, S., BHIMANI, A. D., ARNONE, G. D., ESFAHANI, D. R., AGUILAR, T., ZAKRZEWSKI, J., VENUGOPAL, I., HABIB, N., GALLIA, G. L., LINNINGER, A., CHARBEL, F. T. & MEHTA, A. I. 2018. Magnetic Drug Targeting: A Novel Treatment for Intramedullary Spinal Cord Tumors. *Scientific Reports*, 8, 11417.
- KIM, J., EUN LEE, J., HYEON LEE, S., HO YU, J., LEE, J., GWAN PARK, T. & HYEON, T. 2008. *Designed Fabrication of a Multifunctional Polymer Nanomedical Platform for Simultaneous Cancer-Targeted Imaging and Magnetically Guided Drug Delivery*.
- KIM, S. Y., SHIN, I. G. & LEE, Y. M. 1999. Amphiphilic diblock copolymeric nanospheres composed of methoxy poly(ethylene glycol) and glycolide: properties, cytotoxicity and drug release behaviour. *Biomaterials*, 20, 1033-42.
- KIRCHER, M. F., MAHMOOD, U., KING, R. S., WEISSLEDER, R. & JOSEPHSON, L. 2003. A multimodal nanoparticle for preoperative magnetic resonance imaging and intraoperative optical brain tumor delineation. *Cancer research*, 63, 8122-8125.
- KISELEVA, L., BRILIUTE, J., KHILYAS, I. V., SIMPSON, D. J., FEDOROVICH, V., COHEN, M. & GORYANIN, I. 2015. Magnet-Facilitated Selection of Electrogenic Bacteria from Marine Sediment. *Biomed Res Int*, 2015, 582471.
- KOKS, C. A., GARG, A. D., EHRHARDT, M., RIVA, M., VANDENBERK, L., BOON, L., DE VLEESCHOUWER, S., AGOSTINIS, P., GRAF, N. & VAN GOOL, S. W. 2015. Newcastle disease virotherapy induces long-term survival and tumor-specific immune memory in orthotopic glioma through the induction of immunogenic cell death. *Int J Cancer*, 136, E313-25.
- KOMEILI, A. 2012. Molecular mechanisms of compartmentalization and biomineralization in magnetotactic bacteria. *FEMS Microbiol Rev*, 36, 232-55.
- KOUASSI, G. K., IRUDAYARAJ, J. & MCCARTY, G. 2005. Activity of glucose oxidase functionalized onto magnetic nanoparticles. *Biomagnetic research and technology*, 3, 1.
- KUMAR, M., YIGIT, M., DAI, G., MOORE, A. & MEDAROVA, Z. 2010. Image-Guided Breast Tumor Therapy Using a Small Interfering RNA Nanodrug. *Cancer Research*, 70, 7553-7561.
- KYRTATOS, P. G., LEHTOLAINEN, P., JUNEMANN-RAMIREZ, M., GARCIA-PRIETO, A., PRICE, A. N., MARTIN, J. F., GADIAN, D. G., PANKHURST, Q. A. & LYTHGOE, M. F. 2009. Magnetic Tagging Increases Delivery of Circulating Progenitors in Vascular Injury. *JACC: Cardiovascular Interventions*, 2, 794-802.
- LANDÁZURI, N., TONG, S., SUO, J., JOSEPH, G., WEISS, D., SUTCLIFFE, D. J., GIDDENS, D. P., BAO, G. & TAYLOR, W. R. 2013. Magnetic Targeting of Human Mesenchymal Stem Cells with Internalized Superparamagnetic Iron Oxide Nanoparticles. *Small*, 9, 4017-4026.
- LANFRANCA, M. P., MOSTAFA, H. H. & DAVIDO, D. J. 2014. HSV-1 ICP0: An E3 Ubiquitin Ligase That Counteracts Host Intrinsic and Innate Immunity. *Cells*, 3, 438-454.

- LANGELIER, Y., BERGERON, S., CHABAUD, S., LIPPENS, J., GUILBAULT, C., SASSEVILLE, A. M., DENIS, S., MOSSER, D. D. & MASSIE, B. 2002. The R1 subunit of herpes simplex virus ribonucleotide reductase protects cells against apoptosis at, or upstream of, caspase-8 activation. *J Gen Virol*, 83, 2779-89.
- LANGER, C. J., GADGEEL, S. M., BORGHAEI, H., PAPANIMITRAKOPOULOU, V. A., PATNAIK, A., POWELL, S. F., GENTZLER, R. D., MARTINS, R. G., STEVENSON, J. P., JALAL, S. I., PANWALKAR, A., YANG, J. C., GUBENS, M., SEQUIST, L. V., AWAD, M. M., FIORE, J., GE, Y., RAFTOPOULOS, H. & GANDHI, L. 2016. Carboplatin and pemetrexed with or without pembrolizumab for advanced, non-squamous non-small-cell lung cancer: a randomised, phase 2 cohort of the open-label KEYNOTE-021 study. *Lancet Oncol*, 17, 1497-1508.
- LE BOEUF, F., BATENCHUK, C., VAHA-KOSKELA, M., BRETON, S., ROY, D., LEMAY, C., COX, J., ABDELBARY, H., FALLS, T., WAGHRAY, G., ATKINS, H., STOJDL, D., DIALLO, J. S., KAERN, M. & BELL, J. C. 2013. Model-based rational design of an oncolytic virus with improved therapeutic potential. *Nat Commun*, 4, 1974.
- LE FÈVRE, R., DURAND DUBIEF, M., CHEBBI, I., MANDAWALA, C., LAGROIX, F., VALET, J.-P., IDBAIH, A., ADAM, C., DELATTRE, J.-Y., SCHMITT, C., MAAKE, C., GUYOT, F. & ALPHANDÉRY, E. 2017. Enhanced antitumor efficacy of biocompatible magnetosomes for the magnetic hyperthermia treatment of glioblastoma.
- LEE, J. Y., CHOI, B. I., RYU, J. K., KIM, Y.-T., HWANG, J. H., KIM, S. H. & HAN, J. K. 2011. Concurrent Chemotherapy and Pulsed High-Intensity Focused Ultrasound Therapy for the Treatment of Unresectable Pancreatic Cancer: Initial Experiences. *Korean Journal of Radiology*, 12, 176-186.
- LEFEVRE, C. T. & BAZYLINSKI, D. A. 2013. Ecology, diversity, and evolution of magnetotactic bacteria. *Microbiol Mol Biol Rev*, 77, 497-526.
- LEFEVRE, C. T., FRANKEL, R. B., ABREU, F., LINS, U. & BAZYLINSKI, D. A. 2011. Culture-independent characterization of a novel, uncultivated magnetotactic member of the Nitrospirae phylum. *Environ Microbiol*, 13, 538-49.
- LEMKE, A. J., SENFFT VON PILSACH, M. I., LÜBBE, A., BERGEMANN, C., RIESS, H. & FELIX, R. 2004. MRI after magnetic drug targeting in patients with advanced solid malignant tumors. *European Radiology*, 14, 1949-1955.
- LEOPARDI, R., VAN SANT, C. & ROIZMAN, B. 1997. The herpes simplex virus 1 protein kinase US3 is required for protection from apoptosis induced by the virus. *Proceedings of the National Academy of Sciences of the United States of America*, 94, 7891-7896.
- LI, J., MENGUY, N., GATEL, C., BOUREAU, V., SNOECK, E., PATRIARCHE, G., LEROY, E. & PAN, Y. 2015. Crystal growth of bullet-shaped magnetite in magnetotactic bacteria of the Nitrospirae phylum. *J R Soc Interface*, 12.
- LI, Z., XIANG, J., ZHANG, W., FAN, S., WU, M., LI, X. & LI, G. 2008. Nanoparticle delivery of anti-metastatic NM23-H1 gene improves chemotherapy in a mouse tumor model. *Cancer Gene Ther*, 16, 423-429.
- LIM, S. Y., YUZHALLIN, A. E., GORDON-WEEKS, A. N. & MUSCHEL, R. J. 2016. Targeting the CCL2-CCR2 signaling axis in cancer metastasis. *Oncotarget*, 7, 28697-28710.
- LINARDOU, H. & GOGAS, H. 2016. Toxicity management of immunotherapy for patients with metastatic melanoma. *Ann Transl Med*, 4, 272.
- LINDENMANN, J. & KLEIN, P. A. 1967. VIRAL ONCOLYSIS: INCREASED IMMUNOGENICITY OF HOST CELL ANTIGEN ASSOCIATED WITH INFLUENZA VIRUS. *The Journal of Experimental Medicine*, 126, 93-108.
- LINS, U., FREITAS, F., AACUTE, VIA, KEIM, C. N. & FARINA, M. 2000. Electron Spectroscopic Imaging of Magnetotactic Bacteria: Magnetosome Morphology and Diversity. *Microscopy and Microanalysis*, 6, 463-470.

- LIU, D., WU, W., LING, J., WEN, S., GU, N. & ZHANG, X. 2011a. Effective PEGylation of Iron Oxide Nanoparticles for High Performance In Vivo Cancer Imaging. *Advanced Functional Materials*, 21, 1498-1504.
- LIU, M., GUO, S. & STILES, J. K. 2011b. The emerging role of CXCL10 in cancer (Review). *Oncology letters*, 2, 583-589.
- LIU, X. L., FAN, H. M., YI, J. B., YANG, Y., CHOO, E. S. G., XUE, J. M., FAN, D. D. & DING, J. 2012. Optimization of surface coating on Fe₃O₄ nanoparticles for high performance magnetic hyperthermia agents. *Journal of Materials Chemistry*, 22, 8235-8244.
- LIU, Y., LI, G. R., GUO, F. F., JIANG, W., LI, Y. & LI, L. J. 2010. Large-scale production of magnetosomes by chemostat culture of *Magnetospirillum gryphiswaldense* at high cell density. *Microbial Cell Factories*, 9, 99-99.
- LÜBBE, A. S., BERGEMANN, C., HUHNT, W., FRICKE, T., RIESS, H., BROCK, J. W. & HUHNT, D. 1996. Preclinical Experiences with Magnetic Drug Targeting: Tolerance and Efficacy. *Cancer Research*, 56, 4694-4701.
- LUBBE, A. S., BERGEMANN, C., RIESS, H., SCHRIEVER, F., REICHARDT, P., POSSINGER, K., MATTHIAS, M., DORKEN, B., HERRMANN, F., GÜRTLER, R., HOHENBERGER, P., HAAS, N., SOHR, R., SANDER, B., LEMKE, A. J., OHLENDORF, D., HUHNT, W. & HUHNT, D. 1996. Clinical experiences with magnetic drug targeting: a phase I study with 4'-epidoxorubicin in 14 patients with advanced solid tumors. *Cancer Res*, 56, 4686-93.
- LUKE, J. J., FLAHERTY, K. T., RIBAS, A. & LONG, G. V. 2017. Targeted agents and immunotherapies: optimizing outcomes in melanoma. *Nat Rev Clin Oncol*, 14, 463-482.
- LUSSIGNOL, M., QUEVAL, C., BERNET-CAMARD, M.-F., COTTE-LAFFITTE, J., BEAU, I., CODOGNO, P. & ESCLATINE, A. 2013. The Herpes Simplex Virus 1 Us11 Protein Inhibits Autophagy through Its Interaction with the Protein Kinase PKR. *87*, 859-871.
- MACE, A. T. M., GANLY, I., SOUTAR, D. S. & BROWN, S. M. 2008. Potential for efficacy of the oncolytic Herpes simplex virus 1716 in patients with oral squamous cell carcinoma. *Head & Neck*, 30, 1045-1051.
- MAHMOUDI, M., TACHIBANA, A., GOLDSTONE, A. B., WOO, Y. J., CHAKRABORTY, P., LEE, K. R., FOOTE, C. S., PIECEWICZ, S., BARROZO, J. C., WAKEEL, A., RICE, B. W., BELL III, C. B. & YANG, P. C. 2016. Novel MRI Contrast Agent from Magnetotactic Bacteria Enables In Vivo Tracking of iPSC-derived Cardiomyocytes. *Sci Rep*, 6, 26960.
- MAIER-HAUFF, K., ULRICH, F., NESTLER, D., NIEHOFF, H., WUST, P., THIESEN, B., ORAWA, H., BUDACH, V. & JORDAN, A. 2011. Efficacy and safety of intratumoral thermotherapy using magnetic iron-oxide nanoparticles combined with external beam radiotherapy on patients with recurrent glioblastoma multiforme. *Journal of Neuro-Oncology*, 103, 317-324.
- MANN, S., FRANKEL, R. B. & BLAKEMORE, R. P. 1984a. Structure, morphology and crystal growth of bacterial magnetite. *Nature*, 310, 405-407.
- MANN, S., MOEHC, T. T. & WILLIAMS, R. J. P. 1984b. A high resolution electron microscopic investigation of bacterial magnetite. Implications for crystal growth. *Proceedings of the Royal Society of London. Series B. Biological Sciences*, 221, 385-393.
- MANN, S., SPARKS, N. H., WALKER, M. M. & KIRSCHVINK, J. L. 1988. Ultrastructure, morphology and organization of biogenic magnetite from sockeye salmon, *Oncorhynchus nerka*: implications for magnetoreception. *J Exp Biol*, 140, 35-49.
- MANNUCCI, S., GHIN, L., CONTI, G., TAMBALO, S., LASCIALFARI, A., ORLANDO, T., BENATI, D., BERNARDI, P., BETTERLE, N., BASSI, R., MARZOLA, P. & SBARBATI, A. 2014. Magnetic Nanoparticles from *Magnetospirillum gryphiswaldense* Increase the Efficacy of Thermotherapy in a Model of Colon Carcinoma. *PLoS ONE*, 9, e108959.
- MCBAIN, S. C., YIU, H. H. P. & DOBSON, J. 2008. Magnetic nanoparticles for gene and drug delivery. *International Journal of Nanomedicine*, 3, 169-180.
- MEDAROVA, Z., PHAM, W., FARRAR, C., PETKOVA, V. & MOORE, A. 2007. In vivo imaging of siRNA delivery and silencing in tumors. *Nature medicine*, 13, 372-377.

- MELCHER, A. 2019. Abstract IA27: Oncolytic viruses: Potential for in situ anti-tumor vaccination and combination with checkpoint blockade. 7, IA27-IA27.
- MELCHER, A., PARATO, K., ROONEY, C. M. & BELL, J. C. 2011a. Thunder and lightning: immunotherapy and oncolytic viruses collide. *Mol Ther*, 19, 1008-16.
- MELCHER, A., PARATO, K., ROONEY, C. M. & BELL, J. C. 2011b. Thunder and Lightning: Immunotherapy and Oncolytic Viruses Collide. *Molecular Therapy*, 19, 1008-1016.
- MICHOT, J. M., PRUVOST, R., MATEUS, C., CHAMPIAT, S., VOISIN, A. L., MARABELLE, A. & LAMBOTTE, O. 2018. Fever reaction and haemophagocytic syndrome induced by immune checkpoint inhibitors. *Ann Oncol*, 29, 518-520.
- MILLER, C. G. & FRASER, N. W. 2000. Role of the immune response during neuro-attenuated herpes simplex virus-mediated tumor destruction in a murine intracranial melanoma model. *Cancer Res*, 60, 5714-22.
- MILLER, C. G. & FRASER, N. W. 2003. Requirement of an integrated immune response for successful neuroattenuated HSV-1 therapy in an intracranial metastatic melanoma model. *Molecular Therapy*, 7, 741-747.
- MINETA, T., RABKIN, S. D. & MARTUZA, R. L. 1994. Treatment of Malignant Gliomas Using Ganciclovir-hypersensitive, Ribonucleotide Reductase-deficient Herpes Simplex Viral Mutant. *Cancer Research*, 54, 3963.
- MIYAMOTO, S., INOUE, H., NAKAMURA, T., YAMADA, M., SAKAMOTO, C., URATA, Y., OKAZAKI, T., MARUMOTO, T., TAKAHASHI, A., TAKAYAMA, K., NAKANISHI, Y., SHIMIZU, H. & TANI, K. 2012. Coxsackievirus B3 Is an Oncolytic Virus with Immunostimulatory Properties That Is Active against Lung Adenocarcinoma. 72, 2609-2621.
- MONTEIRO-RIVIERE, N. A., INMAN, A. O. & ZHANG, L. W. 2009. Limitations and relative utility of screening assays to assess engineered nanoparticle toxicity in a human cell line. *Toxicology and Applied Pharmacology*, 234, 222-235.
- MORGAN, R. A., DUDLEY, M. E., WUNDERLICH, J. R., HUGHES, M. S., YANG, J. C., SHERRY, R. M., ROYAL, R. E., TOPALIAN, S. L., KAMMULA, U. S., RESTIFO, N. P., ZHENG, Z., NAHVI, A., DE VRIES, C. R., ROGERS-FREEZER, L. J., MAVROUKAKIS, S. A. & ROSENBERG, S. A. 2006. Cancer Regression in Patients After Transfer of Genetically Engineered Lymphocytes. *Science*, 314, 126-129.
- MORIUCHI, S., OLIGINO, T., KRISKY, D., MARCONI, P., FINK, D., COHEN, J. & GLORIOSO, J. C. 1998. Enhanced tumor cell killing in the presence of ganciclovir by herpes simplex virus type 1 vector-directed coexpression of human tumor necrosis factor-alpha and herpes simplex virus thymidine kinase. *Cancer Res*, 58, 5731-7.
- MUHAREMAGIC, D., ZAMAY, A., GHOBADLOO, S. M., EVGIN, L., SAVITSKAYA, A., BELL, J. C. & BEREZOVSKI, M. V. 2014. Aptamer-facilitated Protection of Oncolytic Virus from Neutralizing Antibodies. *Mol Ther Nucleic Acids*, 3, e167.
- MURAT, D., BYRNE, M. & KOMEILI, A. 2010. Cell biology of prokaryotic organelles. *Cold Spring Harb Perspect Biol*, 2, a000422.
- MUTHANA, M., GIANNOUDIS, A., SCOTT, S. D., FANG, H.-Y., COFFELT, S. B., MORROW, F. J., MURDOCH, C., BURTON, J., CROSS, N., BURKE, B., MISTRY, R., HAMDY, F., BROWN, N. J., GEORGOPOULOS, L., HOSKIN, P., ESSAND, M., LEWIS, C. E. & MAITLAND, N. J. 2011a. Use of Macrophages to Target Therapeutic Adenovirus to Human Prostate Tumors. *Cancer Research*, 71, 1805-1815.
- MUTHANA, M., GIANNOUDIS, A., SCOTT, S. D., FANG, H. Y., COFFELT, S. B., MORROW, F. J., MURDOCH, C., BURTON, J., CROSS, N., BURKE, B., MISTRY, R., HAMDY, F., BROWN, N. J., GEORGOPOULOS, L., HOSKIN, P., ESSAND, M., LEWIS, C. E. & MAITLAND, N. J. 2011b. Use of macrophages to target therapeutic adenovirus to human prostate tumors. *Cancer Res*, 71, 1805-15.
- MUTHANA, M., KENNERLEY, A. J., HUGHES, R., FAGNANO, E., RICHARDSON, J., PAUL, M., MURDOCH, C., WRIGHT, F., PAYNE, C., LYTHGOE, M. F., FARROW, N., DOBSON, J., CONNER, J., WILD, J.

- M. & LEWIS, C. 2015a. Directing cell therapy to anatomic target sites in vivo with magnetic resonance targeting. *Nat Commun*, 6.
- MUTHANA, M., KENNERLEY, A. J., HUGHES, R., FAGNANO, E., RICHARDSON, J., PAUL, M., MURDOCH, C., WRIGHT, F., PAYNE, C., LYTHGOE, M. F., FARROW, N., DOBSON, J., CONNER, J., WILD, J. M. & LEWIS, C. 2015b. Directing cell therapy to anatomic target sites in vivo with magnetic resonance targeting. *Nature Communications*, 6, 8009.
- MUTHANA, M., RODRIGUES, S., CHEN, Y.-Y., WELFORD, A., HUGHES, R., TAZZYMAN, S., ESSAND, M., MORROW, F. & LEWIS, C. E. 2013. Macrophage Delivery of an Oncolytic Virus Abolishes Tumor Regrowth and Metastasis after Chemotherapy or Irradiation. *Cancer Research*, 73, 490-495.
- MUTHANA, M., SCOTT, S. D., FARROW, N., MORROW, F., MURDOCH, C., GRUBB, S., BROWN, N., DOBSON, J. & LEWIS, C. E. 2008a. A novel magnetic approach to enhance the efficacy of cell-based gene therapies. *Gene Therapy*, 15, 902.
- MUTHANA, M., SCOTT, S. D., FARROW, N., MORROW, F., MURDOCH, C., GRUBB, S., BROWN, N., DOBSON, J. & LEWIS, C. E. 2008b. A novel magnetic approach to enhance the efficacy of cell-based gene therapies. *Gene Ther*, 15, 902-910.
- MYKHAYLYK, O., SOBISCH, T., ALMSTÄTTER, I., SANCHEZ-ANTEQUERA, Y., BRANDT, S., ANTON, M., DÖBLINGER, M., EBERBECK, D., SETTLES, M., BRAREN, R., LERCHE, D. & PLANK, C. 2012. Silica-Iron Oxide Magnetic Nanoparticles Modified for Gene Delivery: A Search for Optimum and Quantitative Criteria. *Pharmaceutical Research*, 29, 1344-1365.
- NAIDOO, J., PAGE, D. B., LI, B. T., CONNELL, L. C., SCHINDLER, K., LACOUTURE, M. E., POSTOW, M. A. & WOLCHOK, J. D. 2015. Toxicities of the anti-PD-1 and anti-PD-L1 immune checkpoint antibodies. *Ann Oncol*, 26, 2375-91.
- NASONGKLA, N., BEY, E., REN, J., AI, H., KHEMTONG, C., GUTHI, J. S., CHIN, S. F., SHERRY, A. D., BOOTHMAN, D. A. & GAO, J. 2006. Multifunctional polymeric micelles as cancer-targeted, MRI-ultrasensitive drug delivery systems. *Nano Lett*, 6, 2427-30.
- NAUTS, H. C. & MCLAREN, J. R. 1990. Coley toxins--the first century. *Adv Exp Med Biol*, 267, 483-500.
- NEUBERGER, T., SCHÖPF, B., HOFMANN, H., HOFMANN, M. & VON RECHENBERG, B. 2005. Superparamagnetic nanoparticles for biomedical applications: Possibilities and limitations of a new drug delivery system. *Journal of Magnetism and Magnetic Materials*, 293, 483-496.
- NGUYEN, M. L. & BLAHO, J. A. 2009. Cellular players in the herpes simplex virus dependent apoptosis balancing act. *Viruses*, 1, 965-978.
- NGUYEN, M. L., KRAFT, R. M., AUBERT, M., GOODWIN, E., DIMAIO, D. & BLAHO, J. A. 2007. p53 and hTERT Determine Sensitivity to Viral Apoptosis. 81, 12985-12995.
- NIKAM, D. S., JADHAV, S. V., KHOT, V. M., NINGTHOUJAM, R. S., HONG, C. K., MALI, S. S. & PAWAR, S. H. 2014. Colloidal stability of polyethylene glycol functionalized Co_{0.5}Zn_{0.5}Fe₂O₄ nanoparticles: effect of pH, sample and salt concentration for hyperthermia application. *RSC Advances*, 4, 12662-12671.
- OBEID, M., TESNIERE, A., GHIRINGHELLI, F., FIMIA, G. M., APETOH, L., PERFETTINI, J.-L., CASTEDO, M., MIGNOT, G., PANARETAKIS, T., CASARES, N., MÉTIVIER, D., LAROCLETTE, N., VAN ENDERT, P., CICCOSANTI, F., PIACENTINI, M., ZITVOGEL, L. & KROEMER, G. 2006. Calreticulin exposure dictates the immunogenicity of cancer cell death. *Nature Medicine*, 13, 54.
- ORVEDAHL, A., ALEXANDER, D., TALLOCZY, Z., SUN, Q., WEI, Y., ZHANG, W., BURNS, D., LEIB, D. A. & LEVINE, B. 2007. HSV-1 ICP34.5 confers neurovirulence by targeting the Beclin 1 autophagy protein. *Cell Host Microbe*, 1, 23-35.
- PARK, B.-H., HWANG, T., LIU, T.-C., SZE, D. Y., KIM, J.-S., KWON, H.-C., OH, S. Y., HAN, S.-Y., YOON, J.-H., HONG, S.-H., MOON, A., SPETH, K., PARK, C., AHN, Y.-J., DANESHMAND, M., RHEE, B. G., PINEDO, H. M., BELL, J. C. & KIRN, D. H. 2008. Use of a targeted oncolytic poxvirus, JX-594, in patients with refractory primary or metastatic liver cancer: a phase I trial. *The Lancet Oncology*, 9, 533-542.

- PARK, J. H., SARAVANAKUMAR, G., KIM, K. & KWON, I. C. 2010. Targeted delivery of low molecular drugs using chitosan and its derivatives. *Advanced Drug Delivery Reviews*, 62, 28-41.
- PARK, S. I., LIM, J. H., KIM, J. H., YUN, H. I. & KIM, C. O. 2006. Toxicity estimation of magnetic fluids in a biological test. *Journal of Magnetism and Magnetic Materials*, 304, e406-e408.
- PARK, S. S., DONG, H., LIU, X., HARRINGTON, S. M., KRCO, C. J., GRAMS, M. P., MANSFIELD, A. S., FURUTANI, K. M., OLIVIER, K. R. & KWON, E. D. 2015. PD-1 Restrains Radiotherapy-Induced Abscopal Effect. *Cancer Immunol Res*, 3, 610-9.
- PATEL, M. R. & KRATZKE, R. A. 2013. Oncolytic virus therapy for cancer: the first wave of translational clinical trials. *Translational Research*, 161, 355-364.
- PATEL, S. H., RIMNER, A. & COHEN, R. B. 2017. Combining immunotherapy and radiation therapy for small cell lung cancer and thymic tumors. *Transl Lung Cancer Res*, 6, 186-195.
- PEER, D., KARP, J. M., HONG, S., FAROKHZAD, O. C., MARGALIT, R. & LANGER, R. 2007. Nanocarriers as an emerging platform for cancer therapy. *Nat Nanotechnol*, 2, 751-60.
- PETROVSKI, G., PÁSZTOR, K., OROSZ, L., ALBERT, R., MENCEL, E., MOE, M. C., KAARNIRANTA, K., FACSKÓ, A. & MEGYERI, K. J. J. O. B. 2014. Herpes simplex virus types 1 and 2 modulate autophagy in SIRC corneal cells. 39, 683-692.
- PFANNENSTIEL, L. W., DIAZ-MONTERO, C. M., TIAN, Y. F., SCHARPF, J., KO, J. S. & GASTMAN, B. R. 2019. Immune-Checkpoint Blockade Opposes CD8⁺ T-cell Suppression in Human and Murine Cancer. *Cancer Immunology Research*, 7, 510-525.
- PICCHI, H., MATEUS, C., CHOUAID, C., BESSE, B., MARABELLE, A., MICHOT, J. M., CHAMPIAT, S., VOISIN, A. L. & LAMBOTTE, O. 2018. Infectious complications associated with the use of immune checkpoint inhibitors in oncology: reactivation of tuberculosis after anti PD-1 treatment. *Clin Microbiol Infect*, 24, 216-218.
- PLANK, C., ZELPHATI, O. & MYKHAYLYK, O. 2011. Magnetically enhanced nucleic acid delivery. Ten years of magnetofection—Progress and prospects. *Advanced Drug Delivery Reviews*, 63, 1300-1331.
- POSTOW, M. A., CHESNEY, J., PAVLICK, A. C., ROBERT, C., GROSSMANN, K., MCDERMOTT, D., LINETTE, G. P., MEYER, N., GIGUERE, J. K., AGARWALA, S. S., SHAHEEN, M., ERNSTOFF, M. S., MINOR, D., SALAMA, A. K., TAYLOR, M., OTT, P. A., ROLLIN, L. M., HORAK, C., GAGNIER, P., WOLCHOK, J. D. & HODI, F. S. 2015. Nivolumab and ipilimumab versus ipilimumab in untreated melanoma. *N Engl J Med*, 372, 2006-17.
- POUYSEGUR, J., VOLMAT, V. & LENORMAND, P. 2002. Fidelity and spatio-temporal control in MAP kinase (ERKs) signalling. *Biochem Pharmacol*, 64, 755-63.
- POWER, A. T. & BELL, J. C. 2008. Taming the Trojan horse: optimizing dynamic carrier cell/oncolytic virus systems for cancer biotherapy. *Gene Ther*, 15, 772-779.
- POWER, A. T., WANG, J., FALLS, T. J., PATERSON, J. M., PARATO, K. A., LICHTY, B. D., STOJDL, D. F., FORSYTH, P. A., ATKINS, H. & BELL, J. C. 2007. Carrier cell-based delivery of an oncolytic virus circumvents antiviral immunity. *Mol Ther*, 15, 123-30.
- PRESTWICH, R. J., HARRINGTON, K. J., PANDHA, H. S., VILE, R. G., MELCHER, A. A. & ERRINGTON, F. 2008. Oncolytic viruses: a novel form of immunotherapy. *Expert Rev Anticancer Ther*, 8, 1581-8.
- RAGURAMAN, V. & SUTHINDHIRAN, K. 2019. Comparative ecotoxicity assessment of magnetosomes and magnetite nanoparticles. *International Journal of Environmental Health Research*, 1-13.
- READ, G. S., KARR, B. M. & KNIGHT, K. 1993. Isolation of a herpes simplex virus type 1 mutant with a deletion in the virion host shutoff gene and identification of multiple forms of the vhs (UL41) polypeptide. *Journal of Virology*, 67, 7149-7160.
- REMSSEN, L. G., MCCORMICK, C. I., ROMAN-GOLDSTEIN, S., NILAVER, G., WEISSLEDER, R., BOGDANOV, A., HELLSTRÖM, I., KROLL, R. A. & NEUWELT, E. A. 1996. MR of carcinoma-specific monoclonal antibody conjugated to monocrySTALLINE iron oxide nanoparticles: the potential for noninvasive diagnosis. *American Journal of Neuroradiology*, 17, 411-8.

- RIBAS, A., DUMMER, R., PUZANOV, I., VANDERWALDE, A., ANDTBACKA, R. H. I., MICHELIN, O., OLSZANSKI, A. J., MALVEHY, J., CEBON, J., FERNANDEZ, E., KIRKWOOD, J. M., GAJEWSKI, T. F., CHEN, L., GORSKI, K. S., ANDERSON, A. A., DIEDE, S. J., LASSMAN, M. E., GANSERT, J., HODI, F. S. & LONG, G. V. 2018. Oncolytic Virotherapy Promotes Intratumoral T Cell Infiltration and Improves Anti-PD-1 Immunotherapy. *Cell*, 174, 1031-1032.
- RIEGLER, J., LIEW, A., HYNES, S. O., ORTEGA, D., O'BRIEN, T., DAY, R. M., RICHARDS, T., SHARIF, F., PANKHURST, Q. A. & LYTHGOE, M. F. 2013. Superparamagnetic iron oxide nanoparticle targeting of MSCs in vascular injury. *Biomaterials*, 34, 1987-1994.
- RIEGLER, J., WELLS, J. A., KYRTATOS, P. G., PRICE, A. N., PANKHURST, Q. A. & LYTHGOE, M. F. 2010. Targeted magnetic delivery and tracking of cells using a magnetic resonance imaging system. *Biomaterials*, 31, 5366-5371.
- RINAUDO, M. 2006. Chitin and chitosan: Properties and applications. *Progress in Polymer Science*, 31, 603-632.
- ROBERT, C., RIBAS, A., WOLCHOK, J. D., HODI, F. S., HAMID, O., KEFFORD, R., WEBER, J. S., JOSHUA, A. M., HWU, W. J., GANGADHAR, T. C., PATNAIK, A., DRONCA, R., ZAROOR, H., JOSEPH, R. W., BOASBERG, P., CHMIELOWSKI, B., MATEUS, C., POSTOW, M. A., GERGICH, K., ELASSAISSCHAAP, J., LI, X. N., IANNONE, R., EBBINGHAUS, S. W., KANG, S. P. & DAUD, A. 2014. Anti-programmed-death-receptor-1 treatment with pembrolizumab in ipilimumab-refractory advanced melanoma: a randomised dose-comparison cohort of a phase 1 trial. *Lancet*, 384, 1109-17.
- ROIZMAN, B. 1996. The function of herpes simplex virus genes: a primer for genetic engineering of novel vectors. 93, 11307-11312.
- ROUKOS, D. H., TZAKOS, A. & ZOGRAFOS, G. 2009. Current concerns and challenges regarding tailored anti-angiogenic therapy in cancer. *Expert Rev Anticancer Ther*, 9, 1413-6.
- RUSSELL, S. J. & PENG, K.-W. 2007. Viruses as anticancer drugs. *Trends in Pharmacological Sciences*, 28, 326-333.
- RUSSELL, S. J., PENG, K.-W. & BELL, J. C. 2012. Oncolytic virotherapy. *Nat Biotech*, 30, 658-670.
- SAMANIEGO, L. A., WU, N. & DELUCA, N. A. 1997. The herpes simplex virus immediate-early protein ICP0 affects transcription from the viral genome and infected-cell survival in the absence of ICP4 and ICP27. *Journal of virology*, 71, 4614-4625.
- SAMRA, Z. Q., AHMAD, S., JAVEID, M., DAR, N., ASLAM, M. S., GULL, I. & AHMAD, M. M. 2013. ANTICANCER MEDICINES (DOXORUBICIN AND METHOTREXATE) CONJUGATED WITH MAGNETIC NANOPARTICLES FOR TARGETING DRUG DELIVERY THROUGH IRON. *Preparative Biochemistry and Biotechnology*, 43, 781-797.
- SANCHEZ-ANTEQUERA, Y., MYKHAYLYK, O., VAN TIL, N. P., CENGIZEROGLU, A., DE JONG, J. H., HUSTON, M. W., ANTON, M., JOHNSTON, I. C. D., POJDA, Z., WAGEMAKER, G. & PLANK, C. 2011. Magselectofection: an integrated method of nanomagnetic separation and genetic modification of target cells. *Blood*, 117, e171-e181.
- SANDERS, I., BOYER, M. & FRASER, N. W. 2015. Early nucleosome deposition on, and replication of, HSV DNA requires cell factor PCNA. *J Neurovirol*, 21, 358-69.
- SANFILIPPO, C. M. & BLAHO, J. A. 2006. ICP0 gene expression is a herpes simplex virus type 1 apoptotic trigger. *J Virol*, 80, 6810-21.
- SANTANA, S., BULLIDO, M. J., RECUERO, M., VALDIVIESO, F. & ALDUDO, J. 2012. Herpes simplex virus type I induces an incomplete autophagic response in human neuroblastoma cells. *J Alzheimers Dis*, 30, 815-31.
- SAPET, C., PELLEGRINO, C., LAURENT, N., SICARD, F. & ZELPHATI, O. 2012. Magnetic Nanoparticles Enhance Adenovirus Transduction In Vitro and In Vivo. *Pharmaceutical Research*, 29, 1203-1218.
- SCHADENDORF, D., HODI, F. S., ROBERT, C., WEBER, J. S., MARGOLIN, K., HAMID, O., PATT, D., CHEN, T. T., BERMAN, D. M. & WOLCHOK, J. D. 2015. Pooled Analysis of Long-Term Survival Data

- From Phase II and Phase III Trials of Ipilimumab in Unresectable or Metastatic Melanoma. *J Clin Oncol*, 33, 1889-94.
- SCHINDELIN, J., ARGANDA-CARRERAS, I., FRISE, E., KAYNIG, V., LONGAIR, M., PIETZSCH, T., PREIBISCH, S., RUEDEN, C., SAALFELD, S., SCHMID, B., TINEVEZ, J. Y., WHITE, D. J., HARTENSTEIN, V., ELICEIRI, K., TOMANCAK, P. & CARDONA, A. 2012. Fiji: an open-source platform for biological-image analysis. *Nat Methods*, 9, 676-82.
- SCHÜLER, D. & FRANKEL, R. B. 1999. Bacterial magnetosomes: microbiology, biomineralization and biotechnological applications. *Applied Microbiology and Biotechnology*, 52, 464-473.
- SCULLY, O. J., BAY, B.-H., YIP, G. & YU, Y. 2012. Breast Cancer Metastasis. *Cancer Genomics - Proteomics*, 9, 311-320.
- SELVAN, S. T., TAN, T. T. & YING, J. Y. 2005. Robust, Non-Cytotoxic, Silica-Coated CdSe Quantum Dots with Efficient Photoluminescence. *Advanced Materials*, 17, 1620-1625.
- SENYEI, A., WIDDER, K. & CZERLINSKI, G. 1978. Magnetic guidance of drug-carrying microspheres. *Journal of Applied Physics*, 49, 3578-3583.
- SENZER, N. N., KAUFMAN, H. L., AMATRUDA, T., NEMUNAITIS, M., REID, T., DANIELS, G., GONZALEZ, R., GLASPY, J., WHITMAN, E. & HARRINGTON, K. 2009. Phase II clinical trial of a granulocyte-macrophage colony-stimulating factor–encoding, second-generation oncolytic herpesvirus in patients with unresectable metastatic melanoma. *Journal of Clinical Oncology*, 27, 5763-5771.
- SHAH, N. B., VERCELLOTTI, G. M., WHITE, J. G., FEGAN, A., WAGNER, C. R. & BISCHOF, J. C. 2012. Blood–Nanoparticle Interactions and in Vivo Biodistribution: Impact of Surface PEG and Ligand Properties. *Molecular Pharmaceutics*, 9, 2146-2155.
- SHAPIRO, B. 2009. Towards dynamic control of magnetic fields to focus magnetic carriers to targets deep inside the body. *Journal of Magnetism and Magnetic Materials*, 321, 1594-1599.
- SHARMA, P. & ALLISON, J. P. 2015. The future of immune checkpoint therapy. 348, 56-61.
- SHEN, L.-F., CHEN, J., ZENG, S., ZHOU, R.-R., ZHU, H., ZHONG, M.-Z., YAO, R.-J. & SHEN, H. 2010. The Superparamagnetic Nanoparticles Carrying the E1A Gene Enhance the Radiosensitivity of Human Cervical Carcinoma in Nude Mice. *Molecular Cancer Therapeutics*, 9, 2123-2130.
- SHOWALTER, A., LIMAYE, A., OYER, J. L., IGARASHI, R., KITTIPATARIN, C., COPIK, A. J. & KHALED, A. R. 2017. Cytokines in immunogenic cell death: Applications for cancer immunotherapy. *Cytokine*, 97, 123-132.
- SHUKLA, D. & SPEAR, P. G. 2001. Herpesviruses and heparan sulfate: an intimate relationship in aid of viral entry. *The Journal of clinical investigation*, 108, 503-510.
- SILVA, K. T., LEÃO, P. E., ABREU, F., LÓPEZ, J. A., GUTARRA, M. L., FARINA, M., BAZYLINSKI, D. A., FREIRE, D. M. G. & LINS, U. 2013. Optimization of Magnetosome Production and Growth by the Magnetotactic *Vibrio* magnetotacticus Strain MV-1 through a Statistics-Based Experimental Design. 79, 2823-2827.
- SILVERSTEIN, A., SOOD, R. & COSTAS-CHAVARRI, A. 2016. Breast Cancer in Africa: Limitations and Opportunities for Application of Genomic Medicine. *Int J Breast Cancer*, 2016, 4792865.
- SILVIO, D., MELANIE, K., INGRID, H., ROBERT, M. & MATTHIAS, Z. 2011. Magnetic multicore nanoparticles for hyperthermia—influence of particle immobilization in tumour tissue on magnetic properties. *Nanotechnology*, 22, 265102.
- SIMPSON, S. A., MANCHAK, M. D., HAGER, E. J., KRUMMENACHER, C., WHITBECK, J. C., LEVIN, M. J., FREED, C. R., WILCOX, C. L., COHEN, G. H., EISENBERG, R. J. & PIZER, L. I. 2005. Nectin-1/HvcC mediates herpes simplex virus type 1 entry into primary human sensory neurons and fibroblasts. *Journal of NeuroVirology*, 11, 208-218.
- SINGH, P. K., DOLEY, J., KUMAR, G. R., SAHOO, A. P. & TIWARI, A. K. 2012. Oncolytic viruses & their specific targeting to tumour cells. *The Indian Journal of Medical Research*, 136, 571-584.
- SMITH, K. D., MEZHIR, J. J., BICKENBACH, K., VEERAPONG, J., CHARRON, J., POSNER, M. C., ROIZMAN, B. & WEICHSELBAUM, R. R. 2006. Activated MEK Suppresses Activation of PKR and Enables

- Efficient Replication and In Vivo Oncolysis by $\Delta\gamma₁>34.5$ Mutants of Herpes Simplex Virus 1. *80*, 1110-1120.
- SOTIRIOU, G. A., HIRT, A. M., LOZACH, P.-Y., TELEKI, A., KRUMEICH, F. & PRATSINIS, S. E. 2011. Hybrid, Silica-Coated, Janus-Like Plasmonic-Magnetic Nanoparticles. *Chemistry of Materials*, *23*, 1985-1992.
- SPEAR, P. G. 2004. Herpes simplex virus: receptors and ligands for cell entry. *Cellular Microbiology*, *6*, 401-410.
- STANILAND, S., WARD, B., HARRISON, A., VAN DER LAAN, G. & TELLING, N. 2007. Rapid magnetosome formation shown by real-time x-ray magnetic circular dichroism. *Proceedings of the National Academy of Sciences*, *104*, 19524-19528.
- STANNARD, L. M., FULLER, A. O. & SPEAR, P. G. 1987. Herpes simplex virus glycoproteins associated with different morphological entities projecting from the virion envelope. *Journal of general virology*, *68*, 715-725.
- STUDENY, M., MARINI, F. C., DEMBINSKI, J. L., ZOMPETTA, C., CABREIRA-HANSEN, M., BEKELE, B. N., CHAMPLIN, R. E. & ANDREEFF, M. 2004. Mesenchymal Stem Cells: Potential Precursors for Tumor Stroma and Targeted-Delivery Vehicles for Anticancer Agents. *Journal of the National Cancer Institute*, *96*, 1593-1603.
- SUGIURA, K. & STOCK, C. C. 1952. Studies in a tumor spectrum. I. Comparison of the action of methylbis(2-chloroethyl)amine and 3-bis(2-chloroethyl)aminomethyl-4-methoxymethyl-5-hydroxy-6-methylpyridine on the growth of a variety of mouse and rat tumors. *Cancer*, *5*, 382-402.
- SUN, C., DU, K., FANG, C., BHATTARAI, N., VEISEH, O., KIEVIT, F., STEPHEN, Z., LEE, D., ELLENBOGEN, R. G., RATNER, B. & ZHANG, M. 2010a. PEG-Mediated Synthesis of Highly Dispersive Multifunctional Superparamagnetic Nanoparticles: Their Physicochemical Properties and Function In Vivo. *ACS Nano*, *4*, 2402-2410.
- SUN, J., LI, Y., LIANG, X.-J. & WANG, P. C. 2011. Bacterial Magnetosome: A Novel Biogenetic Magnetic Targeted Drug Carrier with Potential Multifunctions. *Journal of Nanomaterials*, *2011*, 13.
- SUN, J., TANG, T., DUAN, J., XU, P. X., WANG, Z., ZHANG, Y., WU, L. & LI, Y. 2010b. Biocompatibility of bacterial magnetosomes: acute toxicity, immunotoxicity and cytotoxicity. *Nanotoxicology*, *4*, 271-83.
- SUN, J. B., ZHAO, F., TANG, T., JIANG, W., TIAN, J. S., LI, Y. & LI, J. L. 2008. High-yield growth and magnetosome formation by *Magnetospirillum gryphiswaldense* MSR-1 in an oxygen-controlled fermentor supplied solely with air. *Appl Microbiol Biotechnol*, *79*, 389-97.
- TAKASU, A., MASUI, A., HAMADA, M., IMAI, T., IWAI, S. & YURA, Y. 2016. Immunogenic cell death by oncolytic herpes simplex virus type 1 in squamous cell carcinoma cells. *Cancer Gene Therapy*, *23*, 107.
- TAN, G., KASUYA, H., SAHIN, T. T., YAMAMURA, K., WU, Z., KOIDE, Y., HOTTA, Y., SHIKANO, T., YAMADA, S., KANZAKI, A., FUJII, T., SUGIMOTO, H., NOMOTO, S., NISHIKAWA, Y., TANAKA, M., TSURUMARU, N., KUWAHARA, T., FUKUDA, S., ICHINOSE, T., KIKUMORI, T., TAKEDA, S., NAKAO, A. & KODERA, Y. 2015. Combination therapy of oncolytic herpes simplex virus HF10 and bevacizumab against experimental model of human breast carcinoma xenograft. *Int J Cancer*, *136*, 1718-30.
- TANAKA, K., ITO, A., KOBAYASHI, T., KAWAMURA, T., SHIMADA, S., MATSUMOTO, K., SAIDA, T. & HONDA, H. 2005. Intratumoral injection of immature dendritic cells enhances antitumor effect of hyperthermia using magnetic nanoparticles. *International Journal of Cancer*, *116*, 624-633.
- TANAKA, T. & MATSUNAGA, T. 2000. Fully Automated Chemiluminescence Immunoassay of Insulin Using Antibody-Protein A-Bacterial Magnetic Particle Complexes. *Analytical Chemistry*, *72*, 3518-3522.

- TANG, D., KANG, R., COYNE, C. B., ZEH, H. J. & LOTZE, M. T. 2012. PAMPs and DAMPs: signal 0s that spur autophagy and immunity. *Immunological Reviews*, 249, 158-175.
- THOMAS, D. L. & FRASER, N. W. 2003. HSV-1 therapy of primary tumors reduces the number of metastases in an immune-competent model of metastatic breast cancer. *Molecular Therapy*, 8, 543-551.
- THOMAS, M., LU, J. J., GE, Q., ZHANG, C., CHEN, J. & KLIBANOV, A. M. 2005. Full Deacylation of Polyethylenimine Dramatically Boosts Its Gene Delivery Efficiency and Specificity to Mouse Lung. *Proceedings of the National Academy of Sciences of the United States of America*, 102, 5679-5684.
- THOMSON, B. J. 2001. Viruses and apoptosis. *International journal of experimental pathology*, 82, 65-76.
- TODA, M., IIZUKA, Y., KAWASE, T., UYEMURA, K. & KAWAKAMI, Y. 2002. Immuno-viral therapy of brain tumors by combination of viral therapy with cancer vaccination using a replication-conditional HSV. *Cancer Gene Therapy*, 9, 356-364.
- TODA, M., MARTUZA, R. L., KOJIMA, H. & RABKIN, S. D. 1998. In situ cancer vaccination: An IL-12 defective vector/replication-competent herpes simplex virus combination induces local and systemic antitumor activity. *Journal of Immunology*, 160, 4457-4464.
- TODA, M., RABKIN, S. D., KOJIMA, H. & MARTUZA, R. L. 1999. Herpes simplex virus as an in situ cancer vaccine for the induction of specific anti-tumor immunity. *Human Gene Therapy*, 10, 385-393.
- TOPALIAN, S. L., SZNOL, M., MCDERMOTT, D. F., KLUGER, H. M., CARVAJAL, R. D., SHARFMAN, W. H., BRAHMER, J. R., LAWRENCE, D. P., ATKINS, M. B., POWDERLY, J. D., LEMING, P. D., LIPSON, E. J., PUZANOV, I., SMITH, D. C., TAUBE, J. M., WIGGINTON, J. M., KOLLIA, G. D., GUPTA, A., PARDOLL, D. M., SOSMAN, J. A. & HODI, F. S. 2014. Survival, durable tumor remission, and long-term safety in patients with advanced melanoma receiving nivolumab. *J Clin Oncol*, 32, 1020-30.
- TOPP, M. S., KUFER, P., GOKBUGET, N., GOEBELER, M., KLINGER, M., NEUMANN, S., HORST, H. A., RAFF, T., VIARDOT, A., SCHMID, M., STELLJES, M., SCHAICH, M., DEGENHARD, E., KOHNE-VOLLAND, R., BRUGGEMANN, M., OTTMANN, O., PFEIFER, H., BURMEISTER, T., NAGORSEN, D., SCHMIDT, M., LUTTERBUESE, R., REINHARDT, C., BAEUERLE, P. A., KNEBA, M., EINSELE, H., RIETHMULLER, G., HOELZER, D., ZUGMAIER, G. & BARGOU, R. C. 2011. Targeted therapy with the T-cell-engaging antibody blinatumomab of chemotherapy-refractory minimal residual disease in B-lineage acute lymphoblastic leukemia patients results in high response rate and prolonged leukemia-free survival. *J Clin Oncol*, 29, 2493-8.
- TORCHILIN, V. P. 2006. Multifunctional nanocarriers. *Adv Drug Deliv Rev*, 58, 1532-55.
- TORO BEJARANO, M. & MERCHAN, J. R. 2015. Targeting tumor vasculature through oncolytic virotherapy: recent advances. *Oncolytic Virother*, 4, 169-81.
- TRAN, N. & WEBSTER, T. J. 2010. Magnetic nanoparticles: biomedical applications and challenges. *Journal of Materials Chemistry*, 20, 8760-8767.
- TRESILWISED, N., PITHAYANUKUL, P., HOLM, P. S., SCHILLINGER, U., PLANK, C. & MYKHAYLYK, O. 2012a. Effects of nanoparticle coatings on the activity of oncolytic adenovirus-magnetic nanoparticle complexes. *Biomaterials*, 33, 256-69.
- TRESILWISED, N., PITHAYANUKUL, P., HOLM, P. S., SCHILLINGER, U., PLANK, C. & MYKHAYLYK, O. 2012b. Effects of nanoparticle coatings on the activity of oncolytic adenovirus-magnetic nanoparticle complexes. *Biomaterials*, 33, 256-269.
- TRESILWISED, N., PITHAYANUKUL, P., MYKHAYLYK, O., HOLM, P., HOLZMÜLLER, R., ANTON, M., THALHAMMER, S., ADIGÜZEL, D., DÖBLINGER, M. & PLANK, C. 2010a. *Boosting Oncolytic Adenovirus Potency with Magnetic Nanoparticles and Magnetic Force*.
- TRESILWISED, N., PITHAYANUKUL, P., MYKHAYLYK, O., HOLM, P. S., HOLZMULLER, R., ANTON, M., THALHAMMER, S., ADIGUZEL, D., DOBLINGER, M. & PLANK, C. 2010b. Boosting oncolytic

- adenovirus potency with magnetic nanoparticles and magnetic force. *Mol Pharm*, 7, 1069-89.
- TRESILWISED, N., PITHAYANUKUL, P., MYKHAYLYK, O., HOLM, P. S., HOLZMÜLLER, R., ANTON, M., THALHAMMER, S., ADIGÜZEL, D., DÖBLINGER, M. & PLANK, C. 2010c. Boosting Oncolytic Adenovirus Potency with Magnetic Nanoparticles and Magnetic Force. *Molecular Pharmaceutics*, 7, 1069-1089.
- UPRICHARD, S. L. & KNIPE, D. M. 2003. Conformational Changes in the Herpes Simplex Virus ICP8 DNA-Binding Protein Coincident with Assembly in Viral Replication Structures. 77, 7467-7476.
- VACCHELLI, E., EGGERMONT, A., SAUTÈS-FRIDMAN, C., GALON, J., ZITVOGEL, L., KROEMER, G. & GALLUZZI, L. 2013. Trial watch. *Oncolimmunology*, 2, e24612.
- VAN LANDEGHEM, F. K., MAIER-HAUFF, K., JORDAN, A., HOFFMANN, K. T., GNEVECKOW, U., SCHOLZ, R., THIESEN, B., BRUCK, W. & VON DEIMLING, A. 2009. Post-mortem studies in glioblastoma patients treated with thermotherapy using magnetic nanoparticles. *Biomaterials*, 30, 52-7.
- VARGAS, G., CYPRIANO, J., CORREA, T., LEAO, P., BAZYLINSKI, D. A. & ABREU, F. 2018. Applications of Magnetotactic Bacteria, Magnetosomes and Magnetosome Crystals in Biotechnology and Nanotechnology: Mini-Review. *Molecules*, 23.
- VOLL, R. E., HERRMANN, M., ROTH, E. A., STACH, C., KALDEN, J. R. & GIRKONTAITE, I. 1997. Immunosuppressive effects of apoptotic cells. *Nature*, 390, 350-1.
- VON GISE, A., LORENZ, P., WELLBROCK, C., HEMMING, B., BERBERICH-SIEBELT, F., RAPP, U. R. & TROPFMAIR, J. 2001. Apoptosis suppression by Raf-1 and MEK1 requires MEK- and phosphatidylinositol 3-kinase-dependent signals. *Mol Cell Biol*, 21, 2324-36.
- WANG, C., BAO, C., LIANG, S., ZHANG, L., FU, H., WANG, Y., WANG, K., LI, C., DENG, M., LIAO, Q., NI, J. & CUI, D. 2014a. HAI-178 antibody-conjugated fluorescent magnetic nanoparticles for targeted imaging and simultaneous therapy of gastric cancer. *Nanoscale research letters*, 9, 274-274.
- WANG, F., CHEN, C., CHEN, Y., WANG, P., CHEN, C., GENG, D., LI, L. & SONG, T. 2018a. Magnetically targeted photothermal cancer therapy in vivo with bacterial magnetic nanoparticles. *Colloids and Surfaces B: Biointerfaces*, 172, 308-314.
- WANG, R., WU, W., LI, W., HUANG, S., LI, Z., LIU, R., SHAN, Z., ZHANG, C., LI, W. & WANG, S. 2018b. Activation of NLRP3 Inflammasome Promotes Foam Cell Formation in Vascular Smooth Muscle Cells and Atherogenesis Via HMGB1. *Journal of the American Heart Association*, 7, e008596.
- WANG, X., LI, Y., LIU, S., YU, X., LI, L., SHI, C., HE, W., LI, J., XU, L., HU, Z., YU, L., YANG, Z., CHEN, Q., GE, L., ZHANG, Z., ZHOU, B., JIANG, X., CHEN, S. & HE, S. 2014b. Direct activation of RIP3/MLKL-dependent necrosis by herpes simplex virus 1 (HSV-1) protein ICP6 triggers host antiviral defense. *Proc Natl Acad Sci U S A*, 111, 15438-43.
- WESTIN, J. R., CHU, F., ZHANG, M., FAYAD, L. E., KWAK, L. W., FOWLER, N., ROMAGUERA, J., HAGEMEISTER, F., FANALE, M., SAMANIEGO, F., FENG, L., BALADANDAYUTHAPANI, V., WANG, Z., MA, W., GAO, Y., WALLACE, M., VENCE, L. M., RADVANYI, L., MUZZAFAR, T., ROTEM-YEHUDAR, R., DAVIS, R. E. & NEELAPU, S. S. 2014. Safety and activity of PD1 blockade by pidilizumab in combination with rituximab in patients with relapsed follicular lymphoma: a single group, open-label, phase 2 trial. *The Lancet Oncology*, 15, 69-77.
- WHILDING, L. M., ARCHIBALD, K. M., KULBE, H., BALKWILL, F. R., ÖBERG, D. & MCNEISH, I. A. 2013. Vaccinia Virus Induces Programmed Necrosis in Ovarian Cancer Cells. *Molecular Therapy*, 21, 2074-2086.
- WHITE, C. L., TWIGGER, K. R., VIDAL, L., DE BONO, J. S., COFFEY, M., HEINEMANN, L., MORGAN, R., MERRICK, A., ERRINGTON, F., VILE, R. G., MELCHER, A. A., PANDHA, H. S. & HARRINGTON, K. J. 2008. Characterization of the adaptive and innate immune response to intravenous oncolytic reovirus (Dearing type 3) during a phase I clinical trial. *Gene Ther*, 15, 911-20.

- WHITE, D. W., SUZANNE BEARD, R. & BARTON, E. S. 2012. Immune modulation during latent herpesvirus infection. *Immunological reviews*, 245, 189-208.
- WOJTON, J. & KAUR, B. 2010. Impact of tumor microenvironment on oncolytic viral therapy. *Cytokine Growth Factor Rev*, 21, 127-34.
- WONG, J., DAVIES, N., JERAJ, H., VILAR, E., VILJOEN, A. & FARRINGTON, K. 2016. A comparative study of blood endotoxin detection in haemodialysis patients. *Journal of inflammation (London, England)*, 13, 24-24.
- WORKENHE, S. T., POL, J. G., LICHTY, B. D., CUMMINGS, D. T. & MOSSMAN, K. L. 2013. Combining Oncolytic HSV-1 with Immunogenic Cell Death-Inducing Drug Mitoxantrone Breaks Cancer Immune Tolerance and Improves Therapeutic Efficacy. 1, 309-319.
- WORKENHE, S. T., SIMMONS, G., POL, J. G., LICHTY, B. D., HALFORD, W. P. & MOSSMAN, K. L. 2014. Immunogenic HSV-mediated oncolysis shapes the antitumor immune response and contributes to therapeutic efficacy. *Mol Ther*, 22, 123-31.
- WU, Y.-N., CHEN, D.-H., SHI, X.-Y., LIAN, C.-C., WANG, T.-Y., YEH, C.-S., RATINAC, K. R., THORDARSON, P., BRAET, F. & SHIEH, D.-B. 2011. Cancer-cell-specific cytotoxicity of non-oxidized iron elements in iron core-gold shell NPs. *Nanomedicine: Nanotechnology, Biology and Medicine*, 7, 420-427.
- XIA, Z., DICKENS, M., RAINGEAUD, J., DAVIS, R. J. & GREENBERG, M. E. 1995. Opposing effects of ERK and JNK-p38 MAP kinases on apoptosis. *Science*, 270, 1326-31.
- XIANG, L., WEI, J., JIANBO, S., GUILI, W., FENG, G. & YING, L. 2007. Purified and sterilized magnetosomes from *Magnetospirillum gryphiswaldense* MSR-1 were not toxic to mouse fibroblasts in vitro. *Letters in Applied Microbiology*, 45, 75-81.
- XIE, J., CHEN, K. & CHEN, X. 2009. Production, Modification and Bio-Applications of Magnetic Nanoparticles Gestated by Magnetotactic Bacteria. *Nano Res*, 2, 261-278.
- XIE, J., XU, C., KOHLER, N., HOU, Y. & SUN, S. 2007. Controlled PEGylation of Monodisperse Fe₃O₄ Nanoparticles for Reduced Non-Specific Uptake by Macrophage Cells. *Advanced Materials*, 19, 3163-3166.
- XU, J. K., ZHANG, F. F., SUN, J. J., SHENG, J., WANG, F. & SUN, M. 2014. Bio and nanomaterials based on Fe₃O₄. *Molecules*, 19, 21506-28.
- YAN, L., ZHANG, S., CHEN, P., LIU, H., YIN, H. & LI, H. 2012. Magnetotactic bacteria, magnetosomes and their application. *Microbiol Res*, 167, 507-19.
- YE, J., COULOURIS, G., ZARETSKAYA, I., CUTCUTACHE, I., ROZEN, S. & MADDEN, T. L. 2012. Primer-BLAST: A tool to design target-specific primers for polymerase chain reaction. *BMC Bioinformatics*, 13, 134-134.
- YU, X., LI, Y., CHEN, Q., SU, C., ZHANG, Z., YANG, C., HU, Z., HOU, J., ZHOU, J., GONG, L., JIANG, X., ZHENG, C. & HE, S. 2015. Herpes Simplex Virus 1 (HSV-1) and HSV-2 Mediate Species-Specific Modulations of Programmed Necrosis through the Viral Ribonucleotide Reductase Large Subunit R1. *Journal of virology*, 90, 1088-1095.
- YUAN, Z. Y., ZHANG, L., LI, S., QIAN, X. Z. & GUAN, Z. Z. 2003. [Safety of an E1B deleted adenovirus administered intratumorally to patients with cancer]. *Ai Zheng*, 22, 310-3.
- ZAMARIN, D., HOLMGAARD, R. B., RICCA, J., PLITT, T., PALESE, P., SHARMA, P., MERGHOU, T., WOLCHOK, J. D. & ALLISON, J. P. 2017. Intratumoral modulation of the inducible co-stimulator ICOS by recombinant oncolytic virus promotes systemic anti-tumour immunity. *Nature Communications*, 8, 14340.
- ZEYTUNI, N., OFFER, T., DAVIDOV, G. & ZARIVACH, R. 2012. Crystallization and preliminary crystallographic analysis of the C-terminal domain of MamM, a magnetosome-associated protein from *Magnetospirillum gryphiswaldense* MSR-1. *Acta Crystallographica Section F*, 68, 927-930.
- ZHANG, Y., ZHANG, X., JIANG, W., LI, Y. & LI, J. 2011. Semicontinuous culture of *Magnetospirillum gryphiswaldense* MSR-1 cells in an autofermentor by nutrient-balanced and isosmotic feeding strategies. *Appl Environ Microbiol*, 77, 5851-6.

- ZHOU, G. & ROIZMAN, B. 2001. The domains of glycoprotein D required to block apoptosis depend on whether glycoprotein D is present in the virions carrying herpes simplex virus 1 genome lacking the gene encoding the glycoprotein. *Journal of virology*, 75, 6166-6172.
- ZHOU, S., LI, Y., CUI, F., JIA, M., YANG, X., WANG, Y., XIE, L., ZHANG, Q. & HOU, Z. 2014. Development of multifunctional folate-poly(ethylene glycol)-chitosan-coated Fe₃O₄ nanoparticles for biomedical applications. *Macromolecular Research*, 22, 58-66.

Appendix

Table 1: The physicochemical properties of the MNPs

Samples	Diameter (nm)	Electrokinetic potential (mv)	Magnetic susceptibility (SI)	Iron content (mg/l)
MAG	46 ± 5	- 9 ± 2.3	8.164e-5	0.17 ± 0.5
10%PEI90%SF MNPs	70 ± 10	28 ± 8.3	4.635e-5	1.13
50%PEI50%SF MNPs	180 ± 16	47± 10.4	5.7166e-5	0.67
100%PEI MNPs	101 ± 13	68± 2	8.3362e-5	3.1
100%SF MNPs	77 ± 35	-23 ± 1.5	6.5280e-5	1.1

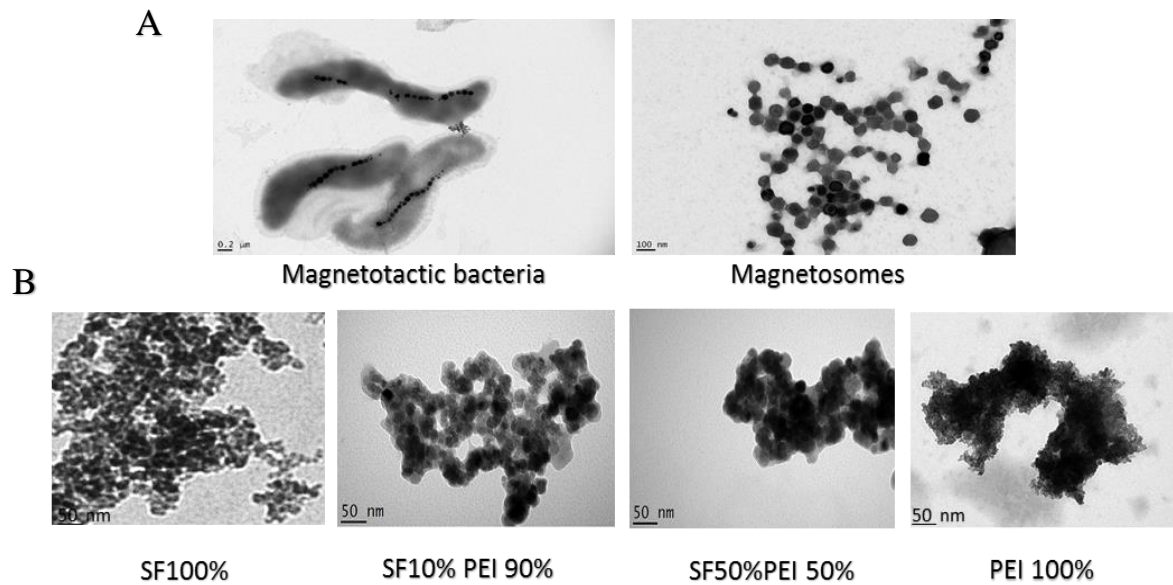


Figure 1: High-resolution Transmission electron microscopy. **A** TEM images of AMB-1 magnetotactic bacteria, grown in cabinet within micro-anaerobic conditions in 1% O₂ gas and 99% nitrogen at 30.1 C° in liquid culture medium which is specific to AMB-1 bacteria (Left image: scale bar-0.2μm). Magnetosomes were purified from AMB-1 and displayed typical cuboidal crystal shapes (Right image: scale bar-100nm). **B** The SF100%, SF10% PEI 90%, SF50%PEI 50% and PEI 100% coated MNPs were much more dense and appeared on top of each other (scale bar-50nm).

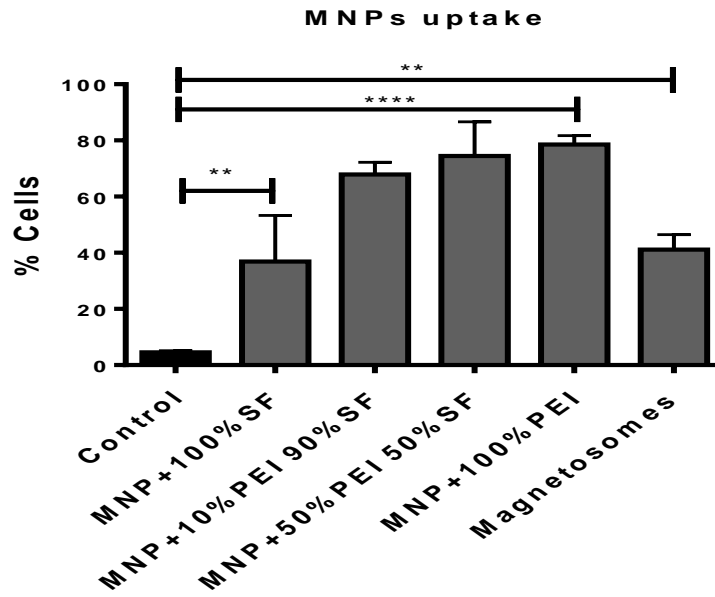
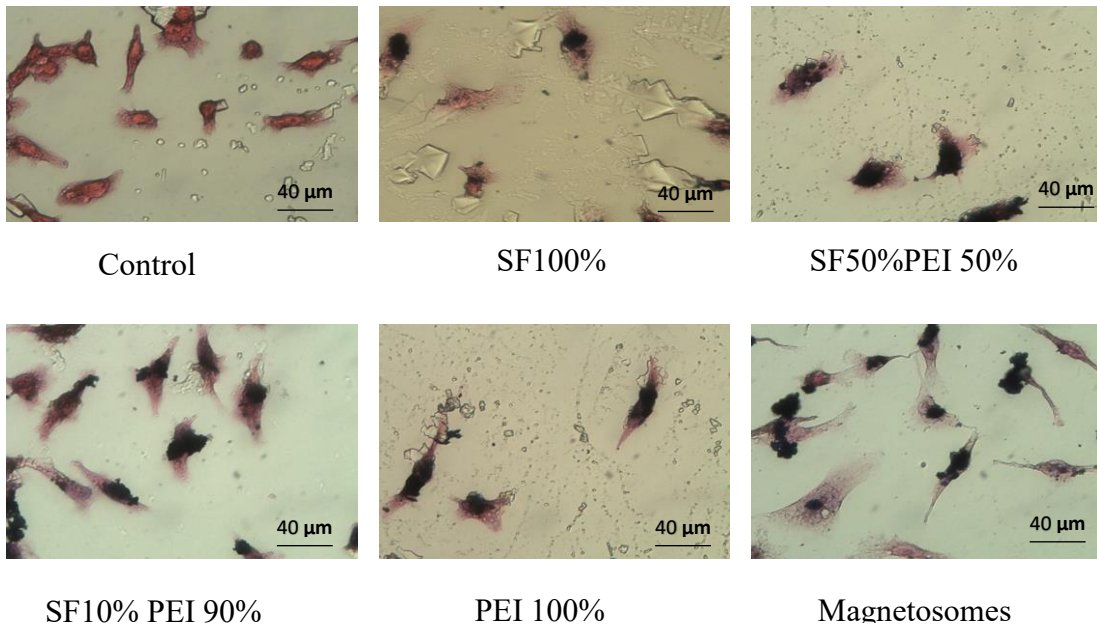
A**B**

Figure 2: MNPs are internalised by MDA-MB-231 cells. MDA-MB-231 cells were incubated with 0.3mg/ml coated MNPs and purified magnetosomes for 24 hours **A** Flow cytometrical analysis of cells revealed uptake of coated MNPs (SF100%, SF 50%PEI 50%, SF 10% PEI 90%, PEI 100%) and magnetosomes resulted in an important increase in cell size and granularity compared to the control (untreated cells). Data are the mean \pm SEM of n=3. **B** Representative Prussian blue images of MDA-MB-231 cells incubated with coated MNPs and magnetosomes. Dark blue staining is the presence of the Prussian blue; pink is the eosin. This was taken at 40 x Magnification using light microscopy.

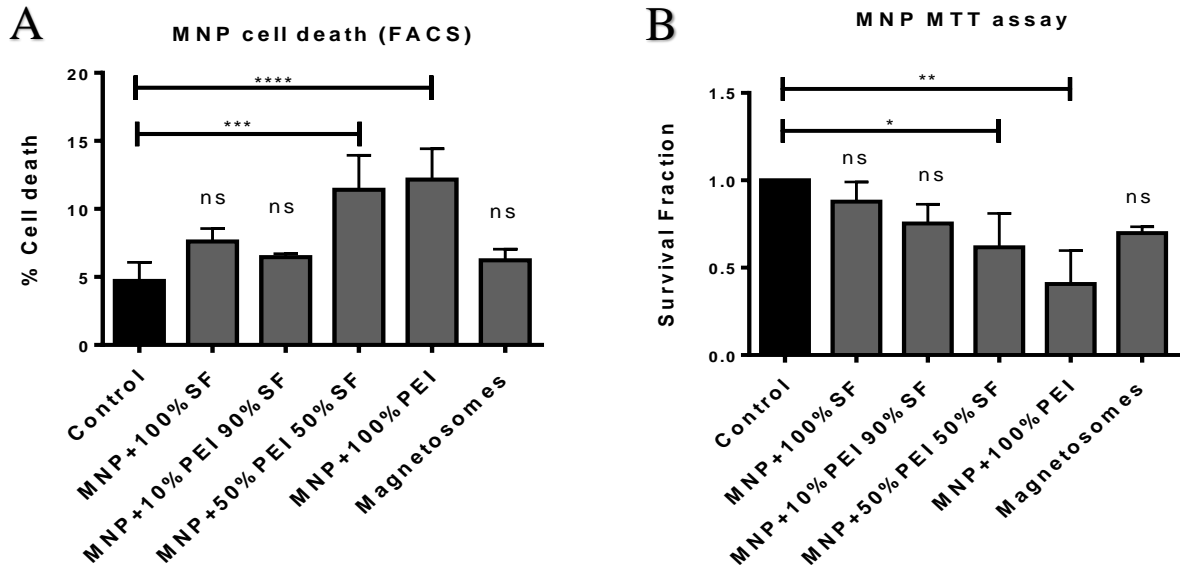


Figure 3: MDA-MB-231 viability following incubation with MNPs. MDA-MB-231 cells were incubated with coated MNPs and purified magnetosomes for 24 hours. Cells were collected and flow cytometry as used to evaluate cell death by the addition of PI immediately prior to analysis. **A** Cell death (PI+ cells) in the presence of MNPs coated with 50% and 100% PEI was significant when compared to the control **B** MTT assay also revealed a significant difference between the control and MNPs coated with 50%PEI/50%SF ($P \leq 0.05$) and 100% PEI ($P \leq 0.01$). No significant change in cell viability was noticed in the presence of 10%PEI/90%SF MNPs or magnetosomes. Data are the mean \pm SEM of $n=4$

Access provided by The University of Sheffield

Access this article on
[ScienceDirect](#)

Breast cancer immunotherapy using magnetised oncolytic viruses

H. AL-Janabi¹, J. Conner², Z. Taher¹, S. Staniland¹, M. Muthana¹
A8

DOI: <https://doi.org/10.1016/j.ejca.2018.01.012>



[Abstract](#) [Full Text](#)

Background: Oncolytic viruses (OV) are encouraging new immunotherapies for cancer. OVs induce immunogenic cell death (ICD) and activate antitumour immunity. However, clinical use has been limited to intratumoural delivery as a result of inadequate tumour targeting following systemic injection, strong anti-viral host immune responses and sequestration by the liver and spleen.

Materials and methods: Bacterial-derived magnetosomes (MAG) were purified from magnetotactic bacteria AMB-1 and washed extensively before assembly with OV (HSV1716) to give MAG-OV complexes. Characterization of the physical, chemical and oncolytic potential of our MAG-OVs was performed. The safety and efficacy of our magnetic viral complexes in combination with magnetic guidance strategies were also assessed *in vivo* in an orthotopic murine mammary carcinoma model (EO771).

Results: Stable MAG-OV complexes of ~90nm diameter successfully infected human and murine breast cancer cells (MDA-MB-231, MCF7, TS1 and EO771 cells in a dose dependant manner), was protected from neutralising antibodies and induced oncolytic cell death. Following MAG-OV infection a significant increase in viral replication (ICP0, gB, ICP8), ICD signals (HMGB1, CALR, ATP) and apoptotic genes (CASP 3, CASP8, FASL) were detected. Intravenous delivery of MAG-OV resulted in reduced tumour burden in the presence of magnetic guidance (MAG/OV 1071mm² vs. OV 1435.7mm², *p* <0.05) and resulted in an increase in tumour-infiltrating T-cells, NK cells and neutrophils.

Conclusions: This study indicates that magnetizing HSV1716 results in viral protection from neutralising antibodies and in combination with magnetic guidance reduces tumour burden and induces antitumour immunity.

Article Tools

[PDF \(41 KB\)](#)

[Email Article](#)

[Add to My Reading List](#)

[Export Citation](#)

[Create Citation Alert](#)

[Cited by in Scopus \(0\)](#)

[Request Permissions](#)

[Order Reprints](#)
(100 minimum order)

Related Articles

European Breast Cancer Conference manifesto on breast centres/units
European Journal of Cancer, Vol. 72
[Open Access](#)

Breast cancer, placenta and pregnancy
European Journal of Cancer, Vol. 115

Impact of age on breast cancer mortality and competing causes of death at 10 years follow-up in the adjuvant TEAM trial
European Journal of Cancer, Vol. 99

